TITLE:

Development of the Inertia Force Driven Hybrid Loading System and Pseudo-Negative Stiffness Control Method for a MR Damper(Dissertation_全文)

AUTHOR(S):

Toyooka, Akihiro

CITATION:

Toyooka, Akihiro. Development of the Inertia Force Driven Hybrid Loading System and Pseudo-Negative Stiffness Control Method for a MR Damper. 京都大学, 2003, 博士(工学)

ISSUE DATE:

2003-03-24

URL:

https://doi.org/10.14989/doctor.k10146

RIGHT:

京都大学学術情報リポジトリ
KURENAI 紅
Kyoto University Research Information Repository

新制
工
1261

Development of the Inertia Force Driven Hybrid Loading System and Pseudo-Negative Stiffness Control Method for a MR Damper

Akihiro TOYOOKA

December 2002

Development of the Inertia Force Driven Hybrid Loading System and Pseudo-Negative Stiffness Control Method for a MR Damper

A Dissertation
Submitted to
the Faculty of Engineering of Kyoto University

In Partial Fulfillment
of the Requirements for the Degree of
Doctor of Engineering

by

Akihiro TOYOOKA

December 2002

Summary

In this dissertation, the Inertia-Force-Driven Loading (I.F.D.L.) system was newly developed to allow an economical and accurate loading environment for energy dissipation devices to characterize the dynamic properties and to comprehend the performances of these devices under the realistic loading conditions.

The objective of this dissertation is to develop a real time substructure hybrid loading experiment system for the IFDL, by which the dynamic interaction between structures and test specimens could be clarified. For this purpose, a control method for the loading device is proposed in order for the equation of motion regarding the IFDL system with damper specimen to be consistent with that for the hypothetical structure. The effectiveness, limitations, and possible error sources have been closely examined through numerical simulations.

After several preliminary identification experiments regarding the test system and the damper specimen, full-scale verification tests are carried out. A single-degree-of-freedom (SDOF) and a multi-degree-of-freedom (MDOF) structural systems are selected as the hypothetical structures in which damper specimen is installed. Also, a constant-current controlled MR damper is used as the passive damper specimen. It is confirmed from the SDOF experiment that the proposed control method could work effectively for replicating the structural response with damper specimen subjected to the arbitrary ground motions. Also, it is observed from MDOF experiment that experimentally obtained results show good agreements with both numerical estimations and previously conducted experimental results.

Another scope of this dissertation is to develop a simple but effective control algorithm for the semi active devices such as MR dampers. In this dissertation, the pseudo-negative stiffness (P.N.S.) control method is examined, in which the control force is given by the combination of the negative stiffness element plus positive damping element. An efficacy of the proposed PNS control is examined both algebraically and numerically. It is shown that the control method is advantageous over the passive device in terms of acceleration reduction. Also, results of the actuator loading experiment so as for the MR damper to realize the PNS control are shown. It is shown from experiment that the MR damper has a capability to generate the proposed PNS hysteresis by precise modeling of the device.

Acknowledgements

This dissertation is a contribution of my six-year of study years as a member of the Structural Dynamic Laboratory of Kyoto University.

First of all, I would like to show my sincere gratitude to my supervisor Professor Iemura of Kyoto University. He not only provided the splendid test facilities and equipments for the structural control research activities, but also shows directions of research with his brilliant inspirations.

I would like to express my sincere appreciation to Professor Matsuhisa and Professor Suzuki of Kyoto University for their invaluable suggestions and critical readings for my dissertation.

Also, I would like to greatly appreciate Associate Professor Igarashi of Kyoto University for his unending instructions and encouragements. His accurate advice and in-depth knowledge lead my research activity to the right way.

I would like to appreciate Dr. Takahashi for his advice, instruction, and encouragement regarding not only research but also various topics during my study year.

As to conduct experiments, involvements and contributions of many persons were indispensable. I thank Mr. Nakanisi for his great effort regarding test system build up and instructions for the equipments. I appreciate Mr. Miyasaka for his contributions to assemble the test facility. Also, I thank Dr. Sunakoda and Mr. Sodeyama for their effort and advice as to the MR damper device. The test facilities and equipments used in the dissertation are financially supported by the Japan Society for the Promotion of Science. Their research grants and funds are fully appreciated.

I would like to express my gratitude to Professor B. F. Spencer, Jr. of University of Illinois at Urbana-Champaign for his sincere and invaluable instructions during my short-term stay in Notre Dame University. I would like to appreciate Professor Henri Gavin of Duke University for providing many ideas on MR dampers and semi active control.

My research activity has been supported by many students and alumni of the Structural Dynamics Laboratory. Particularly, I would like to appreciate Mr. Hitotsumachi, Mr. Fujiwara, Mr. Nakata, Mr. Tanaka, Mr. Suzuki, and Mr. Hirooka for their great

contributions to the research and experiment on structural control. Also, numerous discussions with Mr. M.H. Pradono, Mr. Sogabe, and Dr. Iwata regarding research topics always encourage me to proceed the research. I would like to sincerely appreciate all of the students of the Structural Dynamics Laboratory and my intimate friends for their heartful encouragements.

Finally, I would like to express my sincere gratitude to my father Nagao, my mother Masami, and my sister Akane for their heartful and continuous supports during my student and study years. I would like to dedicate my dissertation to my family.

Table of Contents

List of Figures

List of Tables

List of Photos

Chapter 1

Introduction

1.1 General Remarks

For the decade, many strong earthquakes have occurred one after another in many nations. These earthquakes have caused severe damages to the large-scale infrastructures. It indicates that structures designed with traditional codes are sometimes vulnerable to the strong earthquake motions. In order to avoid such critical damages, structural engineers have been working to figure out different types of structural systems that are robust to the strong motions.

In such a current, structural control techniques are believed to be one of the promising technology for earthquake resistance design. The concept of the structural control is to absorb vibration energy of the structure by introducing auxiliary devices. Efficacy of the structural control technique itself had been proved in early 1960's, and it was first realized in the architectural engineering field. Various types of structural control theories and devices have been recently developed and introduced to the large-scale civil engineering structures.

Among various types of structural control devices, nonlinear hysteresis dampers have been rapidly and widely adopted to the civil structures for retrofitting purpose. These devices include friction damper, oil damper, bingham-plastic damper, etc[1)]. Before introducing such devices, dynamic response calculations should be carried out in order to comprehend the vibration reduction effect and find out optimal location and number of the device. This requires precise frequency-dependent physical or algebraic device models that have been proposed by many researchers. However, it is quite difficult to figure out the appropriate model for specified device because of the existence of the strong nonlinearity. This nonlinearity affect the dynamic response of the target structure, and dynamic interaction between device and structure should be taken into

consideration. For this purpose, so-called 'substructure hybrid experiment' techniques have been developed.

1.2 Substructure Hybrid Experiment

The term 'substructure hybrid' implies the technique that combines the device loading experiment and structural response calculation. The equation of motion of the structure is solved numerically with given earthquake and measured device reaction force, and device is then excited by referring to the calculated structural response. This procedure is iterated at every sample time, and one can get structural response, which the dynamic interaction effect is considered. Particularly, it is called 'real-time substructure hybrid experiment' that the numerical calculation and device loading are simultaneously carried out in real-time. Although this method requires high-speed computers and precisely-driven loading equipments, it could become affordable recently thanks to the remarkable progress in both softwares and hardwares.

Until now, various kinds of test methods have been proposed. Most of them could be classified into two categories from the viewpoint of the loading equipment.

1.2.1 Hydraulic Actuator

The hydraulic actuator is one of the most commonly used equipment for loading experiment. It mainly consists of hydraulic pump unit, reaction wall, accumulator, and servo valves. By adjusting the valve opening, high-pressure oil reserved in the accumulator rushes into the cylinder, and piston could be driven with large stroke and force. It is advantageous for test specimens which require large excitation force and displacement[2–5].

Also, various algorithms and techniques have been proposed in order to conducting the precise real-time experiments. Nakashima investigated the 'operator splitting' numerical integration scheme[6] which is suitable for on-line controlled experiments. Horiuchi *et al.* proposed the compensation method of the response delay of the actuator based on extrapolation[7,8], and extended to the multi-degree-of-freedom system[9] as well as nonlinear structures[10]. The The similar feed-forward based compensation methods are widely utilized to the numerical algorithms development and real-time testing (Darby *et al.*[11]; Nakashima and Masaoka[12]; Nakashima *et al.*[13]).

French *et al.* developed the effective force testing system in which the concrete mass is driven by several hydraulic actuators to generate the large inertia force[14]. They confirmed the effectiveness by conducting a SDOF experiment exposed to the

earthquake[15].

However, maximum force capacity and loading velocity totally depend on the size and number of the accumulator for the actuators. That is to say, quite a large scale of test system and supplemental devices are required. Moreover, realizing high speed loading condition is relatively difficult as the size of the system increases. In many cases, actuator is used for only realizing the required displacement, and velocity dependency of the specimens is sometimes ignored. This method is called 'Pseudo-dynamic experiment', which is mainly used for large-scale test specimens[16, 17].

1.2.2 Shaking Table

The shaking table tests have been also widely conducted. For the shaking table tests, in general, total structures including damper specimens should be put on the table and exposed to the earthquake motions. It follows that quite a large scale test structures as well as high capable shake table should be needed in order to conduct a precise experiments. However, only a limited number of the test facilities are available that can afford the large scale experiments. Also, it is not economical to construct the whole structural system on the shake table each time of experiment. Moreover, it is almost impossible for the large scale structural system such as civil engineering structures to assemble and put on the shake table.

Due to this difficulty, the scaled experiments using small size shake tables and models of both structures and test specimens are widely used for device verification tests. In this case, the scale effects should be carefully examined, otherwise the obtained results do not necessarily represent the behavior of the device or structures under realistic conditions

Alternatively, substructure hybrid loading test system has been developing for the shaking table equipments. Since most of the capable shake tables are driven by the hydraulic actuators, algorithms as well as technologies for the hydraulic actuator systems are directly applicable to the shaking table test systems. Horiuchi *et al.* introduced the response prediction method for compensating the delay of the shake table acceleration and confirm the efficacy of the proposed method using digital signal processors and small shake table[18]. Iemura *et al.* introduced the inverted digital filter of the shake table for compensating the dynamics, and conducted the real time hybrid experiment using the electromagnetic mass damper installed in the nonlinear substructure[19].

Although the shake table test is applicable to the test specimens such as TMDs that are subjected to the acceleration, it is not appropriate for damper specimens loading tests excited with designated displacement and velocity. Moreover, the same obstacles

with the actuator loading tests should be overcome due to the similarity in driving device of the shake table.

1.3 Inertia Force Driven Loading System

As seen in previous sections, it is difficult for existing loading devices to economically and precisely simulate the dynamic interaction between the device and the controlled structure, unless a large-scale structural specimen is used, or a sophisticated testing algorithm is developed and used. It consequently follows that the obtained results do not necessarily represent the behavior of the device or structures under realistic conditions.

In this dissertation, the 'Inertia-Force-Driven-Loading System' is newly developed in order to conduct a real time hybrid loading experiment both economically and precisely. This system consists of the concrete-slab, rubber and roller supports, and active mass driver. The test specimen is attached to the concrete-slab. The concrete-slab as well as the test specimen can be excited with large displacement, velocity, and acceleration by making use of the inertia force of the shaker[20, 21].

This test system has several advantages over the traditional loading test systems as listed below.

1. A precise modeling of the test device is not necessarily required, since full-scale devices can be tested

2. Responses under arbitrary vibration condition can be simulated within the capacity limitation of the shaker device

3. Large displacement, velocity, and load amplitudes can be economically obtained by making use of the resonance response

4. Real-time experiment can be easily carried out for velocity-dependent devices

Due to these advantages, patents are granted for the test system in both Japan and United States of America. The periodical loading experiment utilizing this test facility has been carried out in order to compose the dynamic model of the damper specimen[20, 21]. This dissertation, however, aims to use the test system for the hybrid loading test. Since the damper specimen could not be driven directly, appropriate shaker control method so as to simulate the response under earthquake ground motion should be proposed.

1.4 Semi-Active Control for a MR Damper

An another objective of the research is to develop and examine the simple but effective control algorithm for the semi-active device. The 'semi-active' control refers to as the one of the structural control techniques that realizes the active control method within the physical constraints of the device. Recently, the use of such semi-active devices have been widely spreading to the application for the large scale civil and architectural structures due to their stability and capability. Semi active device always work so as to dissipate energy but never excite the structure, which is clear contrast to the active device such as hydraulic actuators or AMD. Moreover, structural engineers could make use of the abundant of the active control strategies and experiences to design the semi active controller.

Among various types of devices that could realize the semi-active control, magnetorheological (MR) damper is one of the most promising devices. It consists of the MR fluid and electromagnet, followed by accumulators and piston rod. The MR fluid contains micron-sized polarizable particles. By applying the current to the electromagnet, particle chains are formed by the magnetic fields, and fluid shows a semi-solid characteristics. This drastic change is achieved within a few milliseconds, and effective vibration energy dissipation is obtained. Recently, many attentions have been paid to the development of the MR damper and control methods.

Spencer *et al.* examined the effectiveness of the semi-active controlled MR damper to the seismic protection through small scale model structure and damper specimen [22–24]. Also, they introduced the Bouc-Wen based nonlinear phenomenological models that could trace the overall hysteresis with good accuracy for numerical studies, and confirm the versatility through loading experiments of the damper specimens[22, 25, 26]. Gavin *et al.* closely examined the design procedures of the MR damper so as to regulate the electric power consumption and assembled the prototype device[27]. Recently, the large scale MR damper devices that could be applicable to the realistic civil and architectural structures have been developed (Spencer *et al.*[26, 28]; Sodeyama and Sunakoda [29]).

As for control algorithm for semi-active devices, active control laws, such as H_2/LQG, are utilized in many studies (Dyke *et al.*[30]; Spencer *et al.*[22–25, 28]; Sodeyama and Sunakoda [29]; Yamada [31]; Kurata *et al.*[32]; Niwa [33]; Nishitani *et al.* [34]). Various types of control methods for active and semi-active control are summarized by Dyke and Spencer[35].

In general, the active control algorithms offer certain amount of the sensors or sophisticated observes in order to detect the structural response and determine the

command signal. However, it is quite disadvantageous for large scale structures to locate and sustain many sensors, despite the effectiveness of control algorithm itself. Moreover, the control algorithm itself should be as simple as possible, taking into consideration that the existing uncertainty of the structural dynamics and system implementation.

In order to overcome these difficulties, Iemura *et al.* have proposed the 'pseudo-negative control' algorithm for semi active devices[36, 37]. In the control algorithm, the control force is given by the combination of the negative stiffness and positive damping elements. It is quite advantageous from the viewpoint of the device implementation since this algorithm only requires the relative displacement and velocity at the damper location. Moreover, it is expected that this control could work effectively for reducing the acceleration of the structure by apparently elongating the natural period of the system due to the existence of the negative stiffness.

1.5 Organization of the Thesis

The objective of this dissertation is to develop the real time hybrid loading experiment system together with the Inertia Force Driven Loading facility. Also, the conceptual, analytical, and experimental approach for the proposed pseudo-negative stiffness types of semi-active control is described.

In Chapter 2, total setup of the IFDL test system including the sensors, shaker, and control devices is described. The features as well as the locations of devices are closely mentioned, which would be used for the loading experiments.

In Chapter 3, basic algorithm of the shaker control method for the IFDL system to realize the real-time hybrid loading experiment is proposed. In the proposed method, the shaker is commanded so as for the equation of motion regarding the IFDL to consistent with that of the assumed structure. It is shown that any kinds of structural system including nonlinearity and damper specimen can be conducted by utilizing the precisely controlled shaker. The error arises from the existence of the time delay between command and realize of the shaker velocity is analyzed. Also, feasible ground motion level and hypothetical structural properties are examined from the viewpoint of satisfying the physical constraints of the IFDL test system.

In Chapter 4, preliminary identification tests with regard to the IFDL test system, damper specimen, and shaker device are carried out. It is indispensable to compre-

hend the dynamic characteristics for these devices from the viewpoints of the precise numerical simulation and loading experiment. As to damper specimen, the algebraic model is utilized for representing the hysteresis. For shaker dynamics compensation, a PID controller and band-pass filter are designed.

In Chapter 5, real-time hybrid loading experiments are carried out. As hypothetical structures, single-degree-of-freedom (SDOF) as well as multi-degree-of-freedom (MDOF) systems are chosen, both are supposed to be exposed to the resonance periodical motion and historical earthquakes. As test specimen, passive controlled MR damper applying a constant 0 A of current is utilized. The effectiveness of the IFDL test system as well as the proposed control method are confirmed from the SDOF experiments. In case of the MDOF simulation, results of hybrid loading experiment are compared to that of the past research which used the assumed real-scale frame structure.

In Chapter 6, an effectiveness of the proposed 'pseudo-negative stiffness control' is closely examined. It is shown through algebraic approach with SDOF structure that the proposed method works effectively for reducing the acceleration response while not stimulating the displacement response. The efficacy is also examined through numerical simulation of the MDOF structure. Also, the device control experiments so as for the MR damper to generate the pseudo-negative stiffness hysteresis loops are conducted.

In Chapter 7, achievements of this dissertation are summarized in brief, followed by future remarks.

References

(1) Soong, T. T. and Dargush, G. F.: *Passive Energy Dissipation Systems in Structural Engineering*, John Wiley & Sons, 1997.

(2) Igarashi, A.: *On-Line Computer Controlled Testing of Stiff Multi-Degree-Of-Freedom Structural Systems Under Simulated Seismic Loads*, PhD Thesis, University of California, San Diego, 1994.

(3) Igarashi, A., Seible, F., and Hegemier, G. A.: Development of the pseudodynamic technique for testing a full scale 5-story shear wall structure, *U.S.-Japan Seminar on Development and Future Dimension of Structural Testing Techniques*, 1993.

(4) Williams, M. S. and Blakeborough, A. : Laboratory testing of structures under dynamic loads : an introductory review, *The Royal Society of London*, Vol. 359, pp. 1651 – 1669, 2001.

(5) Tanzo, W., Yamada, Y., and Iemura, H.: Substructured Computer-Actuator Hybrid Loading Tests for Inelastic Earthquake Response of Structures, Technical report, School of Civil Engineering, Kyoto University, 1992.

(6) Nakashima, M.: Extension of On-Line Computer Control Method, *U.S.-Japan Seminar on Development and Future Dimension of Structural Testing Techniques*, 1993.

(7) Horiuchi, T., Nakagawa, M., Sugano, M., and Konno, T. : Development of a Real-Time Hybrid Experimental System with Actuator Delay Compensation (1st Report, Compensation Method and Application to Experiments of Single-Degree-of-Freedom Systems) (in Japanese), *Journal of the Japan Society of Mechanical Engineers (Part C)*, Vol. 61, No. 584, pp. 1328 – 1336, 1995.

(8) Horiuchi, T. and Konno, T. : A new method for compensating actuator delay in real-time hybrid experiments, *The Royal Society of London*, Vol. 359, pp. 1893 – 1909, 2001.

(9) Horiuchi, T., Nakagawa, M., Sugano, M., and Konno, T. : Development of a Real-Time Hybrid Experimental System with Actuator Delay Compensation (2nd Report, Application to a Multiple-Degree-of-Freedom System) (in Japanese), *Journal of the Japan Society of Mechanical Engineers (Part C)*, Vol. 62, No. 599, pp. 2563 – 2570, 1996.

(10) Horiuchi, T. and Konno, T. : Development of a Real-Time Hybrid Experimental System with Actuator Delay Compensation (3rd Report,Application to Nonlinear Structural Systems) (in Japanese), *Journal of the Japan Society of Mechanical Engineers (Part C)*, Vol. 64, No. 617, pp. 7 – 14, 1998.

(11) Blakeborough, A., Williams, M. S., Darby, A. P., and Williams, D. M. : The development of real-time substructure testing, *The Royal Society of London*, Vol. 359, pp. 1869 – 1891, 2001.

(12) Nakashima, M. and Masaoka, N. : Real-time on-line test for MDOF systems, *Earthquake Engineering and Structural Dynamics*, Vol. 28, pp. 393 – 420, 1999.

(13) Nakashima, M., Kato, H., and Takaoka, E. : Development of real-time pseudo dynamic testing, *Earthquake Engineering and Structural Dynamics*, Vol. 21, pp. 79 – 92, 1999.

(14) Dimig, J., Shield, C., French, C., Bailey, F., and Clark, A. : Effective Force Testing : A Method of Seismic Simulation Structural Testing, *Journal of Structural Engineering*, pp. 1028 – 1037, 1999.

(15) Shield, C. K., French, C. W., and Timm, J. : Development and implementation of the effective force testing method for seismic simulation of large-scale structures, *The Royal Society of London*, Vol. 359, pp. 1911 – 1929, 2001.

(16) Mahin, S. A. and Shing, P. B. : Pseudodynamic Method for Seismic Testing, *Journal of Structural Engineering*, Vol. 111(7), pp. 1482 – 1503, 1985.

(17) Takanashi, K. and Nakashima, M. : Japanese activities on on-line testing, *Journal of Engineering Mechanics, ASCE*, Vol. 113(7), 1987.

(18) Horiuchi, T., Inoue, M., Konno, T., and Yamagishi, W. : Development of a Real-Time Hybrid Experimental System Using a Shaking Table (1st Report, Proposal of Experiment Concept and Feasibility Study with Rigid Secondary System) (in Japanese), *Journal of the Japan Society of Mechanical Engineers (Part C)*, Vol. 64, No. 622, pp. 1949 – 1956, 1998.

(19) Iemura, H., Igarashi, A., and Tanaka, H.: Substructure Hybrid Shake Table Test Using Digitally Filtered Displacement Compensation Control Scheme (in Japanese), *Proceedings of the 11th JEES*, No. 304, 2002.

(20) Iemura, H., Igarashi, A., and Tanaka, H.: An Experiment Study on a Testing System for Dynamic Characterization of Energy Dissipating Devices (in Japanese),

Proceedings of the Second Japan National Symposium on Structural Control, pp. 243 – 250, 2000.

(21) Iemura, H., Igarashi, A., Toyooka, A., and Suzuki, Y.: Dynamic Loading Experiment of Passive and Semi-Active Dampers Using the Inertia-Force-Driven Loading System, *Proceedings of the 3rd World Conference on Structural Control*, 2002.

(22) Dyke, S. J., Spencer, Jr., B. F., Sain, M. K., and Carlson, J. D.: On the efficacy of magnetorheological dampers for seismic response reduction, *1997 ASME Design Engineering Technical Conferences*, Vol. DETC97VIB3828, 1997.

(23) Dyke, S. J., Spencer, Jr., B. F., Sain, M. K., and Carlson, J. D.: An Experimental Study of MR Dampers for Seismic Protection, *Smart Materials and Structures: Special Issue on Large Civil Structures*, 1997.

(24) Yoshioka, H. and Spencer, Jr., B. F.: Shaking Table Tests on Semi-active Base Isolation System Employing Magnetorheological Damper (in Japanese), *Damping Symposium II*, The Japan Society of Mechanical Engineers, pp. 120–124, 2002.

(25) Yang, G., Jung, H. J., and Spencer, Jr., B. F.: Dynamic model of full-scale MR dampers for civil engineering application, *US-Japan Workshop on Smart Structure for Improved Seismic Performance in Urban Regions*, pp. 213 – 224, 2001.

(26) Yang, G.: *Large-Scale Magnetorheological Fluid Damper for Vibration Mitigation: Modeling, Testing and Control*, PhD Thesis, University of Notre Dame, 2001.

(27) Gavin, H., Hoagg, J., and Dobossy, M.: Optimal design of MR dampers, *US-Japan Workshop on Smart Structure for Improved Seismic Performance in Urban Regions*, pp. 225 –236, 2001.

(28) Yang, G., Spencer, Jr., B. F., Carlson, J. D., and Sain, M. K. : Large-Scale MR Fluid Dampers: Modeling and Dynamic Performance Considerations, *Engineering Structures*, Vol. 24, pp. 309 – 323, 2002.

(29) Sodeyama, H. and Sunakoda, K.: 300kN-MR damper for semi-active vibration control systems, *JSME Dynamics & Design Conference*, 2001.

(30) Dyke, S. J., Spencer, Jr., B. F., Sain, M. K., and Carlson, J. D.: Modeling and Control of Magnetorheological Dampers for Seismic Response Reduction, *Smart Materials and Structures*, Vol. 5, pp. 565 – 575, 1996.

(31) Yamada, K. : Control strategy for variable damping element considering near-future excitation influence, *Earthquake Engineering and Structural Dynamics*, Vol. 29, pp. 1199 – 1217, 2000.

(32) Kurata, N., Kobori, T., Takahashi, M., Ishibashi, T., Niwa, N., Tagami, J., and Midorikawa, H. : Forced Vibration Test of a Building with Semi-Active Damper System, *Earthquake Engineering and Structural Dynamics*, Vol. 29, pp. 629 – 645, 2000.

(33) Niwa, N., Kobori, T., Takahashi, M., Midorikawa, H., Kurata, N., and Mizuno, T. : Dynamic Loading Test and Simulation Analysis of Full-Scale Semi-Active Hydraulic Damper for Structural Control, *Earthquake Engineering and Structural Dynamics*, Vol. 29, pp. 789 – 812, 2000.

(34) Nishitani, A., Nitta, Y., Ikeda, Y., and Ito, A.: Semiactive Seismic Response Control for Building Structures with Variable Slip-Force Level Dampers (in Japanese), *Proceedings of the Second Japan National Symposium on Structural Control*, pp. 85 – 90, 2000.

(35) Dyke, S. J. and Spencer, Jr., B. F.: A Comparison of Semi-Active Control Strategies for the MR Damper, *Proceedings of the IASTED International Conference*, 1997.

(36) Iemura, H. and Pradono, M. H. : Passive and Semi-Active Seismic Response Control of a Cable-Stayed Bridge, *Earthquake Engineering and Structural Dynamics*, Vol. 9, pp. 189 – 204, 2002.

(37) Iemura, H. and Pradono, M. H.: Negative Stiffness Dampers for Seismic Retrofit of a Cable-Stayed Bridg, *Proceeding of Passive Structural Control Symposium*, pp. 7 – 16, 2002.

Chapter 2

Inertia Force Driven Loading System

2.1 General Remarks

In this chapter, outline of the newly developed Inertia-Force-Driven Loading (IFDL) system is introduced. Because of the uniqueness of this loading system, details of the each component, property and whole experimental setup are shown in this chapter.

2.2 IFDL system

Schematics and the test setup of the IFDL test system are shown in Photo 2.1 and Figure. 2.1 respectively. This test system consists of a concrete-slab, rubber bearing, roller supports (Photo 2.3), and a mass-driver device (shaker). Parameters of this test system is shown in Table 2.1

The shaker can be controlled arbitrarily by applying command voltage in real time. The concrete-slab is excited by the transferred inertia force of the mass of the shaker. Since the test specimen that is to be tested is attached to the concrete-slab (Photo 2.2), it is also excited with the stroke, velocity, and acceleration of the slab. The rubber and roller supports are used to restrain the slab displacement and get it back to the original position after tests.

2.3 Sensors

The locations of sensors utilized in this test system is depicted in Figure 2.2.

Photo 2.1: Photo of the IFDL test system

Photo 2.2: Photo of the Attached Damper Specimen

Photo 2.3: Photo of the Rubber and Roller Supports

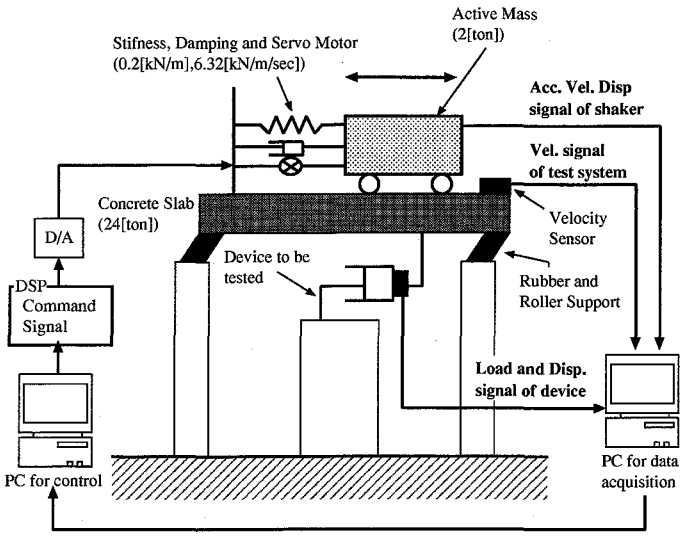

Figure 2.1: Test Set-up of the IFDL test system

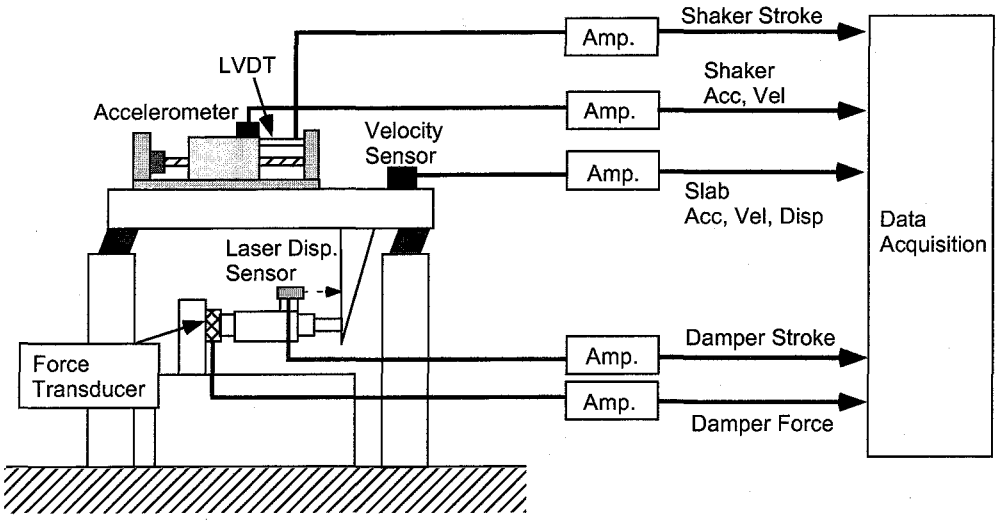

Figure 2.2: Sensor Location

Table 2.1: Parameters of the IFDL Test System

Weight of Slab Mass	26.853 [tonf]
Total Stiffness	344.43 [kN/m]
Total Damping	6.32 [kN/m/sec]
Natural Freq.	0.55 [Hz]
Equivalent Damping	3.86%
Stroke Limit	±10 [cm]

2.3.1 Damper Response Measurement

The force transducer is put between one edge of the damper specimen and the reaction wall. The force transducer amplifier is connected to the force transducer in order to amplify output voltage and eliminate undesirable higher frequency noise. Specifications of these force measurement equipments are shown in Tables 2.2 and 2.3, respectively.

The laser displacement sensor is utilized to measure the stroke, and corresponding stroke velocity is calculated by numerical differentiation. Specification of the laser sensor is shown in Table 2.4.

Table 2.2: Force Transducer Specification

Model	LUK-A-100KNSA1
Rated Capacity	100 kN (10.20 tf)
Rated Output	2001 mV/V
Nonlinearity	0.04 % RO

Table 2.3: Force Transducer Amplifier Specification

Model	DA-16A
Response Frequency	DC - 2.5 kHz
Strain Range	± 50000 μ
S/N Ratio	52 dB p-p
Sensitivity	1 V (at 50μ of strain)
Max. Output	± 5 V
Balance Adjustment	Automatic Electronic Balancer

Table 2.4: Laser Displacement Sensor Specification

Model	LB-300 (Sensor), LB-1200 (Amp.)
Reference Distance	300 mm
Rated Range	± 100 mm
Linearity	0.4 of F.S.
Resolution	50 μm
Output	± 5 V
Luminous Source	Infrared Semiconductor Laser
Spot Diameter	1.2×25 mm

2.3.2 Slab and Shaker Response Measurement

A velocity sensor is installed on the concrete-slab. The velocity sensor together with the amplifier has the capability to measure the displacement, velocity, and acceleration response simultaneously. Among them, displacement and acceleration signals can be obtained from velocity response by analogue integration and differentiation circuits inside the sensor amplifier. Also, accelerometer is located inside the mass of the shaker to measure the absolute acceleration and velocity responses of the mass. The transmitted force is indirectly calculated by the absolute acceleration and the mass of the shaker.

Table 2.5: Velocity Sensor Specification

Type	VSE-15A
Max. Range	± 1000 kine
Sensitivity	0.1 V/kine, 5 mV/gal
Max Output	11 V
Resolution	300 μkine
Linearity	0.05%

2.4 Shaking Device

2.4.1 Specification

The shaker shown in Photo 2.4 is utilized for this IFDL system to generate the inertia force and drive the slab. The shaker is originally intended to be used as the active

Table 2.6: Velocity Sensor Amplifier Specification

Model	AV-200	Max. Output	± 10 V
Frequency Range	Acc : 0.1 - 70 Hz	Precision	Acc : ± 1 %
	Vel : 0.1 - 70 Hz		Vel : ± 1 %
	Dis : 0.1 - 70 Hz		Dis : ± 4 %
Max. Range	Acc : 2000 gal	Resolution	Acc : 0.01 gal
	Vel : 100 kine		Vel : 1 μkine
	Dis : 1000 mm		Dis : 10 μm

Photo 2.4: Photo of the Shaker

mass driver. As shown in the photo, the torque of the servo motor is transmitted to the auxiliary mass through the attached ball screw. The amount of the inertia force totally depends on the weight and the absolute acceleration of the mass. Specification of the shaker is shown in Table 2.7.

2.4.2 Sensors and Control Modes

For the shaker response measurement and control purpose, the accelerometer and the LVDT are installed. The servo motor is driven in real time in accordance with the servo driver command signal. Th servo driver installed in the central control panel has two control modes, velocity controlled operation and torque controlled operation. In the velocity control, rotational speed of the motor is detected by the photo inter-

Table 2.7: Specification of the Shaker

Weight of Mass	2.0 tonf
Weight of Device	3.2 tonf
Stiffness	0.2 kN/m
Damping	6.32 kN/m/sec
Driven Motor	AC Servo 11 kW
Maximum Velocity	150 kine
Stroke Limit	±50 cm
Max. Motor Capacity	0.75 G

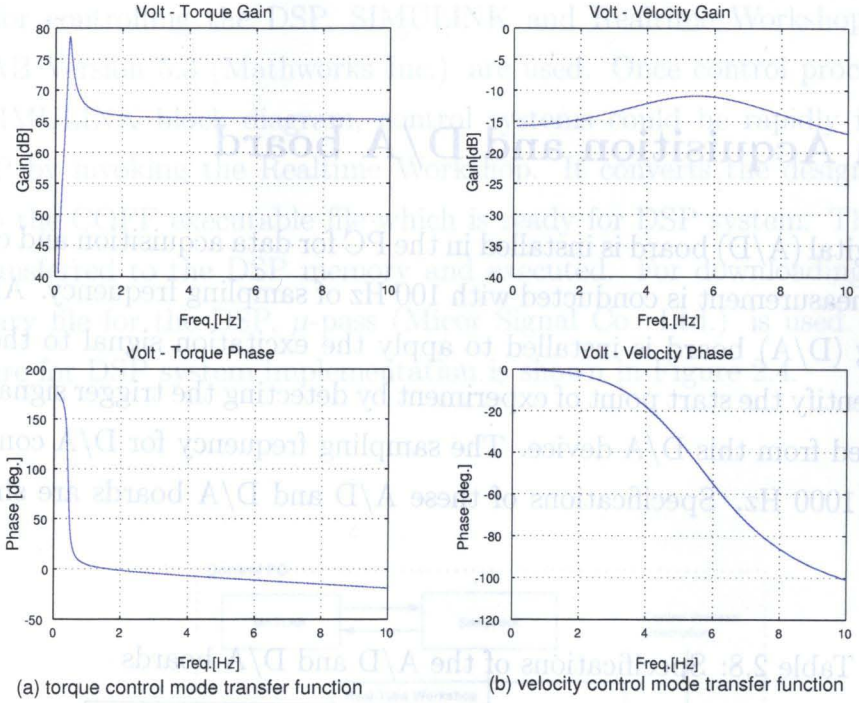

(a) torque control mode transfer function (b) velocity control mode transfer function

Figure 2.3: Primarily Identified Transfer Functions (w/o Load)

ruptor inside the servo motor. Command voltage to the device is then determined by the feedback controller of the servo driver, which amplify the residual value between measured velocity and command signal.

In the torque controlled operation, on the contrary, no such a feedback controller is implemented. The command signal is directly applied to the servo motor, but no compensational operation is applied by the servo driver. For the precise control, velocity controlled operation is selected for this research.

2.4.3 Dynamic Characteristics

In order to conduct the precise loading experiment, shaker should be controlled to follow the command velocity without intolerable time delay. Since the shaker consists of mass, stiffness, and viscous damping elements, transfer function from the command signal to the realized relative velocity shows similar relationship with the single-degree-of-freedom (SDOF) system. The frequency characteristics from the command signal to the realized relative velocity measured by the manufacturer are shown in Figure 2.3.

As observed in Figure 2.3, frequency response of this shaker has a nonlinearity at around the predominant frequency range of the realistic structure. Particularly, nonlinearity in the phase characteristics may cause distortion of the response. The compensation method for the shaker is discussed in Chapter 4 and 5.

2.5 Data Acquisition and D/A board

An analog-to-digital (A/D) board is installed in the PC for data acquisition and control. All of the data measurement is conducted with 100 Hz of sampling frequency. Also, the digital-to-analog (D/A) board is installed to apply the excitation signal to the DSP. The DSP can identify the start point of experiment by detecting the trigger signal (TTL level) commanded from this D/A device. The sampling frequency for D/A conversion is chosen to be 1000 Hz. Specifications of these A/D and D/A boards are shown in Table 2.8

Table 2.8: Specifications of the A/D and D/A boards

	A/D board	D/A board
Manufacturer	Contec Co. Ltd.	Contec Co. Ltd.
Model	AD12-16U(PCI)E	DA12-4
Channels	16	4
Resolution	12bit	12bit
Slot	PCI	PCI
Precision	± 3 LSB	± 3 LSB
Conversion Speed	1 μsec	10 μsec

2.6 Control System

For controlling devices of this test system, the Digital Signal Processor (D.S.P.) is utilized. By introducing the DSP, experiments could be conducted with high-speed sampling and various signal operations in real time. Specifications of the DSP is shown in Table 2.9. A 1000 Hz of sampling frequency is chosen for the real-time operation.

This DSP consists of three boards, main CPU, A/D, and D/A extension units. These boards are connected to the PC through ISA extension slots. All of the measured data necessary for the control is transferred to the DSP through A/D slots, and command voltage signal is determined in accordance with the pre-defined control strategy. Also, the anti-aliasing analog filter is assigned to the each A/D input in order to prevent the aliasing phenomenon.

As for controlling the DSP, SIMULINK and Realtime Workshop together with MATLAB Version 5.3 (Mathworks Inc.) are used. Once control process is described using SIMULINK block diagram, control systems could be rapidly implemented to the DSP by invoking the Realtime Workshop. It converts the designed SIMULINK block to the COFF executable file which is ready for DSP system. This binary file is then transferred to the DSP memory and executed. For downloading and executing the binary file for the DSP, μ-pass (Micor Signal Co. Ltd.) is used. Outline of the procedure for DSP system implementation is shown in Figure 2.4.

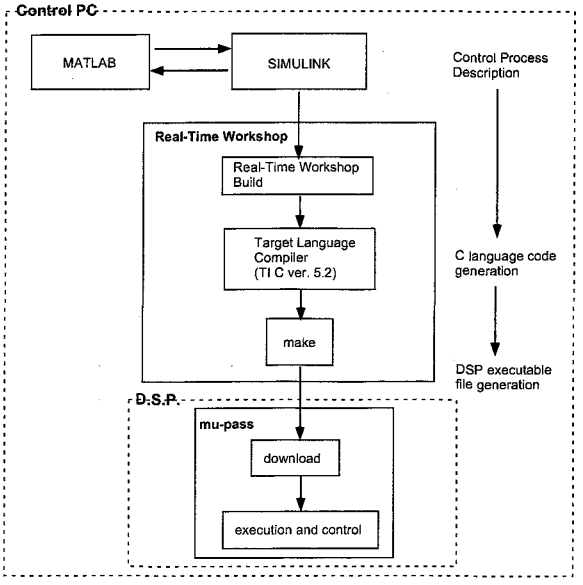

Figure 2.4: Flow of Procedure for Real-Time DSP

Table 2.9: DSP Specification

Processor	TMS320C44 304Pin QFP	
	Bus Type	ISA
	Manufacturer	Texas Instruments
	CPU Clock	50 MHz
	Operation Cycle	40 nsec
	Cache	128 / 32 bit (LRU)
	Floating Point Operation	40 bit
	Integer Operation	32bit
Memory	Local Bus	128kW / 32 bit
	Global Bus	128kW / 32bit
		128 kW / 32bit / 2
	Boot Rom	64kB/ EPROM or 32kB E^2PROM
Host Interface	Dual Port RAM through DPRAM (2K / 16bit) FIFO	
Interruption	Interactive interruption	
Extension Board	2 (2 slots for additional board per each)	
A/D conversion	Module	ADM 12-8 / 2
	Input Channels	8
	Resolution	12bit
	Conversion Time	40 usec
	Conversion Method	Simultaneous Conversion
	Input Voltage Range	± 10 V
D/A conversion	Module	DAM 16-4
	Output Channels	4
	Resolution	16bit
	Conversion Time	9 usec
	Conversion Method	Simultaneous Conversion
	Input Voltage Range	± 10 V

2.7 Hydraulic Actuator

Other than facilities for the IFDL system, hydraulic actuator is also utilized for the loading tests of the damper specimen. Schematic view is shown in Photo 2.5. Frequency characteristics and specification are shown in Figure 2.5 and Table 2.10 respectively. The actuator can be driven under both stroke and load control modes. By utilizing the stroke control mode, the accurate force versus displacement as well as force versus velocity relations can be obtained. Since it is relatively difficult for the IFDL test system to generate the designated displacement, this facility is utilized for the constant-stroke periodical loading tests for composing the dynamic model of the damper specimen.

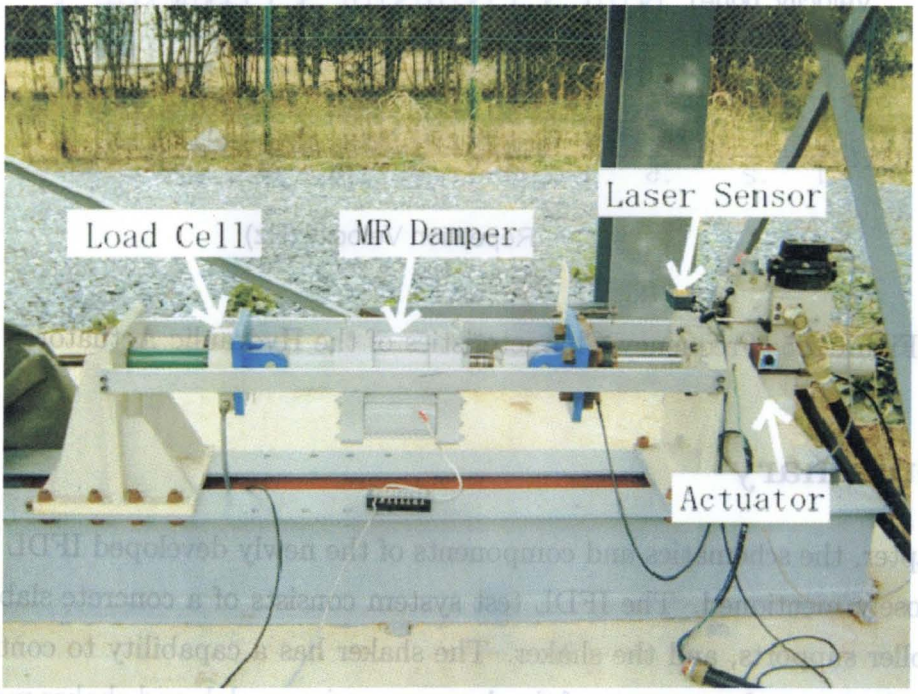

Photo 2.5: Photo of the Actuator Loading System

Table 2.10: Specifications of the Actuator

Type	Hydraulic Servo Actuator
Servo Valve	57 ℓ/min
Maximum Stroke	$\pm$5 cm
Maximum Velocity	20 kine
Sensors	Load Cell (5 tonf), LVDT ($\pm$5 cm)

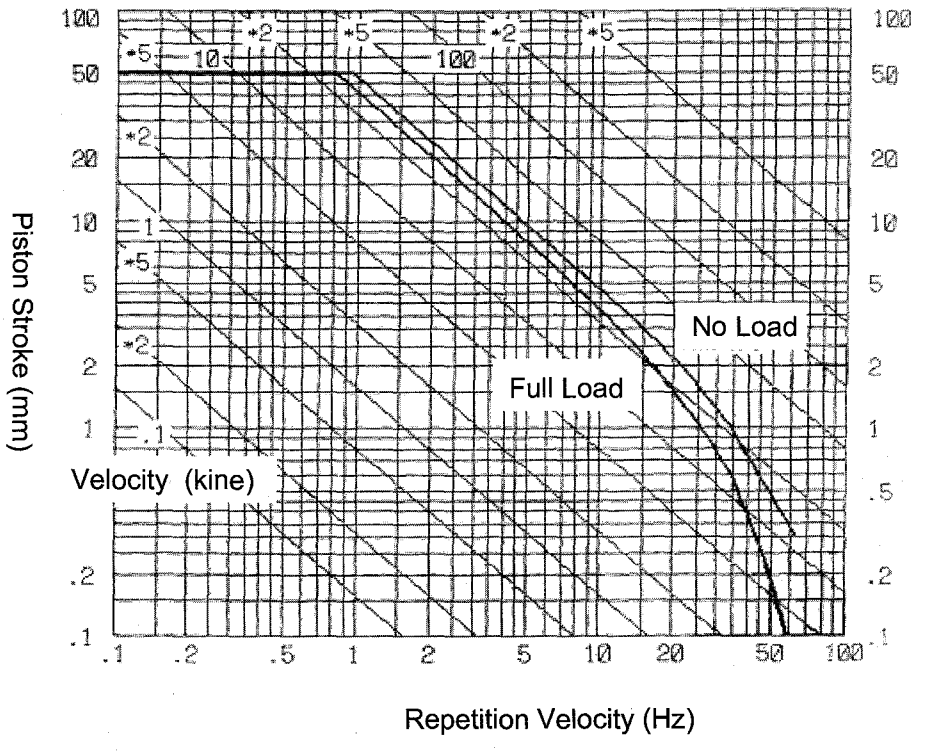

Figure 2.5: Frequency Characteristics of the Hydraulic Actuator

2.8 Summary

In this chapter, the schematics and components of the newly developed IFDL test system are closely mentioned. The IFDL test system consists of a concrete-slab, rubber bearing, roller supports, and the shaker. The shaker has a capability to control arbitrarily by referring to the response of the damper specimen, slab and shaker mass itself. These series of sensors and control equipments are utilized for the element identification tests and full-scale hybrid loading experiments.

References

(1) The MathWorks, Inc.: *Using MATLAB (Version 6)*, 2000.

(2) The MathWorks, Inc.: *Signal Processing Toolbox (Version 5)*, 2000.

(3) The MathWorks, Inc.: *Using Simulink (Version 4)*, 2000.

(4) The MathWorks, Inc.: *Real-Time Workshop (Version 4)*, 2000.

Chapter 3

Real-Time Substructure Hybrid Experiment Development

3.1 General Remarks

One of the main objectives of the IFDL system is to utilize as the real-time substructure hybrid experiment facility. The term 'substructure hybrid' refers to the unique experimental technique that combines the structural response calculation and device loading experiment in real time in order to obtain the response of the assumed structure with nonlinear devices. By introducing this technique, dynamic interaction between structure and device can be clarified without composing a nonlinear model of the device.

In this chapter, a shaker control method is introduced in order to realize the real-time hybrid experiment system with using the IFDL. Simplified SDOF model is used for formulating the control strategy. Effect of the phase delay between command and realization of the shaker force is also discussed.

3.2 Schematics of the Hybrid Experiment

In general, hybrid loading experiments are conducted by solving the following equation of motion step-by-step[1)],

$$[M]\ddot{x}_n + [C]\dot{x}_n + [K]x_n + F_n^{\mathrm{EXP}} = \{P\}_n \tag{3.1}$$

where,

$[M]$: mass matrix ;
$[C]$: damping matrix ;
$[K]$: stiffness matrix ;
$\ddot{x}_n$, $\dot{x}_n$, x_n : structural acceleration, velocity and displacement ;
F_n^{EXP} : device reaction force obtained from loading experiment ; and
$\{P\}_n$: external force.
Also, subscript n expresses the response at step n.

The basic concept of the substructure hybrid loading experiment is to obtain the behavior of the test specimen through loading experiment, while calculating the structural response under assumed external force and measured force. It is derived from Eq.(3.1) that loading experiment and calculation should be carried out simultaneously in real time in order for obtained results to be consistent with the equation of motion of the assumed structure.

In many cases, however, the factor of loading velocity is not taken into consideration because of the limitations of the loading facilities. Particularly, the test methods that statically apply the required stroke to the test specimen have been widely adopted for the devices which characteristics are assumed to depend only on path of displacement. Such methods are called "Pseudo-Dynamic Hybrid Experiment". On the contrary, the test system that conducts loading experiment and calculation in real time is called "Real-Time Hybrid Experiment". For test specimens with velocity-dependent characteristics, such as viscous damper or friction damper, it is appropriate to conduct real-time hybrid experiments to comprehend the dynamics.

In the IFDL system, clear contrast to the actuator loading systems, the inertia force of the shaker is indirectly transferred to the test specimen. Hence, it is relatively difficult to adjust the response magnitude to the designated values. The experiment process and shaker control method should be figured out that are suitable for the IFDL system to conduct the substructure hybrid experiment.

3.3 Hybrid Experiment System Development for the IFDL

Figure 3.1 shows the schematics of the proposed real-time hybrid loading experiment system with using the IFDL system. As shown in this figure, hybrid loading experiment for the IFDL system consists of the following step-by-step procedures:

1. At step n, solve equation of motion regarding assumed structure with currently measured reaction force and assumed ground motion

2. Pick up displacement, velocity, and acceleration at the assumed damper location

3. Calculate the next step command signal for the shaker using the calculated responses

4. Command the shaker in order for the IFDL slab to generate the designated responses

5. Measure reaction force of the test specimen

6. Solve equation of motion regarding assumed structure using measured reaction force and assumed ground motion

7. Back to 1.

It is then obvious that the key to the precise experiment is how to command the shaker so as to realize the designated responses of the hypothetical structure[2].

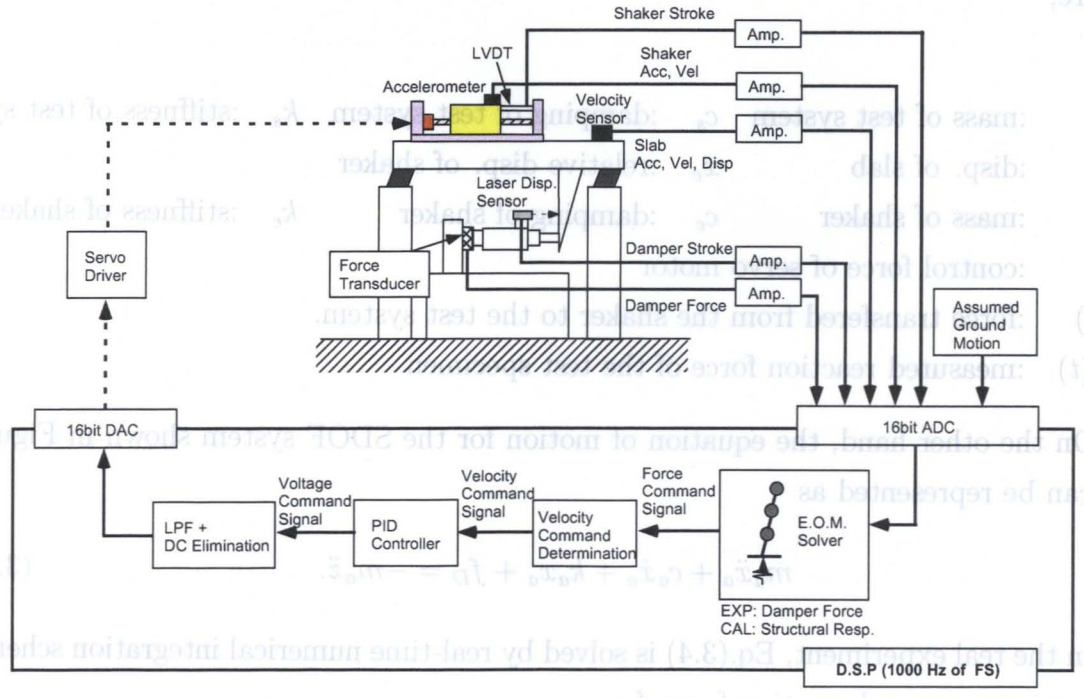

Figure 3.1: Schematics of the Hybrid Experiment using IFDL

3.4 Shaker Control Method

3.4.1 Formulation for A SDOF System

For the simplicity of formulations, a SDOF structure with the damper test specimen exposed to the earthquake ground motion is assumed as a reference structure. The model of the assumed target structure is shown in Figure 3.3. Also, the model of the IFDL system with shaker is shown in Figure 3.2. The main objective is to derive the required command control force of the shaker so as to replicate the dynamic response of the assumed structure.

By referring to Figure 3.2, equations of motions regarding the IFDL test system and shaker are described as follows

$$\begin{cases} m_s\ddot{x}_s + c_s\dot{x}_s + k_s x_s - k_e x_e - c_e x_e + f_D = -u \\ m_e(\ddot{x}_s + \ddot{x}_e) + k_e x_e + c_e \dot{x}_e = u \end{cases} \tag{3.2}$$

or equivalently,

$$\begin{cases} m_s\ddot{x}_s + c_s\dot{x}_s + k_s x_s + f_D = -f(t) \\ m_e(\ddot{x}_s + \ddot{x}_e) = f(t). \end{cases} \tag{3.3}$$

Where,

m_s	:mass of test system	c_s	:damping of test system	k_s	:stiffness of test system
x_s	:disp. of slab	x_e	:relative disp. of shaker		
m_e	:mass of shaker	c_e	:damping of shaker	k_e	:stiffness of shaker
u	:control force of servo motor				
$f(t)$	:force transfered from the shaker to the test system.				
$f_D(t)$	:measured reaction force of the test specimen				

On the other hand, the equation of motion for the SDOF system shown in Figure 3.3 can be represented as

$$m_a\ddot{x}_a + c_a\dot{x}_a + k_a x_a + f_D = -m_a\ddot{z}. \tag{3.4}$$

In the real experiment, Eq.(3.4) is solved by real-time numerical integration scheme with using measured reaction force f_D.

Now, the primary consideration is how to determine the shaker control force $f(t)$ so as for the IFDL system to replicate the designated response $x_a, \dot{x}_a$, and $\ddot{x}_a$.

It follows that the control force is determined so as to meet the following situations.

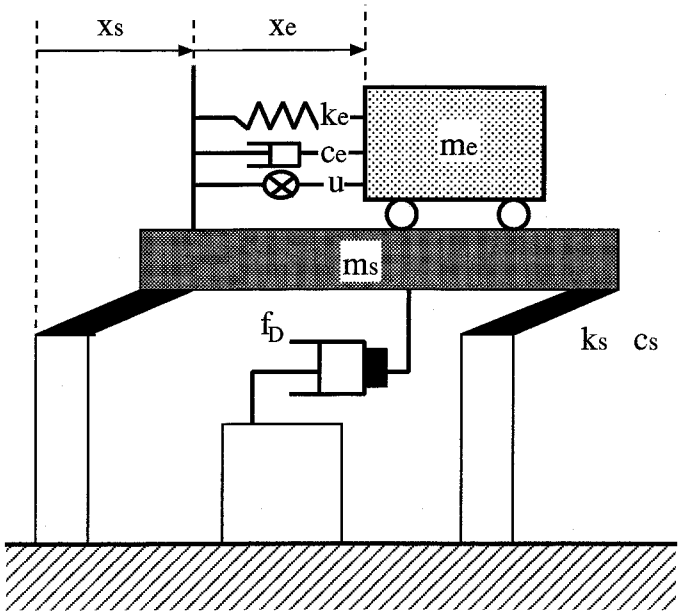

Figure 3.2: Model of the IFDL system with the Shaker

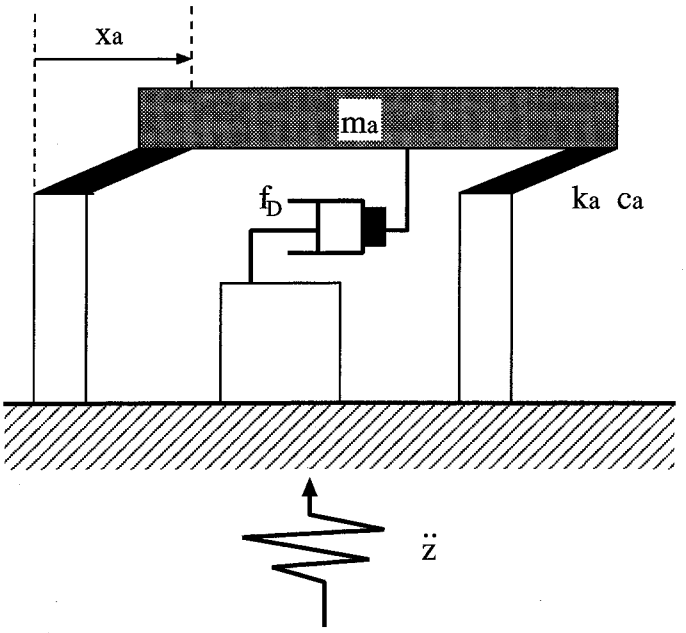

Figure 3.3: Hypothetical SDOF Structure Subjected to the Ground Motion

$$x_s(t) = x_a(t)$$
$$\dot{x}_s(t) = \dot{x}_a(t)$$
$$\ddot{x}_s(t) = \ddot{x}_a(t)$$

Here, attentions should be paid to the two facts; 1) $f(t)$ can be determined arbitrarily 2) both Eqs.(3.3) and (3.4) share the same measured reaction force $f_D(t)$ at the same time. It consequently follows that shaker force $f(t)$ should be given as follows,

$$f(t) = -m_s\ddot{x}_a - c_s\dot{x}_a - k_s x_a - f_D \tag{3.5}$$

or equivalently,

$$f(t) = -m_s(\ddot{x}_a + 2h_s\omega_s\dot{x}_a + \omega_s^2 x_a) - f_D. \tag{3.6}$$

Where, h_s and ω_s are the damping ratio and natural angular frequency of the test system, respectively.

3.4.2 Calculation of Velocity Command Signal

As mentioned in Chapter 2, relative velocity of the mass of the shaker is the only controllable parameter, Eq.(3.6) should be altered to the velocity representation. By substituting Eq.(3.6) into Eq.(3.3), the shaker relative acceleration that realize the given control force f(t) can be represented as follows.

$$\ddot{x}_e = -\ddot{x}_s - \frac{m_s}{m_e}\left(\ddot{x}_a + 2h_s\omega_s\dot{x}_a + \omega_s^2 x_a + \frac{f_D}{m_s}\right) \tag{3.7}$$

Consequently, relative velocity command at time τ can be obtained by taking the integration of Eq. (3.7) under zero initial condition.

$$\dot{x}_e(\tau) = \int_0^\tau \left\{-\ddot{x}_s - \frac{m_s}{m_e}\left(\ddot{x}_a + 2h_s\omega_s\dot{x}_a + \omega_s^2 x_a + \frac{f_D}{m_s}\right)\right\} dt \tag{3.8}$$

3.4.3 Discretized Form

From the experimental implementation point of view, it is convenient to alter Eq.(3.7) to the discretized form.

Consider the n th time step, and derive the shaker command velocity at this step. Eq.(3.7) can be also expressed in a discretized manner as follows.

$$\ddot{x}_e(n) = \frac{\dot{x}_e(n) - \dot{x}_e(n-1)}{\Delta t}$$

$$= -\ddot{x}_s(n) - \frac{m_s}{m_e}\left(\ddot{x}_a(n) + 2h_s\omega_s\dot{x}_a(n) + \omega_s^2 x_a(n) + \frac{f_D(n)}{m_s}\right) \tag{3.9}$$

Where, Δt is a sampling time. This form, however, can not be directly implemented to the test system due to the causality. Acceleration of the slab $\ddot{x}_s$ and damper reaction force f_D at time step n can not be obtained prior to this shaker velocity determination procedure. In order to overcome this problem, $\ddot{x}_s(n)$ and $f_D(n)$ are substituted by the previous responses, $\ddot{x}_s(n-1)$ and $f_D(n-1)$. This assumption could be effective when Δt is substantially small.

Consequently, shaker velocity command signal at time step n is obtained as,

$$\dot{x}_e(n) = \dot{x}_e(n-1) - \Delta t\left\{\ddot{x}_s(n-1) + \frac{m_s}{m_e}\left(\ddot{x}_a(n) + 2h_s\omega_s\dot{x}_a(n) + \omega_s^2 x_a(n) + \frac{f_D(n-1)}{m_s}\right)\right\}. \tag{3.10}$$

Due to the assumption, at least Δt of force transfer time delay is unavoidable.

3.4.4 Application to the MDOF Structure

It should be noted that the proposed method for the SDOF system is ready to be applied to the MDOF structure tests without any modifications. Based on Eq.(3.6), only displacement, velocity and acceleration at the assumed damper location as well as the damper force are needed for determining the shaker control force. In other words, various types of structures can be assumed as the hypothetical system. Figure 3.4 shows the schematic flow of the MDOF substructure hybrid experiment in which the proposed shaker control method is utilized. As shown in this figure, only the responses at the damper location should be replicated by the IFDL test system, regardless of the properties of the assumed structure itself.

3.5 Effect of Time Delay

In the previous discussion, it is assumed that control force generated by the shaker is transferred to the slab and test specimen without any time delay. However, it is obvious that this situation is far from real cases. Many studies regarding hybrid experiments have pointed out that the existence of the time delay in force transfer might cause unacceptable distortions of the obtained results. In this section, the effect of the time delay in shaker force transmission on the response of the IFDL system is examined.

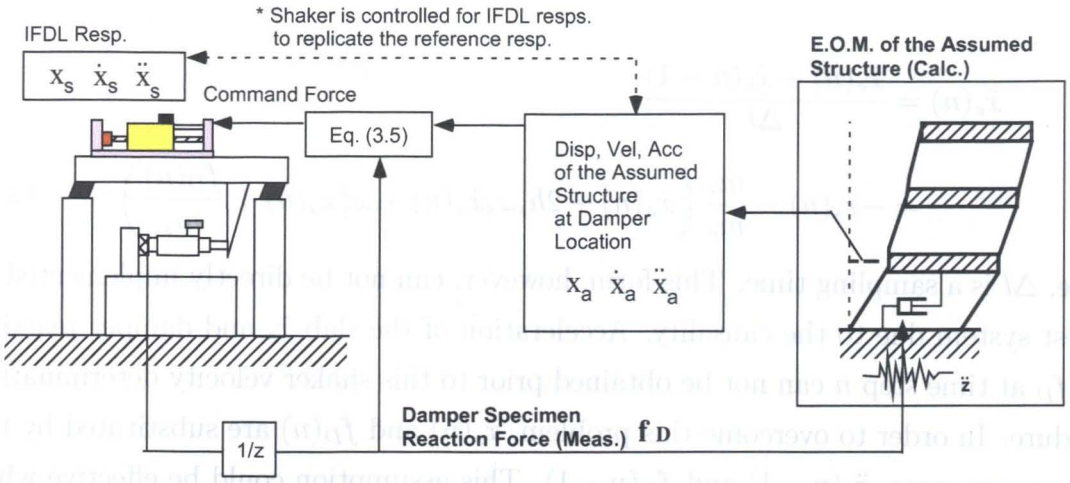

Figure 3.4: Schematics of the MDOF Hybrid Experiment using the IFDL

Suppose the case that the command control force $f(t)$ is transmitted to the slab with a constant δt of time delay. This assumption implies that the time delay is independent from the excitation frequency. The effect of this time delay is inspected by deriving the transfer function from the command force to the displacement response of the test specimen. In the formulation, idealized linear viscous damper is chosen as the model of the test specimen. Also, a unit impulse motion is assumed as ground input.

The equation of motion as to IFDL system with δt of time delay can be written by follows.

$$m_s\ddot{x}_s + c_s\dot{x}_s + k_s x_s + C_D\dot{x}_s + f(t-\delta t) = 0 \tag{3.11}$$

Here, C_D is the damping coefficient for the assumed linear viscous damper specimen.

Applying the Laplace transform of Eq. (3.11) yields

$$(m_s s^2 + c_s s + k_s)X_s(s) + C_D s X_s(s) + e^{-s\delta t}F(s) = 0 \tag{3.12}$$

where, $X_s(s)$ and $F(s)$ are the Laplace transform of the slab displacement $x_s(t)$ and the control force $f(t)$, respectively.

On the other hand, Laplace transform of the displacement response of the assumed SDOF structure $x_a(t)$ under unit impulse ground motion and zero initial condition can be written from Eq.(3.4) as

$$X_a(s) = \frac{-m_a - C_D s X_s(s)}{m_a s^2 + c_a s + k_a}. \tag{3.13}$$

Also, by referring to Eq. (3.6) and Eq. (3.13), the Laplace transform of the shaker

control force $f(t)$ can be obtained as

$$\begin{aligned} F(s) &= (-m_s s^2 - c_s s - k_s)X_a(s) - C_D s X_s(s) \\ &= \frac{(m_s s^2 + c_s s + k_s)}{(m_a s^2 + c_a s + k_a)}(m_a + C_D s X_s(s)) - C_D s X_s(s) \\ &= \frac{B(s)}{A(s)} m_a + C_D s \left(\frac{B(s)}{A(s)} - 1\right) X_s(s) \end{aligned} \tag{3.14}$$

where,

$$\begin{aligned} A(s) &= m_a s^2 + c_a s + k_a \\ B(s) &= m_s s^2 + c_s s + k_s \,. \end{aligned}$$

Substituting Eq.(3.14) to Eq.(3.12) yields,

$$(B(s) + C_D s)X_s(s) + e^{-s\delta t}\left(\frac{B(s)}{A(s)} m_a + C_D s X_s(s)\left(\frac{B(s)}{A(s)} - 1\right)\right) = 0\,. \tag{3.15}$$

Solving this equation regarding $X_s(s)$ gives

$$\left(A(s)B(s) + A(s)C_D s + e^{-s\delta t}(B(s) - A(s))C_D s\right) X_s(s) = -B(s) m_a e^{-s\delta t}. \tag{3.16}$$

Consequently, transfer function $H_{s(w/)}(s)$ from assumed impulse ground motion to the slab displacement $X_s(s)$ with δt of force transmission time delay is obtained as follows.

$$H_{s(w/)}(s) = \frac{-m_a}{A(s)e^{s\delta t} + \left(\frac{A(s)}{B(s)} e^{s\delta t} + \left(1 - \frac{A(s)}{B(s)}\right)\right) C_D s} \tag{3.17}$$

On the other hand, corresponding transfer function without time delay is easily obtained by substituting $\delta t = 0$ into Eq.(3.17), which is,

$$H_{s(w/o)}(s) = \frac{-m_a}{A(s) + C_D s}. \tag{3.18}$$

In order to illustrate the effect of time delay, following transfer function ratio is introduced.

$$Hr(s) = \frac{H_{s(w/o)}}{H_{s(w/)}} \tag{3.19}$$

Here, Maclaurin series expansion is applied to the $e^{s\delta t}$, which is

$$e^{s\delta t} \approx 1 + s\delta t. \tag{3.20}$$

Terms higher than 2nd order are assumed to be substantially small enough to be neglected. Then, Eq.(3.19) can be approximated as follows.

$$Hr(s) \approx 1 + \frac{A(s)(B(s) + C_D s)s}{B(s)(C_D s + A(s))}\delta t \tag{3.21}$$

$$= 1 + s\delta t \left\{ \frac{(s^2 + 2h_s\zeta\gamma\omega_s s + \gamma^2\omega_s^2)\left(s^2 + 2h_s\omega_s s + \omega_s^2 + \dfrac{C_D s}{m_s}\right)}{(s^2 + 2h_s\omega_s s + \omega_s^2)\left(s^2 + 2h_s\zeta\gamma\omega_s s + \gamma^2\omega_s^2 + \dfrac{C_D s}{m_s}\dfrac{1}{\alpha}\right)} \right\} \tag{3.22}$$

Where,

$$\gamma = \frac{\omega_a}{\omega_s} \ , \ \alpha = \frac{m_a}{m_s} \ , \ \zeta = \frac{h_a}{h_s} = \alpha\gamma\frac{c_a}{c_s}.$$

This transfer function ratio consists of the combination of the (transfer function without time delay) plus (fluctuation caused by the time delay) under the case that δt is substantially small. From Eq.(3.22), several effects are estimated;

- Error propagates in accordance with the increase of the time delay δt
- Transfer function is distorted at the natural frequency of the test system.
- Overall power in frequency domain is distorted as δt is getting larger

However, if the damping ratio of the assumed structure is zero, this existing time delay does not affect the resonance response of the assumed structure since second term of Eq.(3.22) disappears at the frequency $s = i\omega_a$.

In order to illustrate the contribution of the time delay, a SDOF simulation is conducted. In the simulation, following hypothetical parameters are used.

- $\gamma = 1.8182$ ($\omega_a = 2\pi \cdot 1$ (rad/sec))
- $\alpha = 20$ ($m_a = 248.53$ton)
- $\zeta = 0$
- $C_D = 200$ (kN/m/sec)

Figures 3.5, 3.6, and 3.7 show transfer functions from unit impulse ground motion to the displacement, velocity, and acceleration responses with various time delay. As observed from these figures, frequency response is distorted at around the natural frequency of the IFDL test system. It is found from results that the predominant natural frequency of the hypothetical structure should not be close to that of the test system in order to avoid the influence of the time delay to the experimental results.

Also, time and frequency responses are calculated for the same SDOF structure. As ground acceleration motion, constant 10 gal of the sweep wave, which has from 0.1 Hz to 5.0 Hz of the frequency component, is selected. Time delays of 0, 0.05, and 0.1 seconds are given as the shaker force transmission delays. Figure 3.8 shows the comparison of the displacement, velocity, acceleration, and damper force with the change of the delay times. Corresponding Fourier spectra are depicted in Figure 3.9. For reference, results of the simulation under ground excitation are also depicted, these are denoted as 'Original'. The comparison of the shaker relative velocity, acceleration, and motor control force are shown in Figure 3.10.

As clearly observed from the time histories with regard to the structure and the shaker, maximum responses are gradually diminished as time delay becomes larger. Horiuchi *et al.* pointed out that the existence of the time delay might increase the apparent damping of the system[3, 4]. The same phenomena can be estimated in this test system. In the frequency responses, algebraically estimated magnification effects are observed at around the natural frequency of the test system.

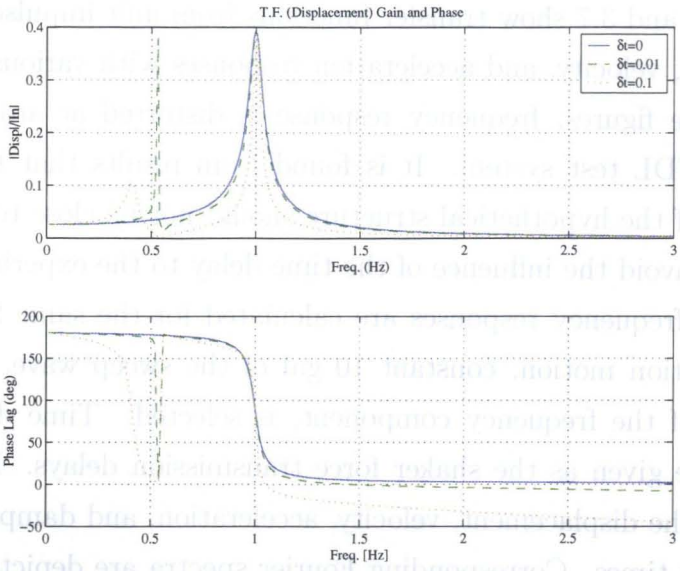

Figure 3.5: Effects of Time Delay on Displacement Transfer Functions

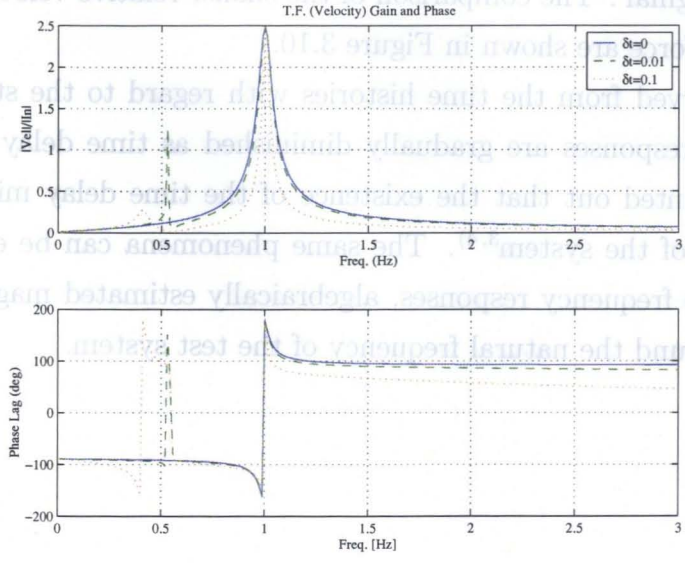

Figure 3.6: Effects of Time Delay on Velocity Transfer Functions

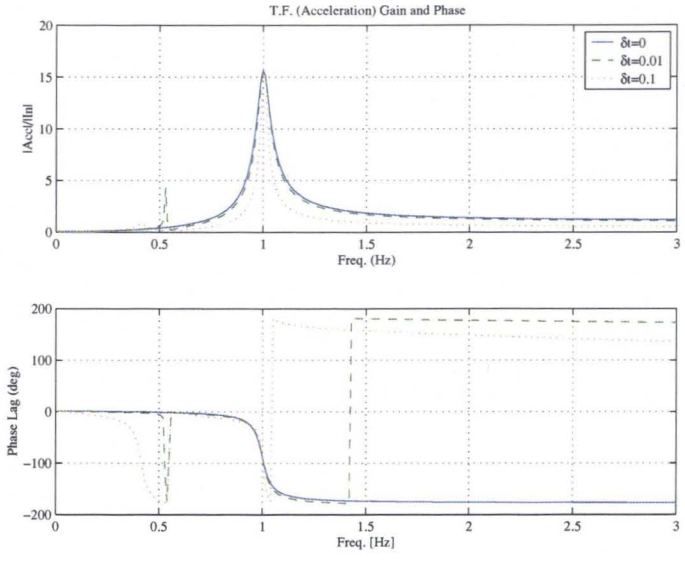

Figure 3.7: Effects of Time Delay on Acceleration Transfer Functions

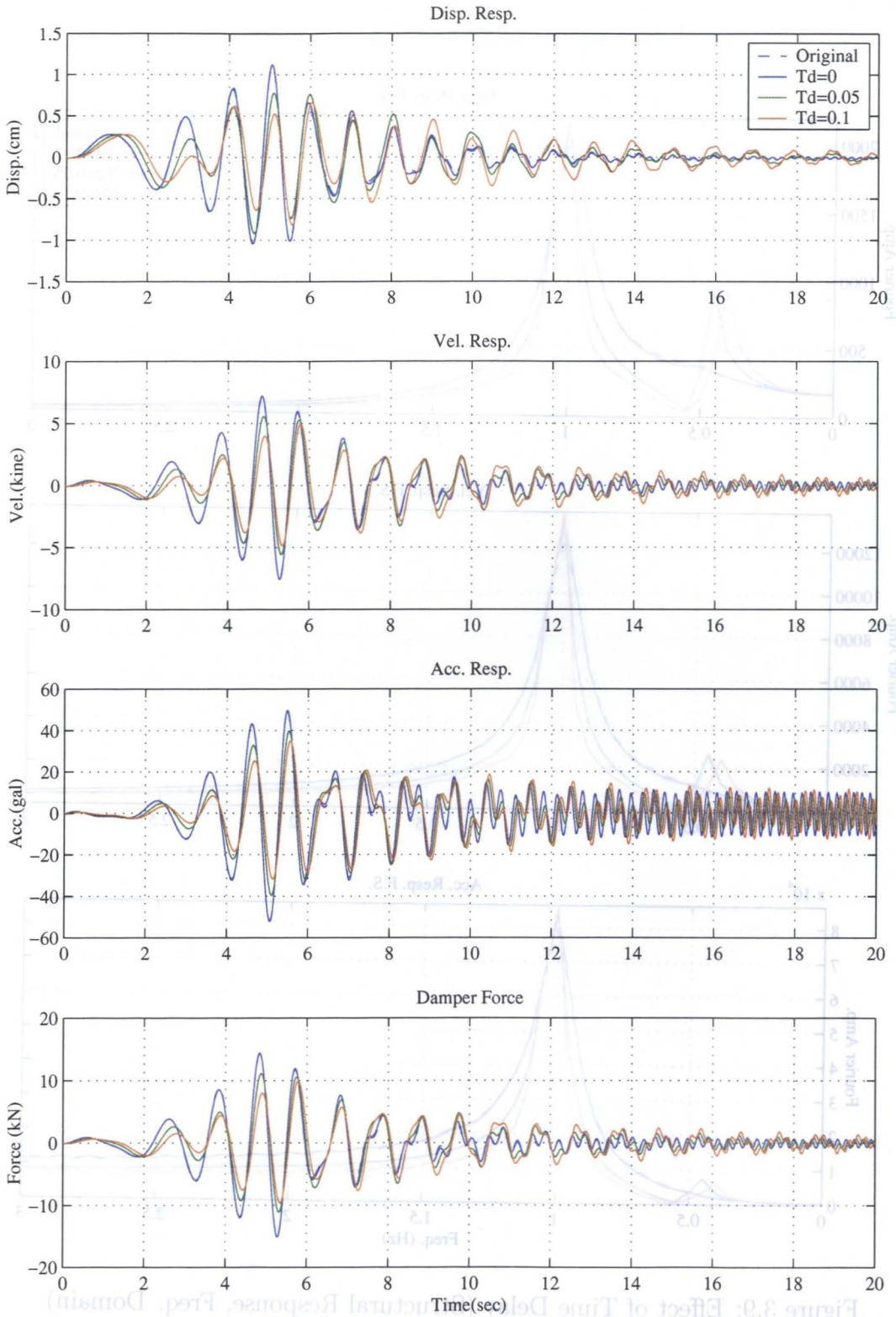

Figure 3.8: Effect of Time Delay (Structural Response, Time Domain)

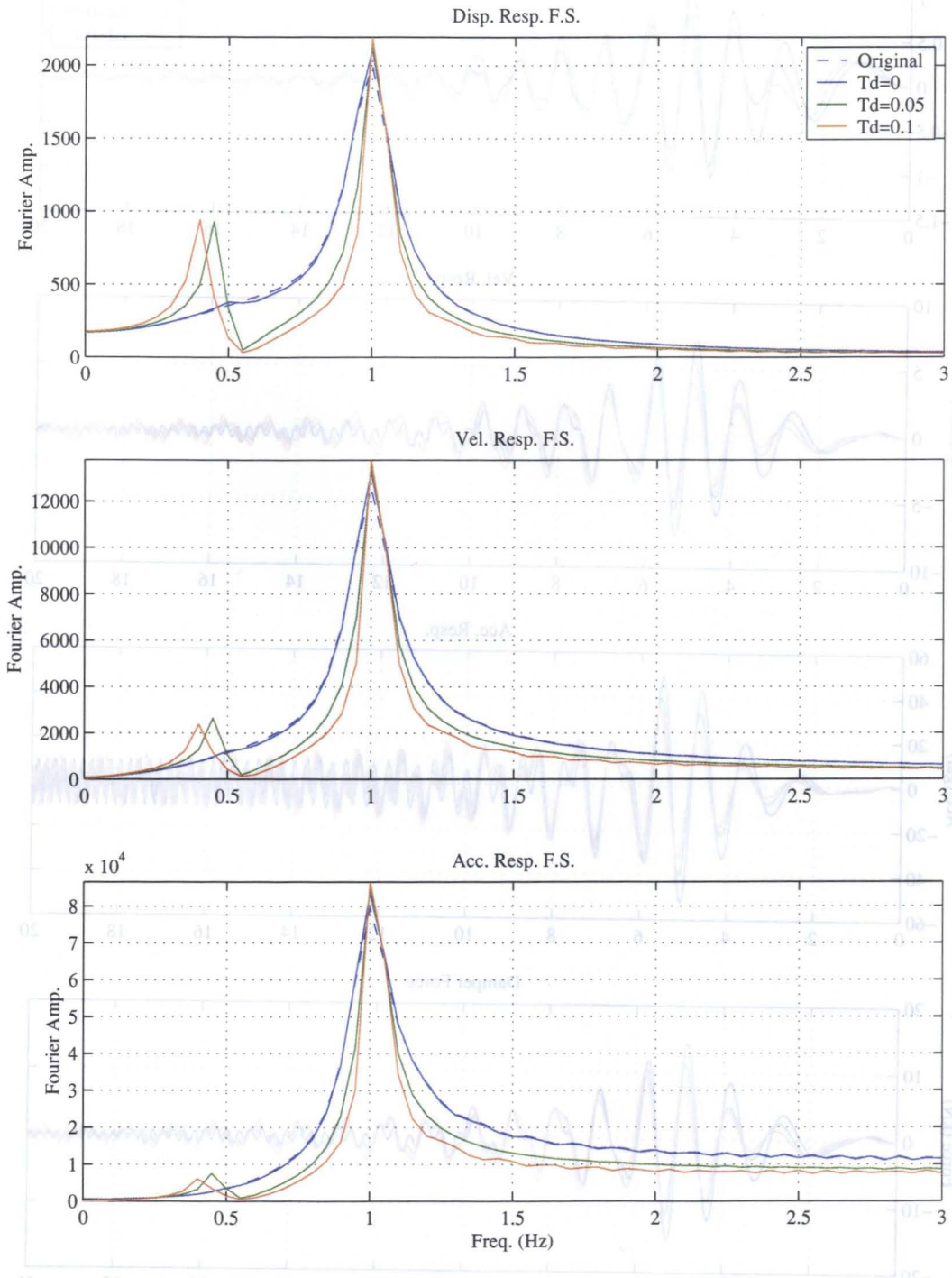

Figure 3.9: Effect of Time Delay (Structural Response, Freq. Domain)

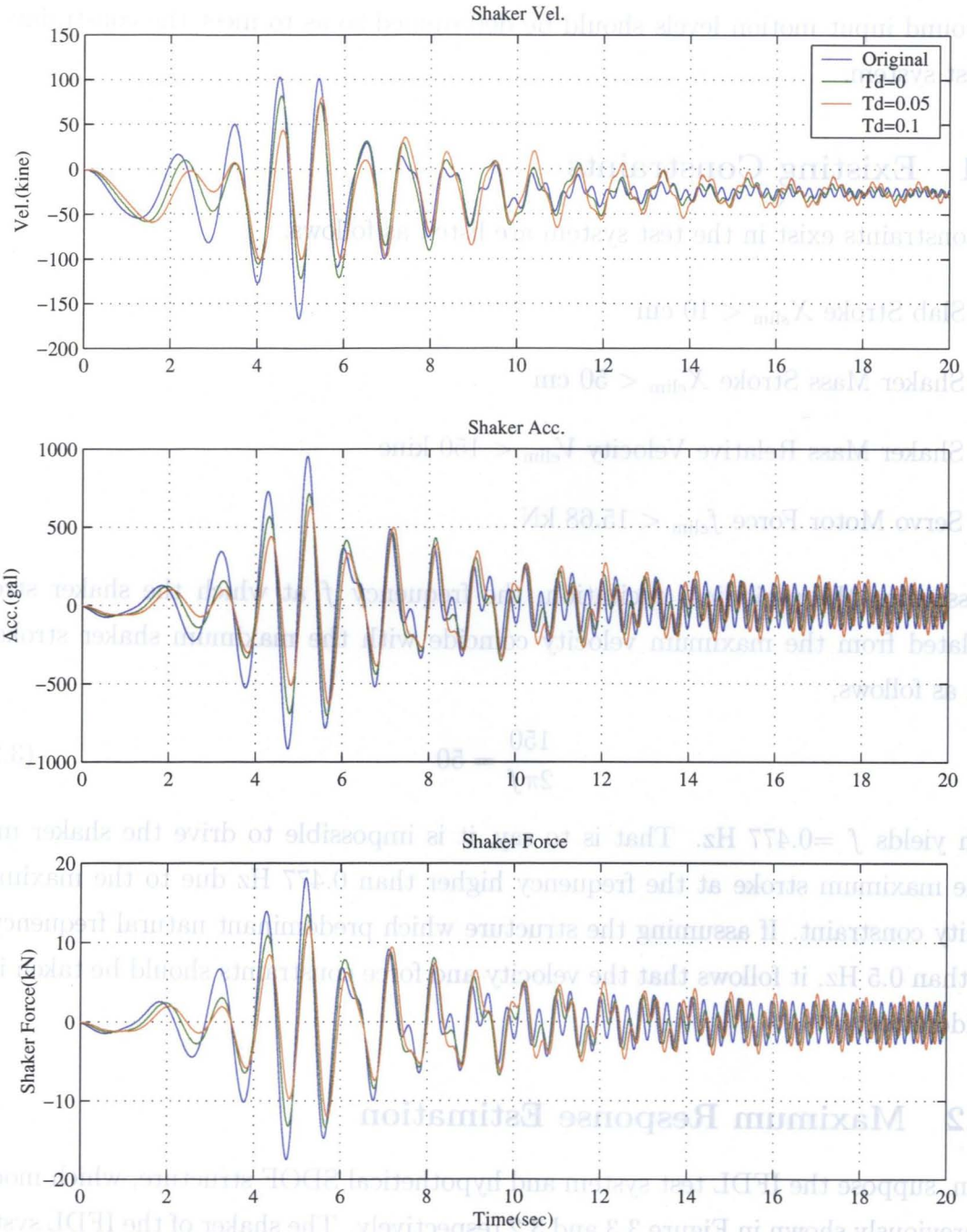

Figure 3.10: Effect of Time Delay (Shaker Response)

3.6 Feasible Capacity of the Test System

The feasible properties of the hypothetical structures for the substructure hybrid experiments are discussed herein. The dynamic properties of the assumed structure and the ground input motion levels should be determined so as to meet the constraints of the test system.

3.6.1 Existing Constraints

The constraints exist in the test system are listed as follows.

- Slab Stroke $X_{slim} < 10$ cm
- Shaker Mass Stroke $X_{elim} < 50$ cm
- Shaker Mass Relative Velocity $V_{elim} < 150$ kine
- Servo Motor Force $f_{elim} < 15.68$ kN

Assuming the periodical excitation, the frequency f at which the shaker stroke calculated from the maximum velocity coincide with the maximum shaker stroke is given as follows,

$$\frac{150}{2\pi f} = 50 \tag{3.23}$$

which yields f =0.477 Hz. That is to say, it is impossible to drive the shaker mass to the maximum stroke at the frequency higher than 0.477 Hz due to the maximum velocity constraint. If assuming the structure which predominant natural frequency is over than 0.5 Hz, it follows that the velocity and force constraints should be taken into consideration.

3.6.2 Maximum Response Estimation

Again, suppose the IFDL test system and hypothetical SDOF structure, which models are previously shown in Figure 3.3 and 3.2 respectively. The shaker of the IFDL system is controlled so as to duplicate the dynamic responses of the SDOF structure, which is exposed to the periodical ground motion.

The objective here is to algebraically derive the maximum steady-state responses of the shaker relative velocity, shaker control force, and slab displacement. These results give the principal information for determining the hypothetical structures and ground motion level in experiments. For simplicity of discussions, it is assumed that a linear

idealized viscous damper is used as the damper test specimen. Also, damping element of the hypothetical structure is neglected.

As shown previously, the equation of motion regarding the IFDL test system and hypothetical SDOF system under periodical earthquake are given as

$$\begin{cases} m_s\ddot{x}_s + c_s\dot{x}_s + k_s x_s + C_D\dot{x}_s + f(t) = 0 \\ m_e(\ddot{x}_s + \ddot{x}_e) = f(t) \end{cases} \tag{3.24}$$

and

$$m_a\ddot{x}_a + C_D\dot{x}_a + k_a x_a = -m_a a e^{i\omega t}. \tag{3.25}$$

Where, ω and a are the excitation frequency and amplitude of the ground motion. From Eq.(3.25), displacement of the SDOF structure can be expressed as follows.

$$\begin{aligned} x_a(t) = \phi e^{i\omega t} &= \frac{-m_a a}{k_a - m_a\omega^2 + C_D i\omega} e^{i\omega t} \\ &= \frac{-a}{\left(\omega_a^2 - \omega^2 + \dfrac{C_D i\omega}{m_a}\right)} e^{i\omega t} \end{aligned} \tag{3.26}$$

The shaker control force $f(t)$ is then given by substituting Eq.(3.26) into Eq.(3.6), which is

$$\begin{aligned} f(t) &= \left\{-k_s - (c_s + C_D)i\omega + m_s\omega^2\right\} \cdot \frac{-a}{\left(\omega_a^2 - \omega^2 + \dfrac{C_D i\omega}{m_a}\right)} e^{i\omega t} \\ &= m_s\left\{\omega_s^2 - \omega^2 + \frac{(c_s + C_D)\, i\omega}{m_s}\right\} \cdot \frac{a}{\left(\omega_a^2 - \omega^2 + \dfrac{C_D i\omega}{m_a}\right)} e^{i\omega t}. \end{aligned} \tag{3.27}$$

Also, corresponding shaker relative acceleration and relative velocity are obtained as follows.

$$\begin{aligned} \ddot{x}_e(t) &= \frac{f(t)}{m_e} - \ddot{x}_s(t) \\ &= \frac{a}{\left(\omega_a^2 - \omega^2 + \dfrac{C_D i\omega}{m_a}\right)} \left\{\frac{m_s}{m_e}\left(\omega_s^2 - \omega^2 + \frac{(c_s + C_D)i\omega}{m_s}\right) - \omega^2\right\} e^{i\omega t} \end{aligned} \tag{3.28}$$

$$\dot{x}_e(t) = \frac{\ddot{x}_e(t)}{i\omega} \tag{3.29}$$

Here, following parameters are introduced in order to obtain the generalized formula.

$$\beta = \frac{\omega_s}{\omega} \ , \ \gamma = \frac{\omega_a}{\omega_s} \ , \ \alpha = \frac{m_a}{m_s}$$

Eqs.(3.26), (3.27), (3.28), and (3.29) can be rewritten as follows.

$$x_a(t) = \frac{-a}{\omega_s^2\left(\gamma^2 - \frac{1}{\beta^2} + \frac{C_D i}{\alpha m_s \omega_s \beta}\right)} e^{i\omega t} \tag{3.30}$$

$$f(t) = \frac{m_s a}{\left(\gamma^2 - \frac{1}{\beta^2} + \frac{C_D i}{\alpha m_s \omega_s \beta}\right)} \left\{1 - \frac{1}{\beta^2} + \frac{(c_s + C_D)i}{m_s \omega_s \beta}\right\} e^{i\omega t} \tag{3.31}$$

$$\ddot{x}_e(t) = \frac{a}{\left(\gamma^2 - \frac{1}{\beta^2} + \frac{C_D i}{\alpha m_s \omega_s \beta}\right)} \left\{\frac{m_s}{m_e}\left(1 - \frac{1}{\beta^2} + \frac{(c_s + C_D)i}{\beta m_s \omega_s}\right) - \frac{1}{\beta^2}\right\} e^{i\omega t} \tag{3.32}$$

$$\dot{x}_e(t) = \frac{a\beta}{i\omega_s\left(\gamma^2 - \frac{1}{\beta^2} + \frac{C_D i}{\alpha m_s \omega_s \beta}\right)} \left\{\frac{m_s}{m_e}\left(1 - \frac{1}{\beta^2} + \frac{(c_s + C_D)i}{\beta m_s \omega_s}\right) - \frac{1}{\beta^2}\right\} e^{i\omega t} \tag{3.33}$$

Assume the case that the frequency of the ground motion corresponds to the natural frequency of the hypothetical SDOF structure, that is $\beta = 1/\gamma$. Then, maximum amplitudes of the slab displacement, shaker control force, shaker relative acceleration, and shaker relative velocity at steady-state are given as,

$$|x_a(t)| = \frac{\alpha m_s a}{C_D \gamma \omega_s} \tag{3.34}$$

$$|f(t)| = \frac{\omega_s \alpha m_s^2 a}{C_D} \sqrt{\left(\frac{(c_s + C_D)}{m_s \omega_s}\right)^2 + \left(\gamma - \frac{1}{\gamma}\right)^2} \tag{3.35}$$

$$|\ddot{x}_e(t)| = \frac{a\alpha m_s \omega_s}{m_e C_D} \sqrt{\left(\frac{(c_s + C_D)}{\omega_s}\right)^2 + \left(m_s\left(\gamma - \frac{1}{\gamma}\right) + m_e \gamma\right)^2} \tag{3.36}$$

$$|\dot{x}_e(t)| = \frac{a\alpha m_s}{m_e C_D} \sqrt{\left(\frac{(c_s + C_D)}{\gamma \omega_s}\right)^2 + \left(m_s\left(1 - \frac{1}{\gamma^2}\right) + m_e\right)^2}. \tag{3.37}$$

It should be noted that the maximum ground motion level as well as hypothetical structural parameters should be determined so as to satisfy the following simultaneous inequality,

$$\begin{cases} |x_a(t)| & < X_{slim}(= 10\,\mathrm{cm}) \\ |f(t)| & < f_{elim}(= 15.68\,\mathrm{kN}) \\ |\dot{x}_e(t)| & < V_{elim}(= 150\,\mathrm{kine}) \end{cases}$$

Since mass ratio α as well as ground motion level a linearly affect the responses, effect of the natural frequency ratio γ is examined herein. For this purpose, following maximum response ratios are introduced.

$$\begin{aligned} R_{x_a} &= |x_a(t)| \,/\, |x_a(t)|_{base} \\ R_f &= |f(t)| \,/\, |f(t)|_{base} \\ R_{\ddot{x}_e} &= |\ddot{x}_e(t)| \,/\, |\ddot{x}_e(t)|_{base} \\ R_{\dot{x}_e} &= |\dot{x}_e(t)| \,/\, |\dot{x}_e(t)|_{base} \end{aligned}$$

Where, subscript $_{base}$ indicates the response of the hypothetical structure in which mass ratio is α, ground level is a, but $\gamma = 1$, i.e. dynamics of the assumed structure coincide with those of the IFDL test system. Figure 3.11 shows the change of these indices with various natural frequency ratio γ. For damping coefficient of the specimen, $C_D = 200$ (kN/m/sec) is used.

As seen in the figure, the acceleration and the control force grow up almost linearly as the natural frequency ratio increases, while the velocity of the shaker closes to the constant value asymptotically. It consequently follows that the major concern on determining the hypothetical structure and ground motion level is the constraint of the shaker control force.

It is also found that the natural frequency of the hypothetical structure should be closer to that of the test system in order to generate the large displacement. In this case, effect of the time delay should be taken into consideration, as seen in previous section. On the contrary, a powerful servo motor is required if conducting the hybrid experiment in which the natural frequency of the hypothetical structure is larger than that of the IFDL test system.

In the real experiment, it is required to carry out preliminary numerical simulations using damper specimen model in order to determine the hypothetical structures and ground motion level. The details of determining the test conditions for several structures and earthquakes will be discussed in Chapter 5.

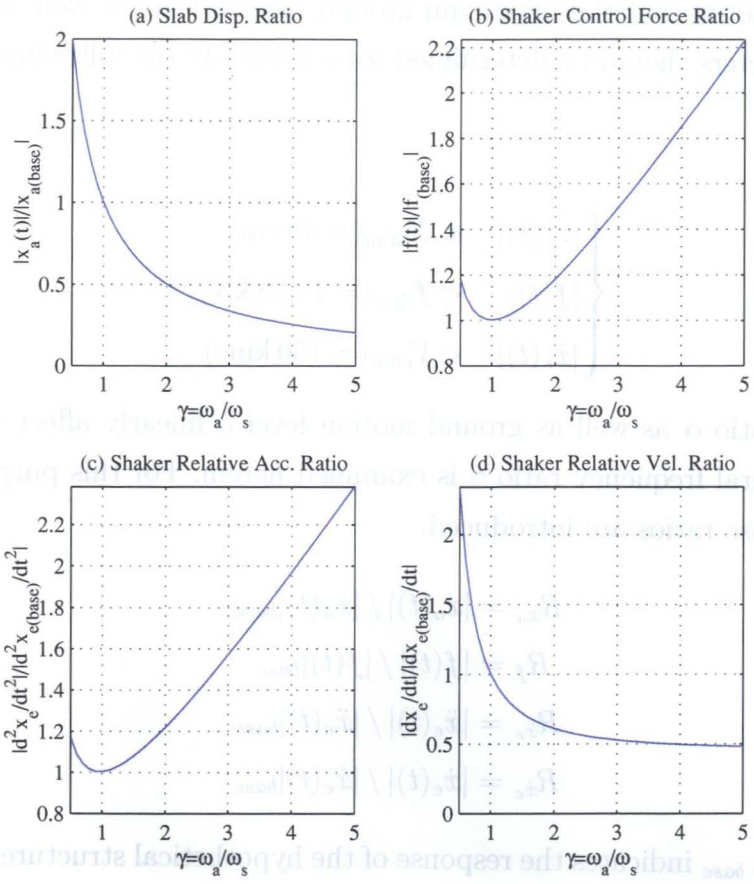

Figure 3.11: Maximum Response Ratios Based on Original Test System

3.7 Summary

In this chapter, a shaker control method for the IFDL test system is proposed, by which the real time hybrid experiment could be realized. In the proposed method, relative velocity of the shaker mass is controlled in real time so as for the IFDL test system response with damper specimen to be consistent with those at the assumed damper location of the hypothetical structure.

The effect of the time delay existing in force transmission is examined by assuming a SDOF system subjected to the impulsive ground motion. It is found that natural frequency of the hypothetical structure should be sufficiently larger than that of the test system in order to avoid the deterioration of the experimental results caused by the time delay. Also, feasible hypothetical structural property are examined for SDOF structure so as not to surpass the physical limitations of the IFDL test system. It is found that the shaker control force capacity should be the major concern for conducting the large-scale experiments.

References

(1) Tanzo, W., Yamada, Y., and Iemura, H.: Substructured Computer-Actuator Hybrid Loading Tests for Inelastic Earthquake Response of Structures, Technical report, School of Civil Engineering, Kyoto University, 1992.

(2) Iemura, H., Igarashi, A., Toyooka, A., and Suzuki, Y.: Dynamic Loading Experiment of Passive and Semi-Active Dampers Using the Inertia-Force-Driven Loading System, *Proceedings of the 3rd World Conference on Structural Control*, 2002.

(3) Horiuchi, T., Inoue, M., Konno, T., and Yamagishi, W. : Development of a Real-Time Hybrid Experimental System Using a Shaking Table (1st Report, Proposal of Experiment Concept and Feasibility Study with Rigid Secondary System) (in Japanese), *Journal of the Japan Society of Mechanical Engineers (Part C)*, Vol. 64, No. 622, pp. 1949 – 1956, 1998.

(4) Horiuchi, T., Nakagawa, M., Sugano, M., and Konno, T. : Development of a Real-Time Hybrid Experimental System with Actuator Delay Compensation (1st Report, Compensation Method and Application to Experiments of Single-Degree-of-Freedom Systems) (in Japanese), *Journal of the Japan Society of Mechanical Engineers (Part C)*, Vol. 61, No. 584, pp. 1328 – 1336, 1995.

(5) Cai, G. and Huang, J. : Discrete-Time Variable Structure Control Method for Seismic-Excited Building Structures with Time Delay in Control, *Earthquake Engineering and Structural Dynamics*, Vol. 31, pp. 1347 – 1359, 2002.

(6) Horiuchi, T., Nakagawa, M., Sugano, M., and Konno, T. : Development of a Real-Time Hybrid Experimental System with Actuator Delay Compensation (2nd Report, Application to a Multiple-Degree-of-Freedom System) (in Japanese), *Journal of the Japan Society of Mechanical Engineers (Part C)*, Vol. 62, No. 599, pp. 2563 – 2570, 1996.

(7) Horiuchi, T. and Konno, T. : Development of a Real-Time Hybrid Experimental System with Actuator Delay Compensation (3rd Report,Application to Nonlinear Structural Systems) (in Japanese), *Journal of the Japan Society of Mechanical Engineers (Part C)*, Vol. 64, No. 617, pp. 7 – 14, 1998.

(8) Horiuchi, T. and Konno, T. : A new method for compensating actuator delay in real-time hybrid experiments, *The Royal Society of London*, Vol. 359, pp. 1893 – 1909, 2001.

(9) Shield, C. K., French, C. W., and Timm, J. : Development and implementation of the effective force testing method for seismic simulation of large-scale structures, *The Royal Society of London*, Vol. 359, pp. 1911 – 1929, 2001.

(10) Nakashima, M. and Masaoka, N. : Real-time on-line test for MDOF systems, *Earthquake Engineering and Structural Dynamics*, Vol. 28, pp. 393 – 420, 1999.

(11) Nakashima, M., Kato, H., and Takaoka, E. : Development of real-time pseudo dynamic testing, *Earthquake Engineering and Structural Dynamics*, Vol. 21, pp. 79 – 92, 1999.

(12) The MathWorks, Inc.: *Using MATLAB (Version 6)*, 2000.

(13) The MathWorks, Inc.: *Signal Processing Toolbox (Version 5)*, 2000.

(14) Chopra, A. K.: *Dynamics of Structures – Theory and Applications to Earthquake Engineering*, Prentice Hall, 2001.

(15) Soong, T. T.: *Active Structural Control*, Longman Scientific & Technical, 1990.

Chapter 4

Preliminary Experiments

4.1 General Remarks

In this chapter, details of the preliminary experiments are mentioned, which are required to conduct hybrid experiment. As shown in the previous chapter, dynamic characteristics of the IFDL system and shaker should be identified with good accuracy. Natural frequency and damping ratio of the test system are identified through free vibration tests. As for the shaker, a PID control method is introduced for compensating the dynamics. The tuning processes of the PID parameters and noise reduction filter are mentioned.

Furthermore, dynamic characteristics of the damper specimen should be also needed for numerical studies. In this research, magnetorheological damper (MR damper) is used. Algebraic model for the MR damper is introduced for numerical simulation as well as hybrid and semi-active experiments. Parameters for the model are identified by periodical excitation tests using both hydraulic actuator and the IFDL system, followed by nonlinear optimization scheme. Total experimental system is then mentioned in brief.

4.2 Structural Identification Test

The mass of the test system is estimated from the volume of the concrete-slab and using the unit weight of the reinforced concrete material, which is 24.853 ton. Given the mass, stiffness and damping ratio are estimated by conducting white noise excitation and the free vibration tests.

In order to estimate the natural frequency of the system, the shaker is driven by a band-limited white noise (DC-10 Hz) under velocity controlled operation, and slab

velocity response is measured as an output. Frequency response ratio from the input to the output magnitudes is calculated at each frequency component. Input command signal and out/in ratio is depicted in Figure 4.1(a) and (b) respectively.

The damping ratio is estimated by the logarithmic decrement[1)] applying to the decaying motion, which is obtained by suddenly stopping the mass of the shaker after several resonance periodical excitation. The velocity response of the test system and the estimated decaying function is shown in Figure 4.1(c).

Consequently, dynamic parameters for the IFDL test system are estimated as shown in Table 4.1.

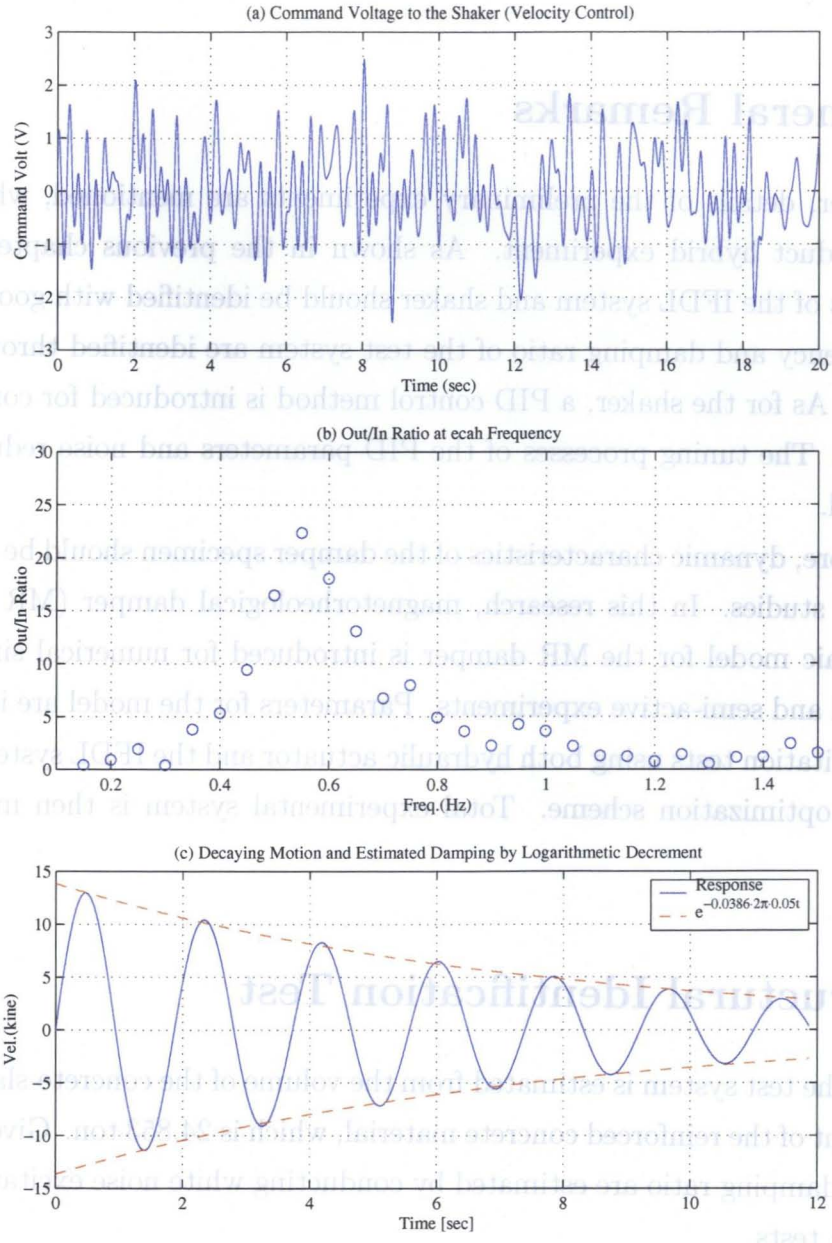

Figure 4.1: Identification Test Results for the IFDL Test System

Table 4.1: Estimated IFDL System Structural Parameters

Mass	24.853 (ton)
Natural Freq.	0.55 (Hz)
Damping Ratio	3.86 %

4.3 Magnetorheological Damper Identification Test

The objective of the IFDL system is to comprehend the dynamic characteristics of the test specimen and structural response without composing the numerical models of the device. Nevertheless, simulation models for the damper specimens are required in this research for calculating the reference results, which will be used to confirm the effectiveness of the IFDL system, hybrid experiment system, and proposed shaker control method.

4.3.1 Design Properties

The magnetorheological(MR) damper, which is shown in Photo 2.5, is chosen as test specimen because of the versatility of its dynamic characteristics with the change of the applied command current[8]. Figure 4.2 shows the schematics of the MR damper. The MR damper consists of the MR fluid, electromagnet, and piston. The MR fluid has the capability to change its viscosity with the change of the exposed magnetic field. The magnetic filed strength can be controlled by applying the current to the electromagnet, and yielding strength of the MR fluid also changes accordingly. Since the vibration energy is dissipated by cutting off the connection of small particles deployed in the MR fluid, force versus stroke hysteresis shows similar relation with that of the friction damper. The design specification of the MR damper is shown in Table 4.2.

For verification purpose of the hybrid experiment system, applied command current is fixed to 0 A, i.e. passive controlled damper is utilized for the verification tests.

4.3.2 Algebraic Model

One of the advantages of the MR damper over traditional passive dampers is that it can change the damping characteristics in real time by simply changing the current applied to the device. In order to realize the required force calculated from the control

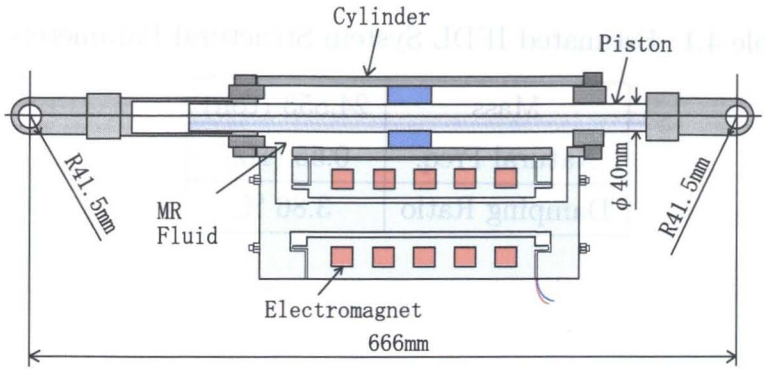

Figure 4.2: Schematics of the Magnetorheological Damper

Table 4.2: Design Specification of the MR damper

Model	MRD-60-kN-100	
Rated Force	60 kN	
Max. Allowable Vel.	25 kine	
Max. Stroke	100 mm (± 50 mm)	
Electromagnet	Coil	0.8 mm, 272 × 5 layer
	Max. Allowable Ampere	3 A
	Max. Resistance	15 Ω
	Inductance	46.4 mH @ 1 kHz

law, relationship between force, stroke, stroke velocity, and applied current should be clarified. [9–12].

In this dissertation, the algebraic model proposed by Gavin *et al.* is used[13]. In this model, the hyperbolic tangent function is introduced for describing the hysteretic characteristics. The device reaction force is given by the following expression.

$$f(x, \dot{x}, V) = f_0(V) \tanh\left(\frac{x}{d_0} + \frac{\dot{x}}{v_0}\right) + k_0 x + c_0 \dot{x} \tag{4.1}$$

Where, d_0, v_0 are parameters that shape the pre-yield region characteristics, $f_0(V)$ determines the maximum force level which is the function of the applied voltage to the device, k_0 is the post yield stiffness, c_0 is the plastic viscosity, and $x, \dot{x}$ are stroke and stroke velocity respectively. These parameters should be identified by utilizing the loading experiment results.

In the original model, the yield force level $f_0(V)$ is assumed to be of the form,

$$f_0(V) = \alpha V^n. \tag{4.2}$$

This model assumes that only the yield force level is the function of the command voltage. In the original model, a constant voltage controlled operation is utilized for controlling the device. However, it has been confirmed that the constant current controlled operation is superior to the constant voltage control due to the rapidness of the response time with the change of the command signal[14]. In this research, constant current control is then utilized, and a slight modification is applied to the yield force level function as shown below.

$$f_0(A) = \alpha A + \beta \tag{4.3}$$

Where, A is the command current (ampere) to the device, and α, β are constant parameters. The parameter β is introduced in order to shape the hysteresis under no command current.

Given yield level function, inverted algebraic model from the required force F_c to the command current A_c can be obtained as follows.

$$A_c = \frac{F_c - k_0 x - c_0 \dot{x}}{\alpha \tanh\left(\frac{x}{d_0} + \frac{\dot{x}}{v_0}\right)} - \frac{\beta}{\alpha} \tag{4.4}$$

This inverted model is used in Chapter 6 for determining the command current to the MR damper so as to trace the desirable force in real time.

Periodical Loading Tests with Hydraulic Actuator

The periodical loading experiments are conducted in order to identify the parameters for the algebraic model under various command currents. The hydraulic actuator loading system shown in Figure 2.5 is used for the test. Also, 0, 0.25, 0.5, 0.75, 1, 1.5 and 2 A of the constant command currents are applied to the MR damper. The identification is carried out with the following procedures[15];

1. Base parameters d_0, v_0, k_0 and c_0 are determined using 1 Hz, 1 cm of periodical excitation test results. As command current, a case of 0.25 A is selected.

2. The yielding force level $f_0(A)$ for all of the command currents are determined, while parameters obtained in Step 1 are used

3. The parameters α and β are determined by least square regression, which represent the relation between yielding force level and command current. The estimated relationship is shown in Figure 4.10

4. The effectiveness of the identified model is confirmed by calculating the force response using measured stroke and stroke velocity of the 2 Hz, 1cm of periodical excitation test, and compared with measured force.

Consequently, the MR damper model based on 1 Hz, 1 cm of sinusoidal experiment is obtained as follows.

$$f(x, \dot{x}, A) = (14.88A + 0.7334) \tanh\left(\frac{x}{0.9862} + \frac{\dot{x}}{0.7959}\right) + 0.2648\dot{x} \qquad (4.5)$$

x : Stroke (cm)

$\dot{x}$: Stroke Velocity (kine)

A : Command Current (A)

Figures 4.3 $\sim$ 4.9 show comparisons of the force, stroke versus force, and stroke velocity versus force relations of the 1 Hz, 1 cm of sinusoidal excitations between measured data and calculated results by Eq.(4.5). Also, same comparisons with 2 Hz, 1cm of sinusoidal loadings are shown in Figures 4.11 $\sim$ 4.17. As quantitative index for confirming the accuracy of the obtained model, the amount of the energy absorbance is calculated and compared, which is shown in Table 4.3. It is found from the table that obtained model based on 1 Hz, 1 cm of sinusoidal excitation tests could well trace the 2 Hz, 1 cm of measured data. From these results, the identified model has a good accuracy for tracing the overall hysteretic characteristics.

Table 4.3: Comparison of the Energy Absorbance (2 Hz, 1cm of Sinusoid)

Command Current (A)	0	0.25	0.5	0.75	1.0	1.5	2.0
Meas. (kJ)	2.90	5.94	8.96	11.9	14.9	20.5	26.1
Estimated (kJ)	2.58	5.47	9.03	12.6	15.7	20.9	24.6
Error (%)	11.0	7.90	0.78	6.05	5.92	1.61	5.86

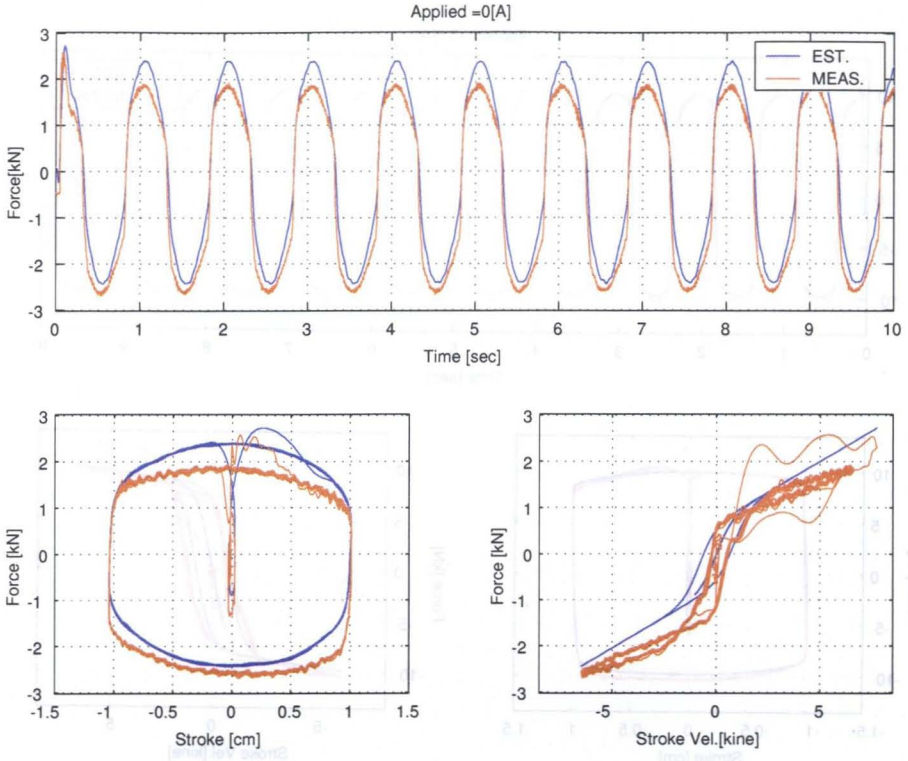

Figure 4.3: Comparison of Hysteresis at Command Amp = 0 A (1 Hz, 1 cm)

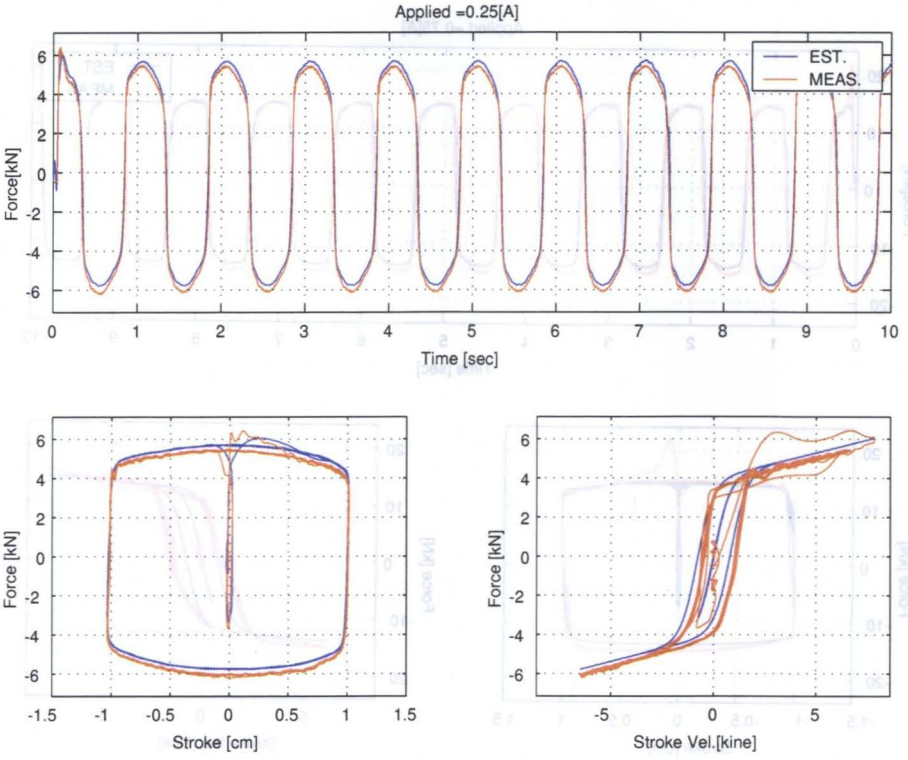

Figure 4.4: Comparison of Hysteresis at Command Amp = 0.25 A (1 Hz, 1 cm)

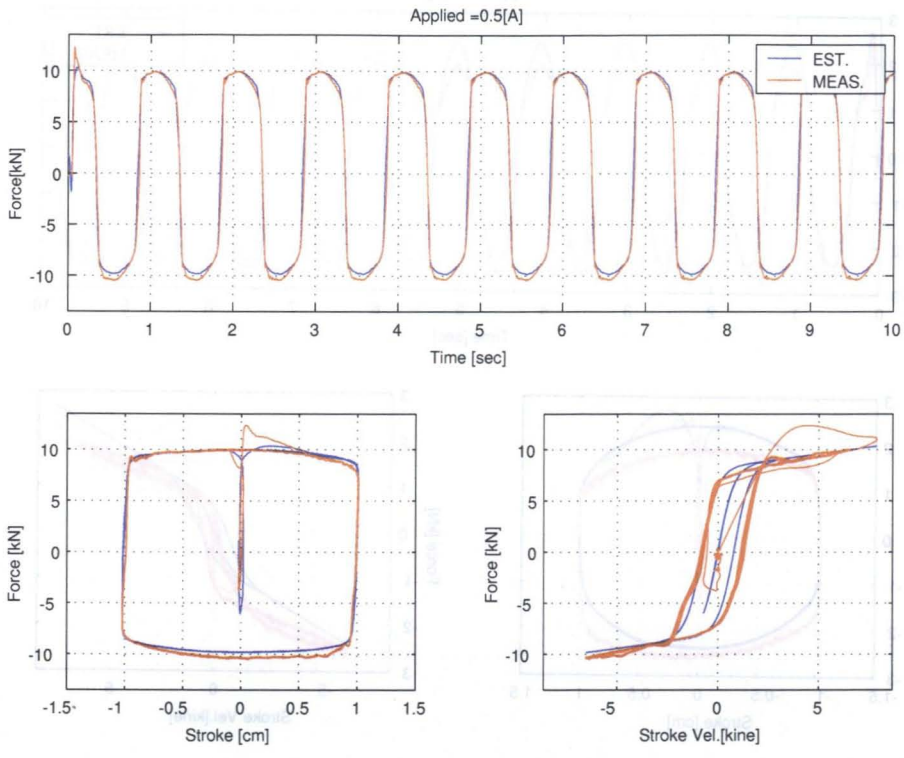

Figure 4.5: Comparison of Hysteresis at Command Amp = 0.5 A (1 Hz, 1 cm)

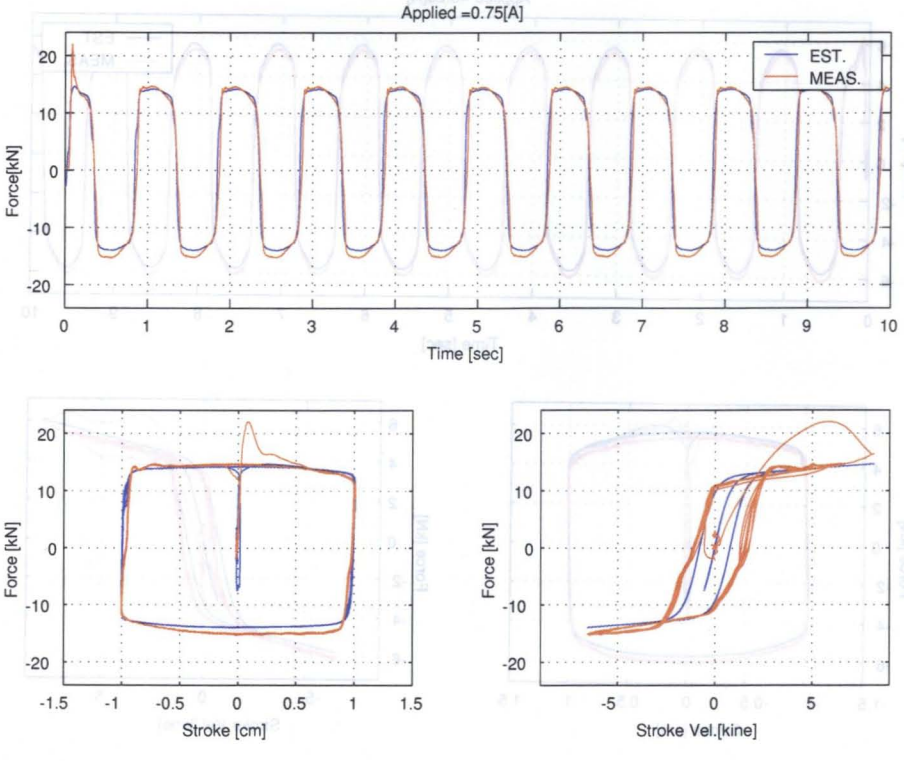

Figure 4.6: Comparison of Hysteresis at Command Amp = 0.75 A (1 Hz, 1 cm)

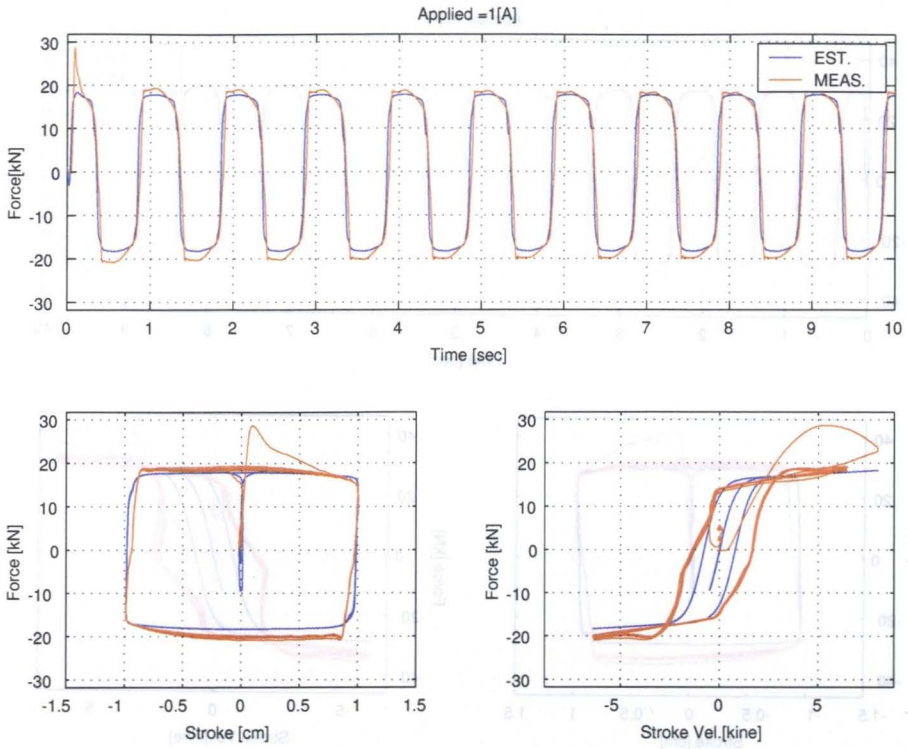

Figure 4.7: Comparison of Hysteresis at Command Amp = 1 A (1 Hz, 1 cm)

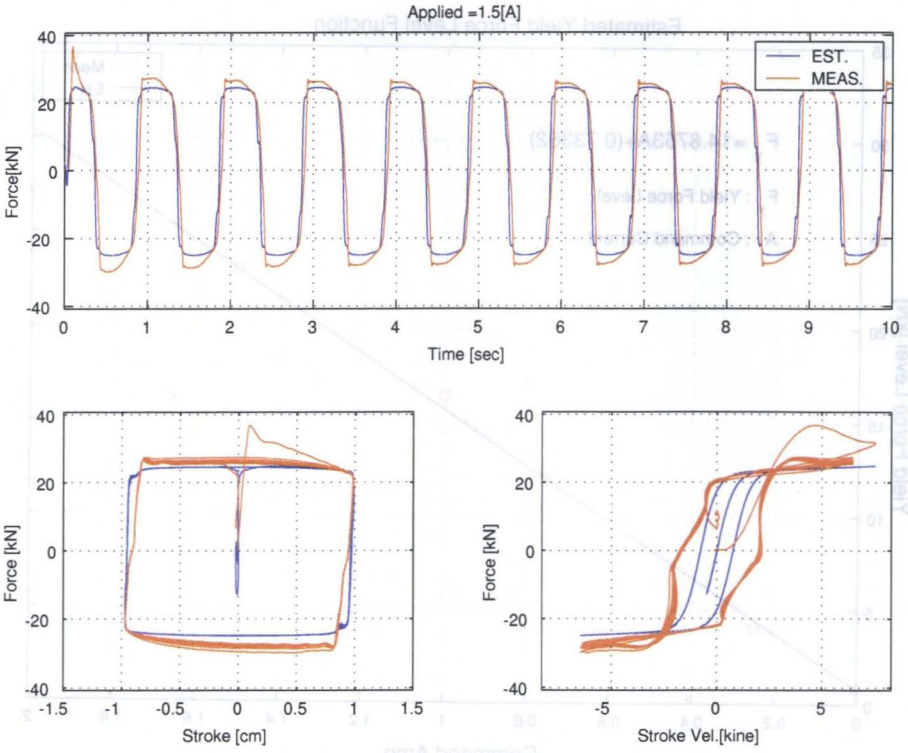

Figure 4.8: Comparison of Hysteresis at Command Amp = 1.5 A (1 Hz, 1 cm)

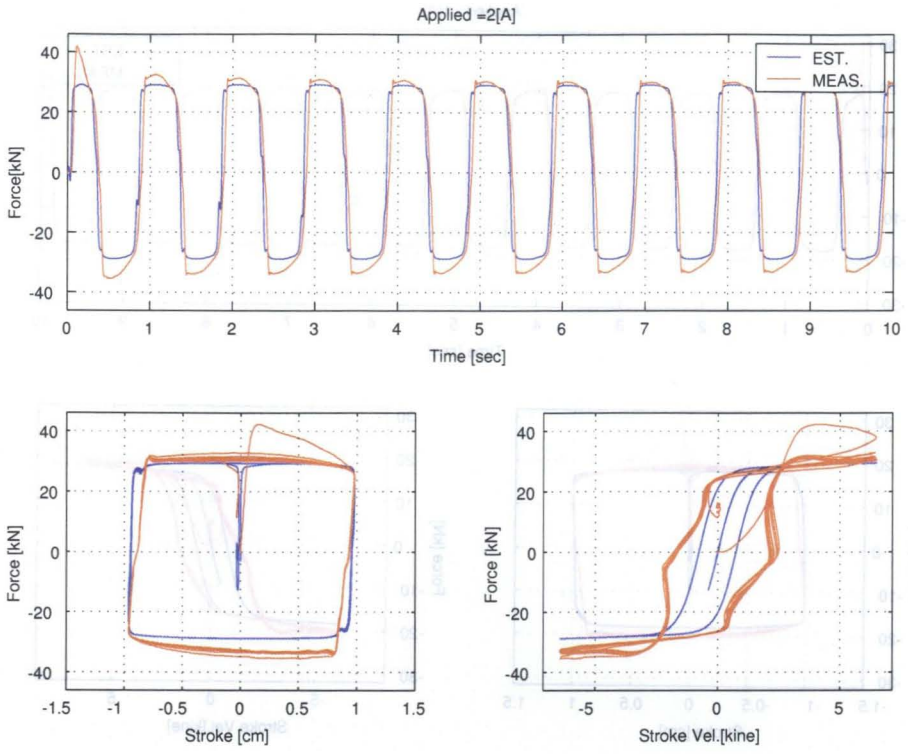

Figure 4.9: Comparison of Hysteresis at Command Amp = 2 A (1 Hz, 1 cm)

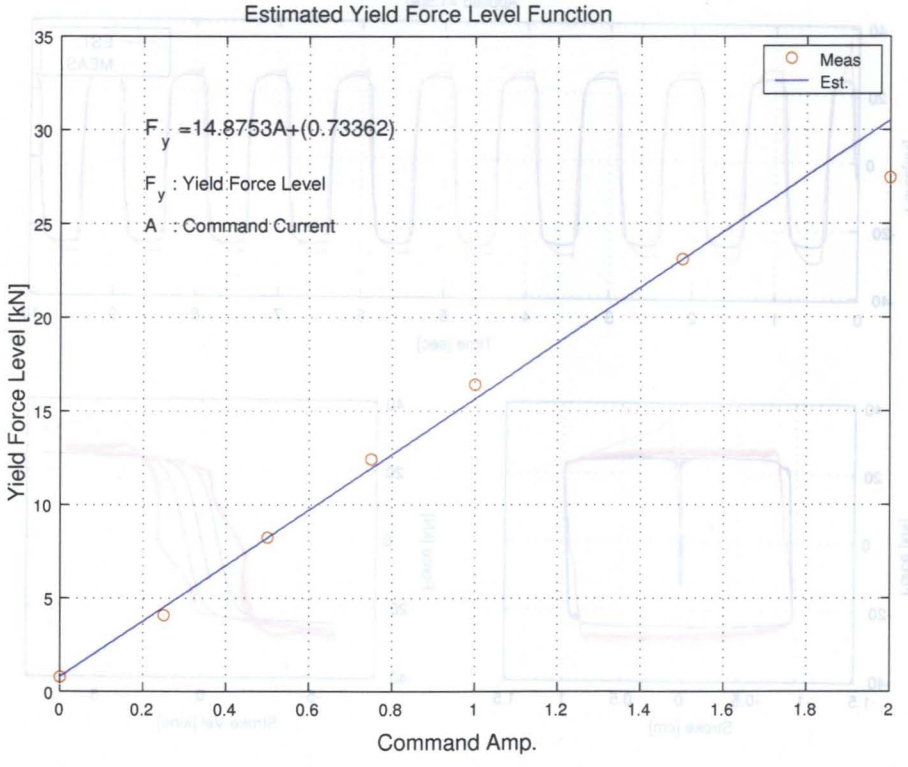

Figure 4.10: Yield Force Level at each Command Ampere and Estimation

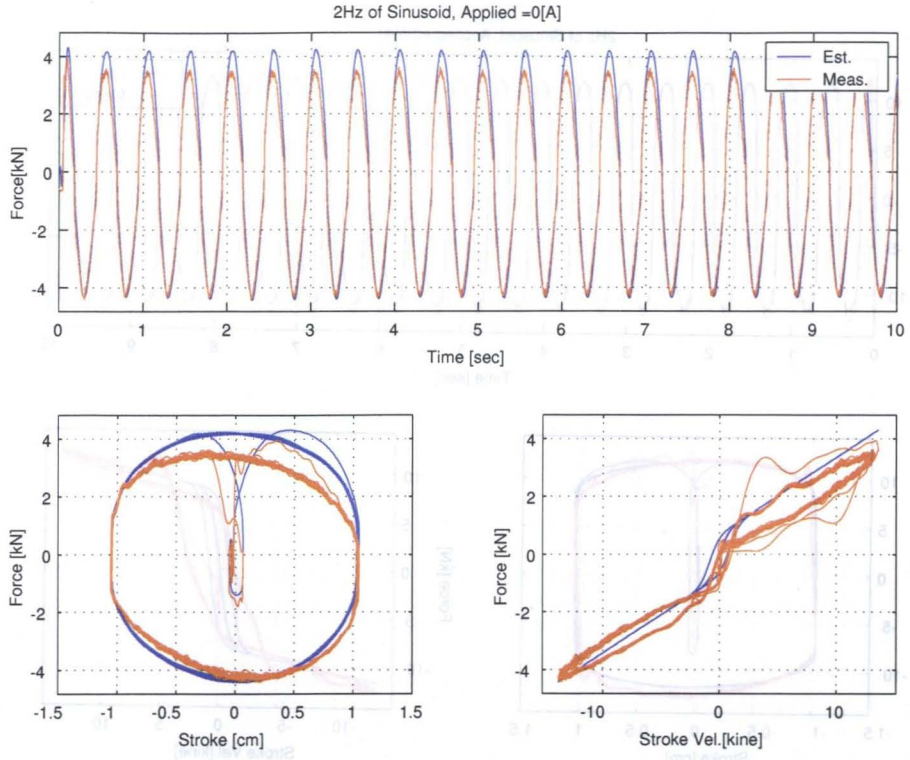

Figure 4.11: Comparison of Hysteresis at Command Amp = 0 A (2 Hz, 1 cm)

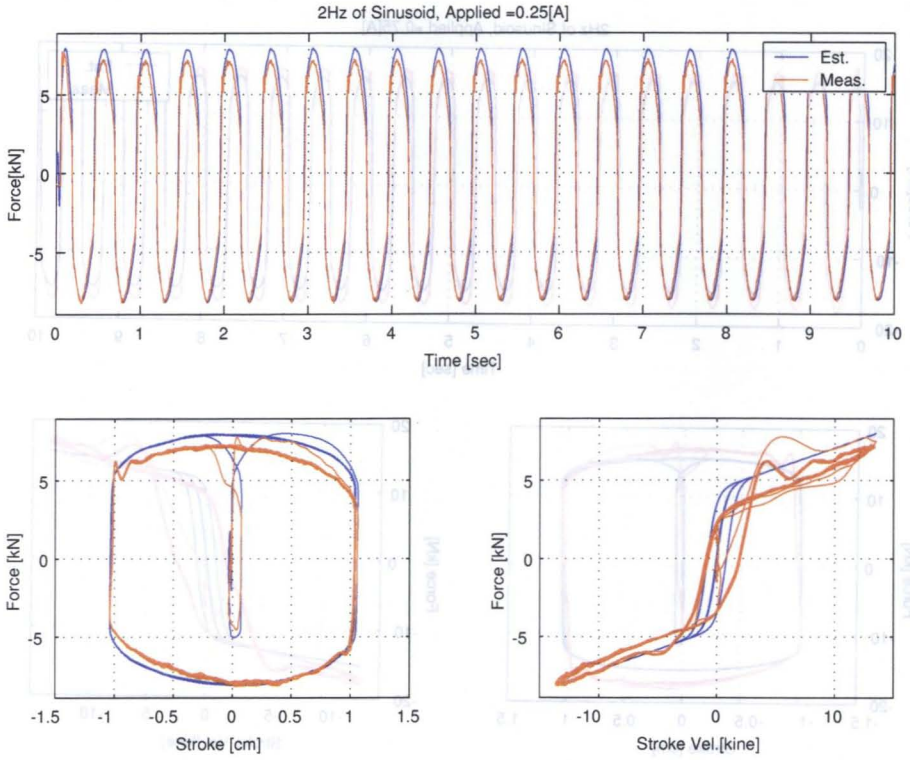

Figure 4.12: Comparison of Hysteresis at Command Amp = 0.25 A (2 Hz, 1 cm)

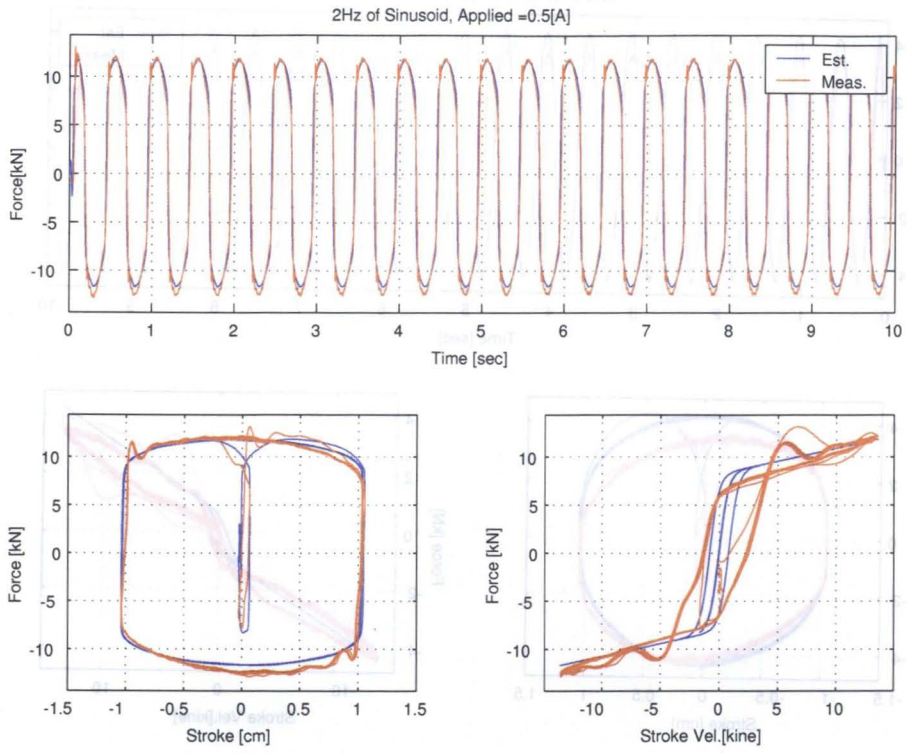

Figure 4.13: Comparison of Hysteresis at Command Amp = 0.5 A (2 Hz, 1 cm)

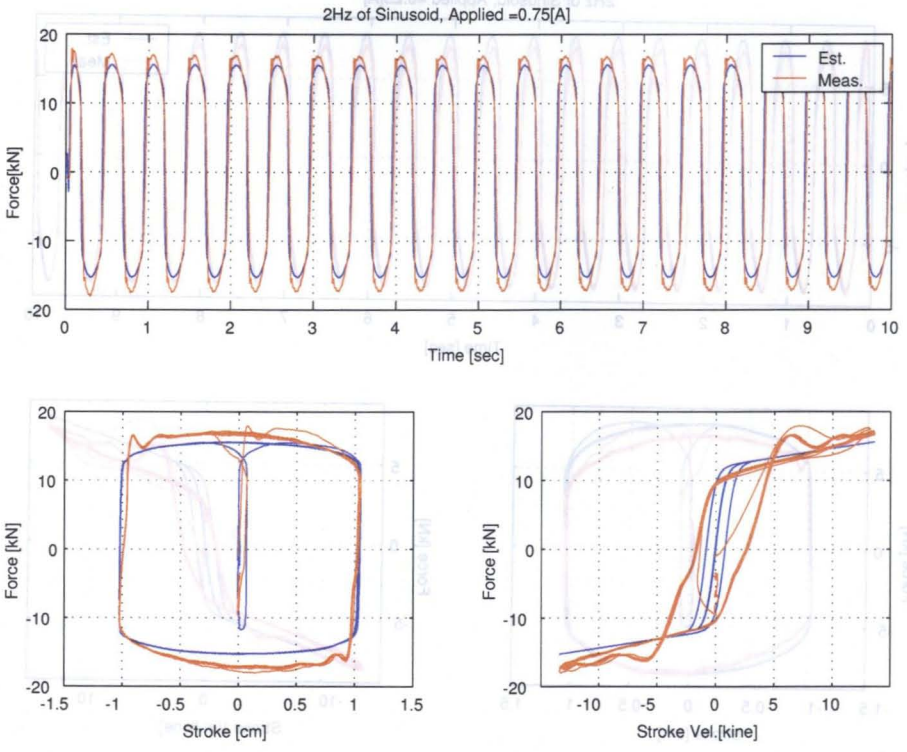

Figure 4.14: Comparison of Hysteresis at Command Amp = 0.75 A (2 Hz, 1 cm)

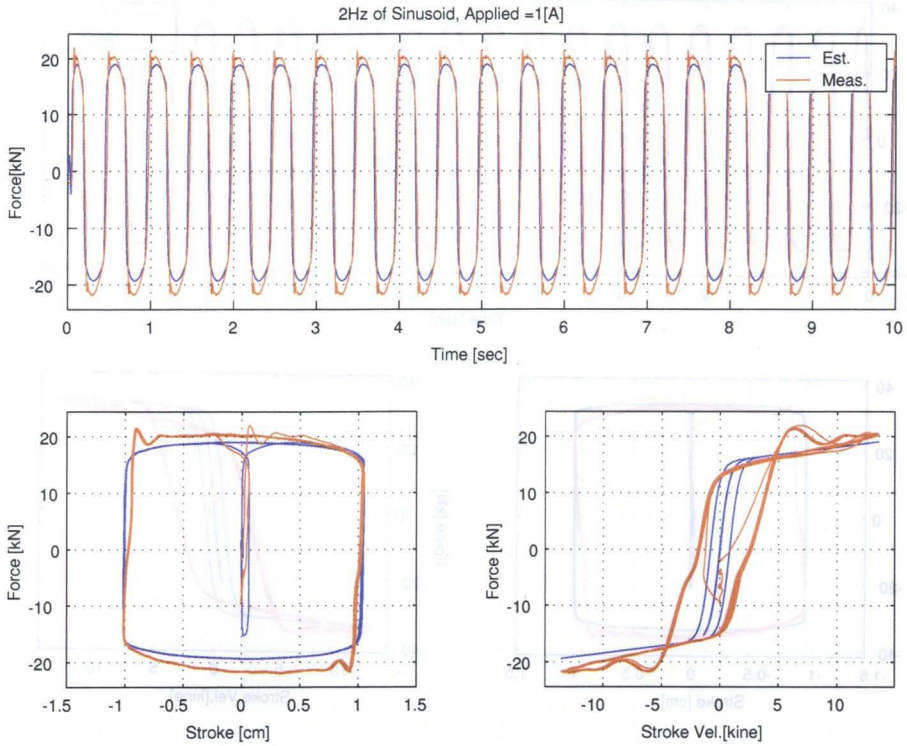

Figure 4.15: Comparison of Hysteresis at Command Amp = 1 A (2 Hz, 1 cm)

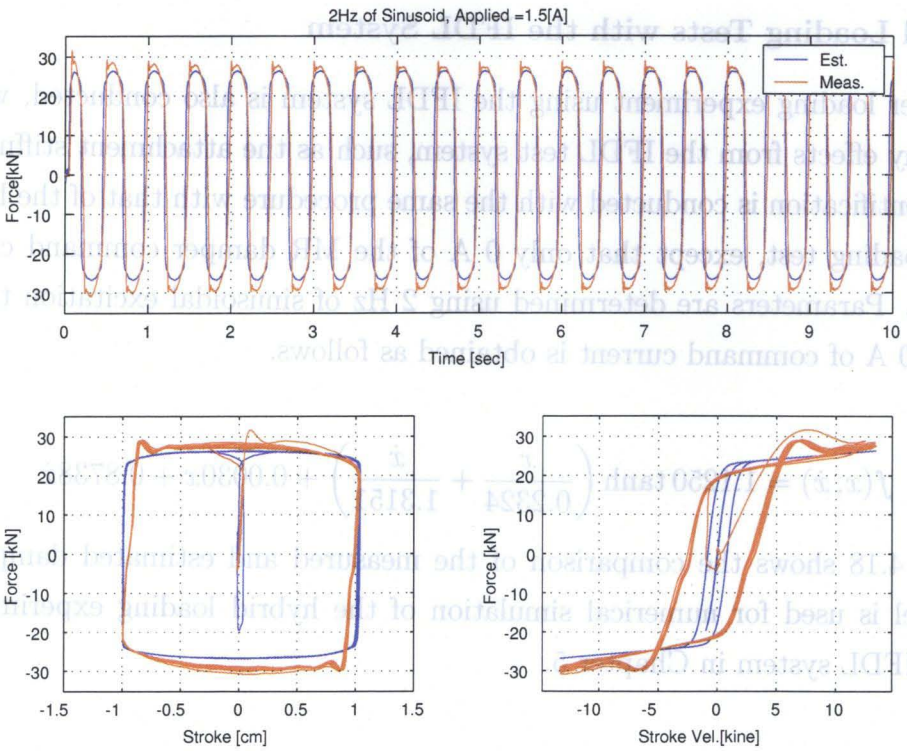

Figure 4.16: Comparison of Hysteresis at Command Amp = 1.5 A (2 Hz, 1 cm)

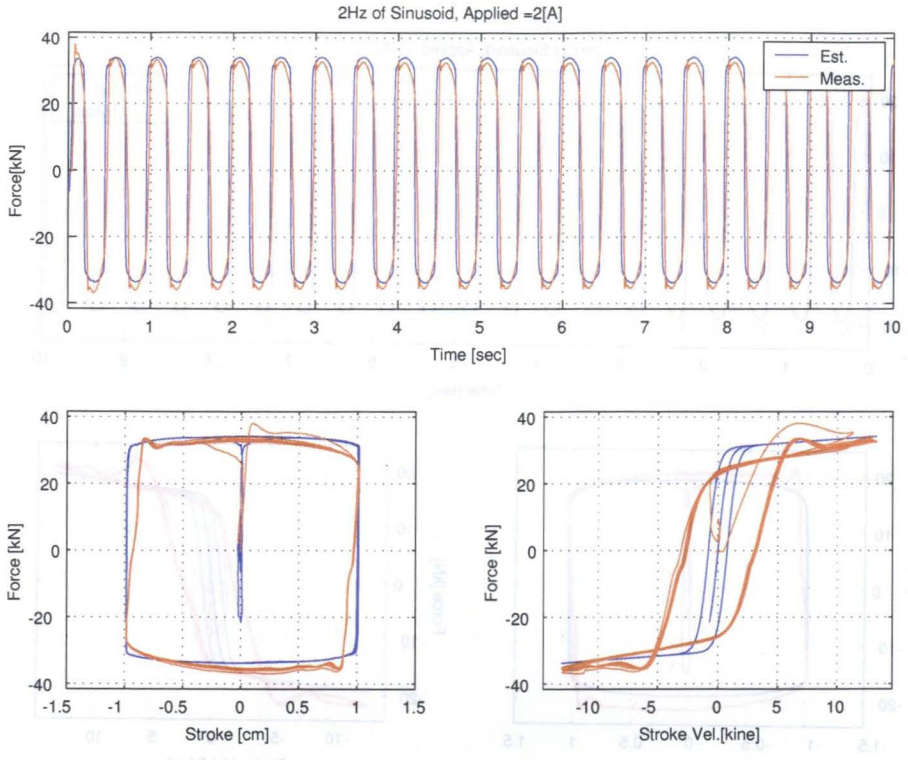

Figure 4.17: Comparison of Hysteresis at Command Amp = 2 A (2 Hz, 1 cm)

Periodical Loading Tests with the IFDL System

The damper loading experiment using the IFDL system is also conducted, which includes many effects from the IFDL test system, such as the attachment stiffness.

The identification is conducted with the same procedure with that of the hydraulic actuator loading test, except that only 0 A of the MR damper command current is considered. Parameters are determined using 2 Hz of sinusoidal excitation test. The model for 0 A of command current is obtained as follows.

$$f(x,\dot{x}) = 1.1250 \tanh\left(\frac{x}{0.2324} + \frac{\dot{x}}{1.3151}\right) + 0.0030x + 0.8738\dot{x} \tag{4.6}$$

Figure 4.18 shows the comparison of the measured and estimated damper force. This model is used for numerical simulation of the hybrid loading experiment with using the IFDL system in Chapter 5.

4.4 Shaker Dynamics Compensation

As shown in Chapter 3, it is essential for the hybrid experiment to control the motion of the shaker so as to trace the command signal as precise as possible. However, the

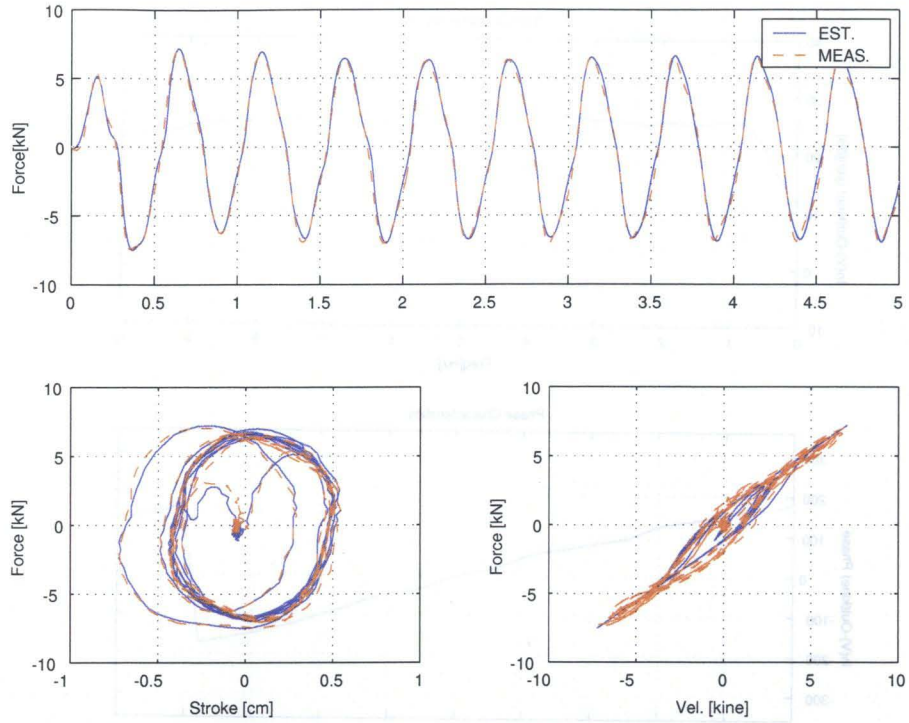

Figure 4.18: Comparison of Hysteresis at Command Amp = 0 A (2 Hz)

shaker has its own dynamics by nature, particularly in phase characteristics. In this section, shaker motion compensation method based on PID tuning is introduced. Also, the band-pass digital filter which reduce the noise and DC components is designed.

4.4.1 Original Device Dynamics

To begin with, transfer function of the shaker without any compensations is examined. The MR damper device is set to the IFDL test system and command current is held to be 0 A through the test. The shaker is driven with the velocity contort mode, and band-limited white noise (from 0.5 Hz to 20 Hz) is selected as velocity command signal.

Figure 4.19 shows the measured frequency characteristics of the shaker under velocity controlled operation. As observed from the figure, this device has linear but relatively large phase lag, contrast to the good gain shape. From this result, shaker transfer function is estimated as follows[16, 17].

$$H(s) = \frac{-4.5632 \cdot s^4 + 551.58 \cdot s^3 - 53913 \cdot s^2 + 2.5695 \times 10^6 \cdot s - 5.7146 \times 10^7}{1.0000 \cdot s^4 + 56.674 \cdot s^3 + 5578.1 \cdot s^2 + 1.2798 \times 10^5 \cdot s + 3.8598 \times 10^6} \quad (4.7)$$

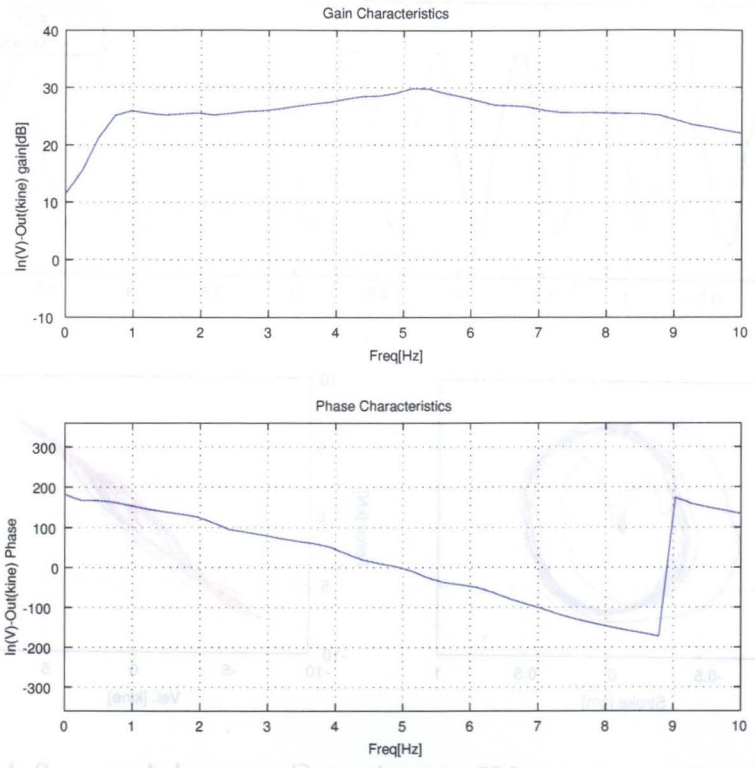

Figure 4.19: Estimated Characteristics of the Shaker w/o Compensation

4.4.2 PID Controller

The PID controller[18] is introduced for compensating the dynamics of the shaker. Due to its simpleness and clear physical meanings, the PID controller is one of the most commonly used method for compensating the plant dynamics[19–21]. In this research, the compensation block shown in Figure 4.20 is assembled.

The measured data required for the compensation block are the relative velocity and stroke of the shaker mass. A band-pass filter $P(s)$ is applied to the command signal

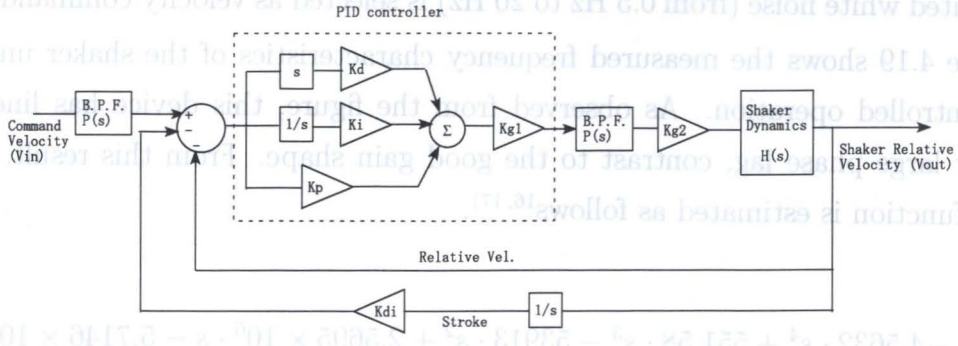

Figure 4.20: Block Diagram for the Shaker Dynamics Compensation

as the pre-filter in order to eliminate the undesirable signals. The residue between the command and measured relative velocity is taken at every sample time, and passed to the PID controller block. In the PID block, proportional (K_p), derivative (K_d), and integration (K_i) gains are multiplied to the error signal. K_{g1} gain is introduced to adjust the polarity. Then, a band-pass filter is again applied to the command voltage, followed by the overall magnification gain K_{g2}.

Also, mass displacement data is fed back so as not for the shaker mass to drift from the central position. The small but non-zero external noise comes into the velocity command signal, and it causes the drift of the mass. The amount of the gain K_{di} for the mass stroke should be as small as possible in order not to deteriorate the accuracy of the velocity control. These parameters are determined through shaker loading experiments, which is mentioned in Chapter 5.

From Figure 4.20, the transfer function from velocity command signal to the voltage command signal with PID controller is derived as follows.

$$H_{io}(s) = \frac{V_{out}}{V_{in}} = \frac{sP(s)G(s)}{s(1+G(s)) + K_{di}G(s)} \tag{4.8}$$

$$\text{where, } G(s) = k_{g1}k_{g2}P(s)\left(K_p + K_d s + \frac{K_i}{s}\right)H(s) \tag{4.9}$$

4.4.3 Band-Pass Filter

Due to the bias in the measured data, the command velocity signal may drift from the base line. In fact, it is observed in series of experiments that this existence of the velocity drift also cause the position drift of the mass, and tests are terminated after the upper limit of the shaker mass stroke is detected. Furthermore, undesirable higher frequency component may degrade the stability of the shaker control. In order to avoid these problems, band-pass digital filter is introduced. This filter is intended to eliminate the frequency components under 0.4 Hz and over 25 Hz, which is realized by the Chebyshev IIR filter[16, 22]. The digital filter transfer function with 1000 Hz of sampling frequency is designed as follows.

$$P(z) = g \cdot H_1(z) \cdot H_2(z) \cdot H_3(z) \tag{4.10}$$

$$H_1(z) = \frac{1.00000000000000 - 0.00000000426277z^{-1} - 1.00000000426277z^{-2}}{1.00000000000000 - 1.71627179477815z^{-1} + 0.71654433108907z^{-2}}$$

$$H_2(z) = \frac{1.00000000000000 - 1.80922220206838z^{-1} + 1.00000000000001z^{-2}}{1.00000000000000 - 1.74767323411886z^{-1} + 0.81082040017573z^{-2}}$$

$$H_3(z) = \frac{1.00000000000000 - 1.99999949254145z^{-1} + 0.99999999573721z^{-2}}{1.00000000000000 - 1.99904804722753z^{-1} + 0.99904946672524z^{-2}}$$

$$g = 0.04675252691119$$

In order to stabilize the real-time calculation in the experiment, the filter transfer function is represented and implemented by the second-order sections form[22].

Figure 4.21 shows the magnitude, phase, and group delay characteristics of the designed digital filter. Also, Figure 4.22 shows zeros/poles locations of the filter.

Despite the effectiveness of the designed filter, its nonlinear phase characteristics might alter the output velocity. This effect is also compensated by the PID controller.

4.5 Controller for the Hybrid Experiment

Based on proposed shaker control method and practical considerations, a SIMULINK block diagram for the DSP to realize the real-time hybrid experiment is assembled, which is depicted in Figure 4.23. The procedure at each step for obtaining the command voltage to the shaker device is as follows.

1. Measure shaker and structural response as well as damper force
2. Solve E.O.M under given earthquake data and measured response (4th order Runge-Kutta method is utilized for numerical integration)
3. Pick up displacement, velocity, and acceleration at the assumed damper location
4. Calculate command velocity based on Eq.(3.8)
5. Pass through PID controller and band-pass filter
6. Output command voltage from D/A
7. Back to step 1.

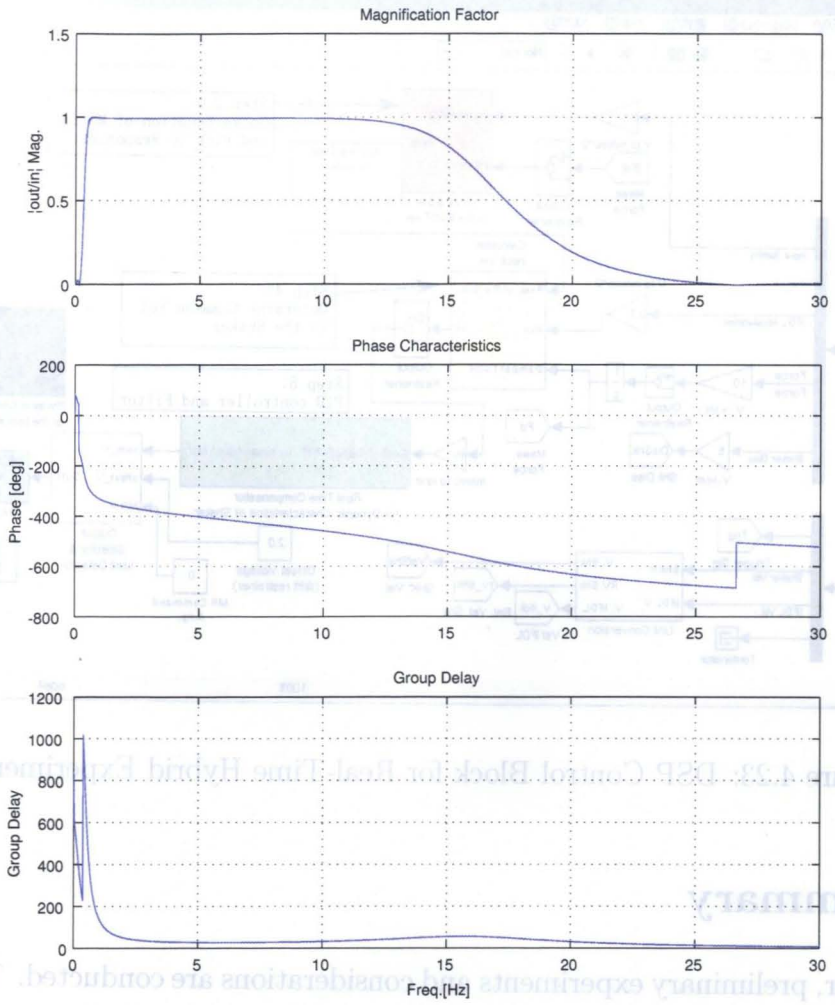

Figure 4.21: Characteristics of the Designed Digital Filter

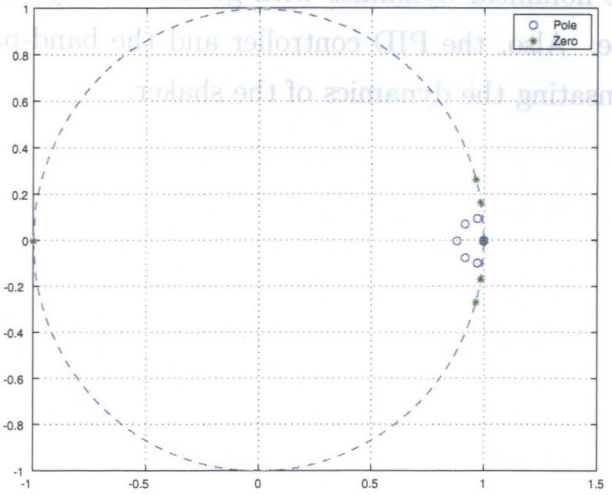

Figure 4.22: Zero Pole Locations

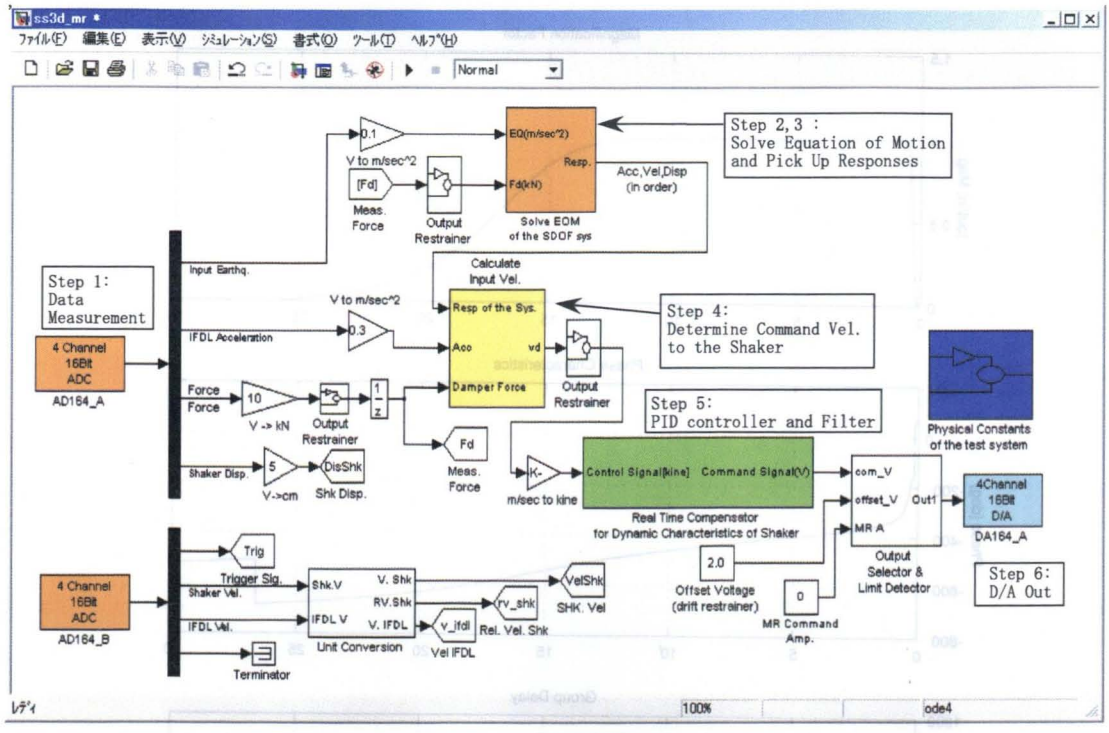

Figure 4.23: DSP Control Block for Real-Time Hybrid Experiment

4.6 Summary

In this chapter, preliminary experiments and considerations are conducted. The natural frequency and damping ratio of the test system are identified. Then, series of periodical loading experiments are carried out to compose the algebraic model of the MR damper test specimen as a function of command current. It is confirmed that the identified model could trace the nonlinear dynamics with good accuracy from the viewpoint of the energy absorbance. Also, the PID controller and the band-pass digital filter are introduced for compensating the dynamics of the shaker.

References

(1) Chopra, A. K.: *Dynamics of Structures – Theory and Applications to Earthquake Engineering*, Prentice Hall, 2001.

(2) Ribakov, Y. and Gluck, J. : Active Control of MDOF Structures with Supplemental Electrorheological Fluid Dampers, *Earthquake Engineering and Structural Dynamics*, Vol. 28, pp. 143 – 156, 1999.

(3) Soda, S., Kusumoto, H., and Hagiwara, N.: Basic Study on Capacity Control of Magneto-Rheological Fluid Damper by Electric Current, *Damping Symposium II*, The Japan Society of Mechanical Engineers, pp. 105–109, 2002.

(4) Nakaya, N., Shiraishi, T., and Morishita, S.: Vibration Control of Structure by MR Damper, *Damping Symposium II*, The Japan Society of Mechanical Engineers, pp. 110–114, 2002.

(5) Iwata, N., Soda, S., Sodeyama, H., Sunakoda, K., and Fujitani, H.: Experimental Study on Mechanical Properties of A Bypass Type Magnetorheological Fluid Damper, *Proceedings of the Second Japan National Symposium on Structural Control*, pp. 15 – 20, 2000.

(6) Matsuhisa, H. and Pan, G.: Study on Vibration Control with Magnetorheological Damper, *Damping Symposium II*, The Japan Society of Mechanical Engineers, pp. 149 – 154, 2002.

(7) Yi, F., Dyke, S. J., Frech, S., and Carlson, J. D.: Investigation of Magnetorheological Dampers for Earthquake Hazard Mitigation, *Proceedings of the Second World Conference on Structural Control*, pp. 349 – 357, 1998.

(8) Sodeyama, H. and Sunakoda, K.: 300kN-MR damper for semi-active vibration control systems, *JSME Dynamics & Design Conference*, 2001.

(9) Dyke, S. J., Spencer, Jr., B. F., Sain, M. K., and Carlson, J. D.: Modeling and Control of Magnetorheological Dampers for Seismic Response Reduction, *Smart Materials and Structures*, Vol. 5, pp. 565 – 575, 1996.

(10) Spencer, Jr., B. F., Dyke, S. J., Sain, M. K., and Carlson, J. D. : Phenomenological Model of a Magnetorheological Damper, *Journal of Engineering Mechanics*, Vol. 3, pp. 230 – 238, 1997.

(11) Dyke, S. J., Spencer, Jr., B. F., Sain, M. K., and Carlson, J. D.: On the efficacy of magnetorheological dampers for seismic response reduction, *1997 ASME Design Engineering Technical Conferences*, Vol. DETC97VIB3828, 1997.

(12) Yang, G., Jung, H. J., and Spencer, Jr., B. F.: Dynamic model of full-scale MR dampers for civil engineering application, *US-Japan Workshop on Smart Structure for Improved Seismic Performance in Urban Regions*, pp. 213 – 224, 2001.

(13) Gavin, H., Hoagg, J., and Dobossy, M.: Optimal design of MR dampers, *US-Japan Workshop on Smart Structure for Improved Seismic Performance in Urban Regions*, pp. 225 –236, 2001.

(14) Yang, G.: *Large-Scale Magnetorheological Fluid Damper for Vibration Mitigation: Modeling, Testing and Control*, PhD Thesis, University of Notre Dame, 2001.

(15) The MathWorks, Inc.: *Optimization Toolbox (Version 2)*, 2000.

(16) The MathWorks, Inc.: *Signal Processing Toolbox (Version 5)*, 2000.

(17) Ljung, L.: *System Identification Toolbox (Version 5)*, 2000.

(18) Clark, R. N.: *Control System Dynamics*, Cambridge University Press, 1996.

(19) Fujita, T., Shimazaki, M., Tanaka, K., Ohyama, H., Nakamura, Y., Murakoshi, K., Nora, H., and Miyano, H. : Large-Scale Mode Experiment of Hybrid Mass Damper with Convertible Active and Passive Modes Using Servomotor for Vibration Control of Tall Buildings (in Japanese), *Journal of the Japan Society of Mechanical Engineers*, pp. 3755 – 3761, 1994.

(20) Fujita, T., Bessho, T., Hora, H., Tanaka, K., and Nakamura, Y. : Control Methods for Active Mass Damper Using Linear Motor for Vibration Control of Tall Buildings, *Journal of the Japan Society of Mechanical Engineers*, pp. 1154 – 1161, 1998.

(21) Chu, S. Y., Soong, T. T., Lin, C. C., and Chen, Y. Z. : Time-Delay Effect and Compensation on Direct Output Feedback Controlled Mass Damper Systems, *Earthquake Engineering and Structural Dynamics*, Vol. 31, pp. 121 – 137, 2002.

(22) Mitra, S. K.: *Digital Signal Processing – A Computer-Based Approach*, McGraw Hill, 2002.

(23) Soong, T. T.: *Active Structural Control*, Longman Scientific & Technical, 1990.

Chapter 5

Real-Time Experimental Verifications with Passive Damper

5.1 General Remarks

In this chapter, series of real-time substructure hybrid experiments are carried out in order to confirm the effectiveness of the proposed shaker control method and assembled test setup. Several types of structures are assumed as the target structural systems, in which damper specimen is installed. After tuning the PID parameters for the shaker dynamics compensation, periodical and earthquake excitation tests are carried out using the MR damper. The obtained measurement data is compared with the numerical simulation results utilizing the algebraic model for the damper specimen.

5.2 Problem Definitions

5.2.1 Model Structures

Two different types of systems are selected as hypothetical structures, in which the MR damper specimen is assumed to be installed.

SDOF Model

This system consists of the single mass, spring, and damping elements. These properties are selected so as to differ from that of the original IFDL test system. It is intended that results obtained in this simplified case give the basic informations for conducting the loading experiment of more complicated multi-degree-of-freedom (MDOF) structural systems.

JDS Model

The adjacent structure, which consists of 3-story and 5-story frame buildings, is selected as a MDOF structure. The full-scale structures were constructed in the Disaster Prevention Research Institute, Kyoto University. The original purpose of these structures is to confirm the effectiveness of the joint damper system (JDS) through full-scale experiments[1–3]. The JDS is one of the structural control methods that reduce vibration response by coupling several structures with the energy dissipation devices[4–8]. This technique works effectively if each structure has different dynamic properties from others, since the connecting devices dissipate energy effectively by making use of the relative responses between structures.

The experimental verification tests using variable-orifice viscous damper had been carried out, connecting 3rd floors of the 3-story and 5-story frame structures[1–3]. In this dissertation, the MR damper is assumed to be installed at the same location.

5.2.2 Test Specimen

The MR damper that characteristics are closely examined in Chapter 4, is used as the test specimen. For the simplicity of discussions, the command current to the device is fixed to 0 A through all experiments, i.e. the passive device similar to the viscous-elastic damper is utilized for the test. The algebraic model represented by Eq.(4.6) is used for the numerical simulations to trace the behavior of the device.

5.2.3 Assumed Ground Motions

As to the assumed ground motions to which structures are exposed, three different types of waveforms are chosen; resonance sinusoidal waves, El Centro NS and JMA Kobe NS ground motions. In the following discussions, abbreviated notations "ECNS" and "KBNS" are used to represent the El Centro NS and Kobe NS ground motions.

Figures 5.1 and 5.2 show time histories and mean power spectral densities of the El Centro NS and Kobe NS inputs, respectively. Maximum excitation level for each structure are determined by preliminary numerical simulations so as to meet the physical constraints of the shaker and test system shown in Table 5.1.

5.3 Shaker Control

Prior to the loading experiments, parameters for the PID control of the shaker should be determined which are suitable for each experiment condition. Initial guessed param-

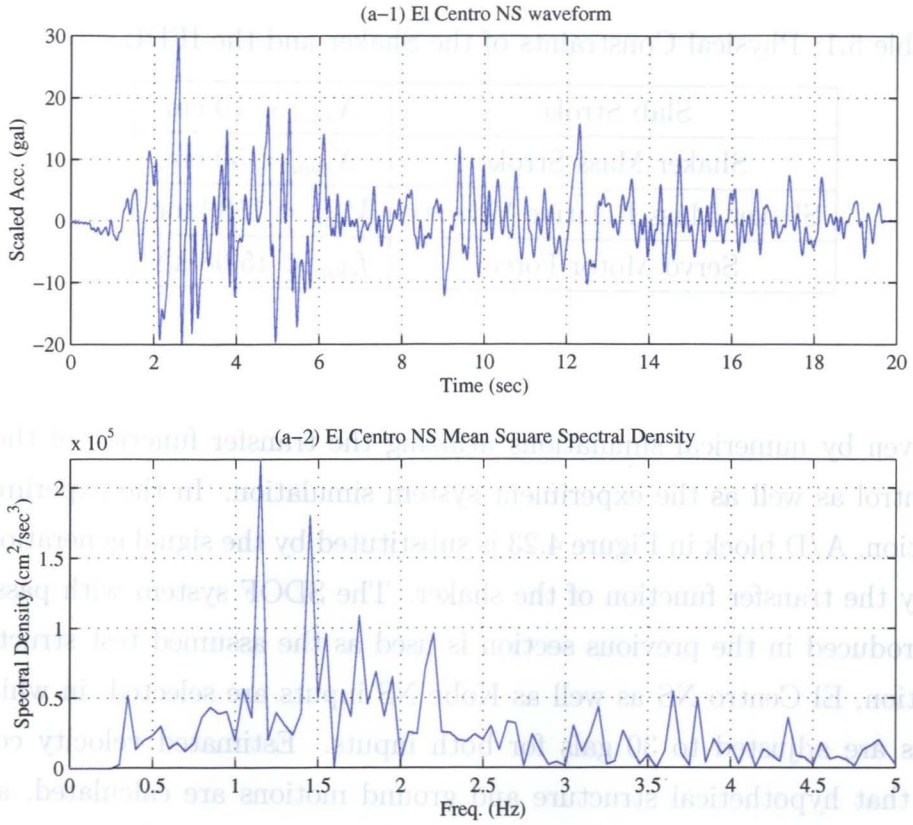

Figure 5.1: El Centro NS waveform

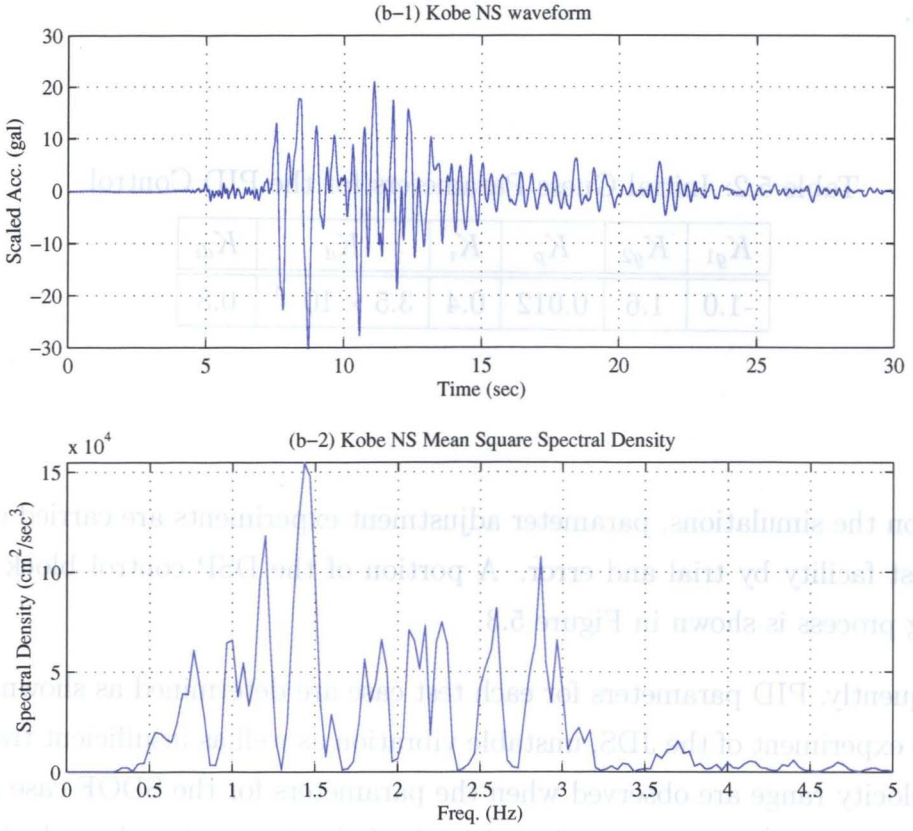

Figure 5.2: JMA Kobe NS wavefrom

Table 5.1: Physical Constraints of the Shaker and the IFDL system

Slab Stroke	$X_{\text{slim}} < 10$ cm
Shaker Mass Stroke	$X_{\text{elim}} < 50$ cm
Shaker Mass Relative Velocity	$V_{\text{elim}} < 150$ kine
Servo Motor Force	$f_{\text{elim}} < 15.68$ kN

eters are given by numerical simulations utilizing the transfer function of the shaker without control as well as the experiment system simulation. In the experiment system simulation, A/D block in Figure 4.23 is substituted by the signal generation block, and D/A by the transfer function of the shaker. The SDOF system with passive MR damper introduced in the previous section is used as the assumed test structure. As ground motion, El Centro NS as well as Kobe NS inputs are selected, in which maximum levels are adjusted to 30 gals for both inputs. Estimated velocity command signals for that hypothetical structure and ground motions are calculated, and PID parameters are tuned so as to minimize the standard deviation of the in-out shaker relative velocity time histories. Table 5.2 shows the numerically obtained initial guess parameters.

Table 5.2: Initial Guess Parameters for the PID Control

K_{g1}	K_{g2}	K_p	K_i	K_d	K_{di}
-1.0	1.6	0.012	0.4	3.5×10^{-4}	0.8

Based on the simulations, parameter adjustment experiments are carried out using the real test facility by trial and error. A portion of the DSP control block used for this tuning process is shown in Figure 5.3.

Consequently, PID parameters for each test case are determined as shown in Table 5.3. In the experiment of the JDS, unstable vibration as well as insufficient traceability at large velocity range are observed when the parameters for the SDOF case are used. Efficacy of these parameters is confirmed in the following sections by calculating the transfer function of the shaker relative velocity from commands to measurements.

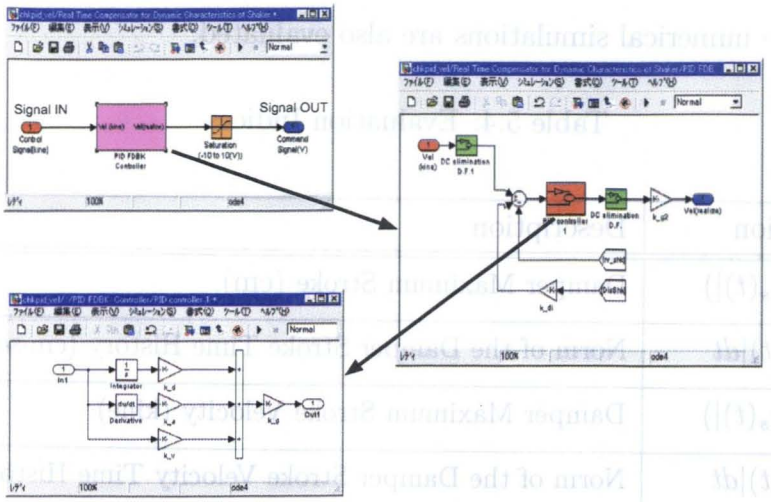

Figure 5.3: DSP Control Block for Parameter Tuning

Table 5.3: Experimentally Obtained Parameters for the PID Control

CASE	K_{g1}	K_{g2}	K_p	K_i	K_d	K_{di}
SDOF	-1.0	1.7	0.029	0.48	3.0×10^{-4}	0.95
JDS	-1.0	1.75	0.025	0.48	3.0×10^{-4}	0.84

5.4 Simulation Properties and Evaluation Indices

In the following sections, experimentally obtained responses are compared with those of the idealized simulations. In the simulations, dynamics of the shaker and the time delay are not taken into consideration. At each time step, the control force calculated from Eq.(3.6) is transmitted to the IFDL slab. The equation of motion is then solved using the external shaker control force and damper specimen reaction force obtained from Eq.(4.6). The reaction force is also used to determine the shaker control force at the next step. Finally, shaker displacement, velocity, and acceleration are calculated by using the control force and the slab acceleration. A 4th order Runge-Kutta method with 0.001 sec of time step is chosen for numerical integration.

In order to comprehend the effectiveness of the IFDL test system and proposed shaker control method quantitatively, evaluation indices shown in Table 5.4 are introduced herein. Other than maximum response, norm values are also calculated to comprehend the overall traceability. For JDS structure, velocities at the top floors of both 3DOF and 5DOF structures are also evaluated.

These indices are calculated for every test case and its simulation, and errors from

the results of the numerical simulations are also evaluated.

Table 5.4: Evaluation Indices

Index	Definition	Description
E_s	$\max(\lvert x_s(t)\rvert)$	Damper Maximum Stroke (cm)
Nr_s	$\int_0^T \lvert x_s(t)\rvert dt$	Norm of the Damper Stroke Time History (cm·sec)
E_{sv}	$\max(\lvert \dot{x}_s(t)\rvert)$	Damper Maximum Stroke Velocity (kine)
Nr_{sv}	$\int_0^T \lvert \dot{x}_s(t)\rvert dt$	Norm of the Damper Stroke Velocity Time History (kine·sec)
E_f	$\max(\lvert f_D(t)\rvert)$	Damper Maximum Force (kN)
Nr_f	$\int_0^T \lvert f_D(t)\rvert dt$	Norm of the Damper Force Time History (kN·sec)
E_{ev}	$\max(\lvert \dot{x}_e(t)\rvert)$	Shaker Maximum Relative Velocity (kine)
Nr_{ev}	$\int_0^T \dot{x}_e(t)dt$	Norm of the Shaker Velocity Time History (kine·sec)
E_{ef}	$\max(\lvert f(t)\rvert)$	Shaker Maximum Control Force (kN)
Nr_{ef}	$\int_0^T \lvert f(t)\rvert dt$	Norm of the Shaker Force Time History (kN·sec)
E_{de}	$\int_0^T f_D(t)\dot{x}_s(t)dt$	Energy Absorbance of the Damper Specimen (kJ)
E_{3R}	$\max(\lvert \dot{x}_{33}(t)\rvert)$	3DOF 3F Maximum Velocity (JDS only) (kine)
Nr_{3R}	$\int_0^T \lvert \dot{x}_{33}(t)\rvert dt$	Norm of the 3DOF 3F Velocity Time History (JDS only) (kine·sec)
E_{5R}	$\max(\lvert \dot{x}_{55}(t)\rvert)$	5DOF 5F Maximum Velocity (JDS only) (kine)
Nr_{5R}	$\int_0^T \lvert \dot{x}_{55}(t)\rvert dt$	Norm of the 5DOF 5F Velocity Time History (JDS only) (kine·sec)

5.5 SDOF System Experiment

5.5.1 Assumed Structure

To begin with, a single-degree-of-freedom (SDOF) system is chosen as the target structure. Structural parameters are shown in Table 5.5. The mass is assumed to be 10 times as large as that of the original IFDL test system, and the stiffness is selected so that natural frequency of the system becomes 1 Hz. Also, damping ratio of the structure without damper specimen is selected to be 2%.

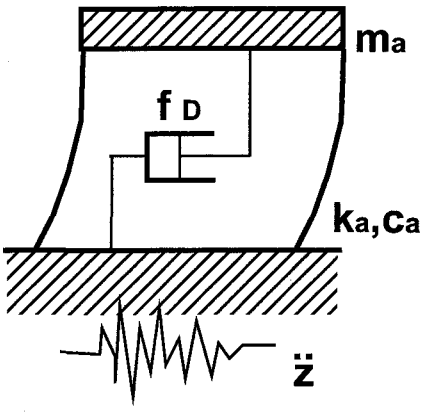

Figure 5.4: Target Structure (SDOF system)

Table 5.5: SDOF System Properties

Mass (ton)	248.53 ($10\times m_s$)
Natural Freq. (Hz)	1.0
Damping Ratio (%)	2.0

5.5.2 Preliminary Simulation

The feasible amplitude level for each assumed ground motion is determined prior to the experiment. With ground motions and estimated MR damper model represented by Eq.(4.6), the numerical simulations are conducted. The maximum ground motion levels for the experiment should be determined by taking these maximum responses and physical constraints of the test system into account. The limitations being considered are previously shown in Table 5.1.

Figures 5.5, 5.6, and 5.7 show relations between input ground motion level and maximum responses.

Consequently, it is determined that experiments are conducted with the maximum ground motion levels shown in Table 5.6.

Table 5.6: Test Property (SDOF structure)

Waveform	Maximum Level
Sinusoid (1.0 Hz)	5 gal
El Centro NS	30 gal
Kobe NS	30 gal

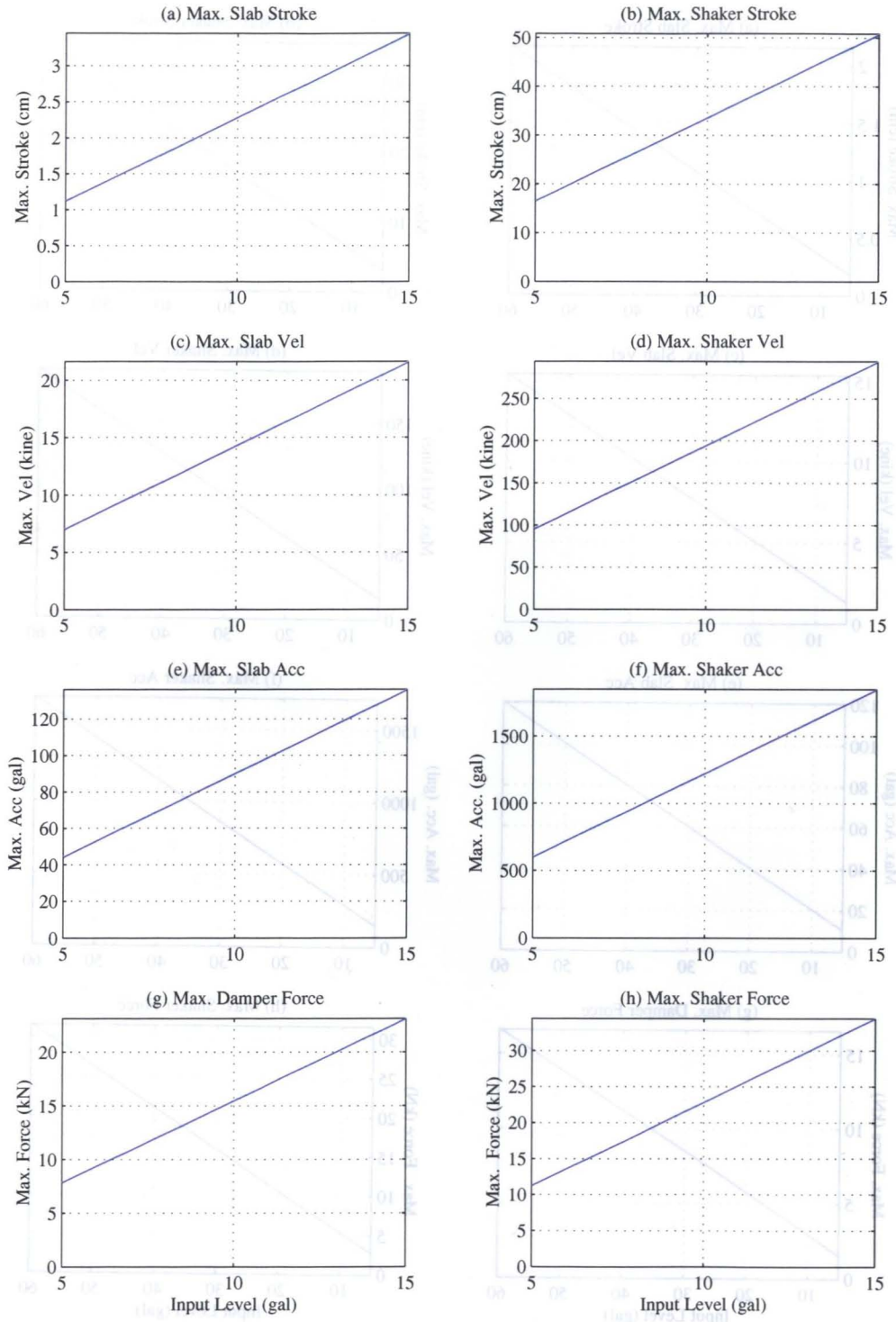

Figure 5.5: Maximum Input Level and Response (Sin 1 Hz)

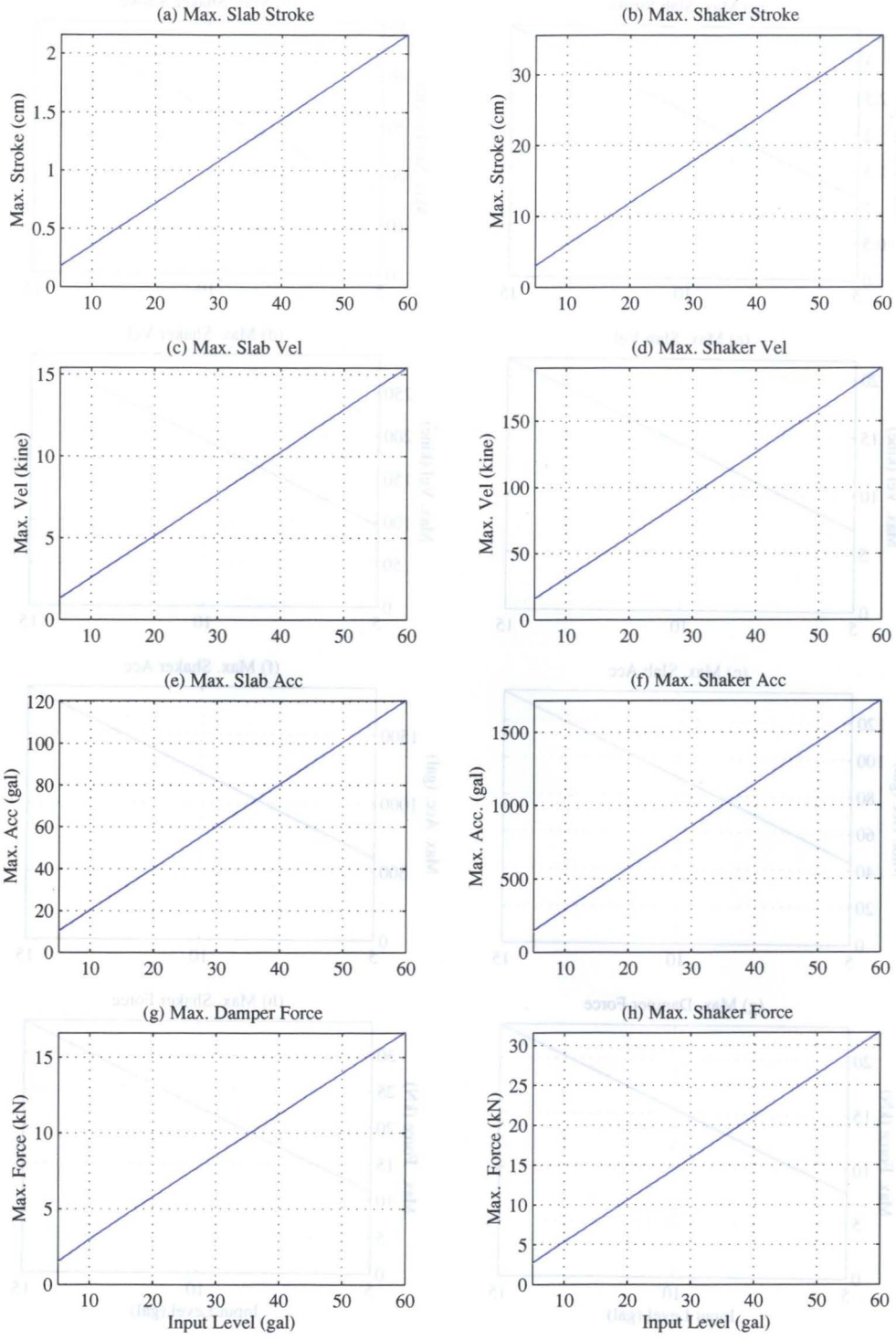

Figure 5.6: Maximum Input Level and Response (ECNS)

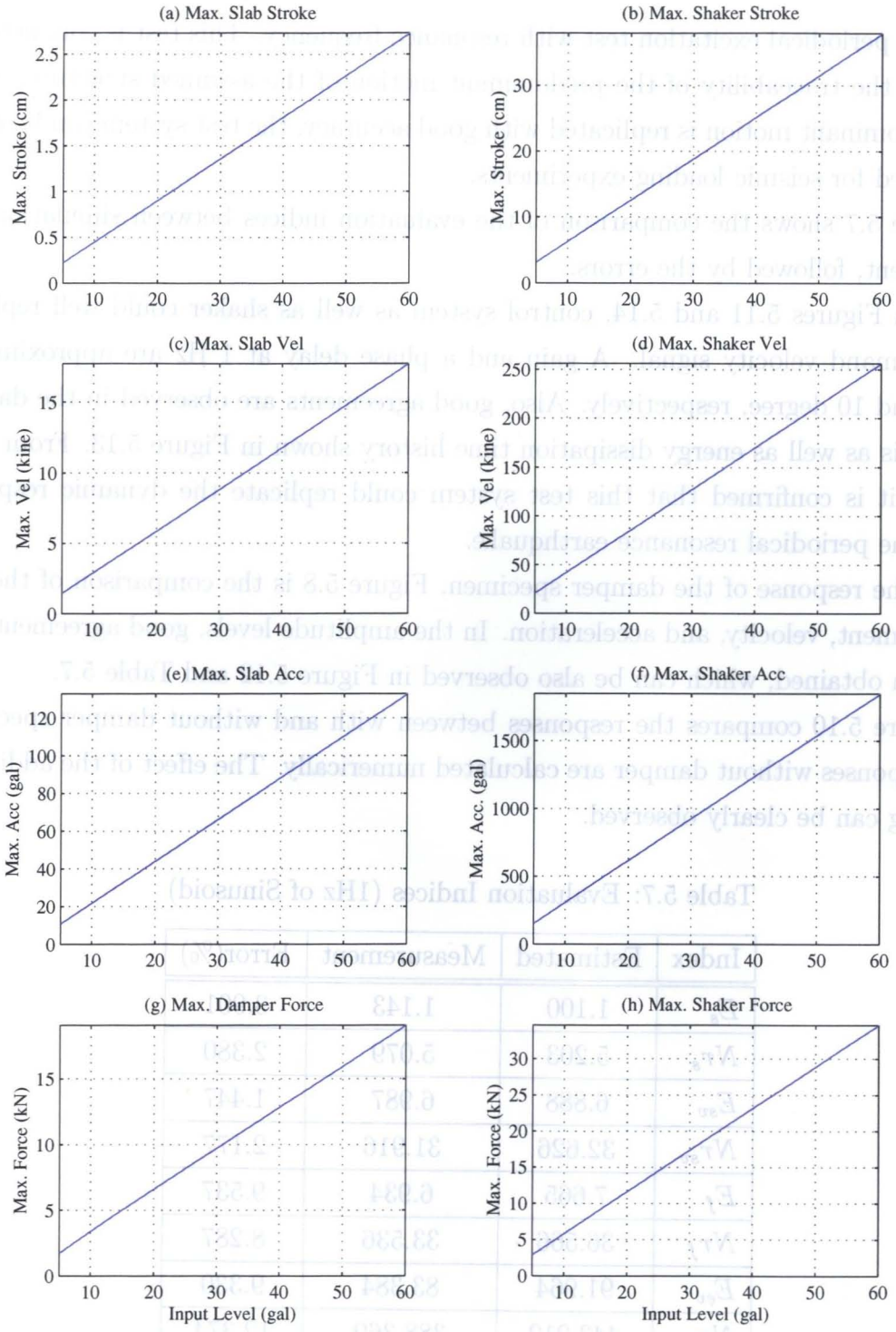

Figure 5.7: Maximum Input Level and Response (KBNS)

5.5.3 Experimental Results and Discussions

1 Hz of Sinusoid

This is a periodical excitation test with resonance frequency. This test is conducted to evaluate the traceability of the predominant motion of the assumed structure. Once the predominant motion is replicated with good accuracy, the test system can be ready to be used for seismic loading experiments.

Table 5.7 shows the comparison of the evaluation indices between simulation and experiment, followed by the errors.

From Figures 5.11 and 5.14, control system as well as shaker could well replicate the command velocity signal. A gain and a phase delay at 1 Hz are approximately -2 dB and 10 degree, respectively. Also, good agreements are observed in the damper hysteresis as well as energy dissipation time history shown in Figure 5.13. From these results, it is confirmed that this test system could replicate the dynamic responses under the periodical resonance earthquake.

As the response of the damper specimen, Figure 5.8 is the comparison of the slab displacement, velocity, and acceleration. In the amplitude levels, good agreements can be again obtained, which can be also observed in Figure 5.12 and Table 5.7.

Figure 5.10 compares the responses between with and without damper specimen. The responses without damper are calculated numerically. The effect of the additional damping can be clearly observed.

Table 5.7: Evaluation Indices (1Hz of Sinusoid)

Index	Estimated	Measurement	Error(%)
E_s	1.100	1.143	3.901
Nr_s	5.203	5.079	2.380
E_{sv}	6.888	6.987	1.447
Nr_{sv}	32.626	31.916	2.177
E_f	7.665	6.934	9.537
Nr_f	36.566	33.536	8.287
E_{ev}	91.964	83.384	9.330
Nr_{ev}	443.212	388.369	12.374
E_{ef}	10.793	10.187	5.617
Nr_{ef}	51.551	44.239	14.184
E_{de}	1.618	1.394	13.834

El Centro NS Wave

On the basis of the results obtained in the periodical excitation tests, earthquake excitation tests are conducted. Table 5.8 shows the comparison of the evaluation indices.

From Figures 5.18 and 5.21, the PID control could work effectively for the wide-range command signal. The gain at 1 Hz is approximately -2 dB.

Regarding the damper response, it is observed from Figure 5.20 that estimated algebraic model gives slight a large reaction force at around maximum velocity. Since the model is composed based on periodical excitations, it may not represent the wide-range hysteretic characteristic precisely. Nevertheless, the difference is limited to the tolerable amount from the viewpoint of the energy absorbance. Good agreement can be observed in the maximum stroke and stroke velocity, which can be found in Figure 5.15. In the after-shock motion, experimental results show the larger responses. Several factors are thought to be the major reason for the phenomenon. One of them is the effect of the time delay. In general, the control error is accumulated as time goes, and it may distort the control signal of the shaker. Another possibility is the nonlinearity existing in the test system and damper specimen. Since the concrete-slab is supported by the rubber and roller supports in the IFDL test system, the strong nonlinear phenomena such as friction take place in the small response region, and so is the shaker device. It goes without saying that the uncertainties in the damper algebraic model and identified IFDL dynamics in the small response region might have great effect on the simulation. In the frequency domain response shown in Figure 5.19, however, good agreement in both peak values and tendency can be observed.

Figure 5.17 compares the responses between with and without damper specimen. As observed, only a slight contribution from the additional damping appears.

Kobe NS Wave

As another earthquake loading test, Kobe NS input is selected. Figure 5.27 shows the comparison of the damper responses between simulation and measurement. Although a slight difference appears in the damper stroke, good agreement can be observed in the energy absorbance time history. Also, from Figure 5.28, the shaker compensation process works again effectively in this case. The gain at 1 Hz is also approximately -2 dB. Figures 5.22 and 5.26 shows the time histories and corresponding frequency responses of the damper specimen. Compared to the El Centro NS input, better agreement can be obtained, particularly in the post-shock regions. From Figure 5.24, effectiveness of the damper in response reductions can be observed.

Table 5.8: Evaluation Indices (ECNS)

Index	Estimated	Measurement	Error(%)
E_s	1.020	0.981	3.795
Nr_s	3.220	3.582	11.262
E_{sv}	7.338	7.017	4.384
Nr_{sv}	21.420	23.221	8.407
E_f	8.134	6.543	19.559
Nr_f	24.442	32.317	32.219
E_{ev}	87.844	72.007	18.029
Nr_{ev}	289.512	310.536	7.262
E_{ef}	14.646	11.393	22.208
Nr_{ef}	39.816	36.622	8.023
E_{de}	0.670	0.621	7.390

Table 5.9: Evaluation Indices (KBNS)

Index	Estimated	Measurement	Error(%)
E_s	1.363	1.333	2.234
Nr_s	4.835	5.258	8.745
E_{sv}	8.920	8.511	4.591
Nr_{sv}	31.120	33.214	6.728
E_f	9.816	8.350	14.942
Nr_f	35.389	46.445	31.243
E_{ev}	125.414	104.268	16.862
Nr_{ev}	414.440	441.370	6.498
E_{ef}	17.142	12.992	24.211
Nr_{ef}	51.709	51.114	1.152
E_{de}	1.094	1.030	5.838

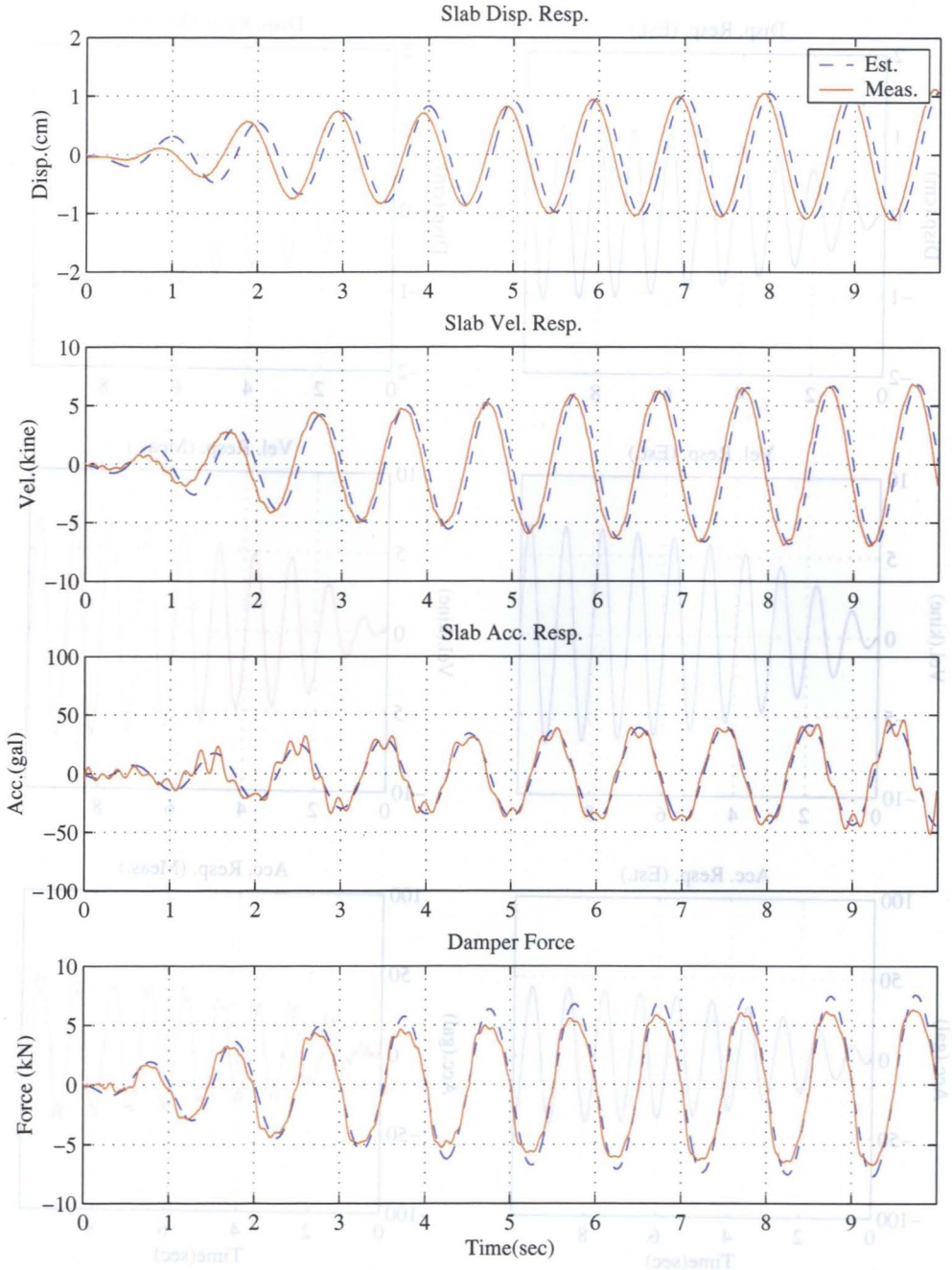

Figure 5.8: Comparison of the Structural Response (Sin 1 Hz, 5 gal)

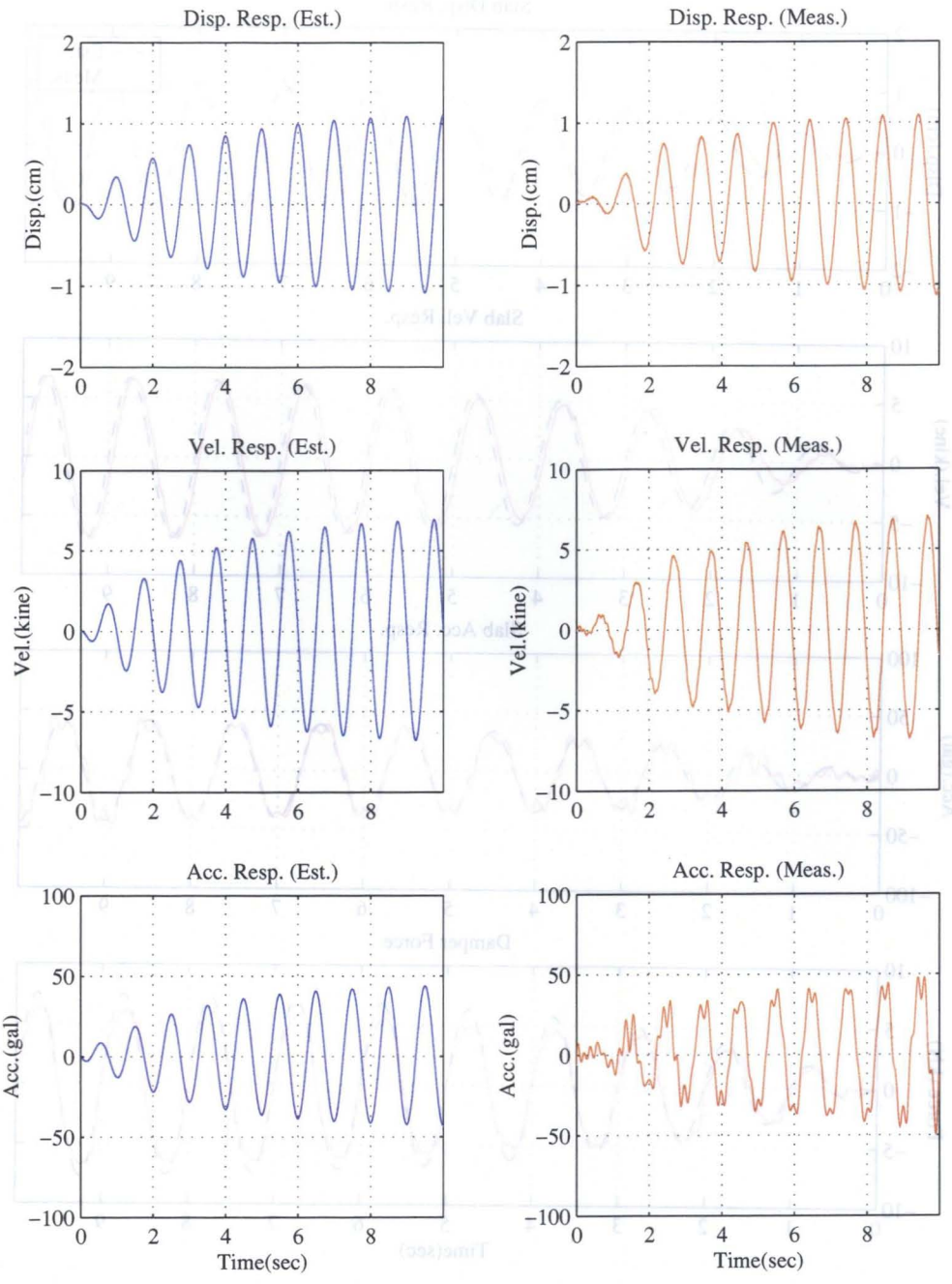

Figure 5.9: Comparison of the Structural Response (Sin 1 Hz, 5 gal)

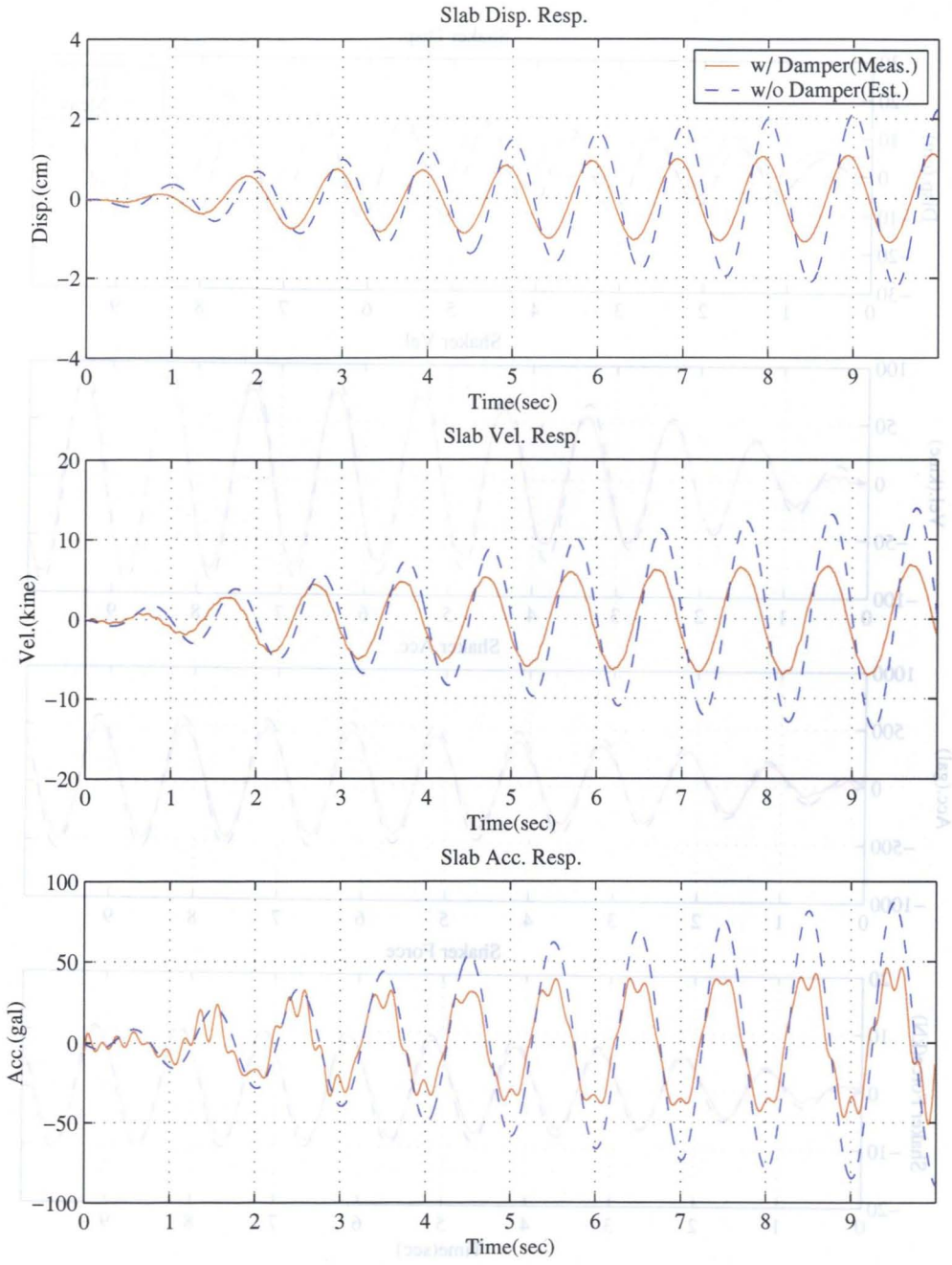

Figure 5.10: Comparison of the Structural Response (Sin 1 Hz, w/ & w/o damper)

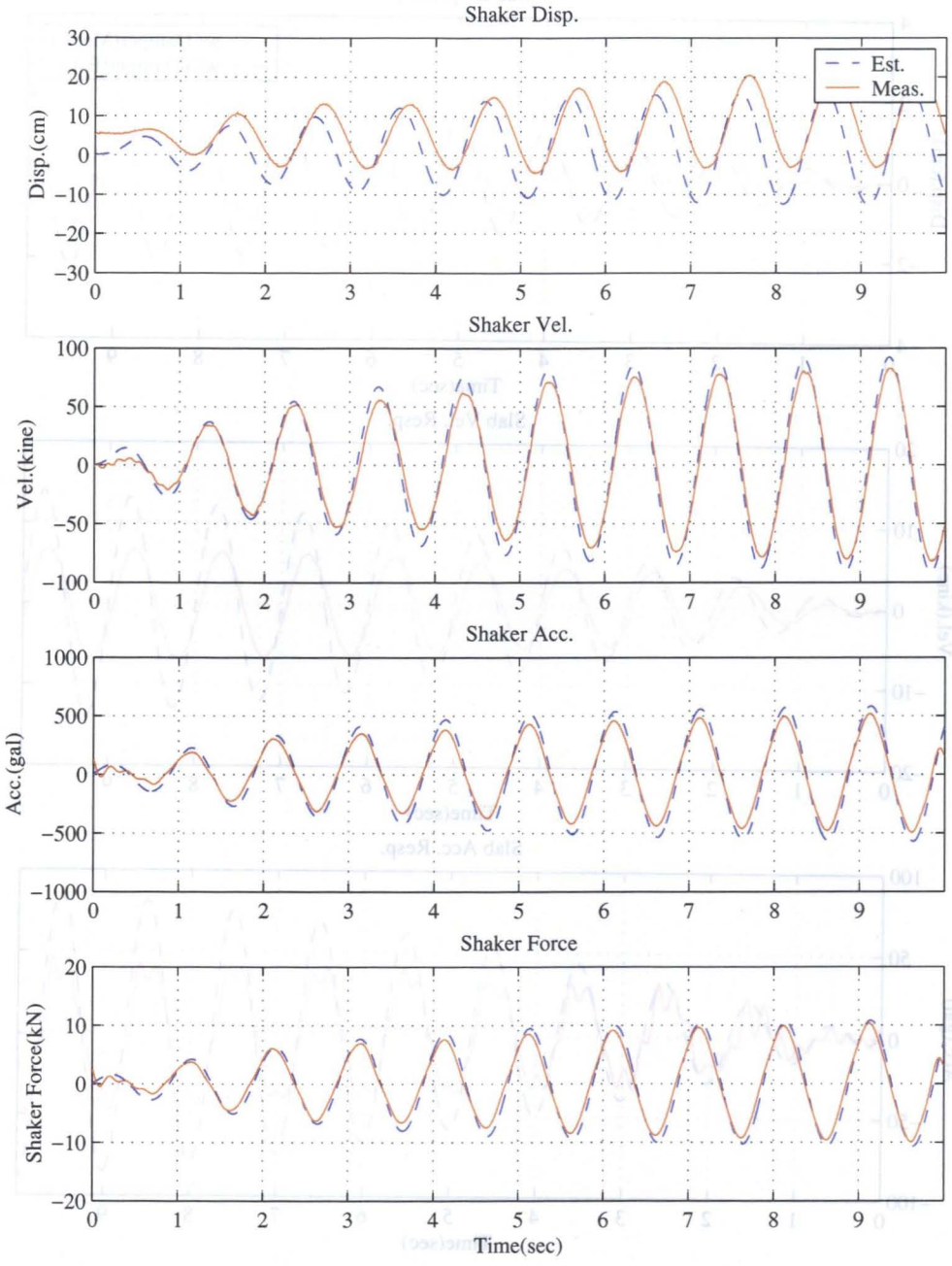

Figure 5.11: Shaker Response (Sin 1 Hz, 5 gal)

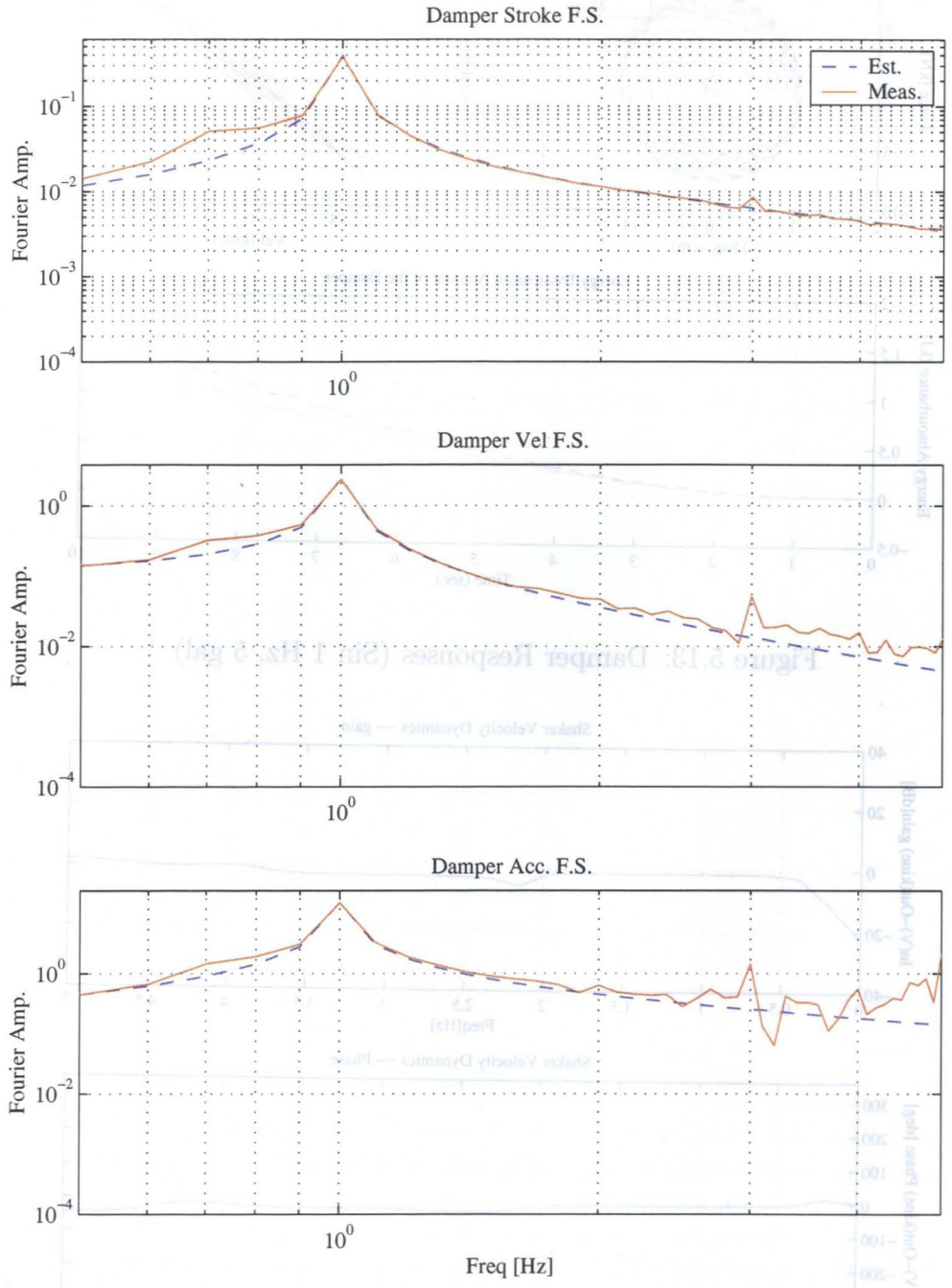

Figure 5.12: Comparison of Fourier Spectra (Sin 1 Hz, 5 gal)

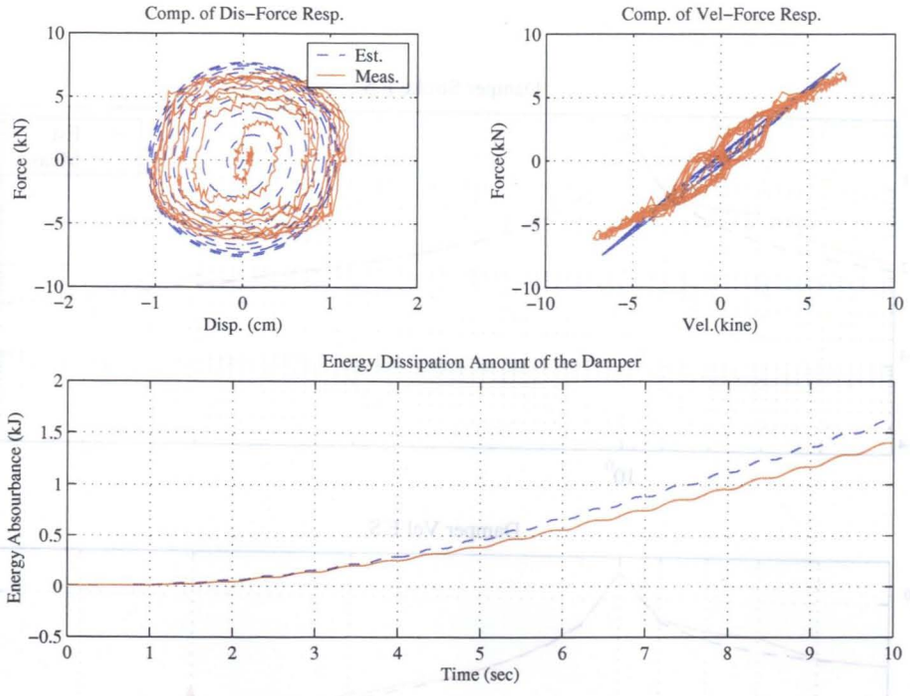

Figure 5.13: Damper Responses (Sin 1 Hz, 5 gal)

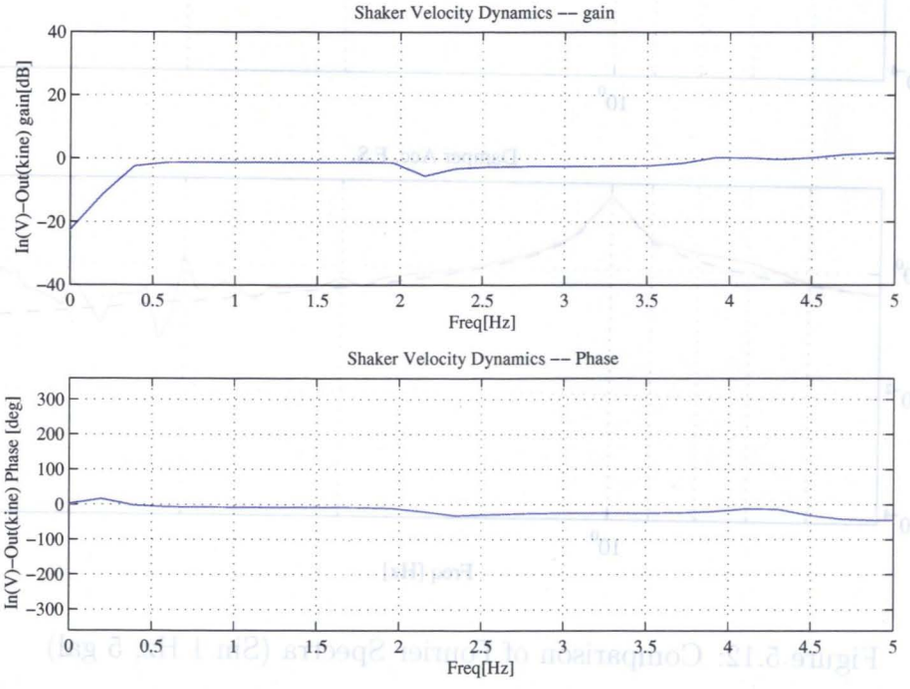

Figure 5.14: Transfer Function from Command to the Shaker Relative Velocity

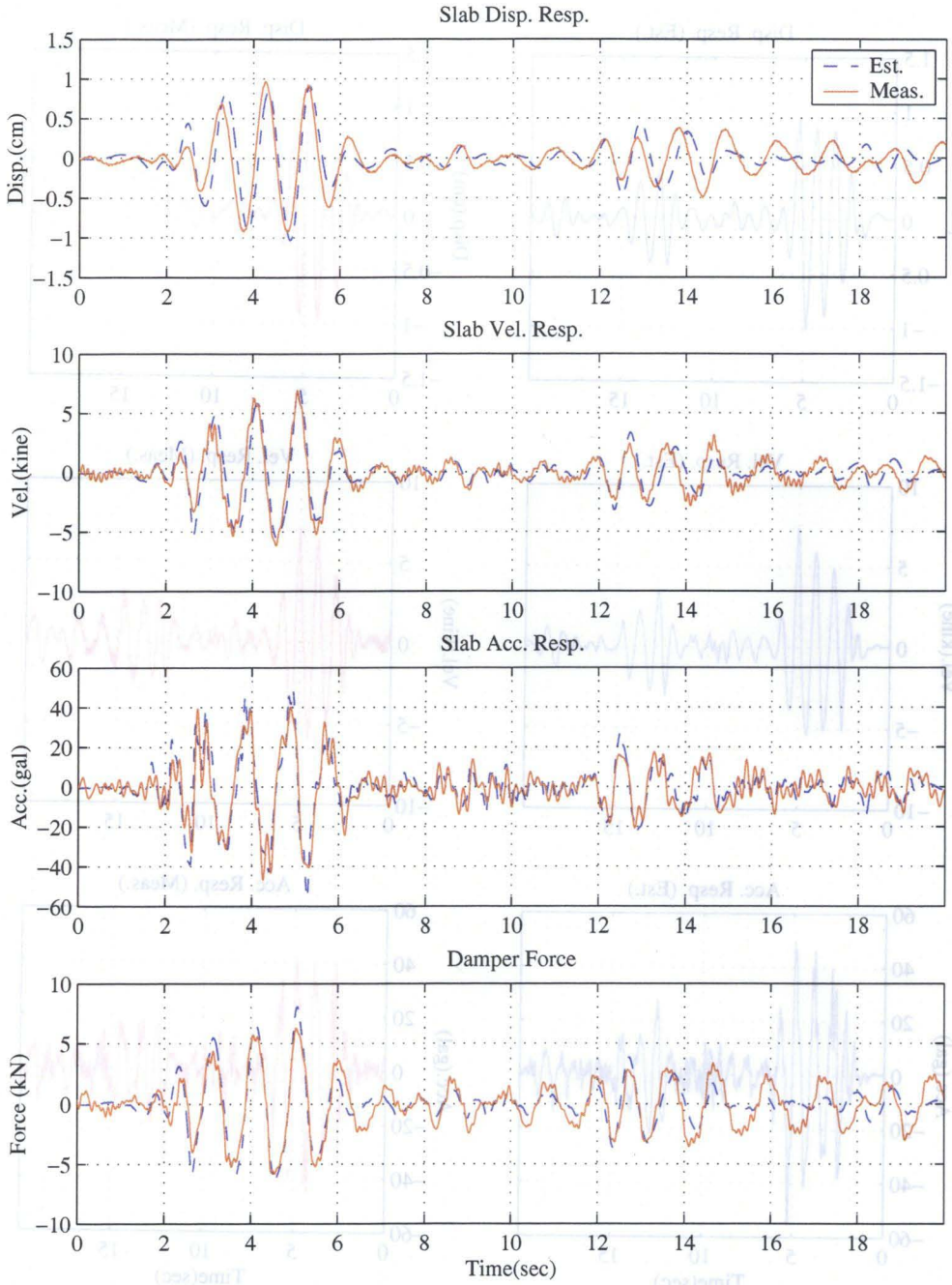

Figure 5.15: Comparison of the Structural Response (ECNS 30gal)

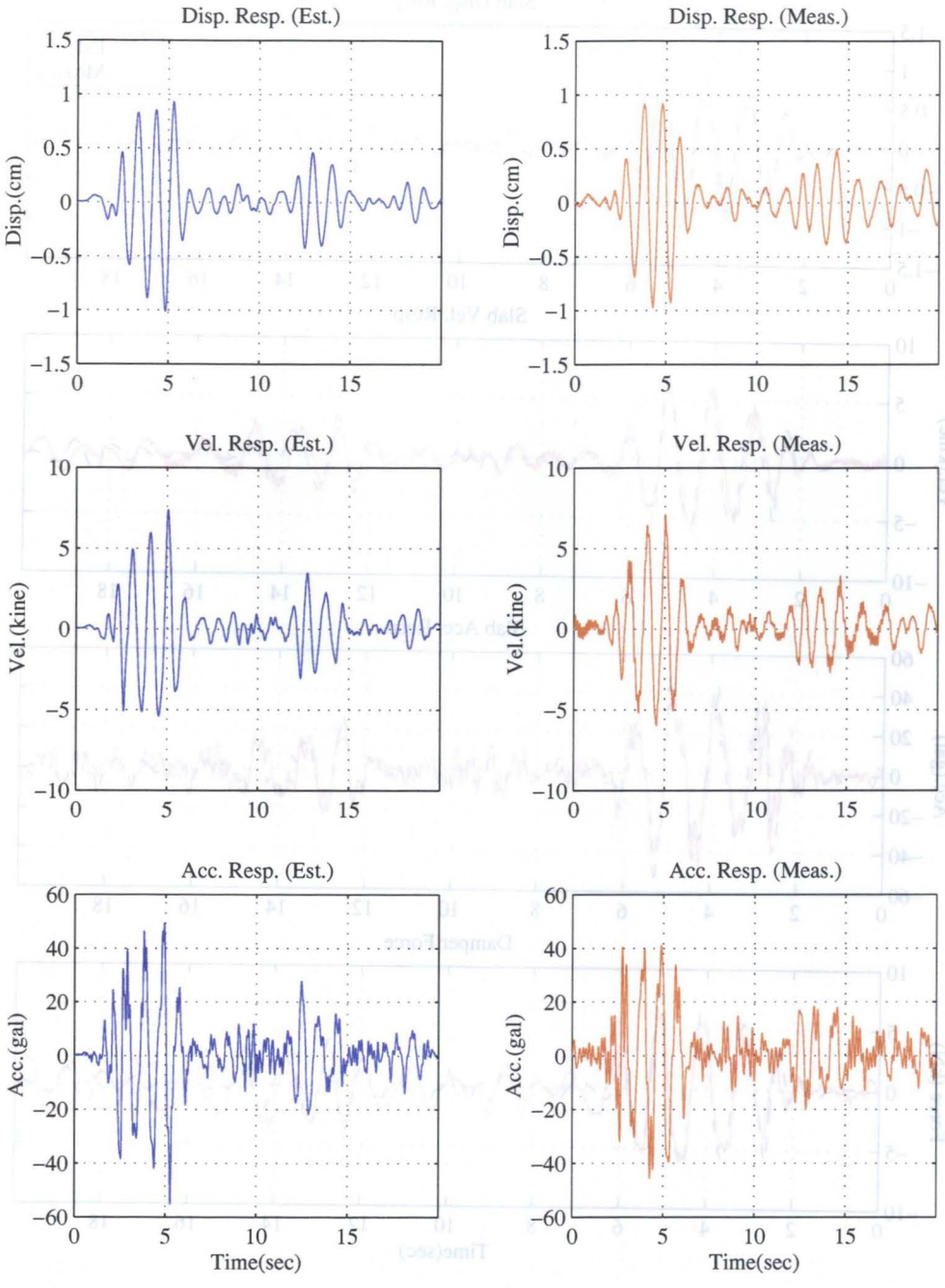

Figure 5.16: Comparison of the Structural Response(ECNS 30gal)

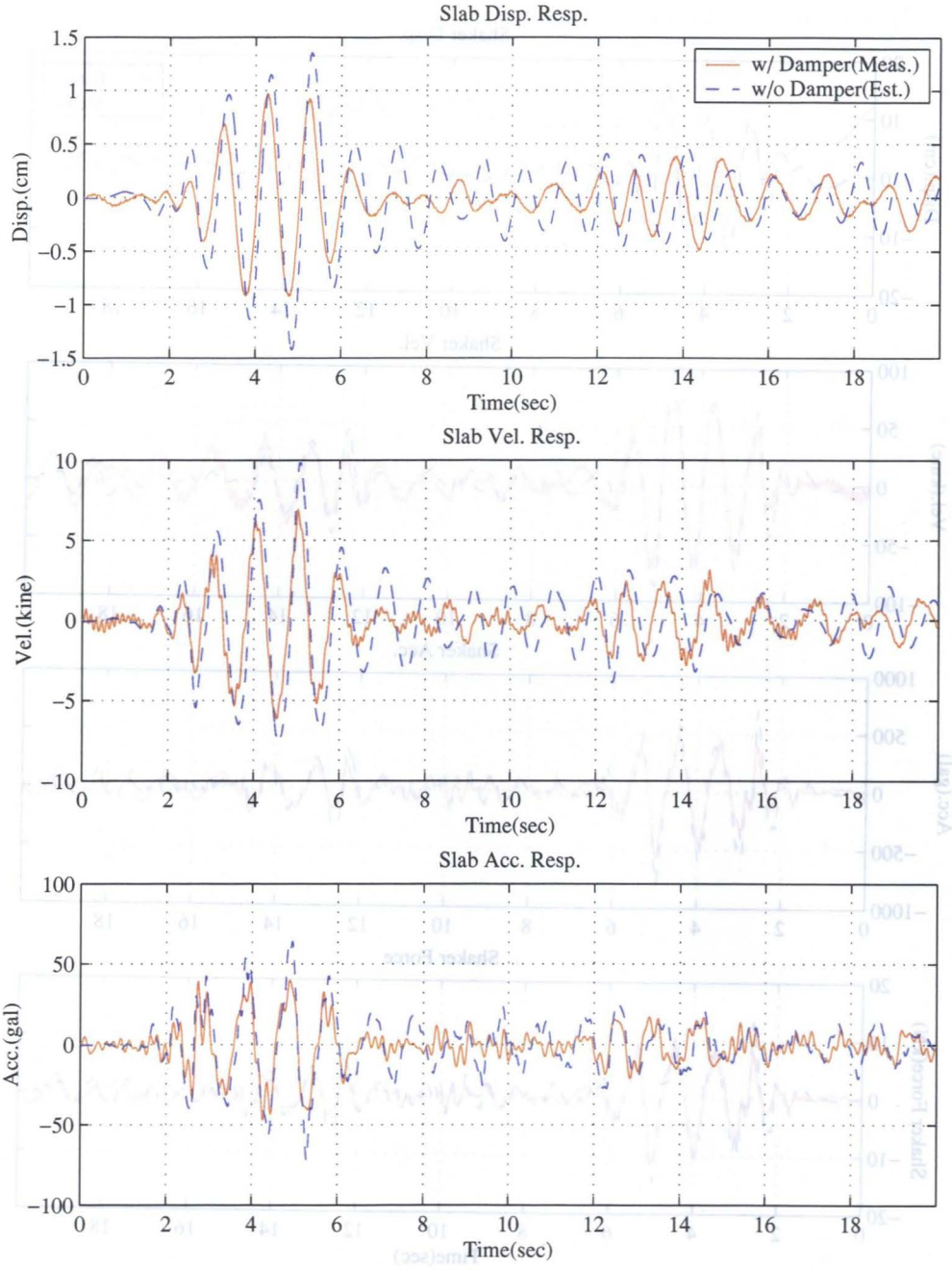

Figure 5.17: Comparison of the Structural Response (ECNS 30gal, w/ & w/o damper)

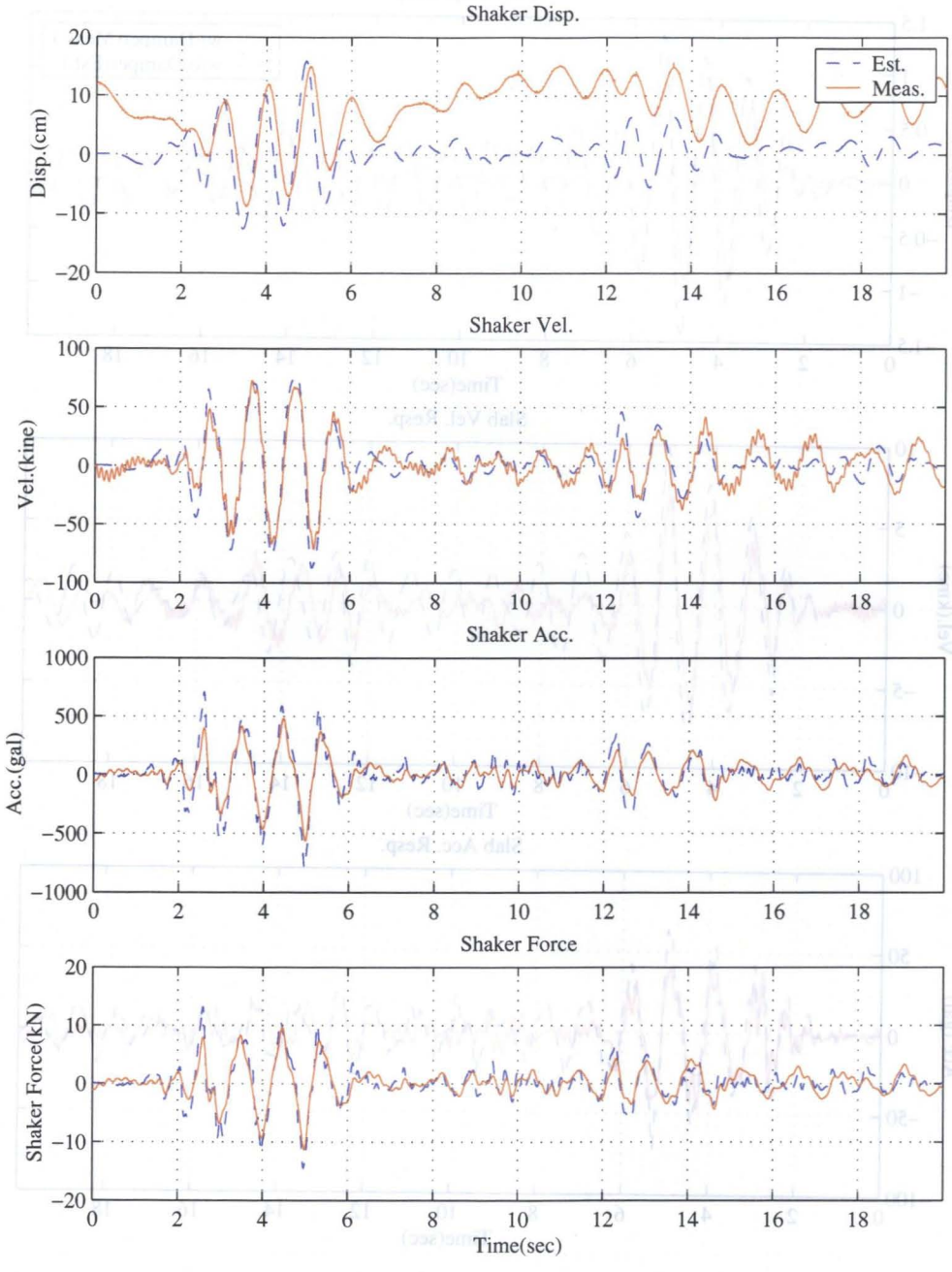

Figure 5.18: Shaker Response (ECNS 30gal)

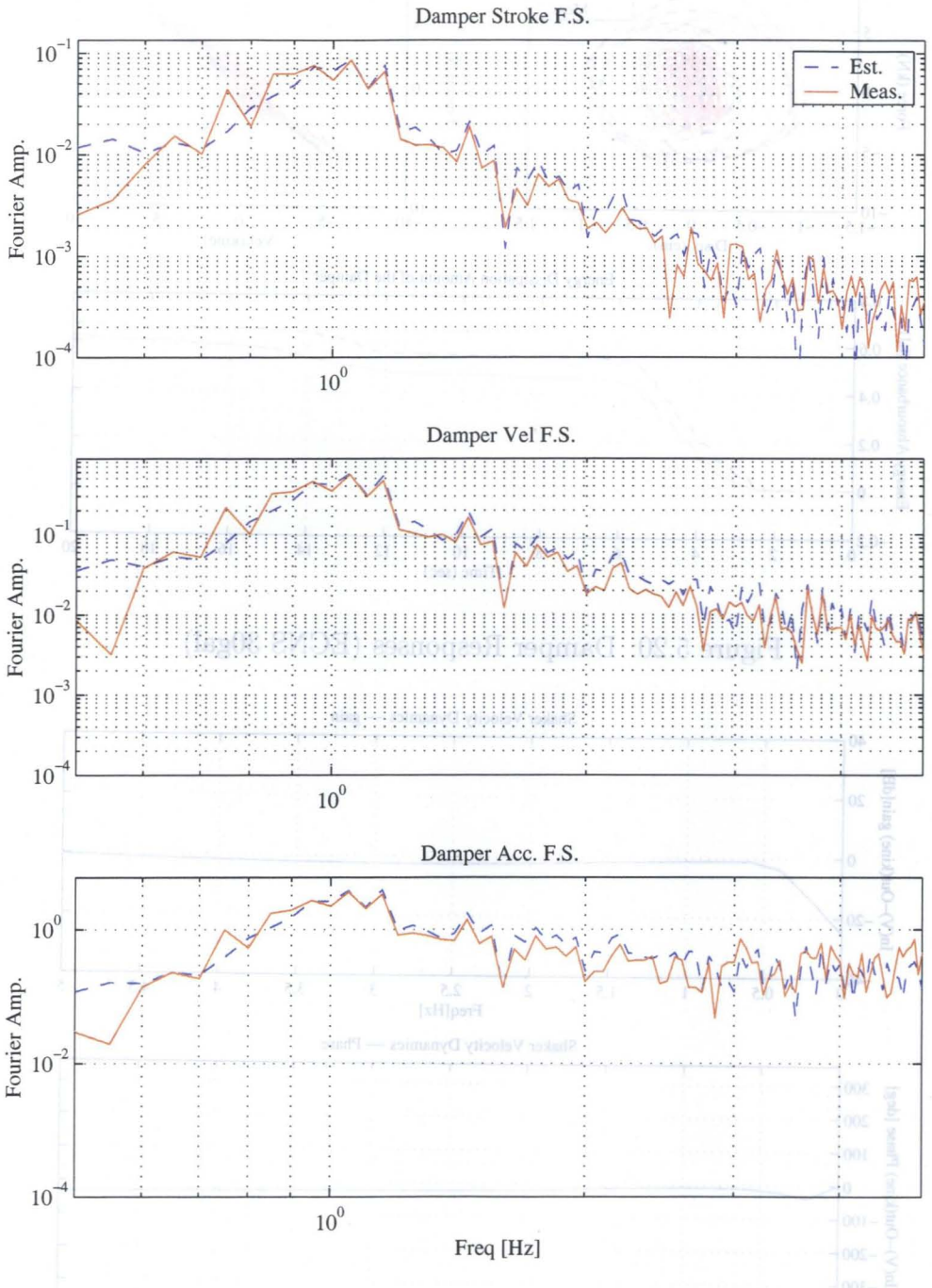

Figure 5.19: Comparison of Fourier Spectra (ECNS 30gal)

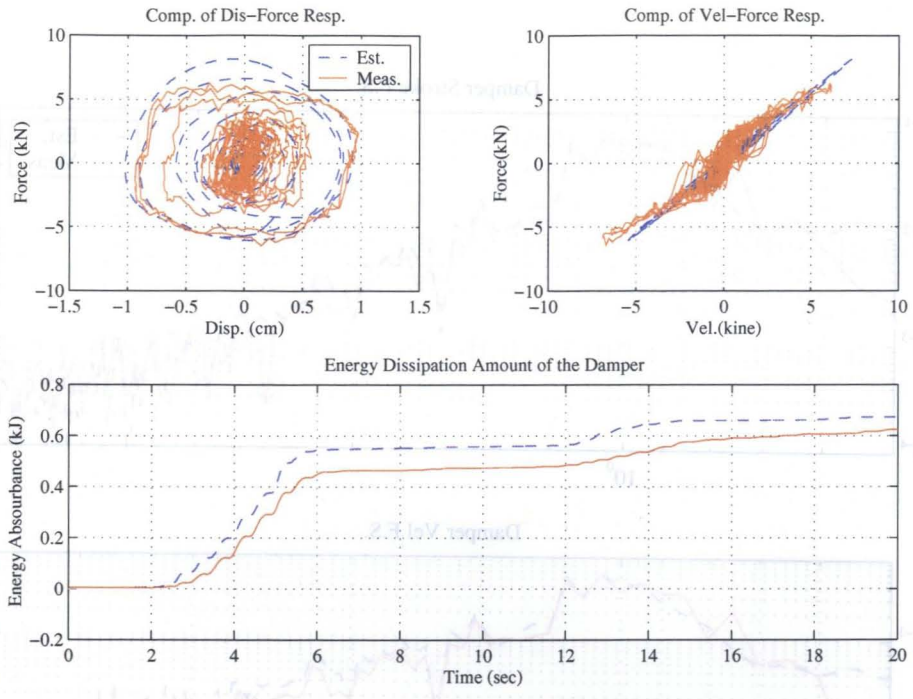

Figure 5.20: Damper Responses (ECNS 30gal)

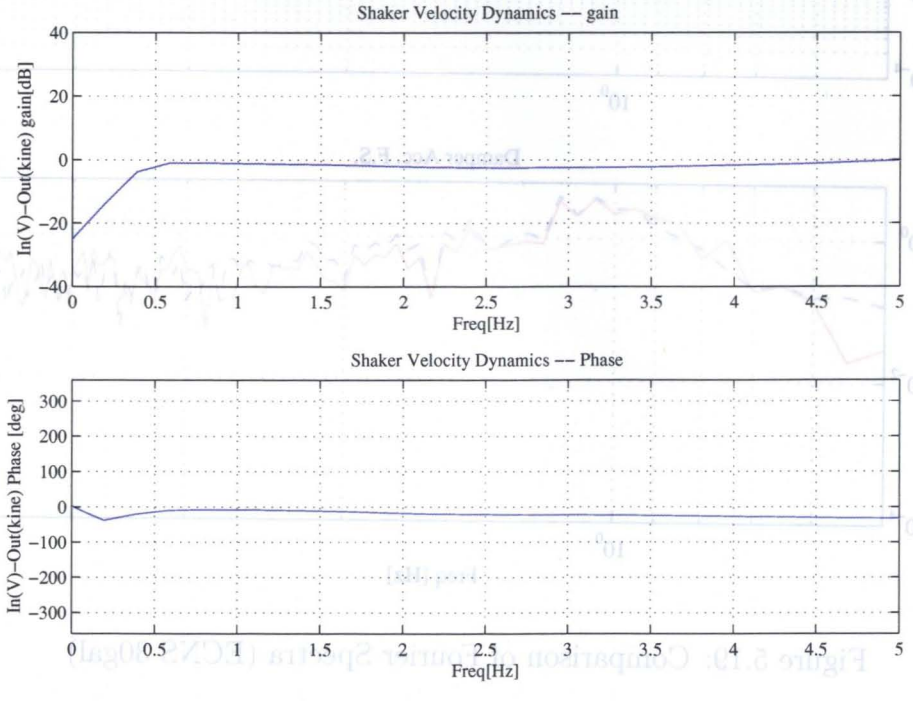

Figure 5.21: Transfer Function from Command to the Shaker Relative Velocity

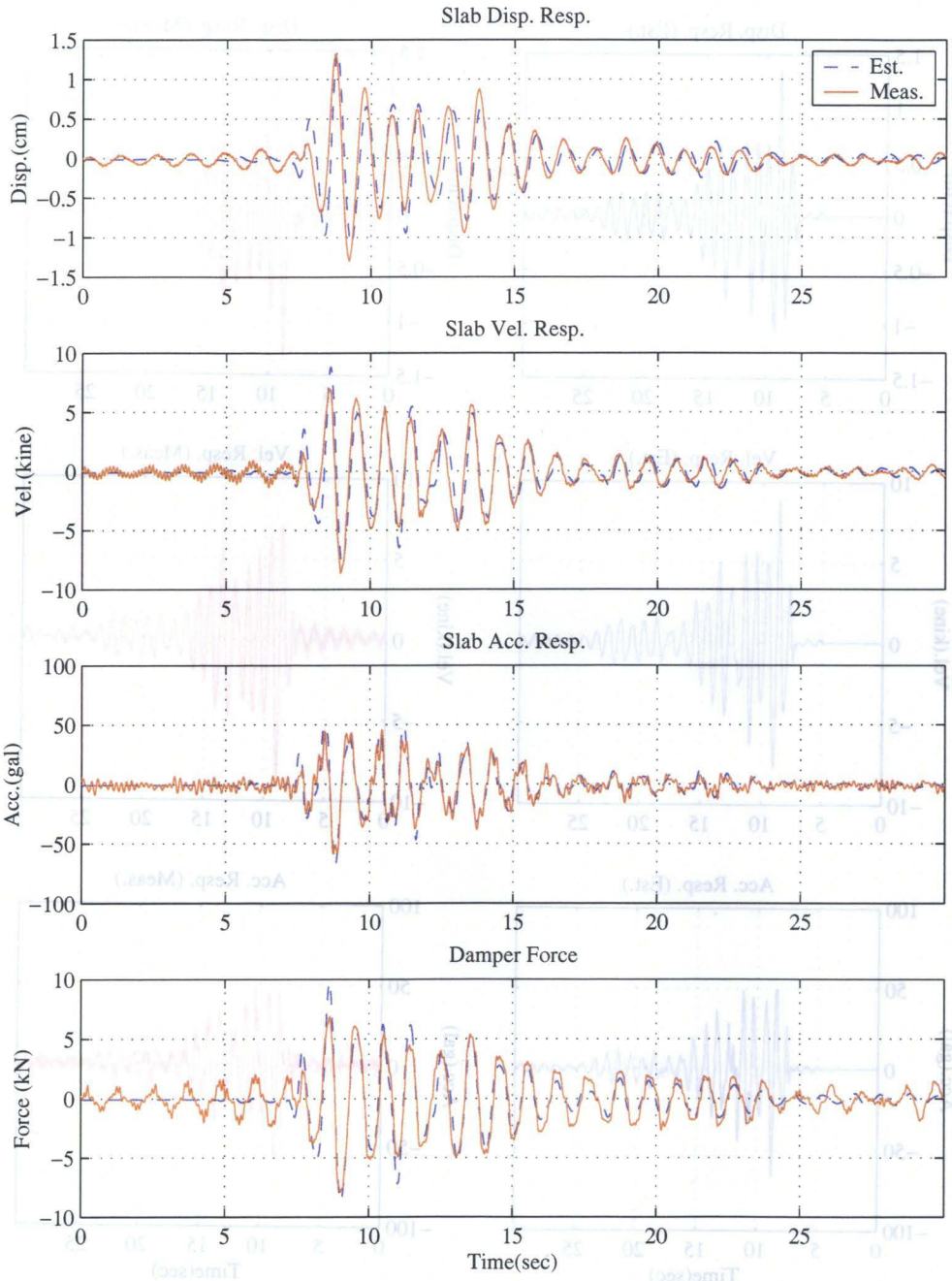

Figure 5.22: Comparison of the Structural Response (KBNS 30gal)

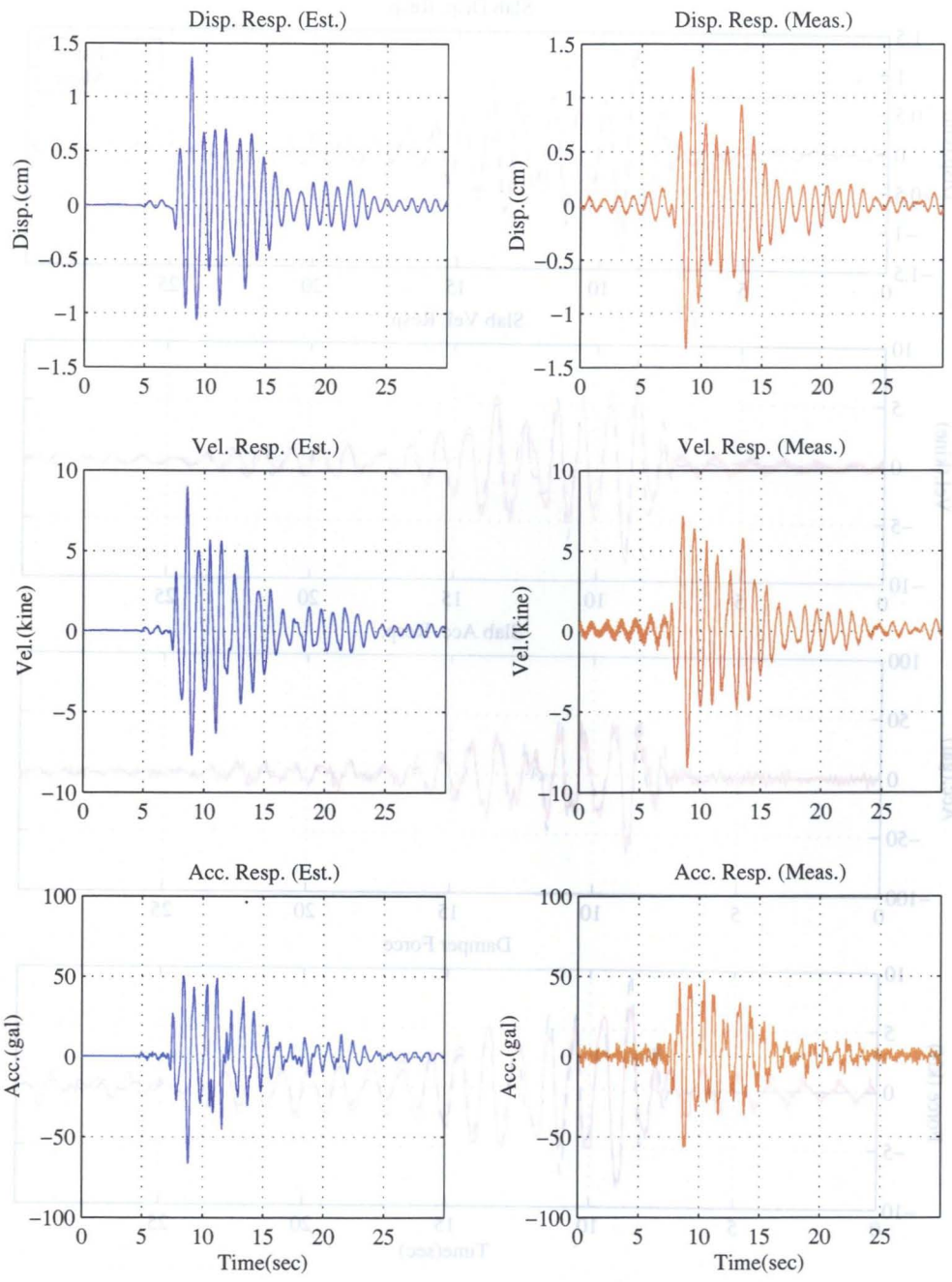

Figure 5.23: Comparison of the Structural Response(KBNS 30gal)

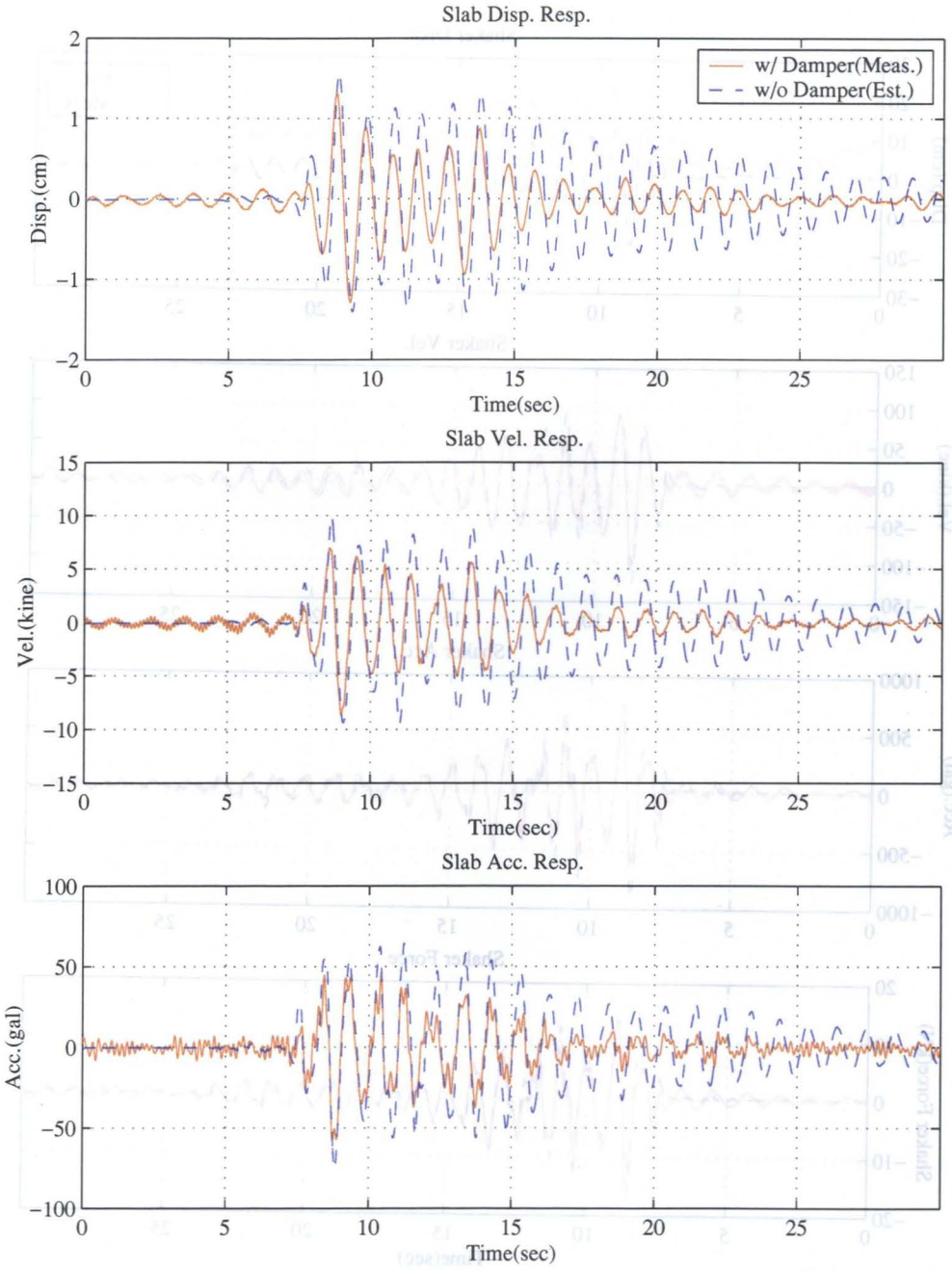

Figure 5.24: Comparison of the Structural Response (KBNS 30gal, w/ & w/o damper)

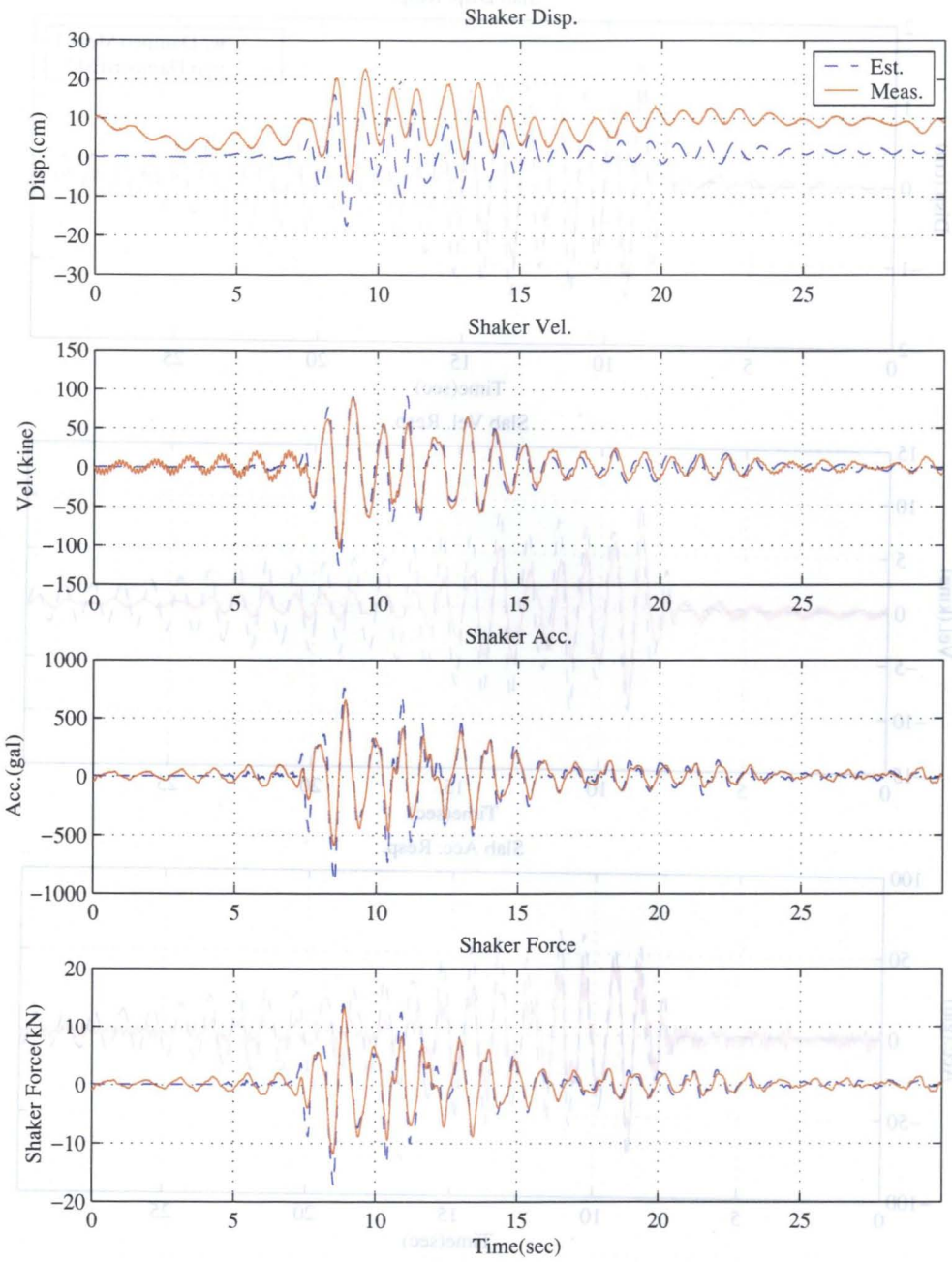

Figure 5.25: Shaker Response (KBNS 30gal)

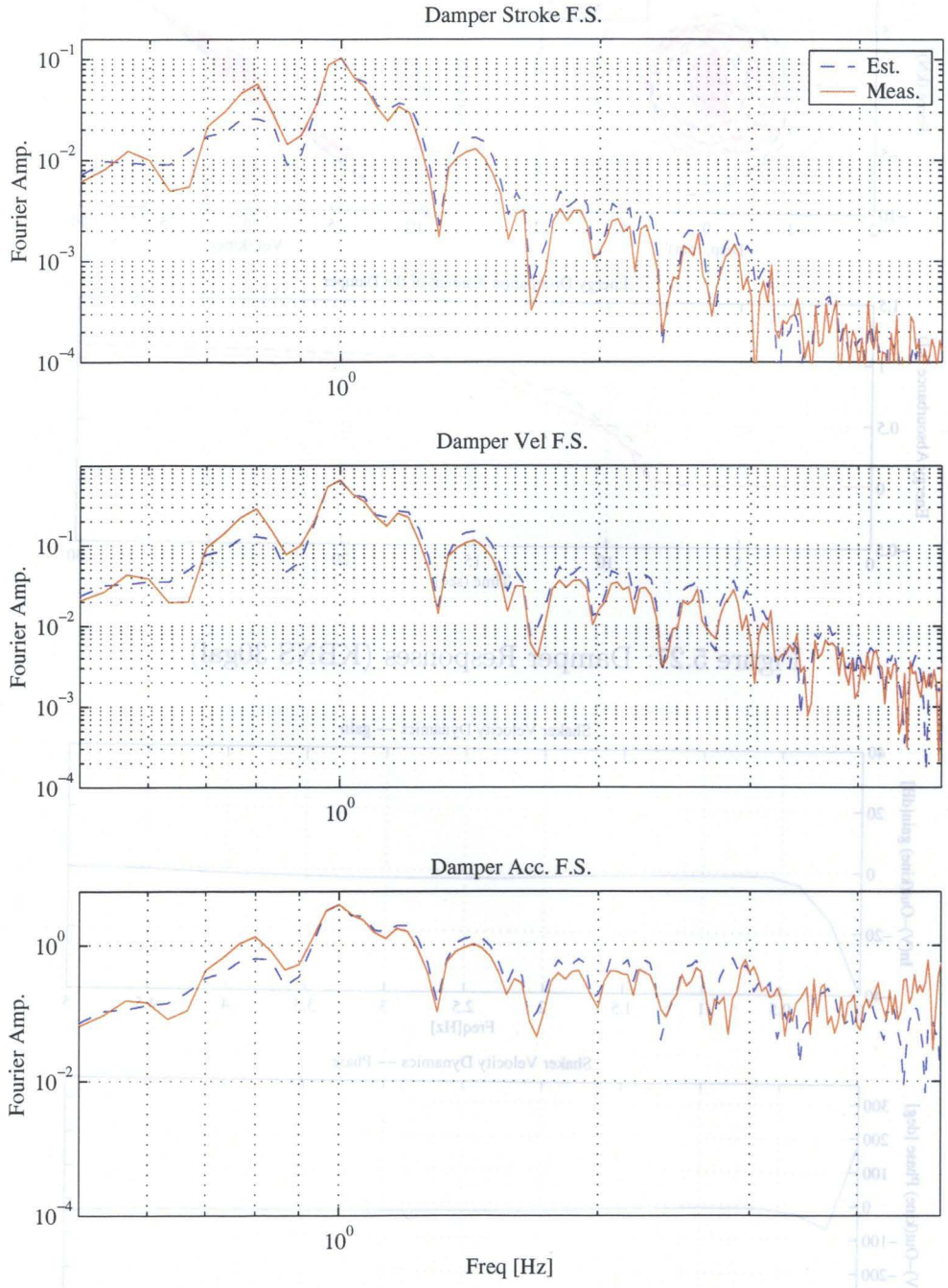

Figure 5.26: Comparison of Fourier Spectra (KBNS 30gal)

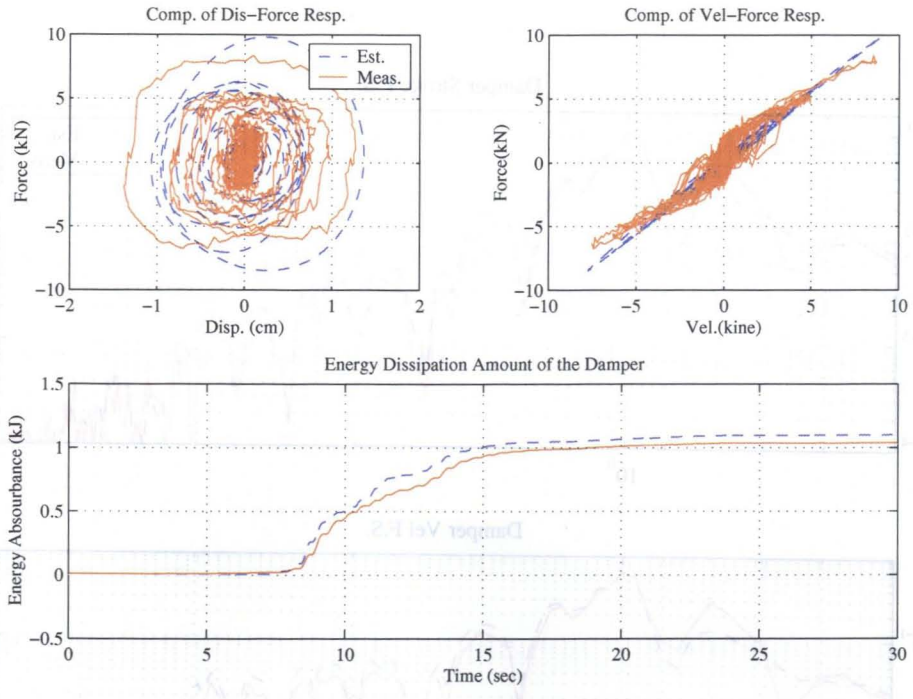

Figure 5.27: Damper Responses (KBNS 30gal)

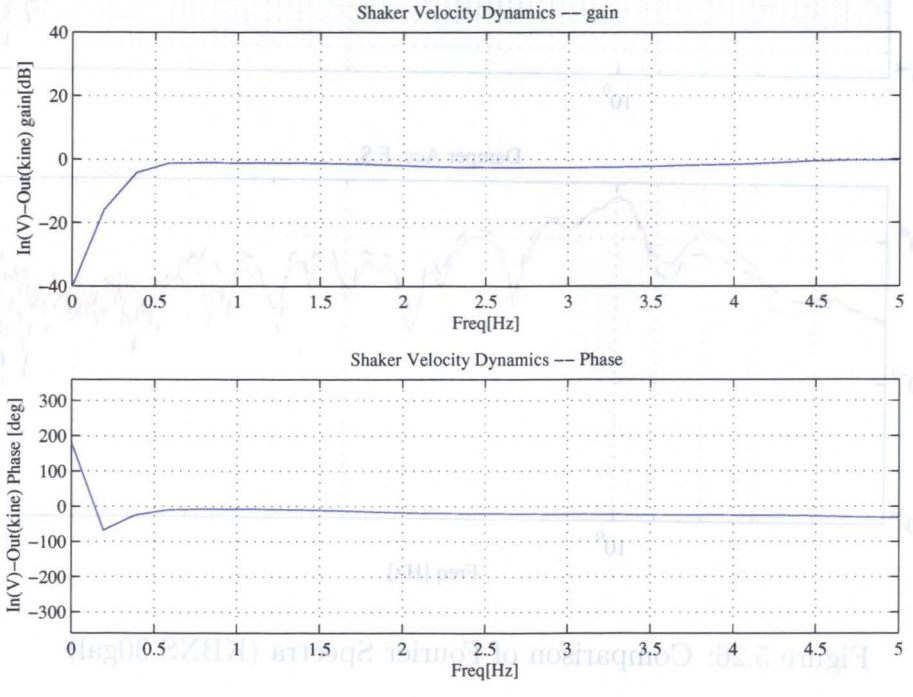

Figure 5.28: Transfer Function from Command to the Shaker Relative Velocity

5.6 MDOF System Experiment

5.6.1 Assumed Structure

The experiment assuming the MDOF structure is also conducted. The model structure is depicted in Figure 5.29. Damper specimen is attached between 3rd floors of each frame structure. In the experiment, the relative displacement, velocity, and acceleration at the damper location are calculated and replicated by the IFDL test system. Table 5.10 and 5.11 shows the properties of both structures. One of the main objectives to conduct a MDOF experiment is to examine the potential to replicate multiple modes.

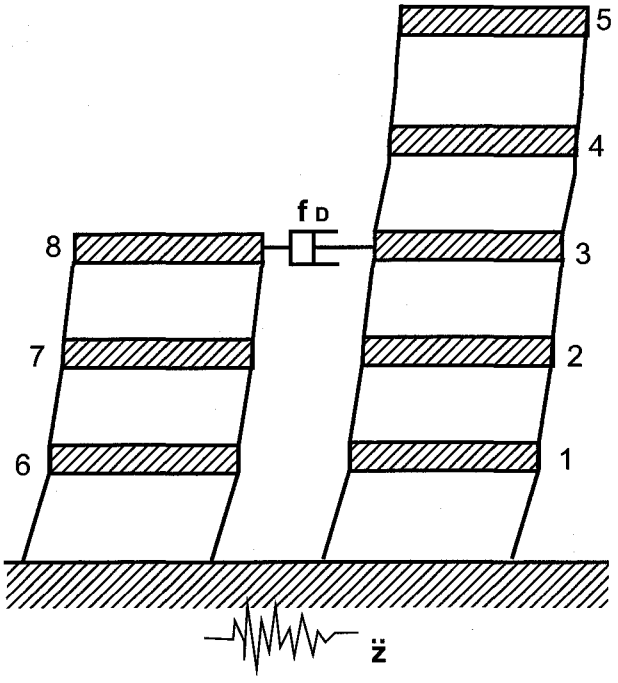

Figure 5.29: Target Structure (Joint Damper System)

5.6.2 Preliminary Simulation

The same preliminary studies with those for the SDOF structure are carried out for the assumed MDOF system in order to determine the ground motion levels. Figures 5.30, 5.31, 5.32, and 5.33 show relations between input ground motion level and maximum responses. As frequencies for the periodical ground motions, 1.75 Hz and 2.41 Hz are selected, which correspond to the natural frequencies of the uncoupled 5-story and 3-story frame structures. Other than those, El Centro NS and Kobe NS inputs are again assumed as earthquake ground motions. Table 5.12 shows the maximum ground

Table 5.10: Structural Parameters (5DOF)

Mode	1st	2nd	3rd	4th	5th
Natural Freq. (Hz)	1.75	5.42	9.17	14.35	18.68
Damping Ratio (%)	1.28	1.0	0.8	0.9	1.1
Total Mass (ton)	163.1				

Table 5.11: Structural Parameters (3DOF)

Mode	1st	2nd	3rd
Natural Freq. (Hz)	2.41	7.23	13.91
Damping Ratio (%)	1.47	4.5	5.5
Total Mass (ton)	61.17		

Table 5.12: Test Property (JDS structure)

Waveform	Maximum Level
Sinusoid (1.75 Hz)	10 gal
Sinusoid (2.41 Hz)	10 gal
El Centro NS	30 gal
Kobe NS	30 gal

motion levels for the experiment, which are determined by taking into account the several constraints of the test system shown in Table 5.1. From these figures, it is found that the estimated response exceeds maximum force capacity in some cases. However, unstable vibrations are observed when using the ground motions that meet the force constraints. In such a reason, ground motion levels shown Table 5.1 are determined from the viewpoint of preventing the unstable motions of the shaker device.

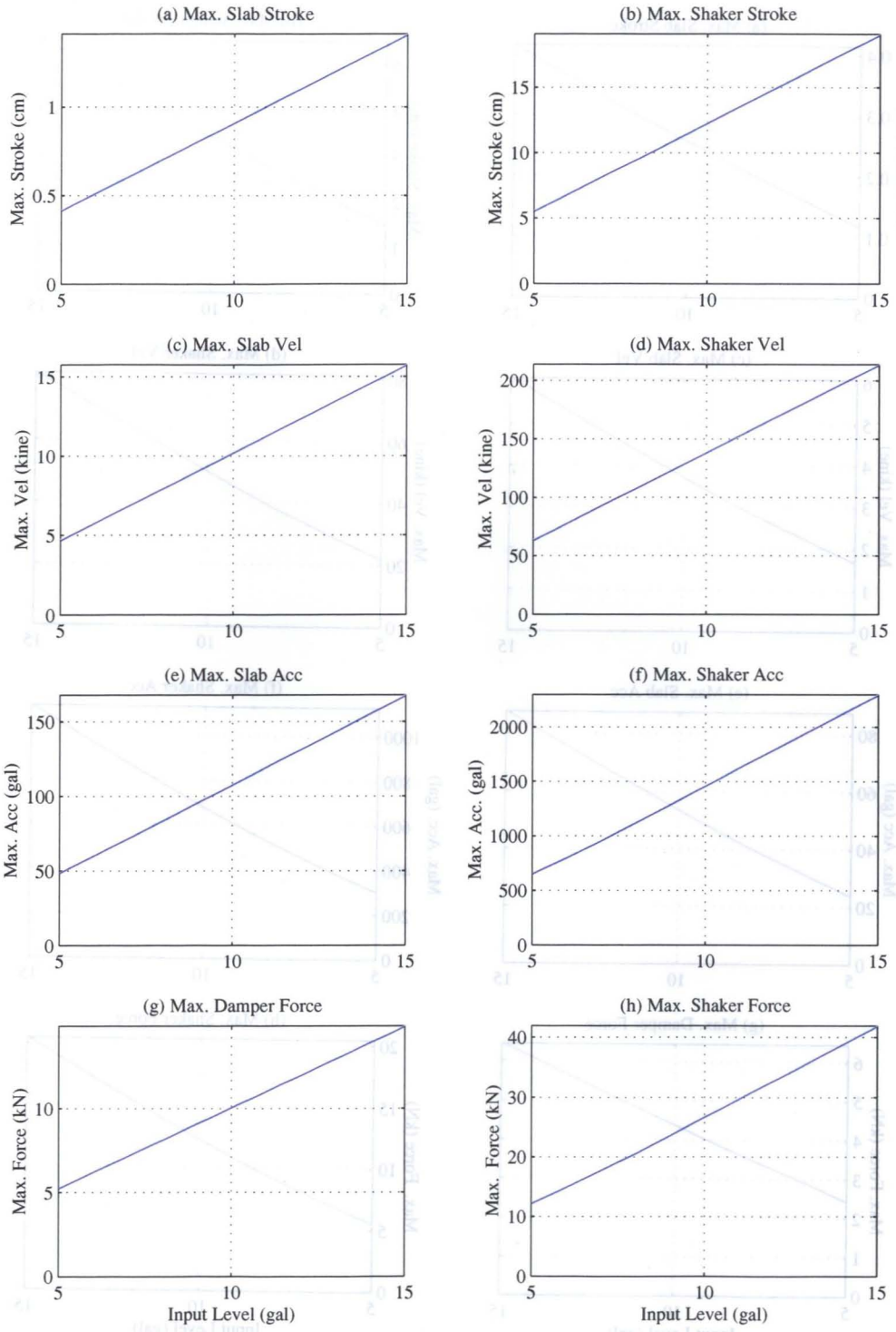

Figure 5.30: Maximum Input Level and Response (Sin 1.75 Hz)

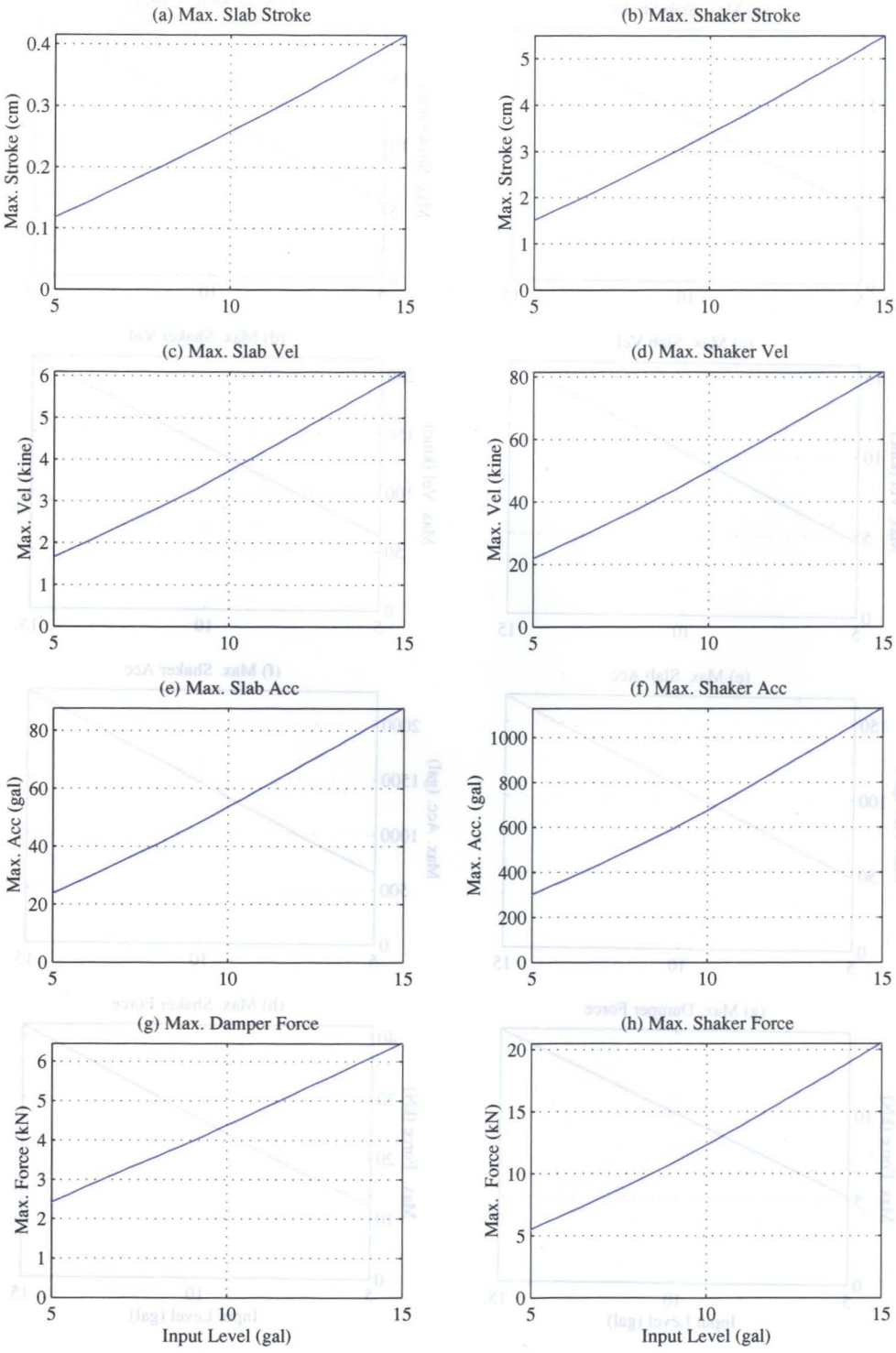

Figure 5.31: Maximum Input Level and Response (Sin 2.41 Hz)

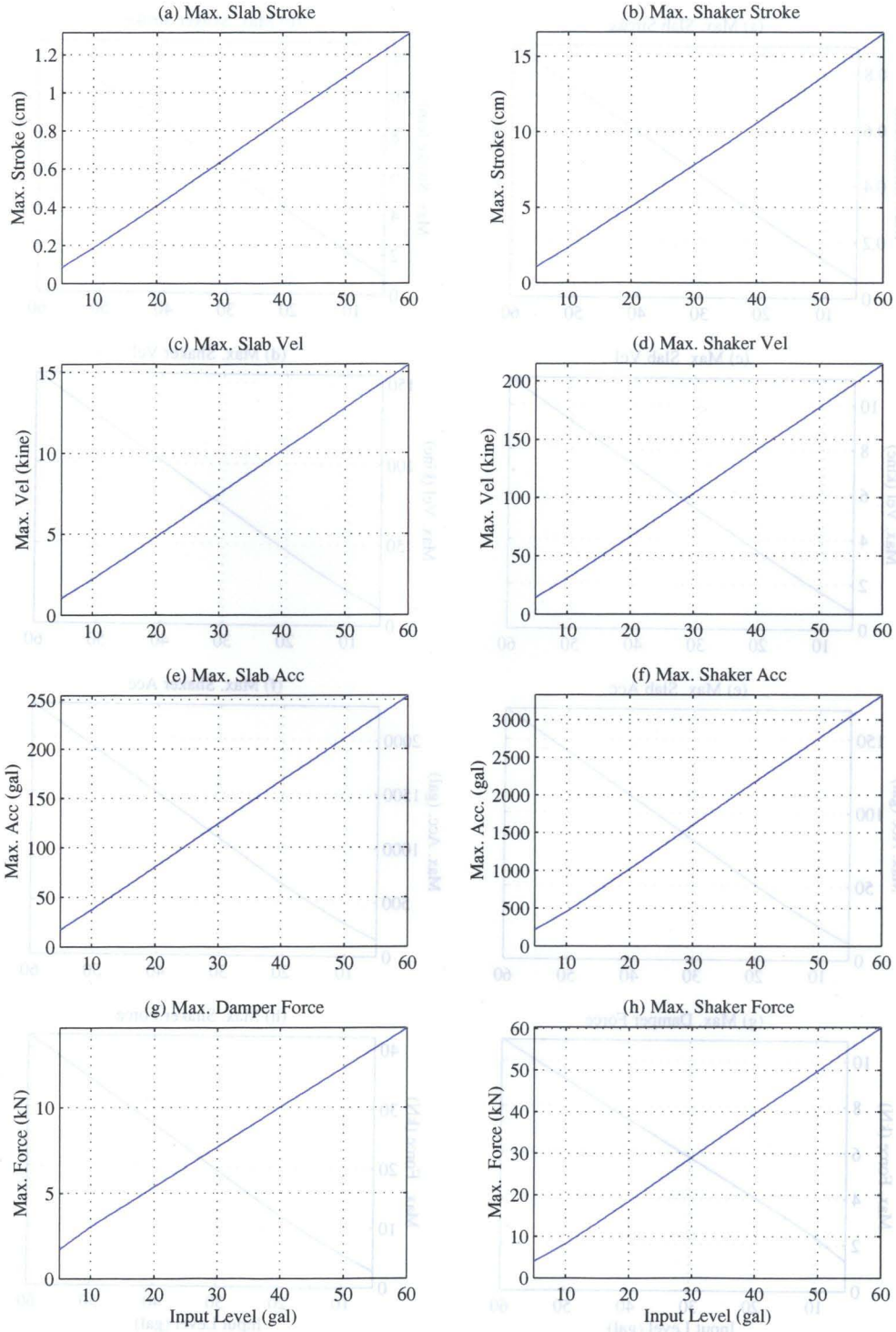

Figure 5.32: Maximum Input Level and Response (ECNS)

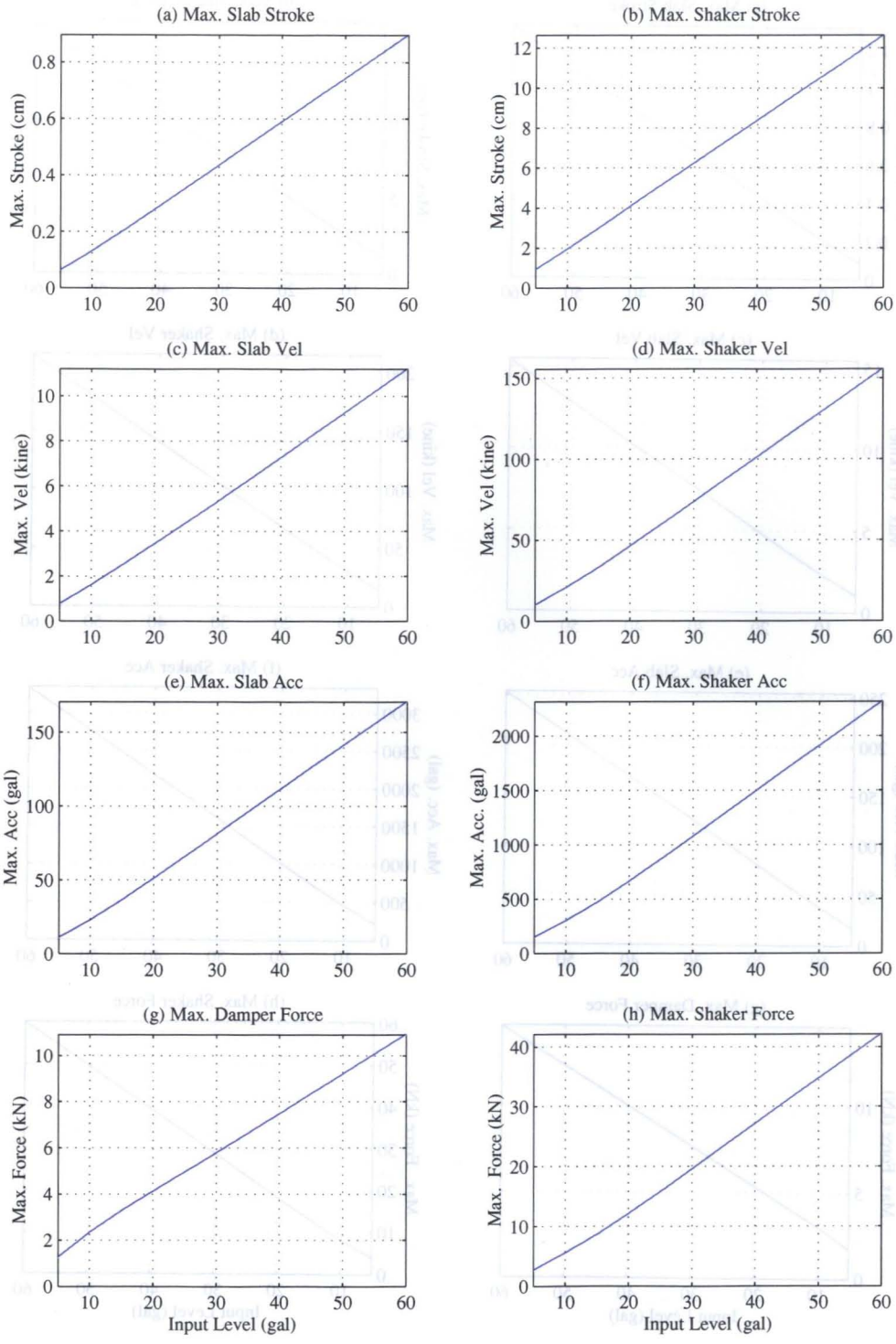

Figure 5.33: Maximum Input Level and Response (KBNS)

5.6.3 Experimental Results and Discussions

Sinusoid (1.75 Hz)

This is a periodical excitation test with 1st mode resonance frequency of the 5-story frame structure. Table 5.13 shows the comparison of the evaluation indices between simulation and experiment.

From Figures 5.37 and 5.39, the realized maximum velocity is approximately 18% less than the commanded. Things are even worse in the norm response comparison. As pointed out in Chapter 3, this deficiency might arise from the time delay between command and shaker movement. Figure 5.37 shows that commanded force exceeds the limitation of the sensor and servo motor capacities. It affects the damper hysteresis and energy dissipation depicted in Figure 5.38, particular in absorbance energy.

As the response of the damper specimen depicted in Figure 5.34, however, relative response between two structures are traced with good accuracy. In the frequency response shown in Figure 5.40, frequency and amount at the peak shows good agreement. In acceleration response, however, higher frequency components are magnified. Also, in displacement spectrum, elements close to the natural frequency of the test system are slightly magnified, which can be regarded as the effect of the time delay.

Figure 5.36 compares the responses between with and without damper specimen. By introducing the joint damper, relative response is reduced to almost a half of the uncoupled cases.

Figure 5.41 shows the comparison of the 5th floor velocity of the 5-story frame and 3rd floor of the 3-story between simulation and experiment. Measured data are results of the real time calculation during loading experiment. Apart from the slight difference in the amplitude level at steady state response, overall characteristics show the good agreement. Figure 5.42 shows the comparison between with and without joint damper. It should be noted that response of the top floor of the 3-story structure becomes larger compared to the original uncoupled structure. The reason of this phenomenon is that the response of the 3-story frame is influenced by that of the 5-story frame. This effect has been observed in the past series of experiments using this real-scale test facility[2, 3].

Sinusoid (2.41 Hz)

The sinusoidal loading experiment which frequency is adjusted to the 1st mode natural frequency of the 3-story frame is conducted as well. Table 5.14 shows the comparison of the evaluation indices between simulation and experiment.

It is observed From Figures 5.46 and 5.48 that shaker response is slightly larger than

Table 5.13: Evaluation Indices (Sin 1.75Hz)

Index	Estimated	Measurement	Error(%)
E_s	0.914	0.967	5.818
Nr_s	4.408	3.643	17.366
E_{sv}	10.223	10.195	0.275
Nr_{sv}	48.584	41.162	15.277
E_f	10.058	9.424	6.308
Nr_f	50.499	40.779	19.249
E_{ev}	134.094	110.137	17.866
Nr_{ev}	634.480	481.793	24.065
E_{ef}	25.710	24.232	5.749
Nr_{ef}	130.207	96.778	25.673
E_{de}	3.302	2.198	33.434
E_{3R}	3.896	3.833	1.607
Nr_{3R}	20.893	18.176	13.005
E_{5R}	16.092	21.306	32.396
Nr_{5R}	78.672	95.435	21.307

commanded. It is also observed from the damper hysteresis and energy dissipation shown in Figure 5.47, strong nonlinearity that can not be traced by the estimated model is observed. The existing nonlinearity in the damper specimen and test system at the small response region takes place and deteriorates the estimation of the response. Furthermore, from the viewpoint of the transfer characteristics from shaker force to the slab displacement, it is disadvantageous to stimulate the higher frequency regions from the IFDL system natural frequency. In order to overcome this problem, the IFDL natural frequency should be adjusted to be close to that of the hypothetical structure so as to make use of the resonance response.

Figure 5.43 shows the damper response comparison. The relatively larger error values in response is regarded as the results of the nonlinearity. The large difference is also observed in Figure 5.50, particularly in 3rd floor velocity of the 3-story structure. Since the damper location of the 3-story structure is its top floor, 1st mode vibration of the structure could be easily stimulated. Then, the uncertainty observed in the damper hysteresis might cause the difference in the response of the top floor between simulations and experiments. In fact, from results shown in Figure 5.45, top floor

velocity of the 5-story structure is not affected so much by the damper specimen, clear contrast to that of the 3-story structure.

Table 5.14: Evaluation Indices (Sin 2.41Hz)

Index	Estimated	Measurement	Error(%)
E_s	0.258	0.337	30.494
Nr_s	1.322	1.658	25.423
E_{sv}	3.713	5.347	43.987
Nr_{sv}	19.711	25.058	27.127
E_f	4.363	5.322	21.996
Nr_f	25.478	23.719	6.905
E_{ev}	49.668	60.693	22.198
Nr_{ev}	260.794	306.022	17.342
E_{ef}	12.252	14.908	21.680
Nr_{ef}	73.927	80.193	8.476
E_{de}	0.620	0.631	1.729
E_{3R}	3.587	5.661	57.826
Nr_{3R}	20.723	31.964	54.245
E_{5R}	3.677	3.451	6.142
Nr_{5R}	15.064	14.219	5.611

El Centro NS Wave

This test is an earthquake loading experiment. Table 5.15 shows the comparison of the evaluation indices between simulation and experiment.

From Figures 5.55 and 5.58, shaker could not trace the command velocity at around the peak response region. It is observed from the shaker command force time history that the commanded force exceeds the upper limitation of the device. In the experiment, however, unstable oscillation of the shaker as well as the deterioration of the measured waveforms are observed when assuming the smaller ground motion level than 30 gal. Since the objective of the experiment is to illustrate the efficacy of the test system and the control method, this difficulty could overcome by utilizing the more capable shaker. In fact, as seen in the figure 5.52, the proposed control method works effectively to duplicate the overall dynamic response apart from the slight inconsistency at the peak. In lower frequency regions, magnification of the gain is observed, which

is thought to be the effect of the time delay.

As for the top floor response of both structures depicted in Figure 5.59, overall waveforms shows good agreements, which is also observed in frequency response. Also, Figure 5.60 shows the comparison of the top floor response with and without damper. It is found that joint damper system works effectively for the response reduction of the 5-story structure. In frequency response, natural frequencies of both 5-story and 3-story structures are shifted to be closer. These results are totally consistent to the past research for the joint damper system with this structure. The full-scale experiment using the real frame structures have pointed out that both structures can no longer respond independently due to the coupling effect of the device[2, 3]. That is to say, these two structure are altered to the one 8-DOF structural system. In the hybrid experiment using the IFDL, the same phenomenon can be clearly observed.

Table 5.15: Evaluation Indices (ECNS)

Index	Estimated	Measurement	Error(%)
E_s	0.614	0.571	6.893
Nr_s	1.857	1.923	3.535
E_{sv}	7.275	5.903	18.851
Nr_{sv}	21.510	24.832	15.444
E_f	7.482	6.689	10.591
Nr_f	28.807	28.356	1.563
E_{ev}	96.984	81.733	15.725
Nr_{ev}	280.258	285.903	2.014
E_{ef}	25.868	15.851	38.725
Nr_{ef}	63.476	49.569	21.910
E_{de}	0.671	0.458	31.696
E_{3R}	5.299	4.356	17.791
Nr_{3R}	13.327	16.504	23.845
E_{5R}	10.969	10.681	2.626
Nr_{5R}	34.249	43.902	28.188

Kobe NS Wave

Structural responses are also examined under Kobe NS input motion. Table 5.16 shows the comparison of the evaluation indices between simulation and experiment.

From Figure 5.64 and 5.66, deficiency in the shaker velocity gain is observed. This results could not be improved even if the control gain of the PID controller increases. Instead, the undesirable reaction of the shaker is observed in that case.

In the damper specimen response depicted in Figure 5.61 and 5.65, estimated response does not show good agreement with measurement due to the nonlinear characteristics of the damper specimen. This nonlinearity may not take place if conducting experiments with assuming more stronger earthquake motions. However, due to the physical constraints of the the command velocity as well as shaker control force, it is impossible for this prototype experiment facility to conduct the loading experiment with larger ground motion. In the frequency response shown in Figure 5.67, however, good agreements can be observed in both peak response and overall tendency. This indicates that the major problem of conducting the experiment with the IFDL test system is the lack of the velocity amplitude level and corresponding transmitted force of the shaker. Since the proposed method itself has the capability to trace the frequency response characters of the assumed structure,more precise experiment could be carried out by utilizing more powerful shaker, or alternatively adjusting the natural frequency of the IFDL test system.

As for the top floor response of both structures depicted in Figure 5.68, overall waveforms shows good agreements, particularly in that for the 5-story structure. It is also clearly observed in the frequency response.

The effect of the coupling structure can be again observed in Figure 5.69. This figure shows that joint damper does not work efficiently under Kobe NS earthquake motion. The past study has also found that the passive joint damper system for this test frame structures does not work so effective under Kobe NS earthquake due to the natural frequencies of the target structure and frequency characteristics of the ground motion[2, 3]. Similar characteristics could be observed by utilizing the IFDL test system.

Table 5.16: Evaluation Indices (KBNS)

Index	Estimated	Measurement	Error(%)
E_s	0.439	0.439	0.163
Nr_s	1.858	2.300	23.760
E_{sv}	5.367	5.552	3.433
Nr_{sv}	22.285	31.772	42.573
E_f	5.814	6.543	12.531
Nr_f	30.126	34.741	15.319
E_{sv}	71.779	65.044	9.383
Nr_{sv}	291.726	371.321	27.284
E_{sf}	19.075	15.621	18.108
Nr_{sf}	68.151	60.936	10.587
E_e	0.643	0.481	25.271
E_{3R}	4.602	5.430	18.006
Nr_{3R}	15.548	22.357	43.795
E_{5R}	7.801	9.095	16.596
Nr_{5R}	32.399	45.589	40.712

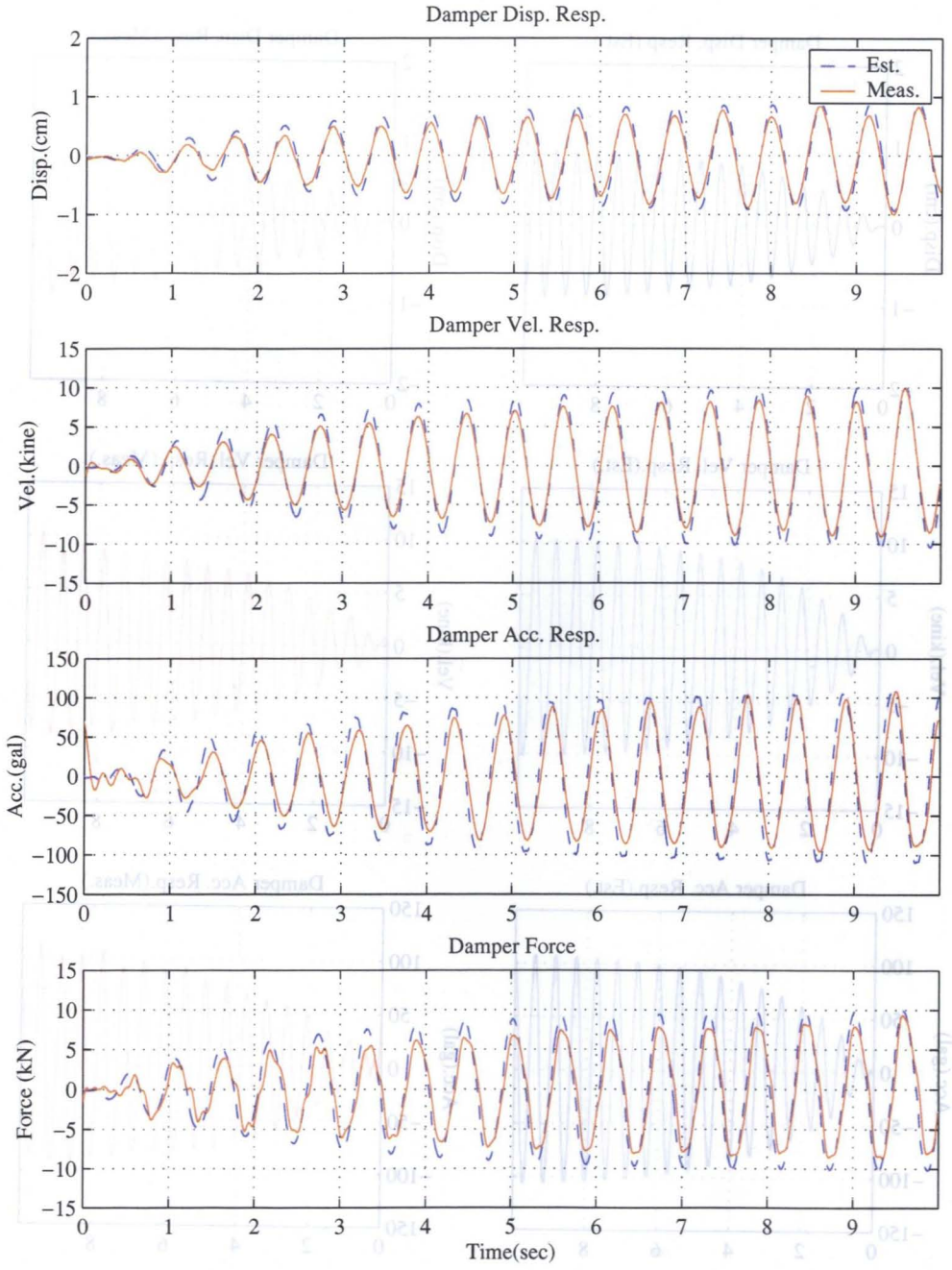

Figure 5.34: Comparison of the Structural Response (Sin 1.75 Hz, 10 gal)

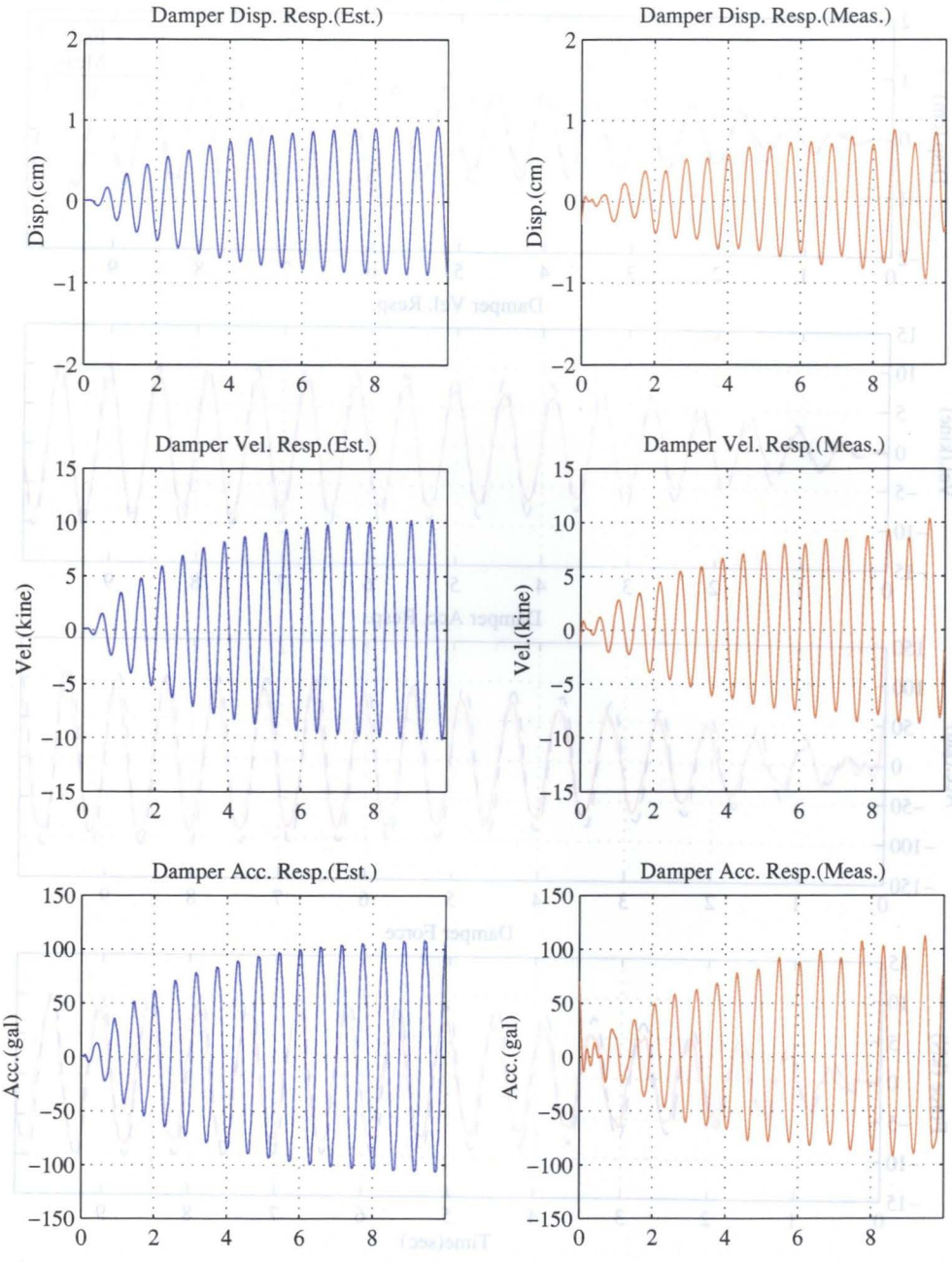

Figure 5.35: Comparison of the Structural Response (Sin 1.75 Hz, 10 gal)

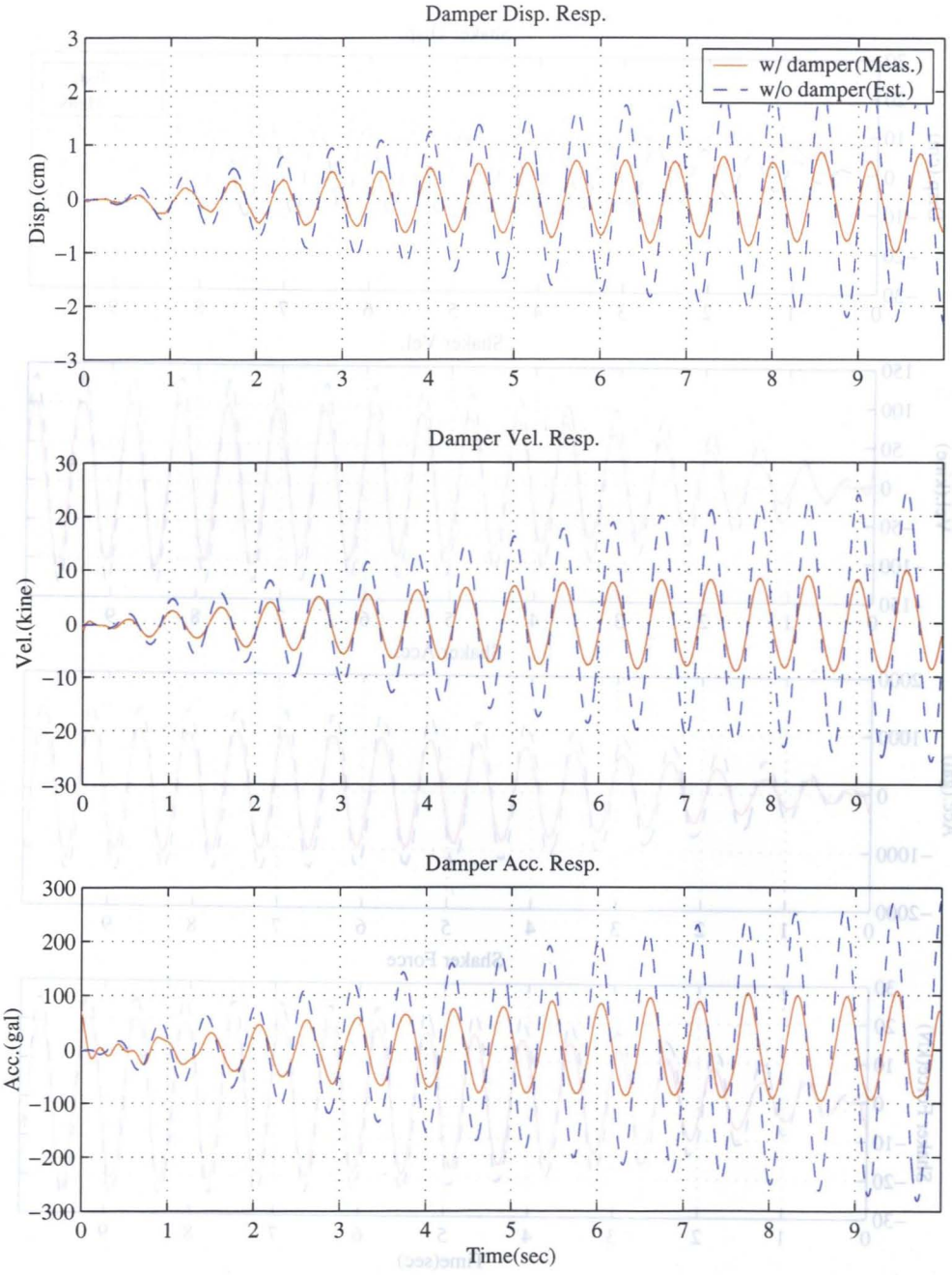

Figure 5.36: Comparison of the Structural Response (Sin 1.75 Hz, w/ & w/o damper)

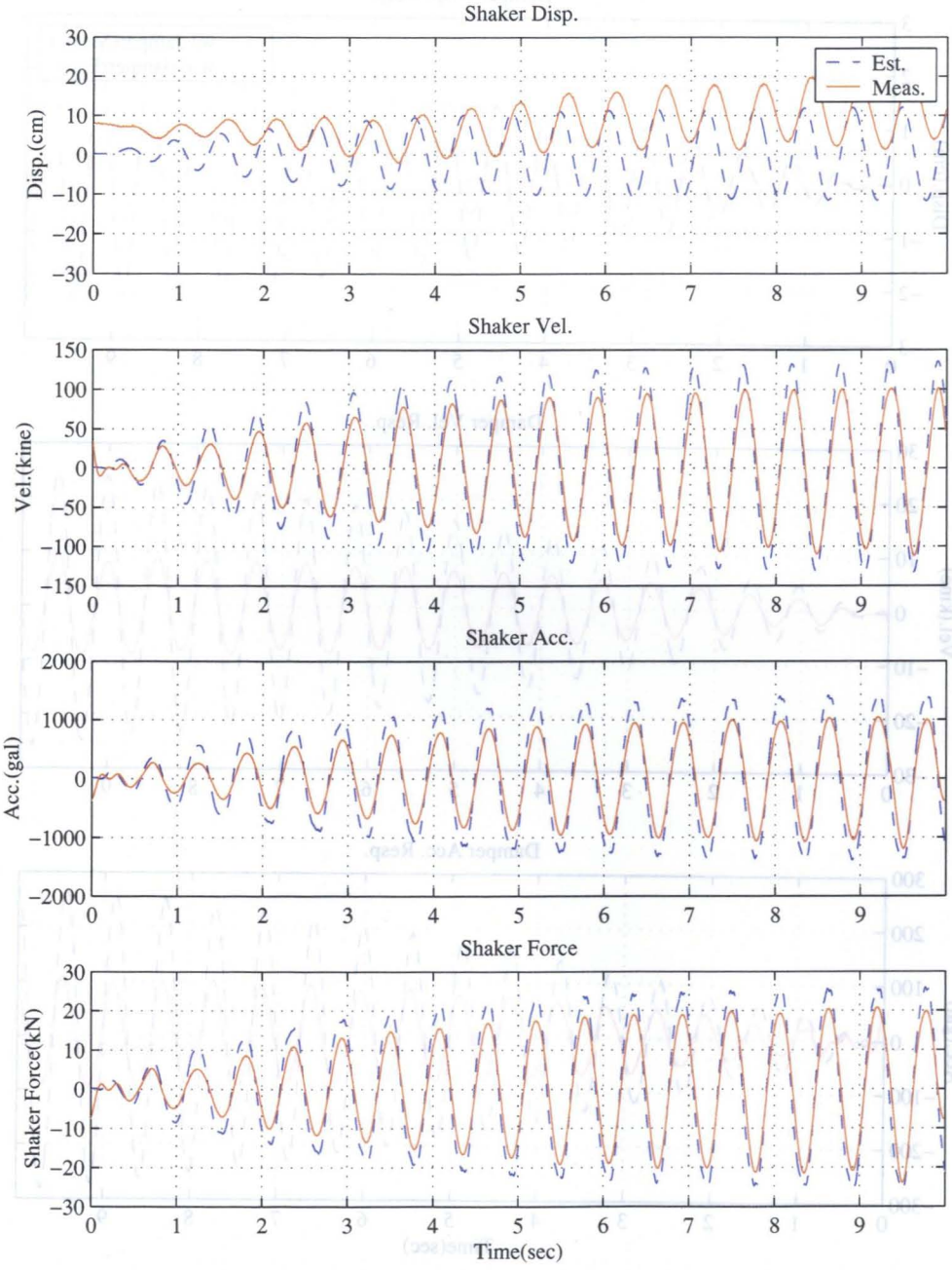

Figure 5.37: Shaker Response (Sin 1.75 Hz, 10 gal)

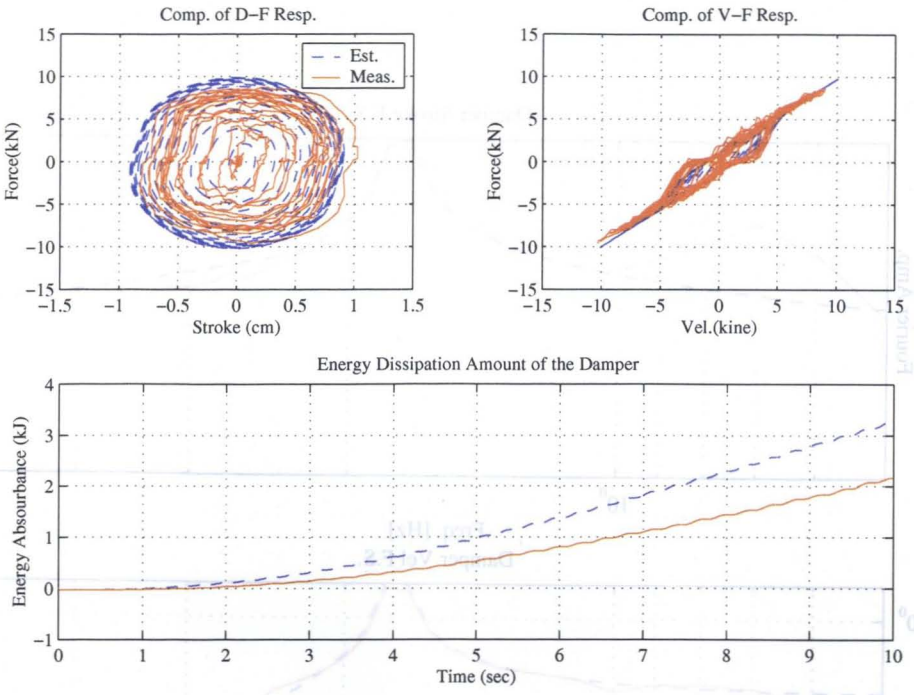

Figure 5.38: Damper Responses (Sin 1.75 Hz, 10 gal)

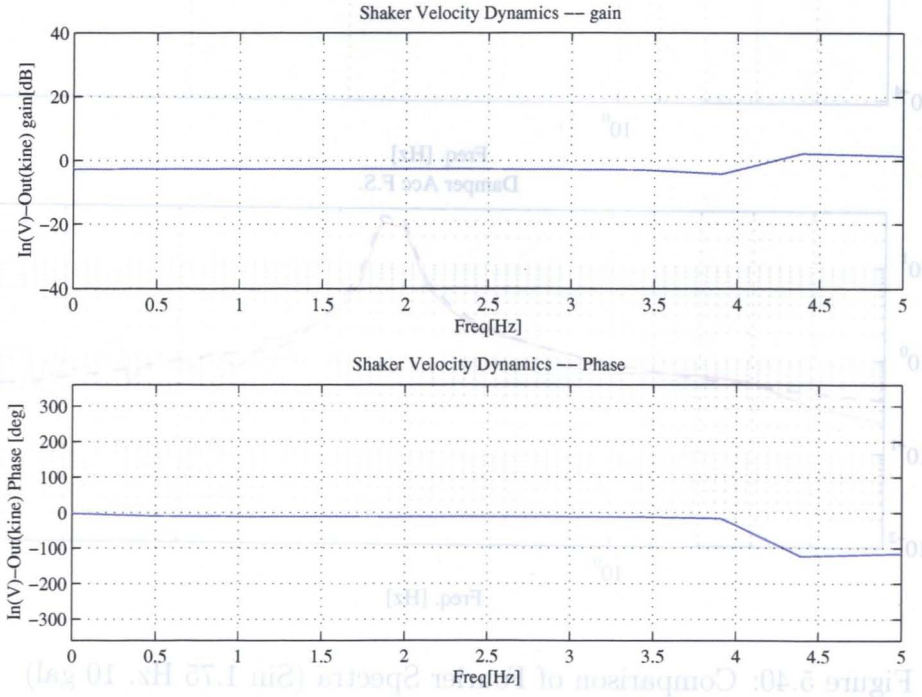

Figure 5.39: Transfer Function from Command to the Shaker Relative Velocity

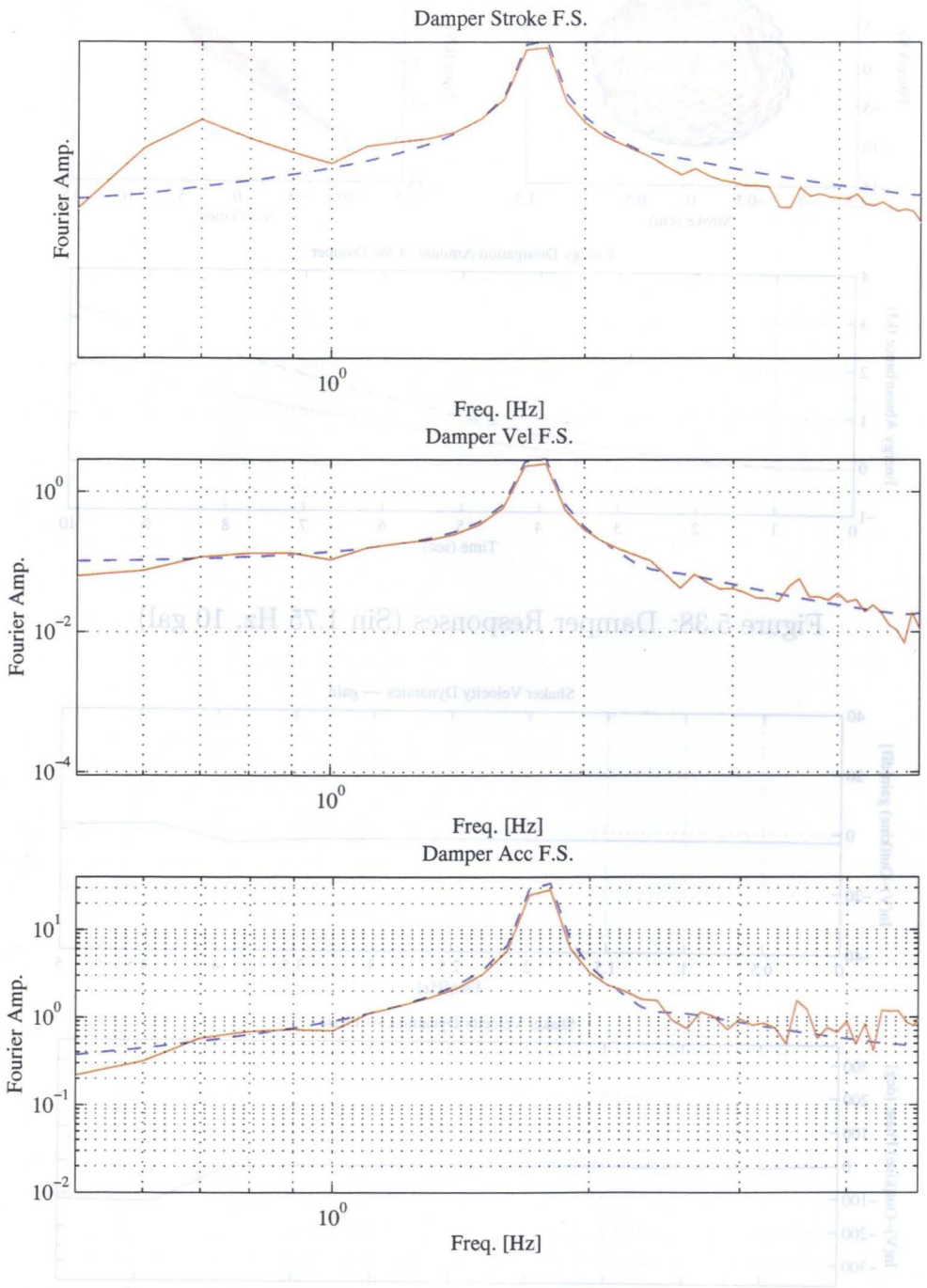

Figure 5.40: Comparison of Fourier Spectra (Sin 1.75 Hz, 10 gal)

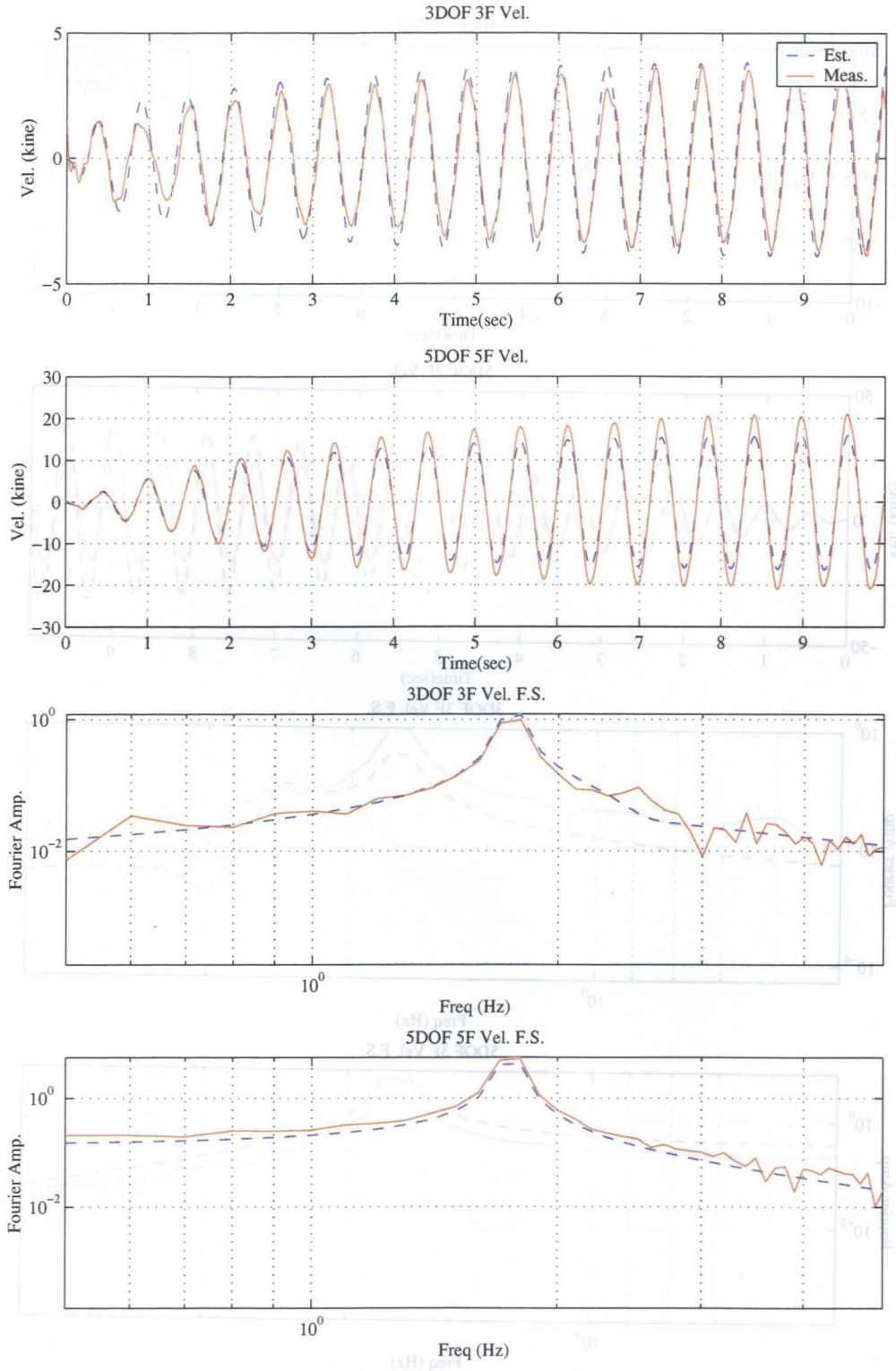

Figure 5.41: Comparison of Fourier Spectra (Sin 1.75 Hz, 10 gal)

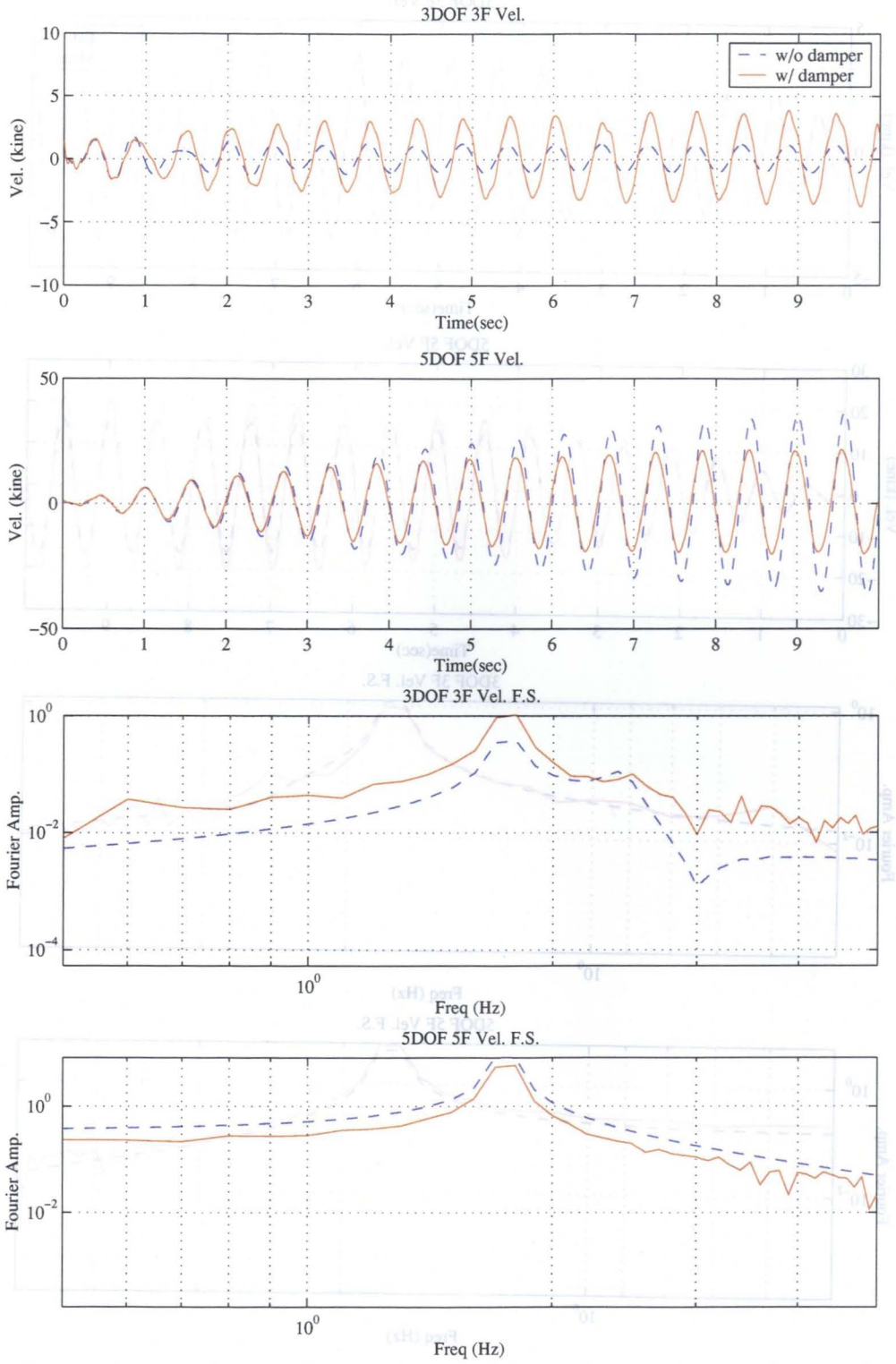

Figure 5.42: Comparison of Fourier Spectra (Sin 1.75 Hz, 10 gal)

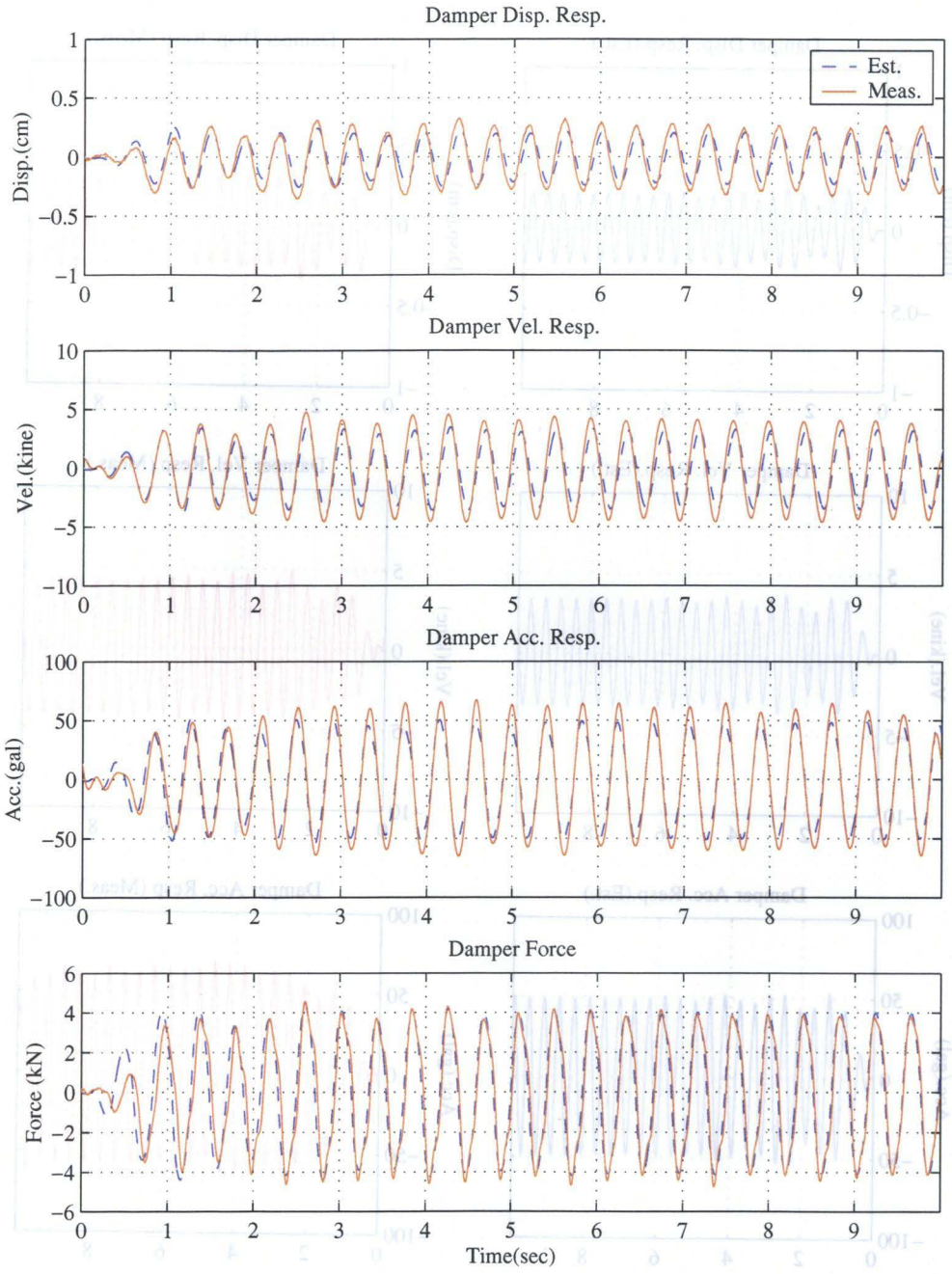

Figure 5.43: Comparison of the Structural Response (Sin 2.41 Hz, 10 gal)

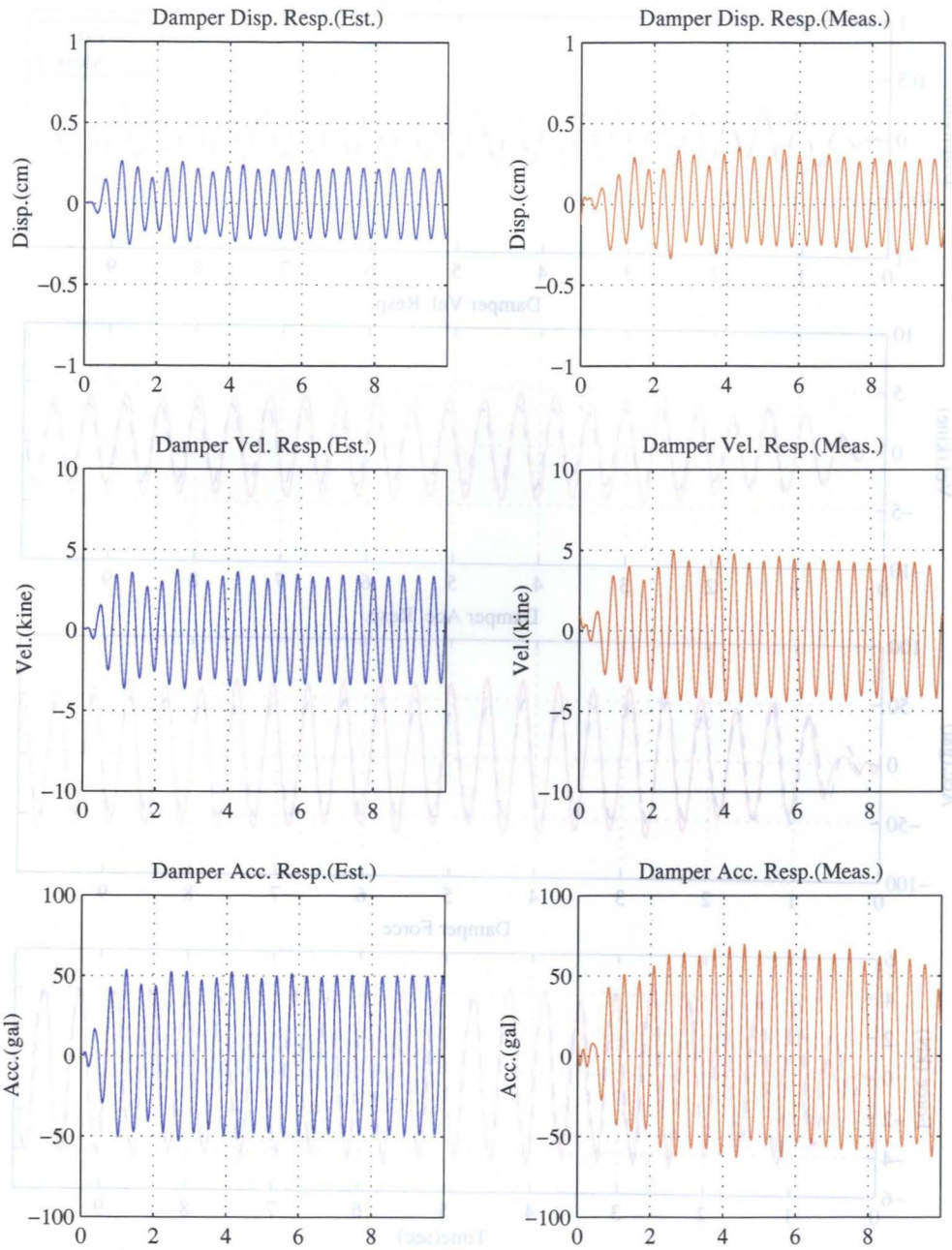

Figure 5.44: Comparison of the Structural Response (Sin 2.41 Hz, 10 gal)

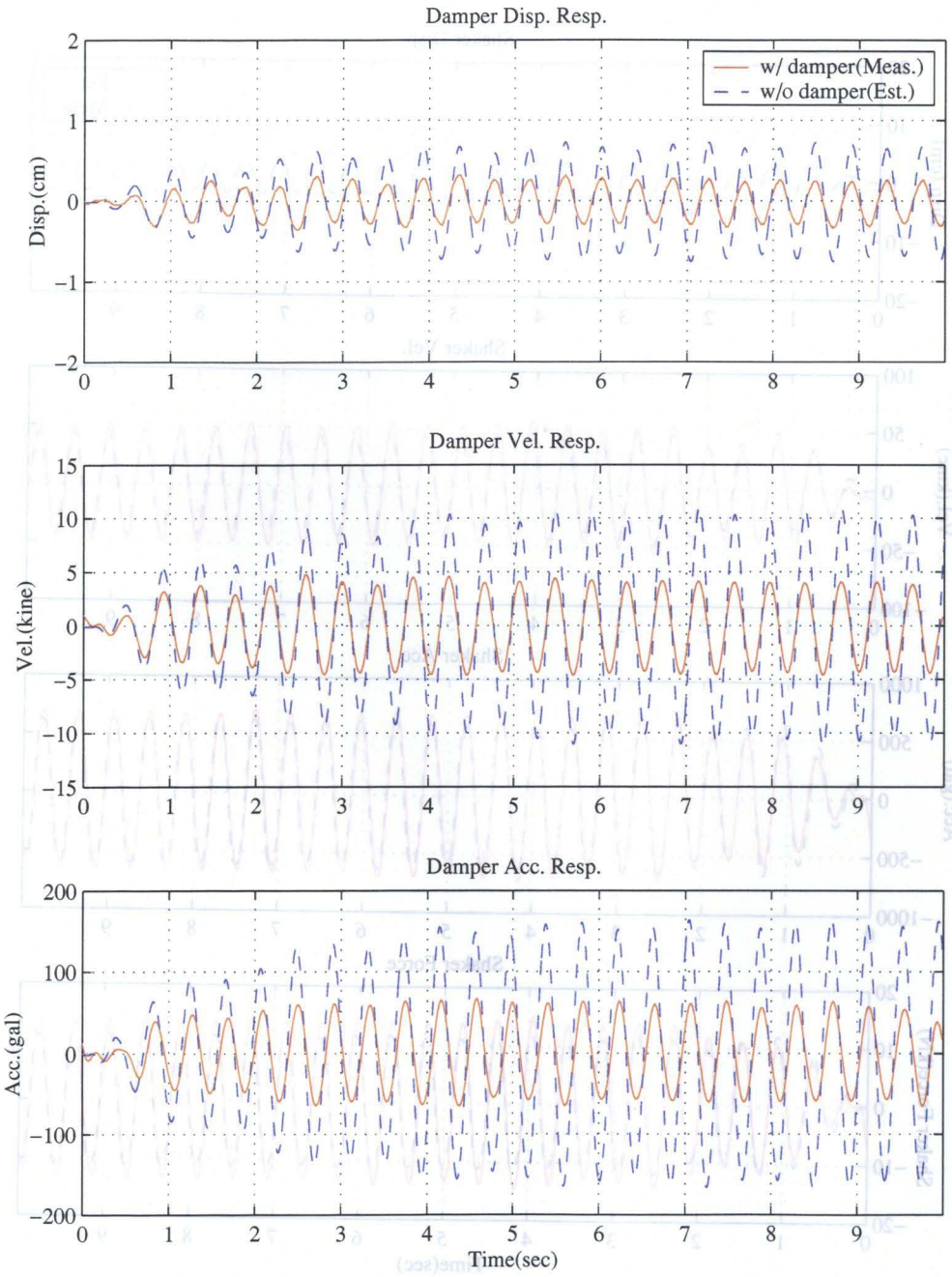

Figure 5.45: Comparison of the Structural Response (Sin 2.41 Hz, w/ & w/o damper)

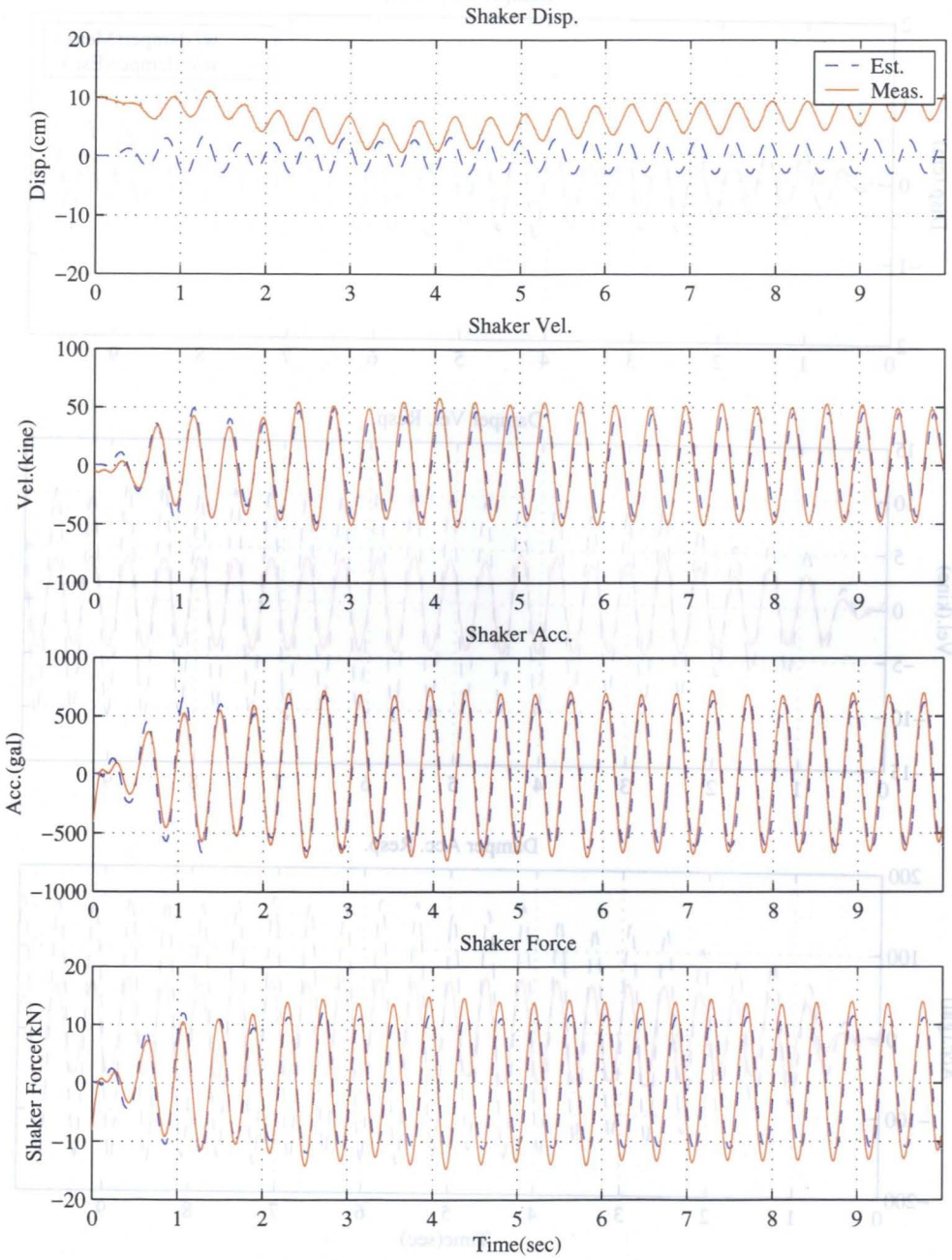

Figure 5.46: Shaker Response (Sin 2.41 Hz, 10 gal)

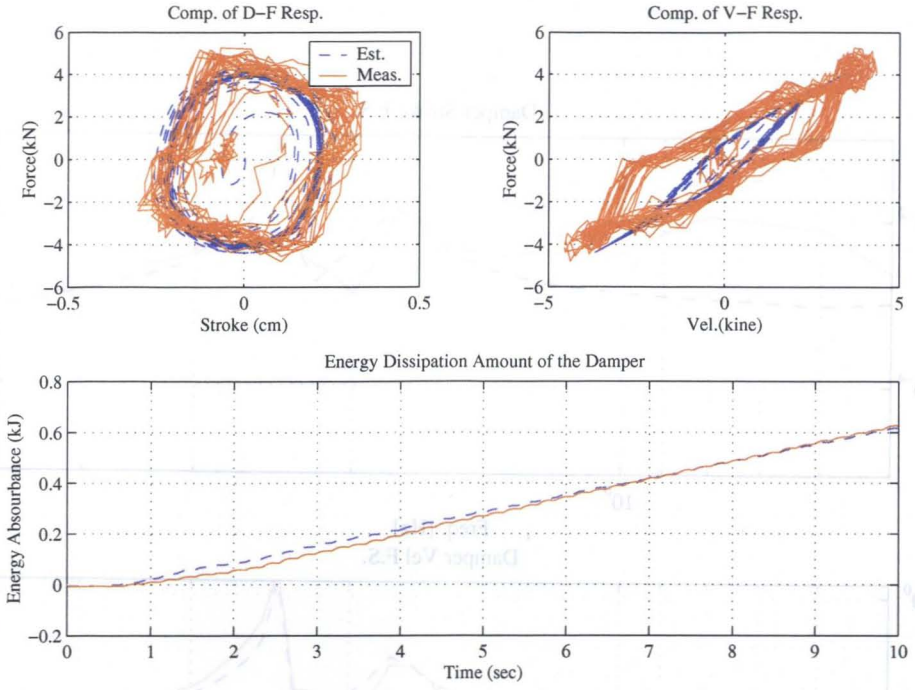

Figure 5.47: Damper Responses (Sin 2.41 Hz, 10 gal)

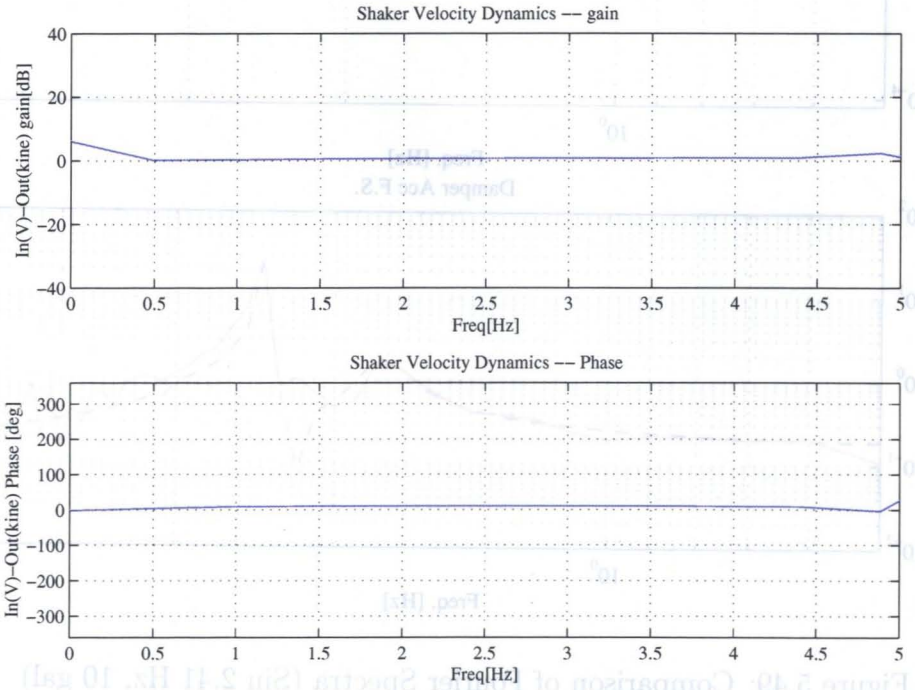

Figure 5.48: Transfer Function from Command to the Shaker Relative Velocity

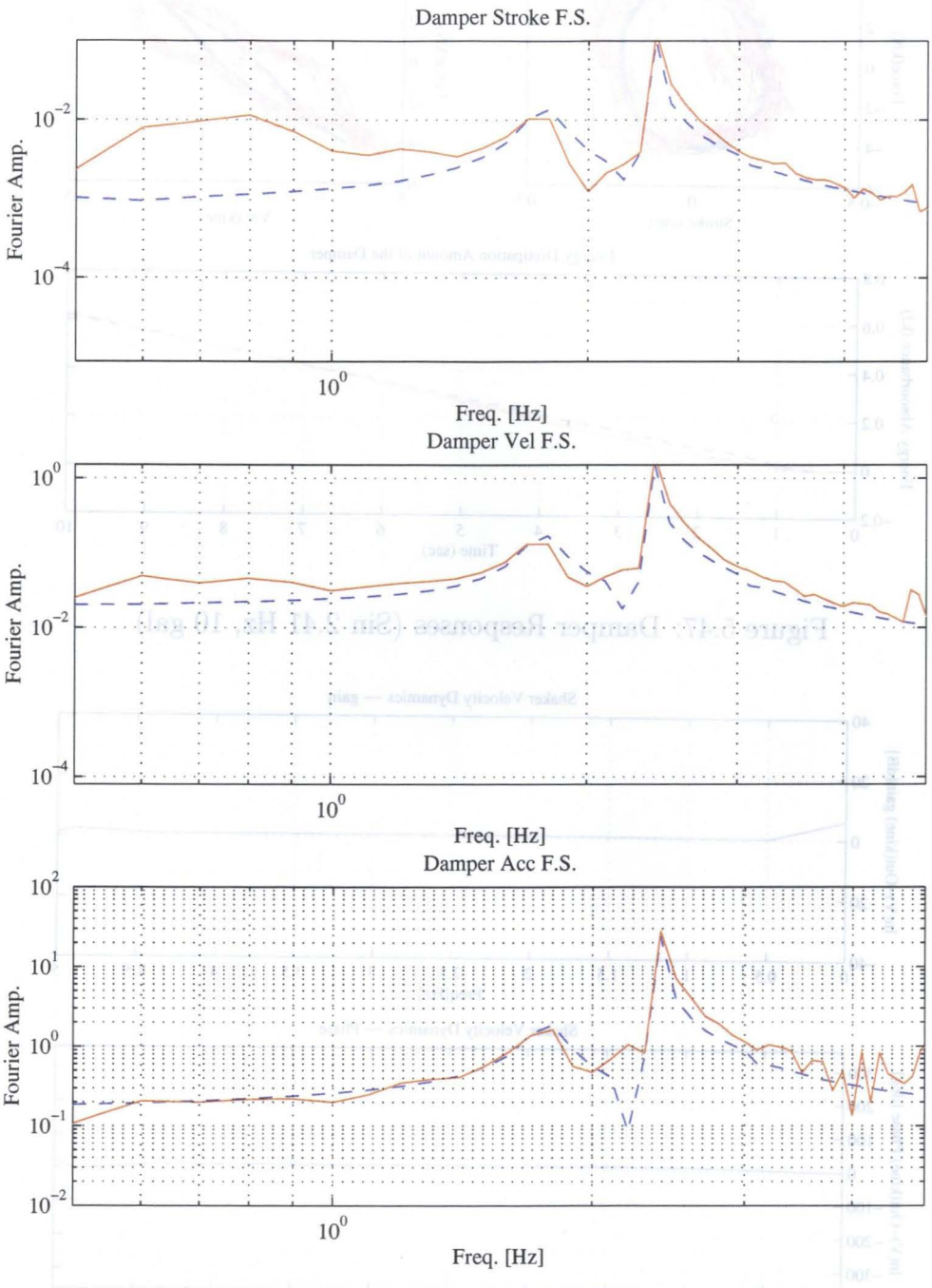

Figure 5.49: Comparison of Fourier Spectra (Sin 2.41 Hz, 10 gal)

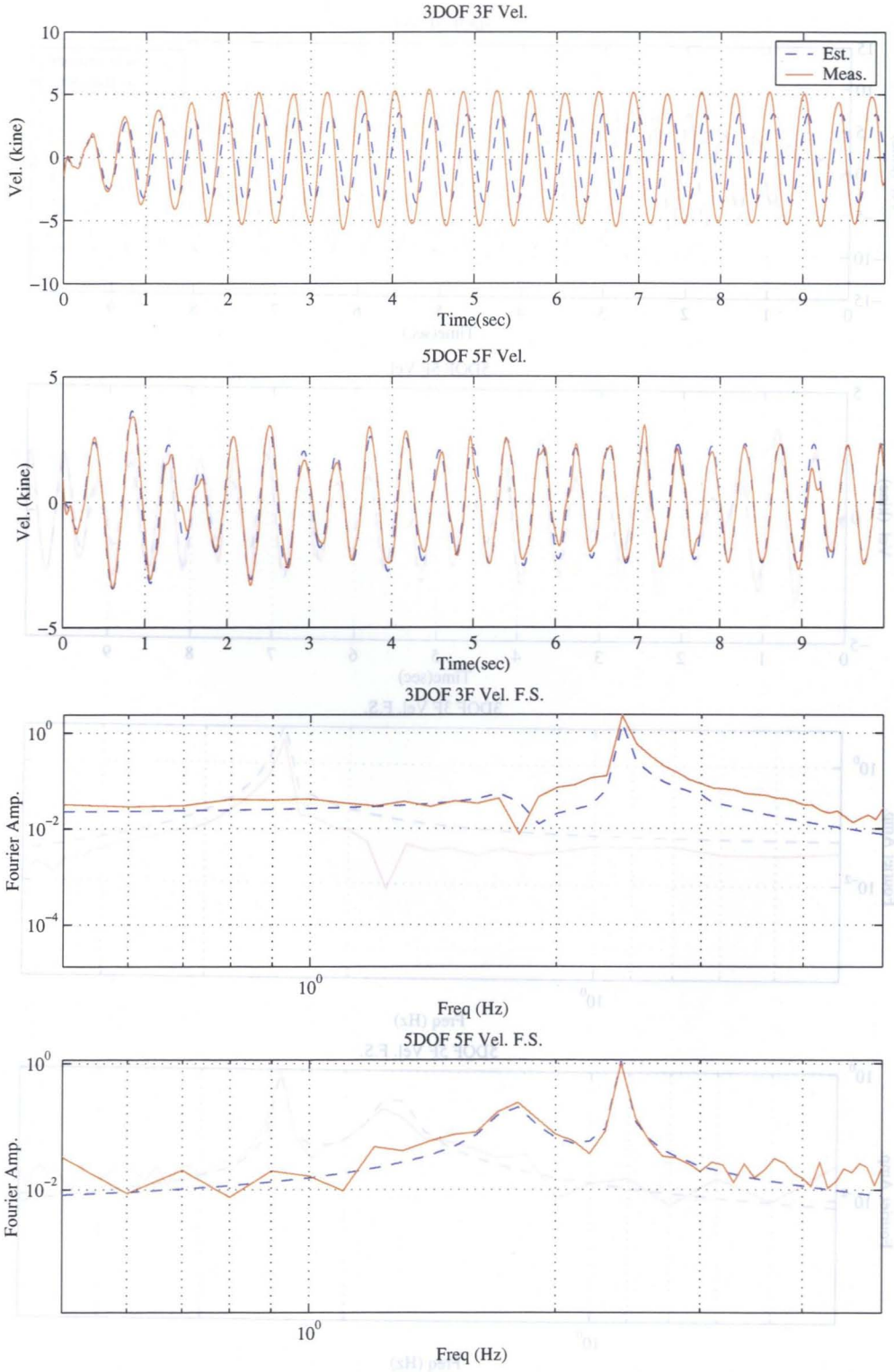

Figure 5.50: Comparison of Fourier Spectra (Sin 2.41 Hz, 10 gal)

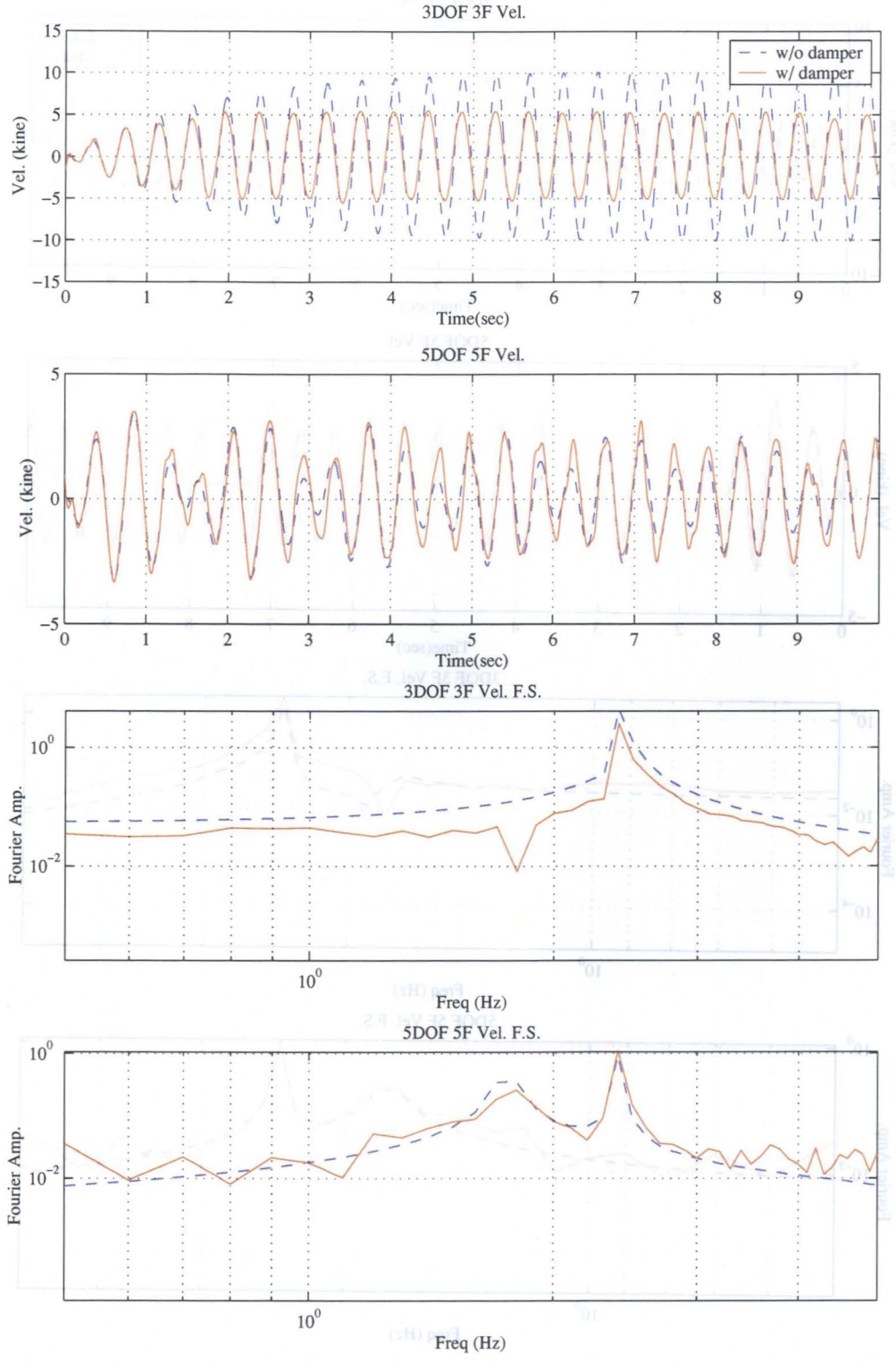

Figure 5.51: Comparison of Fourier Spectra (Sin 2.41 Hz, 10 gal)

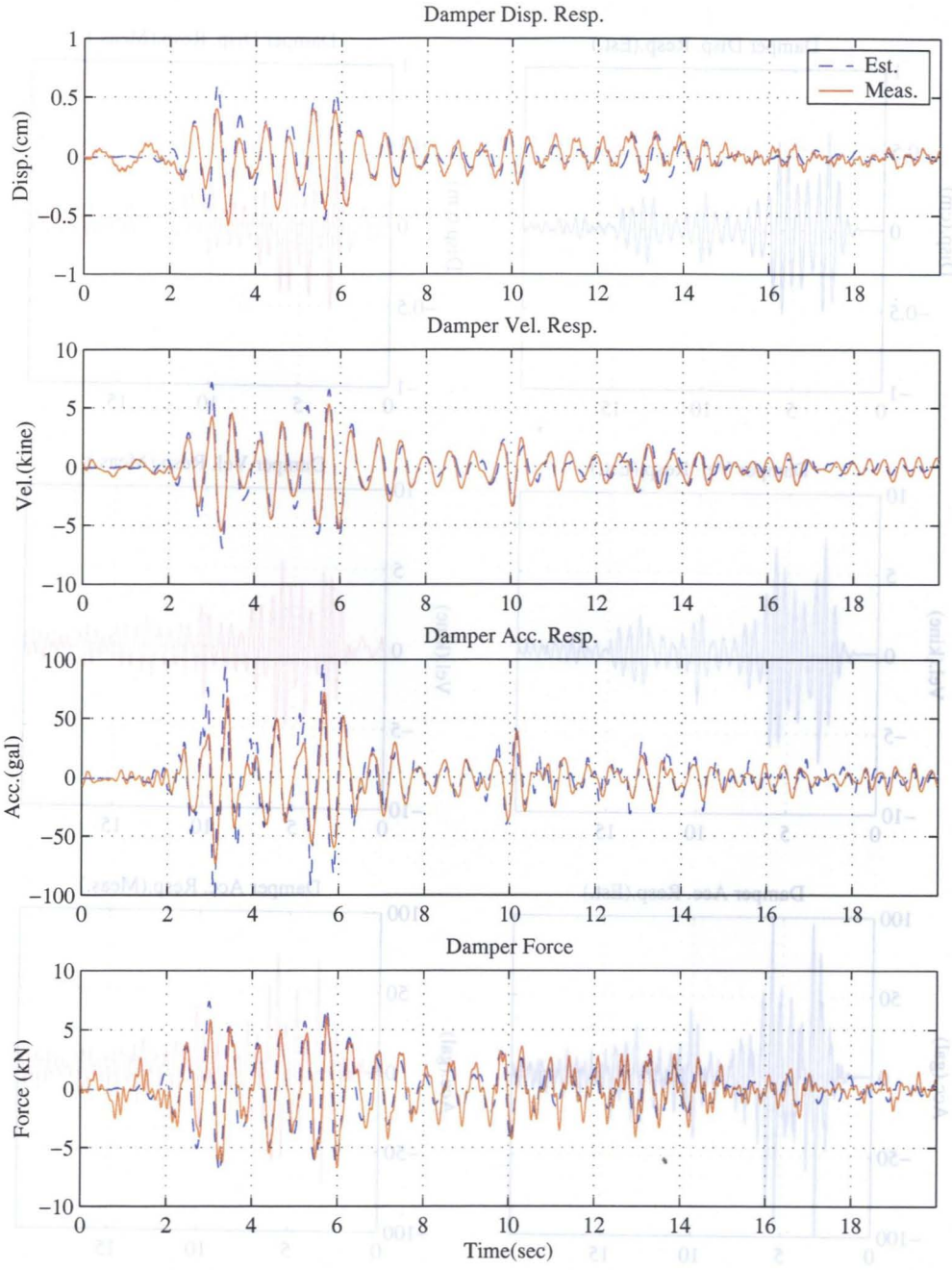

Figure 5.52: Comparison of the Structural Response (ECNS 30gal)

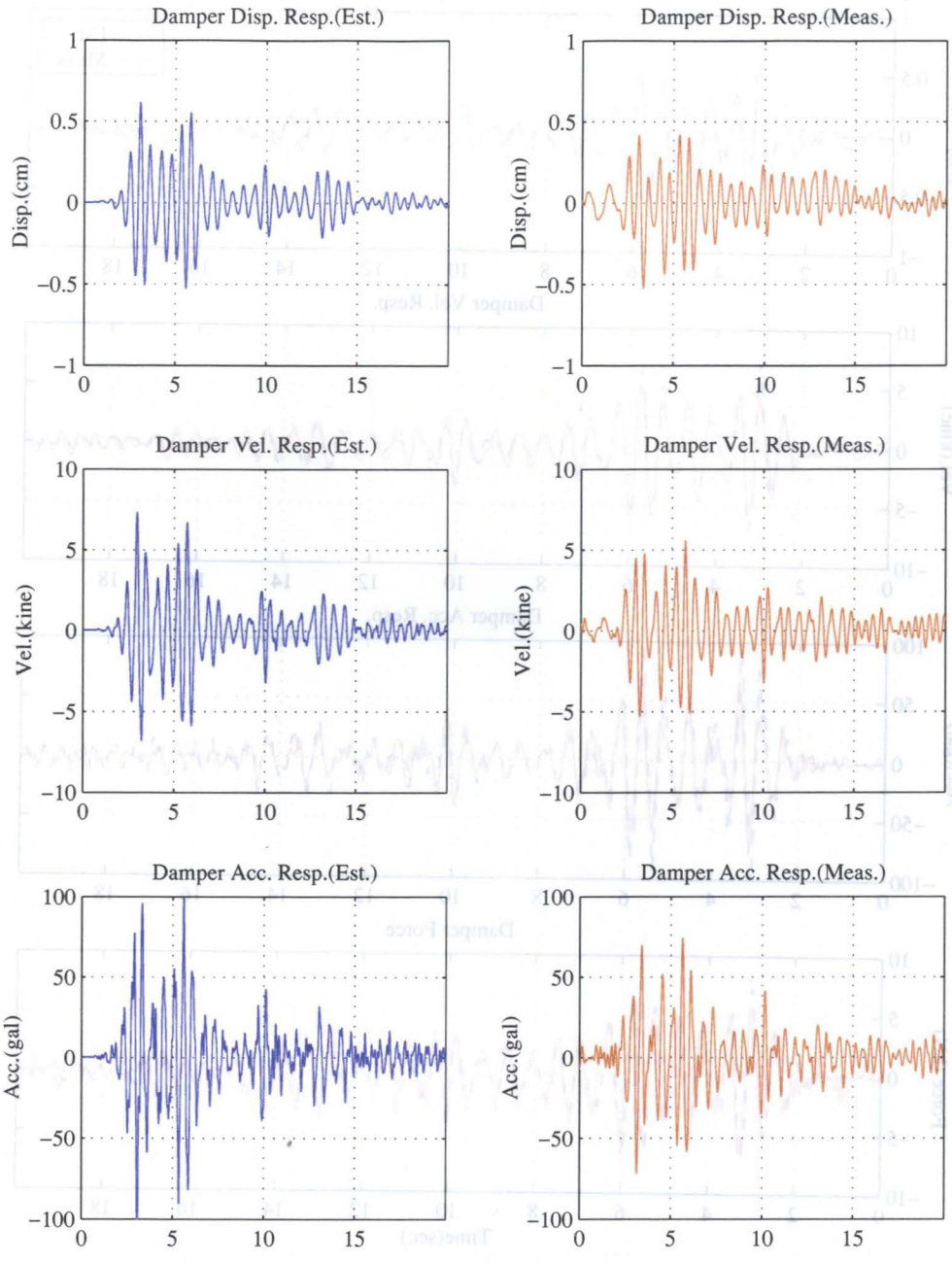

Figure 5.53: Comparison of the Structural Response(ECNS 30gal)

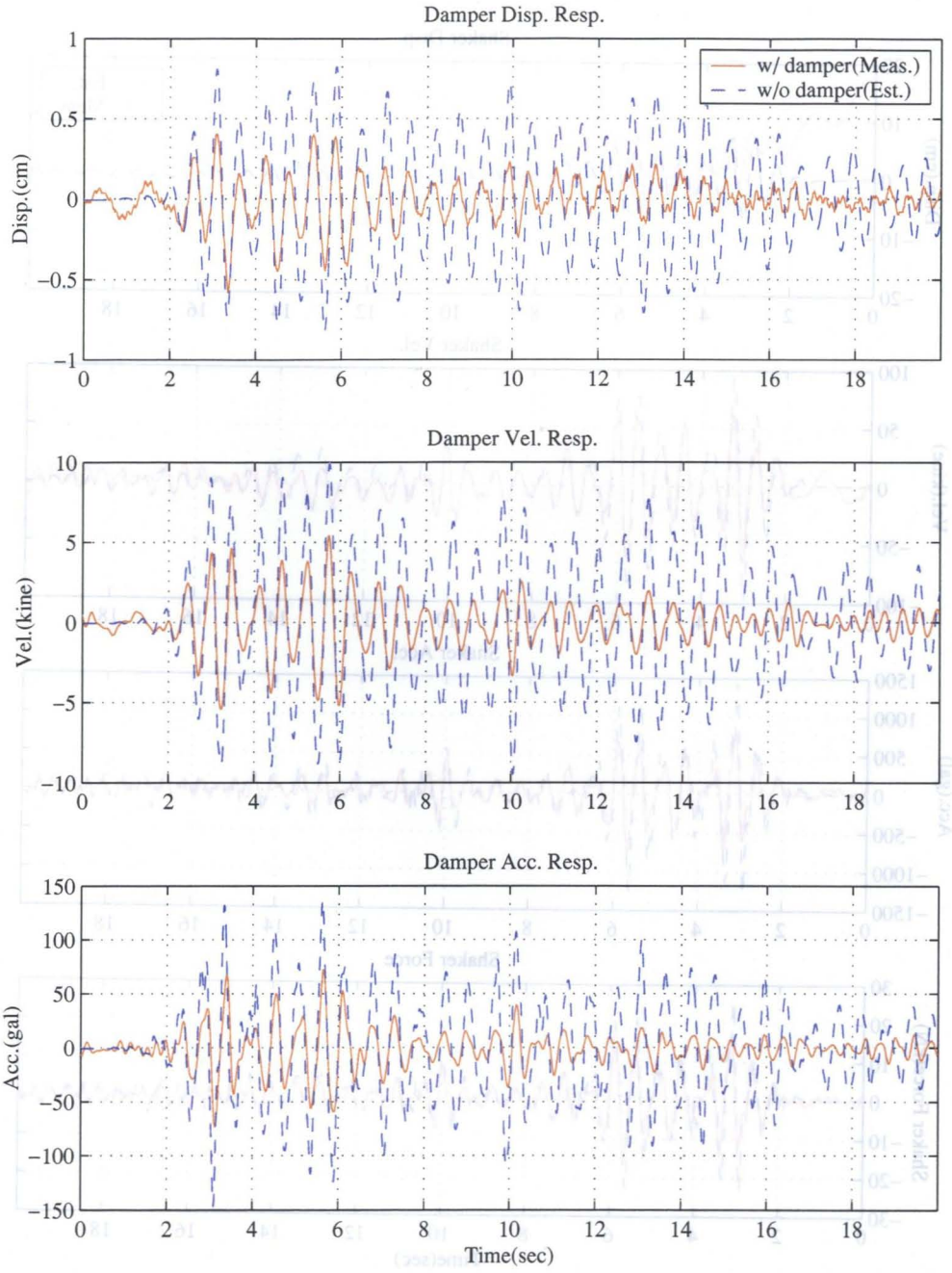

Figure 5.54: Comparison of the Structural Response (ECNS 30gal, w/ & w/o damper)

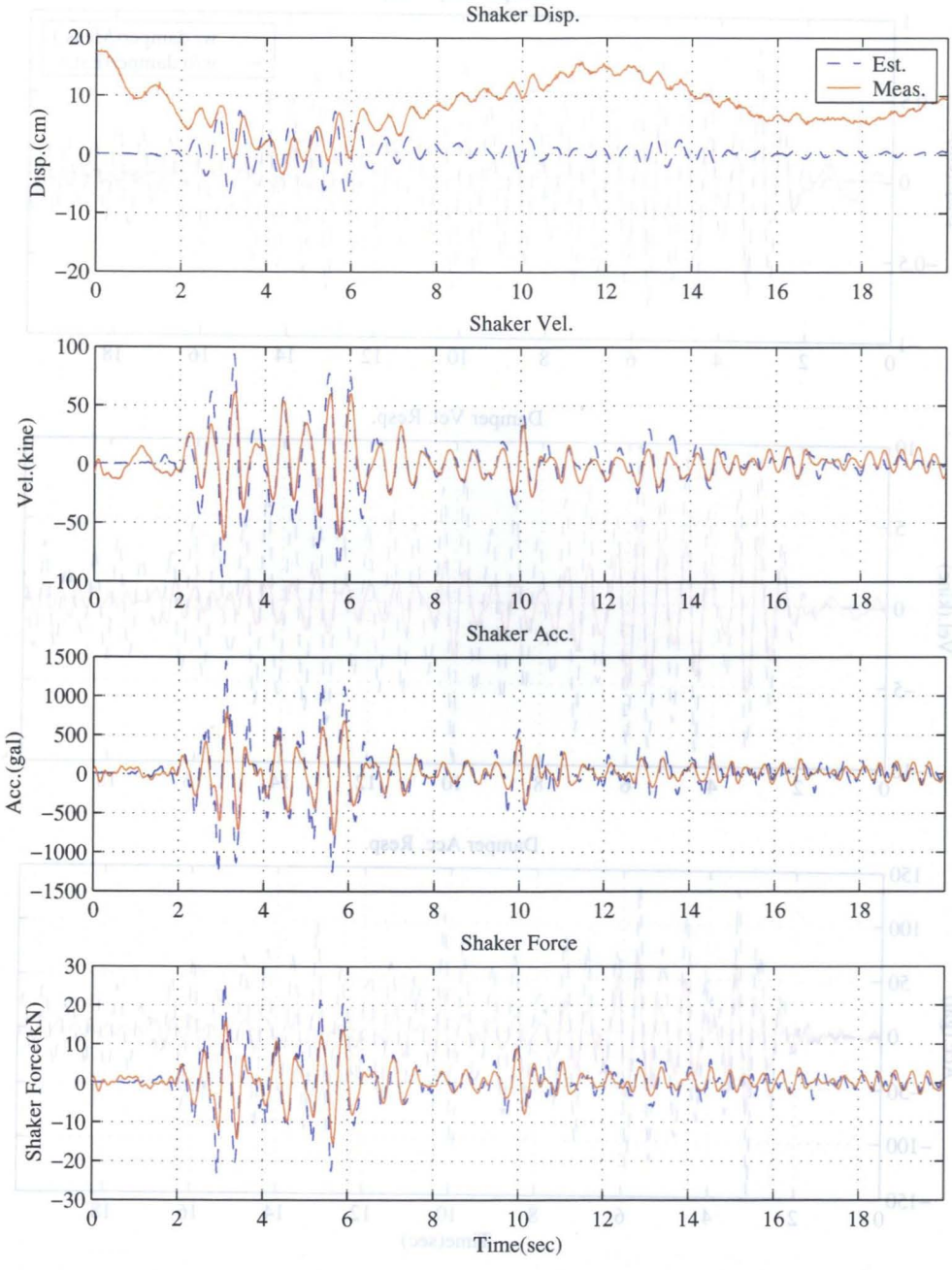

Figure 5.55: Shaker Response (ECNS 30gal)

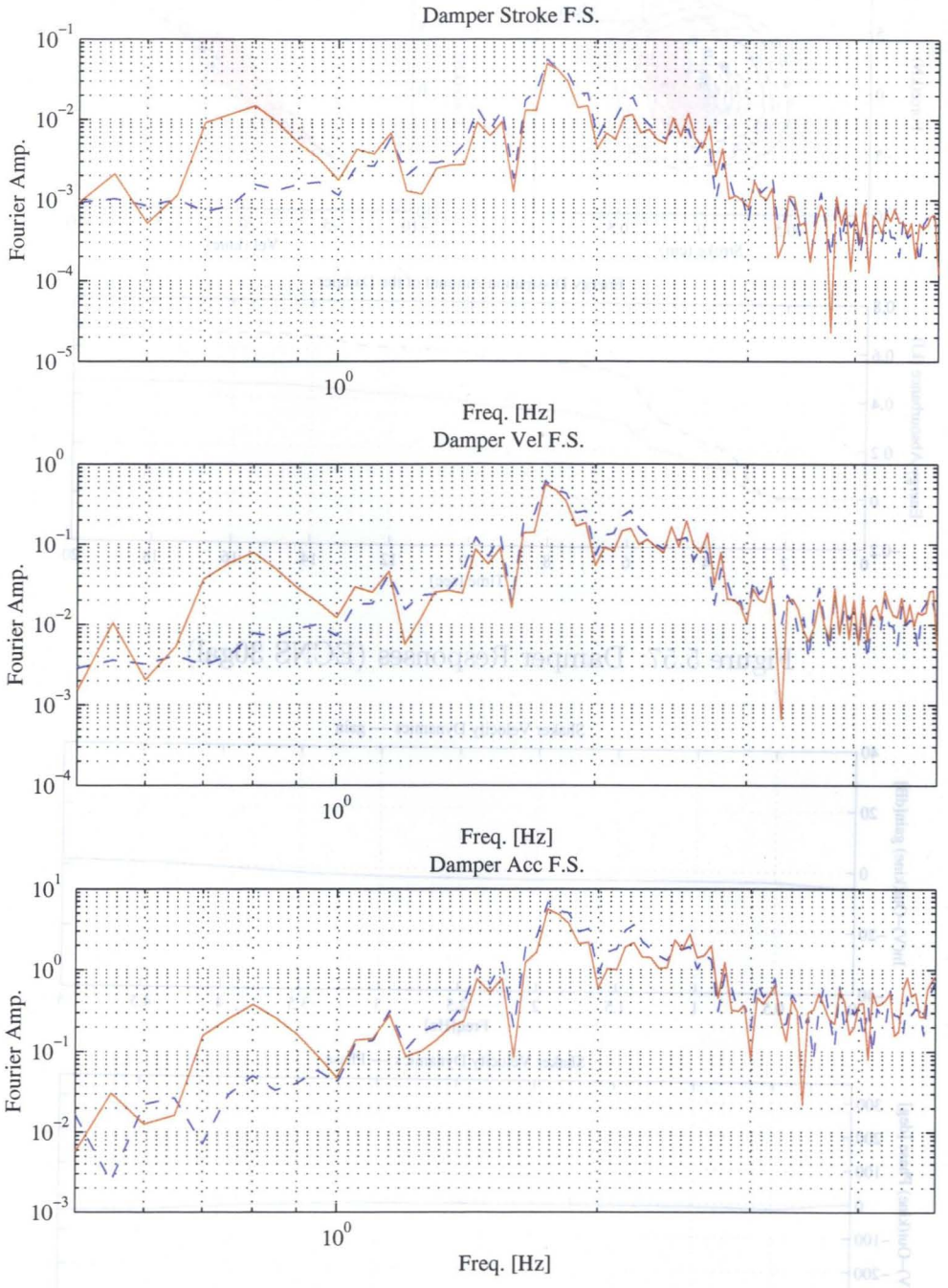

Figure 5.56: Comparison of Fourier Spectra (ECNS 30gal)

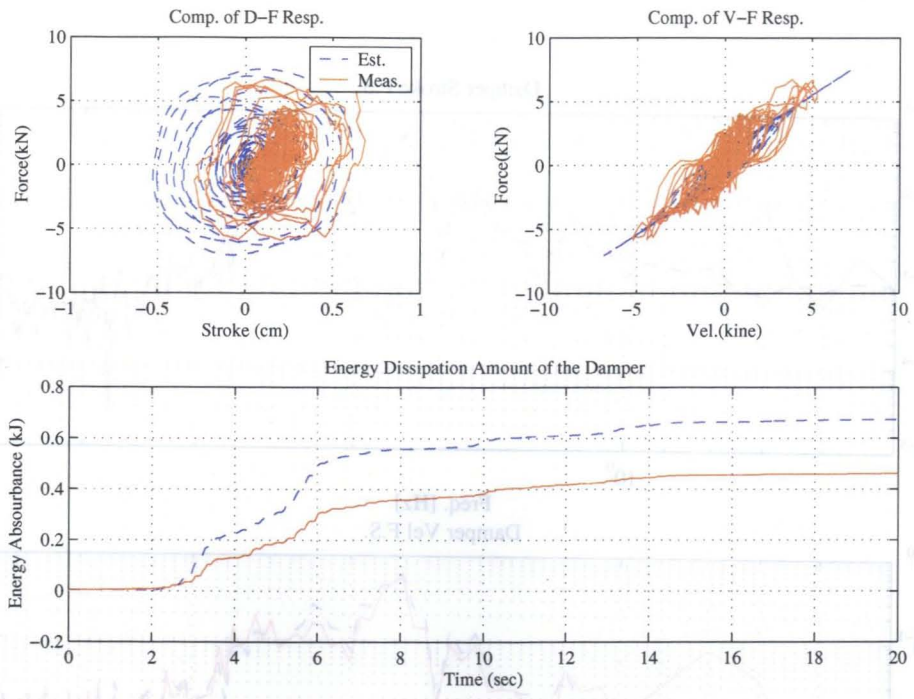

Figure 5.57: Damper Responses (ECNS 30gal)

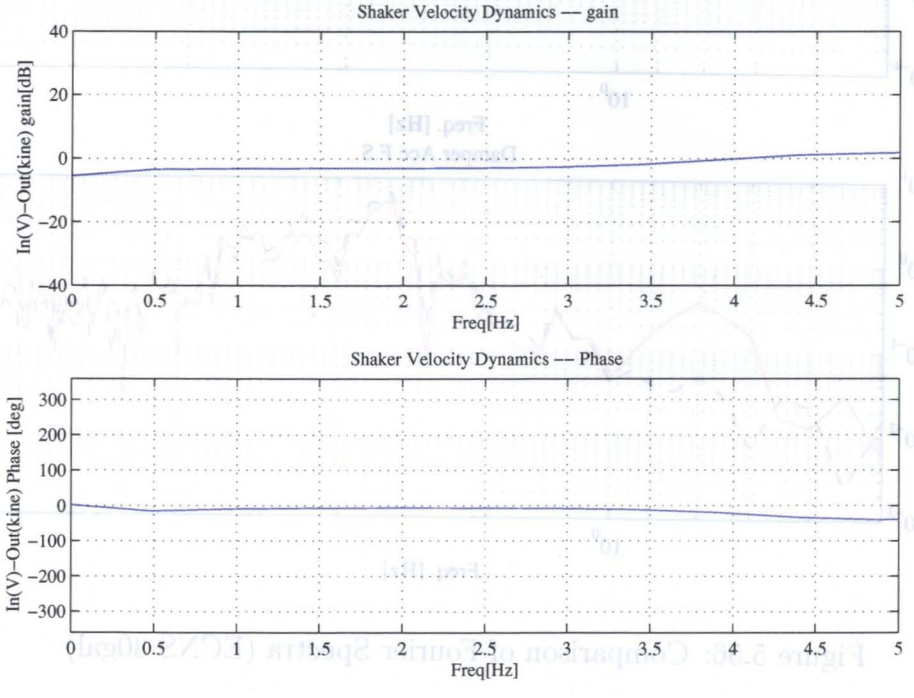

Figure 5.58: Transfer Function from Command to the Shaker Relative Velocity

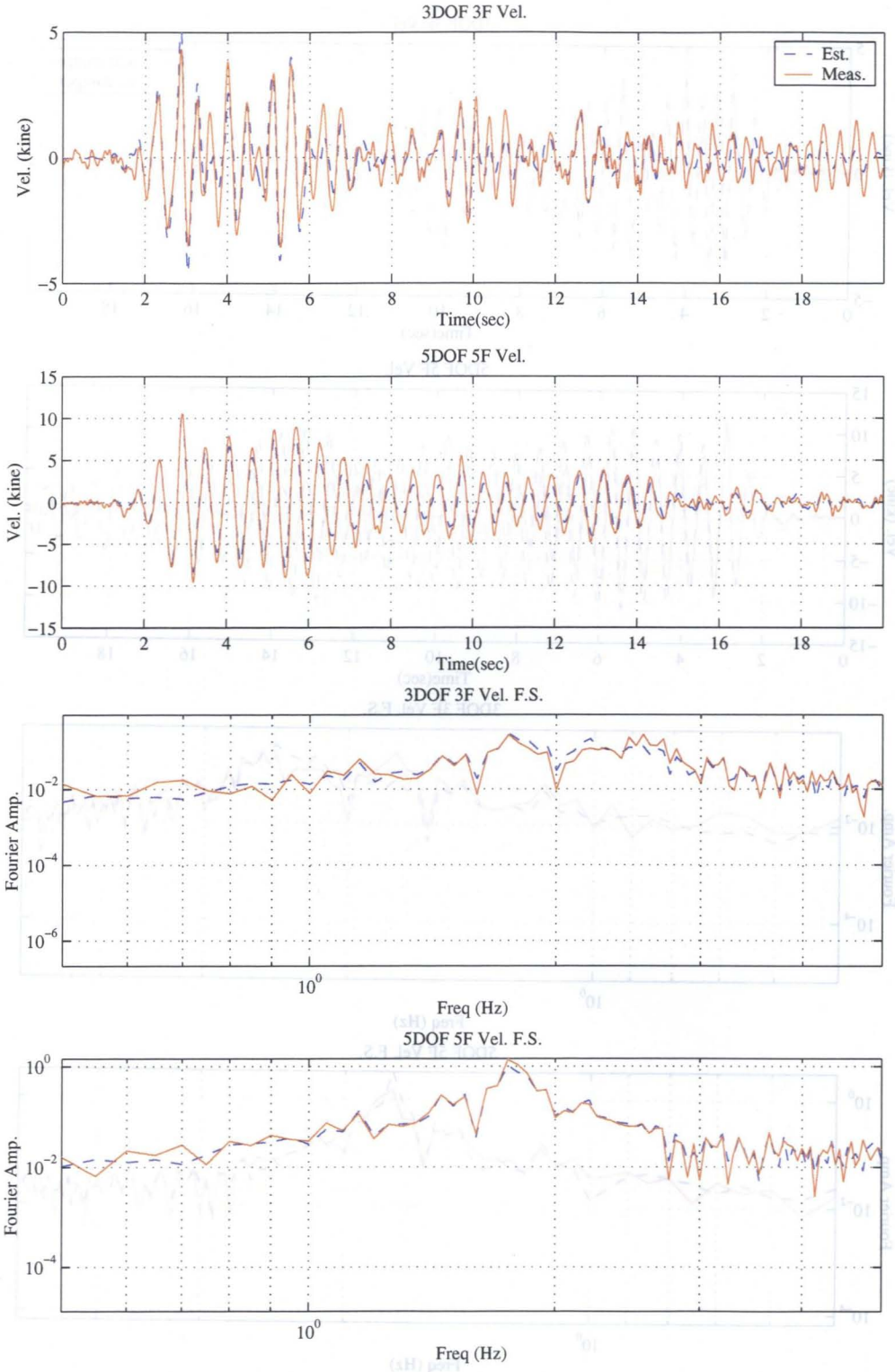

Figure 5.59: Comparison of Fourier Spectra (ECNS 30gal)

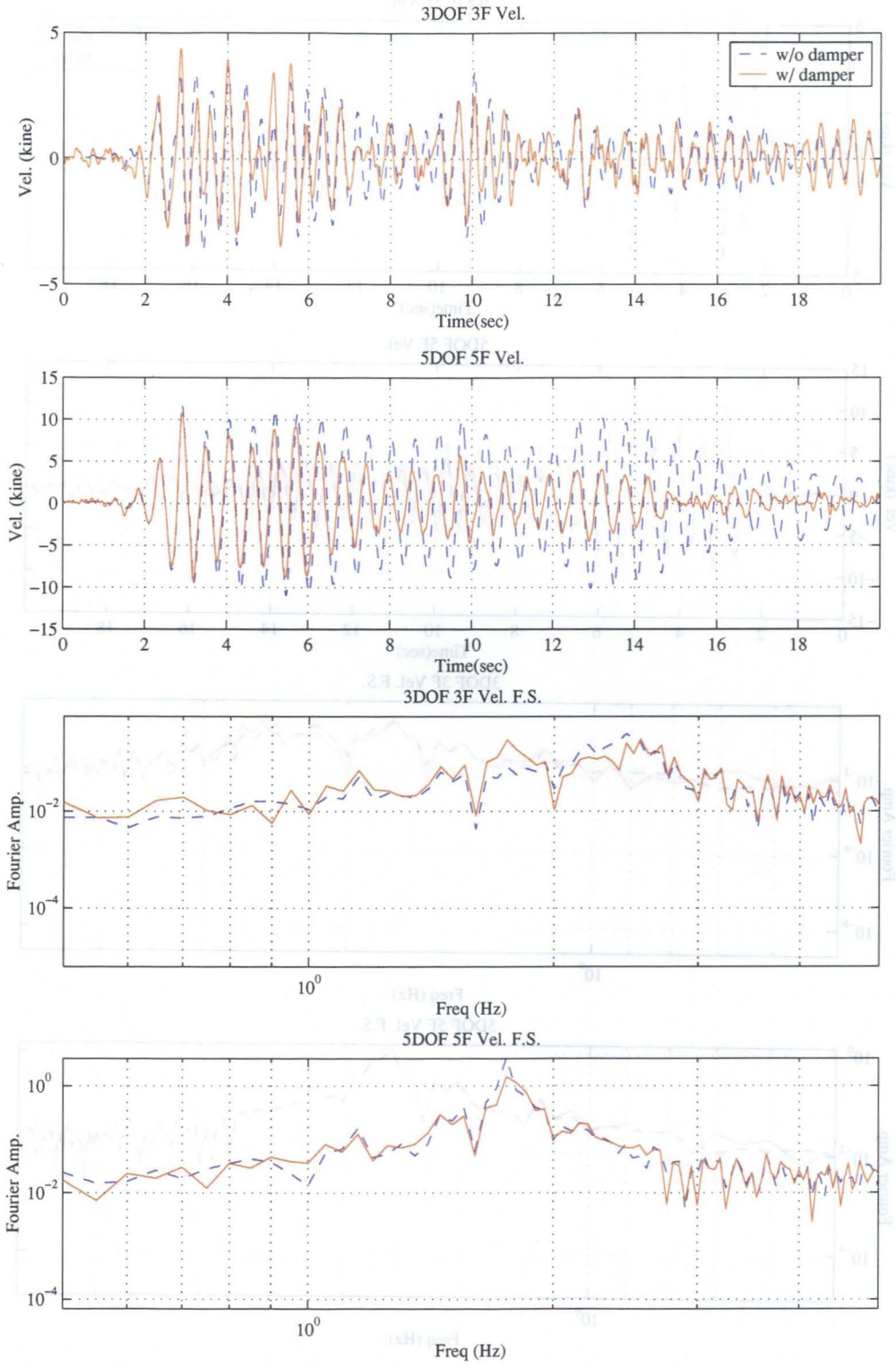

Figure 5.60: Comparison of Fourier Spectra (ECNS 30gal)

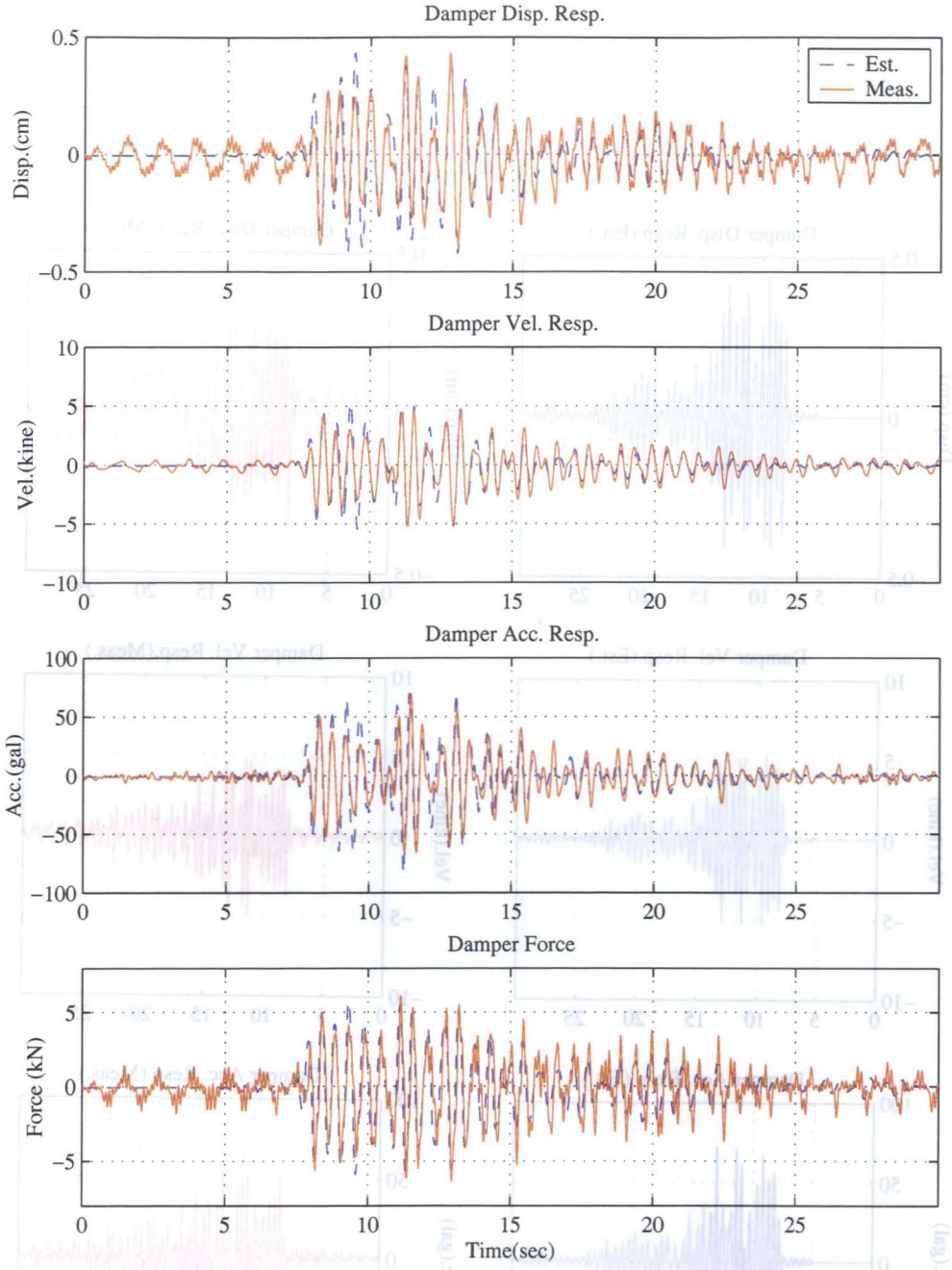

Figure 5.61: Comparison of the Structural Response (KBNS 30gal)

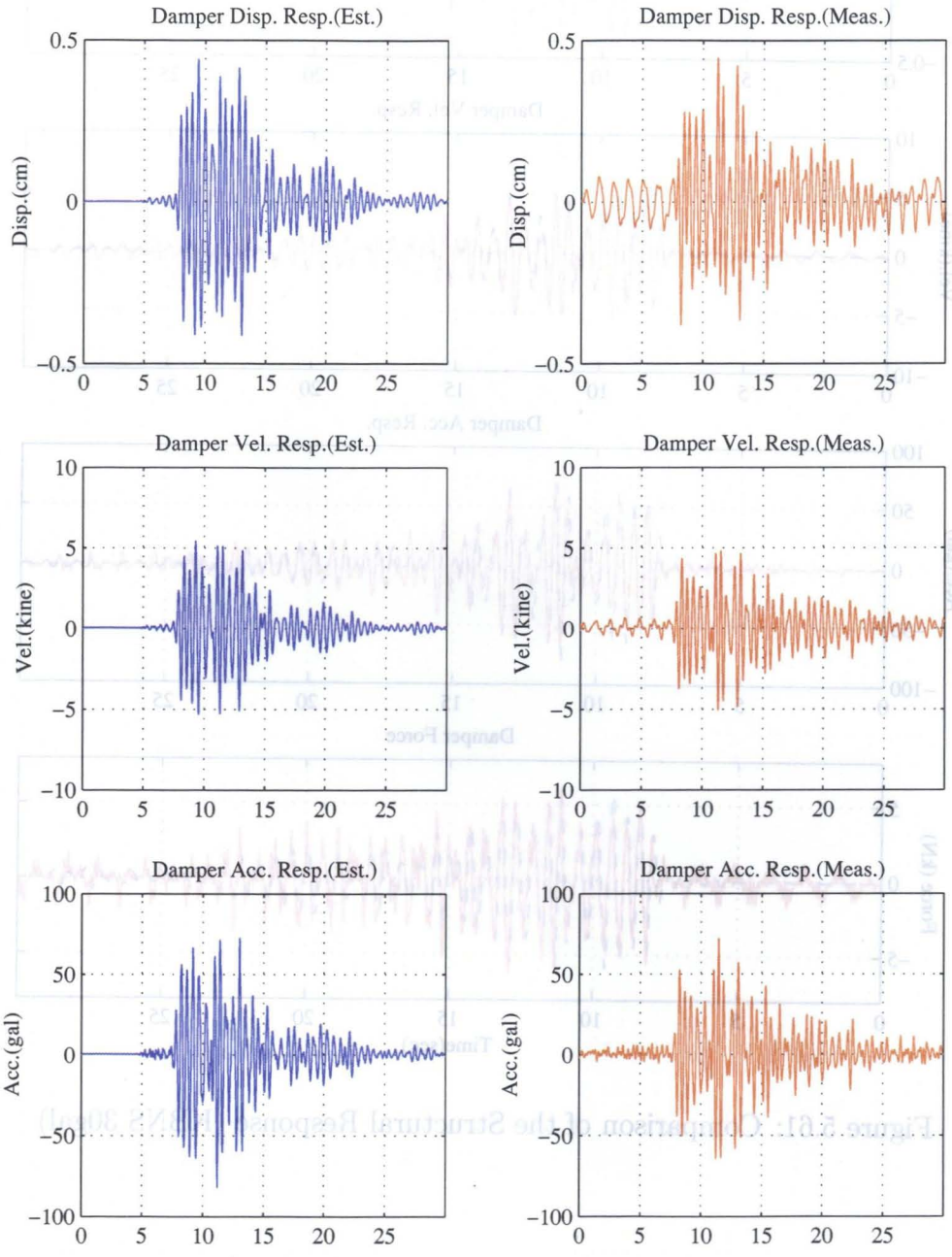

Figure 5.62: Comparison of the Structural Response(KBNS 30gal)

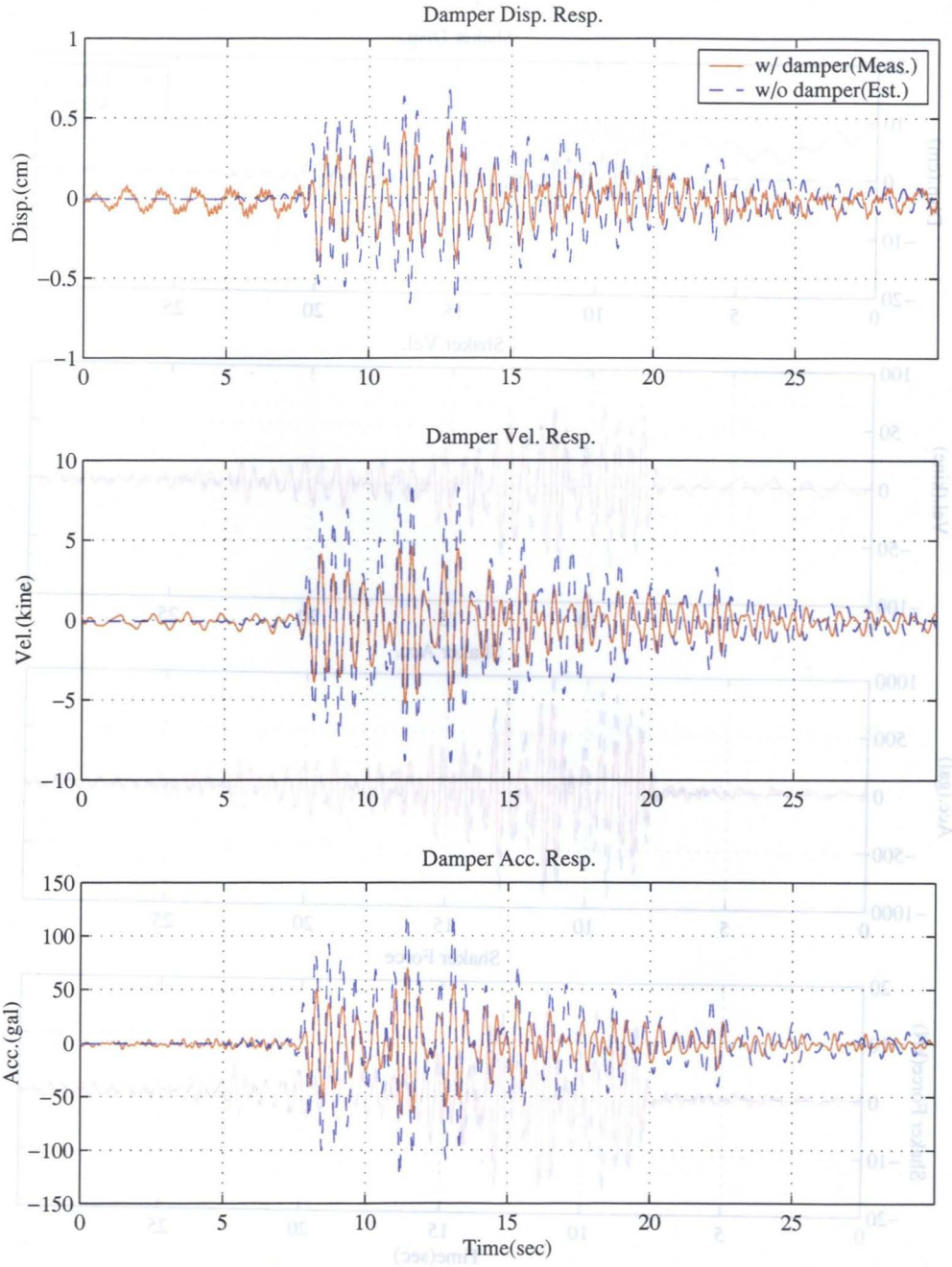

Figure 5.63: Comparison of the Structural Response (KBNS 30gal, w/ & w/o damper)

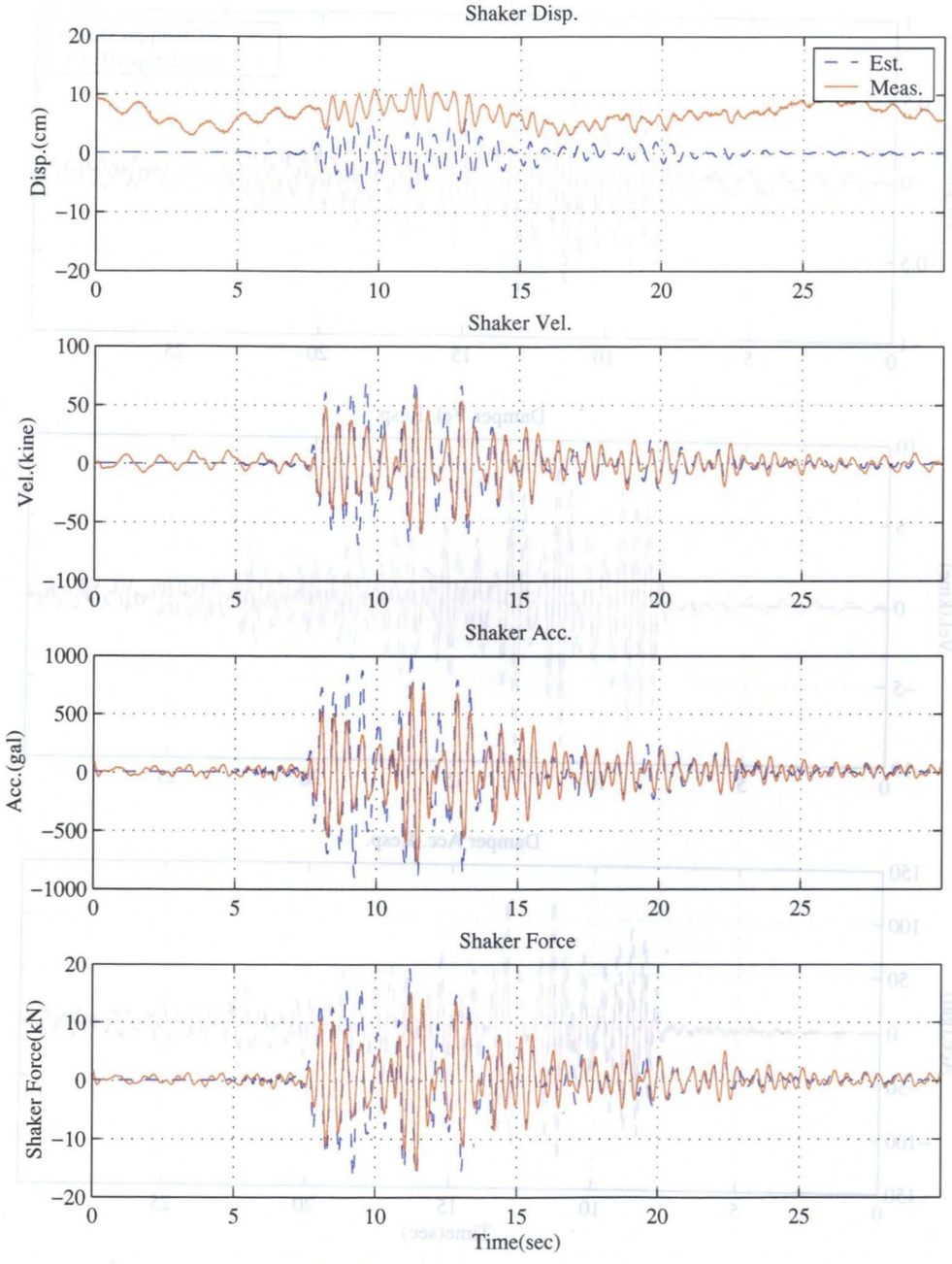

Figure 5.64: Shaker Response (KBNS 30gal)

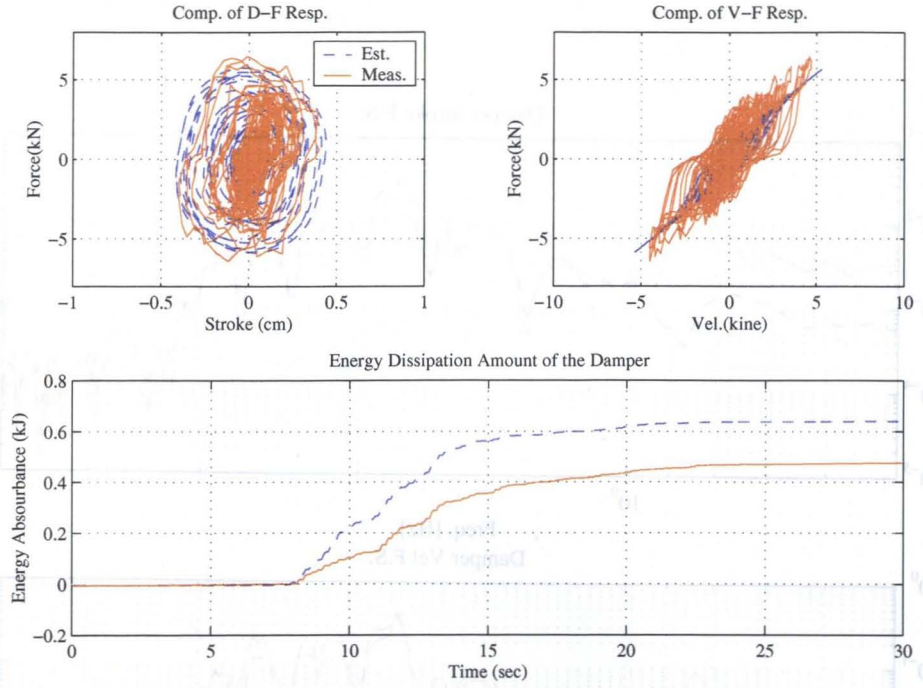

Figure 5.65: Damper Responses (KBNS 30gal)

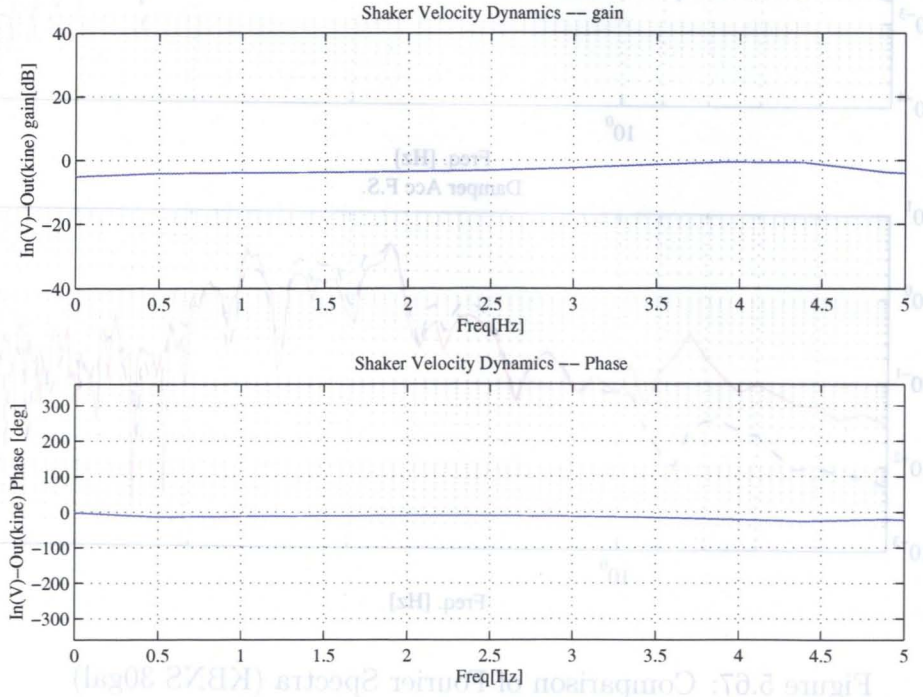

Figure 5.66: Transfer Function from Command to the Shaker Relative Velocity

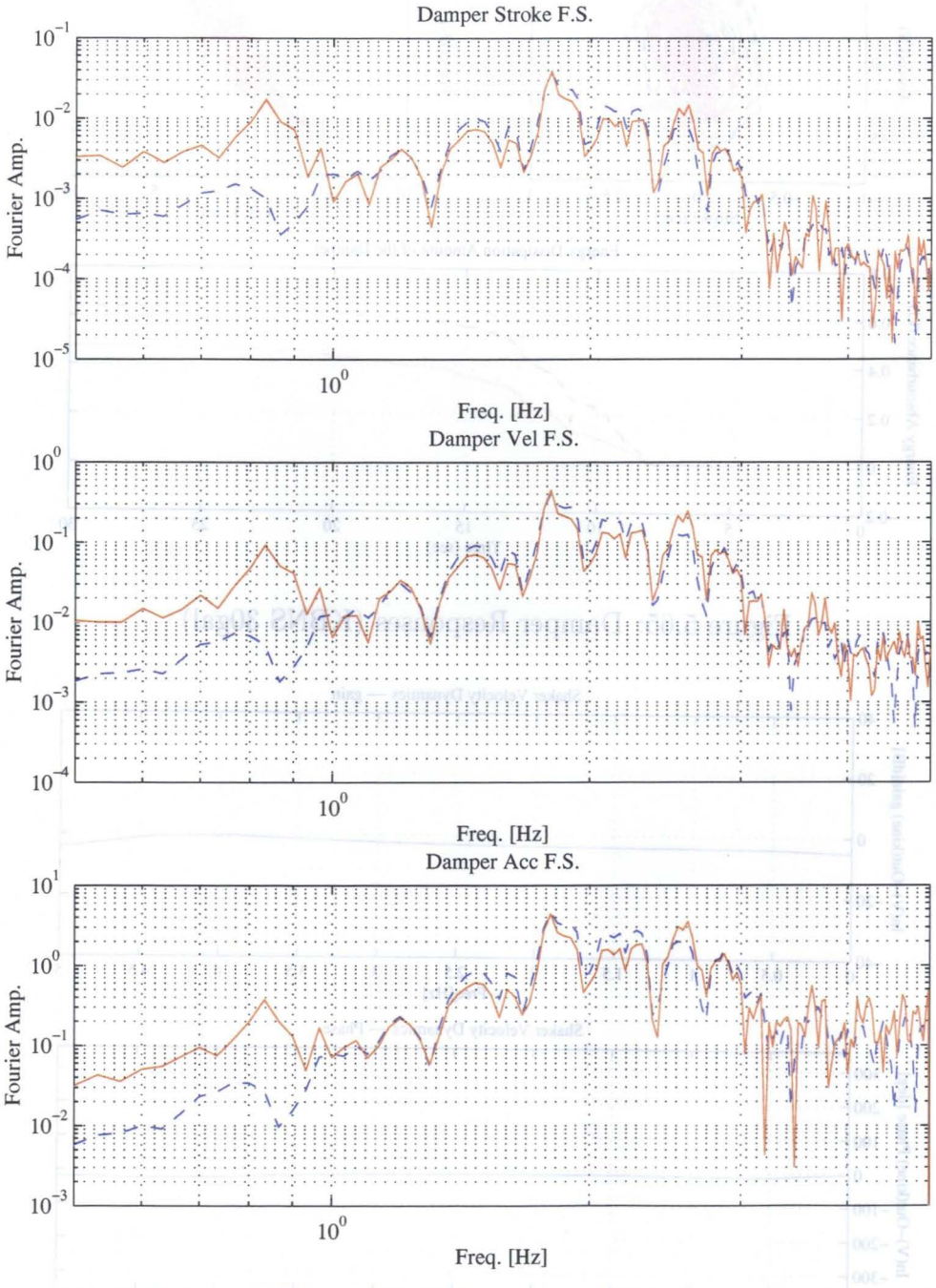

Figure 5.67: Comparison of Fourier Spectra (KBNS 30gal)

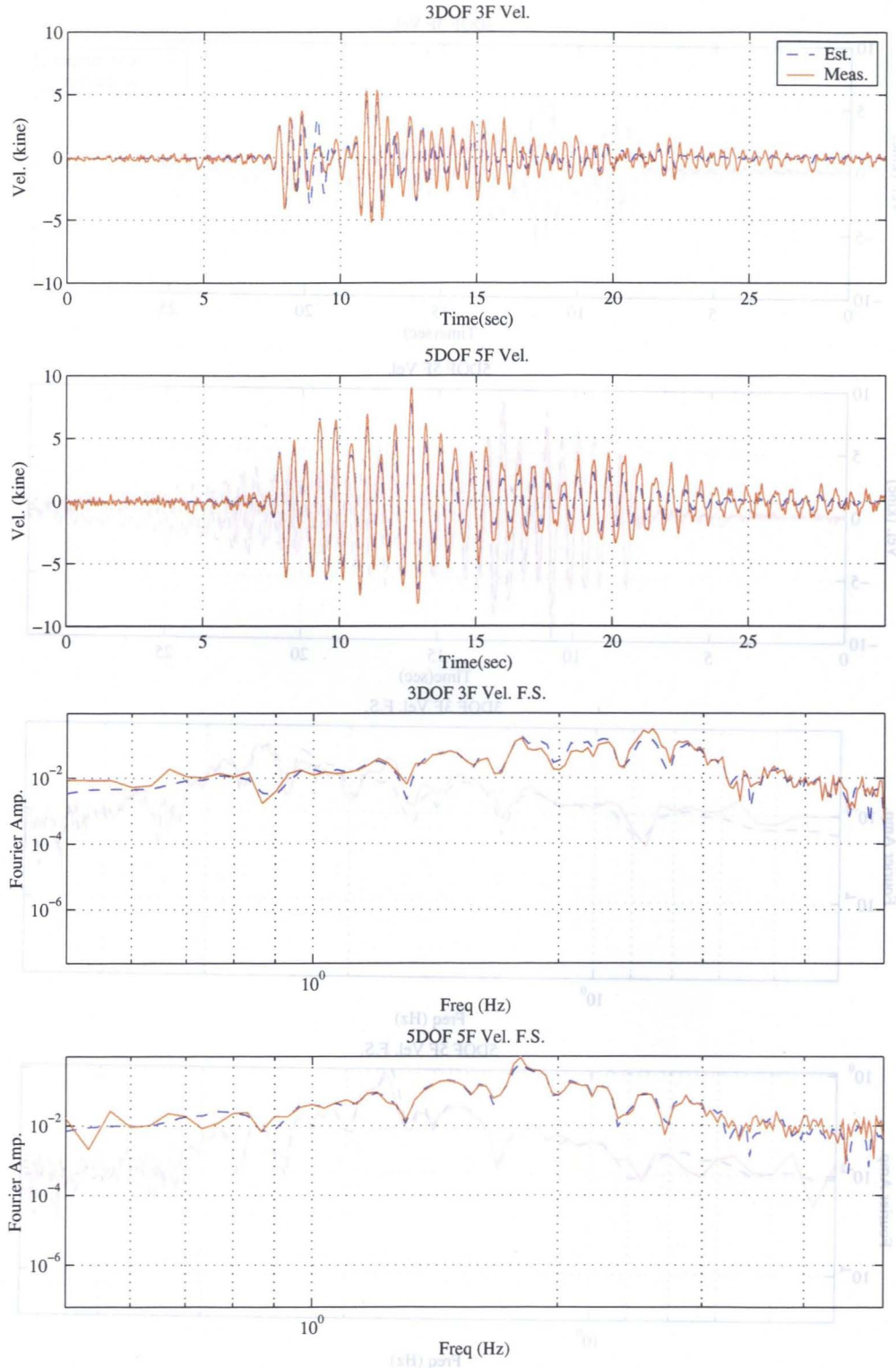

Figure 5.68: Comparison of Fourier Spectra (KBNS 30gal)

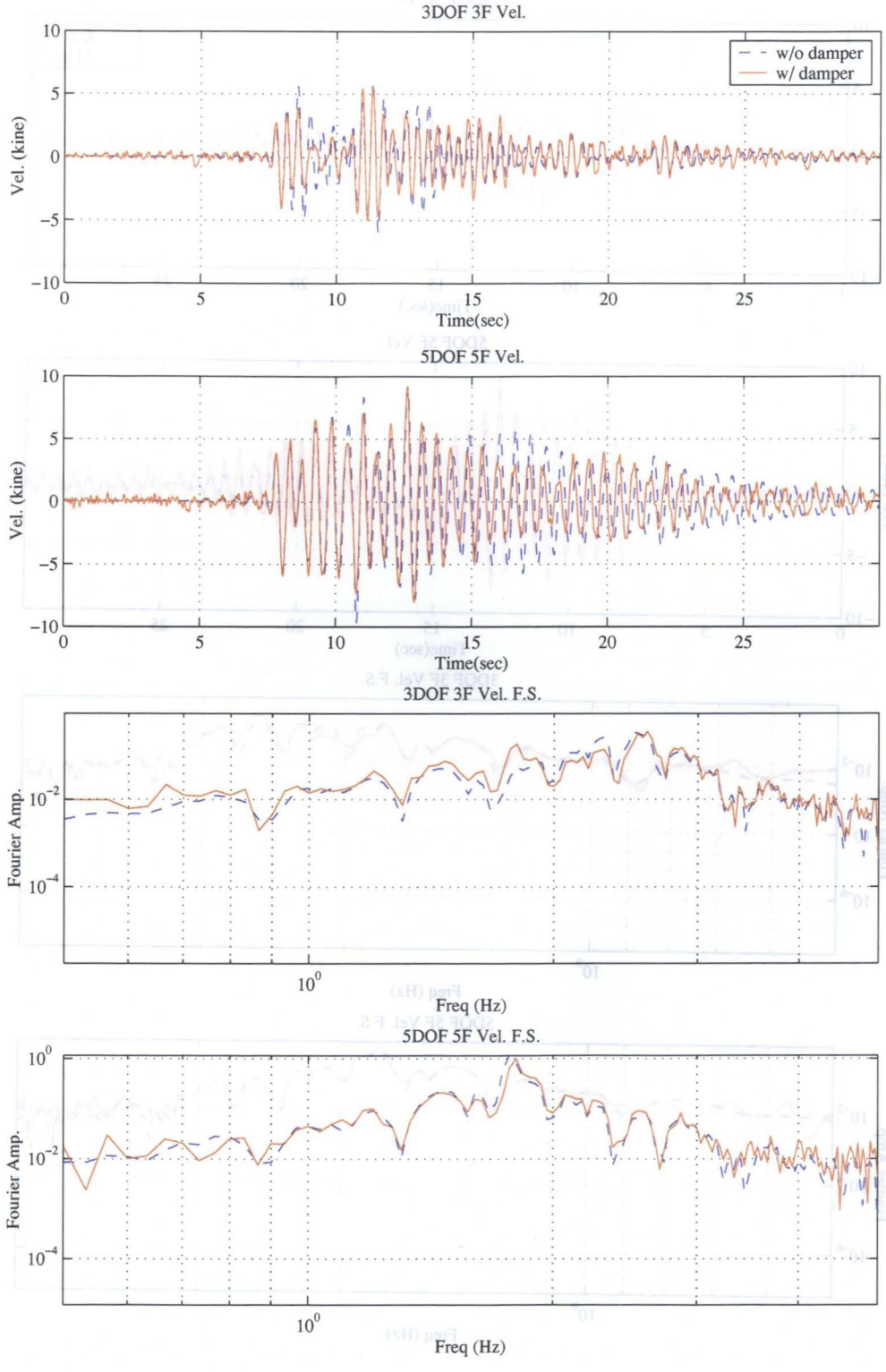

Figure 5.69: Comparison of Fourier Spectra (KBNS 30gal)

5.7 Summary

The achievements mentioned in this chapter are the main objective of this dissertation. Efficacy of the proposed shaker control method and the IFDL system for being used as the real time hybrid system is confirmed through full-scale experiment. As damper specimen, passive controlled MR damper is utilized in which command current is kept to be a constant 0 A.

Following things could be found from the SDOF structure test:

- In the resonance sinusoidal ground motion test, it is confirmed proposed shaker control method works effectively, and good agreements are observed between simulation and experiment
- The identified damper model could trace the measured behavior with good accuracy
- Good agreements in maximum response level and overall trends could be observed in the earthquake loading tests
- A shaker compensation method is found to be effective for command signals with wide-range frequency components

Also, results of the MDOF structure test are listed below:

- A structural model for the joint damper system experiment is used as hypothetical structure in order to compare with past experimental results
- In the resonance sinusoidal ground motion test which frequency corresponds to the natural frequency of the 5-story frame structure, damper as well as top floor responses could be replicated with good accuracy. Effects of coupling structures could be also observed
- On the contrary, when adjusted to the natural frequency of the 3-story frame structure, obtained results are slightly larger compared to the estimation. It is thought that the lack of the traceability of the estimated damper might cause difference
- In the earthquake excitation tests, effect of the coupling structures could be clearly observed, in which natural frequencies of the both structures become closer. Effective response reduction is observed in 5-story structure under El Centrol NS input, clear contrast to that of the 3-story structure. Under Kobe

NS input, joint damper system does not work so effectively. These all results coincide with those of the previously conducted full-scale experiment

- Dynamics of the joint damper system with passive damper are well traced without using the real structural systems

- Deficiency in the shaker force and velocity are observed in some test cases, particularly when assuming the high frequency motion. In order to overcome this difficulty, more powerful servo motor should be introduced. Alternatively, natural frequency of the test system should be closer to that of the hypothetical structure by replacing the rubber supports.

On the whole, it is confirmed that the proposed shaker control method together with the PID compensation work quite effectively for realizing the real time hybrid loading experiment. Particularly, in the MDOF tests, the overall trends in frequency domain observed from the results coincide with that of the full-scale experiment results. It is advantageous to trace the dynamics of the structural system with damper specimen without constructing the total structures. However, a more capable shaker or changing the dynamic properties of the IFDL test system itself, are required for conducting the experiment with larger amount of the ground motion level. It is also advantageous from the viewpoint of avoiding the uncertain behaviors that might take place in the small response regions.

References

(1) Iemura, H., Igarashi, A., and Toyooka, A.: Full-scale Structural Vibration Control Experiments Using Joint Damper System, *Proceedings of the Second Japan National Symposium on Structural Control*, pp. 121 – 128, 2000.

(2) Iemura, H., Igarashi, A., and Toyooka, A. : Full-Scale Experiment of the Joint Damper System for Structural Vibration Control (in Japanese), *Journal of Structural Mechanics and Earthquake Engineering*, pp. 91 – 101, 7 2002.

(3) Iemura, H., Igarashi, A., and Nakata, N.: Full-scale Verification Tests of Semi-active Control of Structures Using Variable Joint Damper System, *Proceedings of the 3rd World Conference on Structural Control*, 2002.

(4) Iwanami, K., Suzuki, K., and Seto, K. : Vibration Control Method of Parallel Structures Connected to Each Other with Damper and Spring (in Japanese), *Journal of the Japan Society of Mechanical Engineers (Part C)*, pp. 2975 – 2980, 10 1993.

(5) Seto, K., Toba, Y., Matsumoto, Y., and Doi, F. : Vibration Controlling and Modeling Methods for Flexible Structures Arranged in Parallel (Basic Study for Realizing Super-Tall Buildings) (in Japanese), *Journal of the Japan Society of Mechanical Engineers (Part C)*, pp. 1899 – 1905, 5 1995.

(6) Abe, M. and Fujino, Y. : Optimal Design of Passive Energy Dissipation Devices for Seismic Protection of Bridges (in Japanese), *Journal of Structural Mechanics and Earthquake Engineering*, pp. 241 – 252, 10 1998.

(7) Luco, J. E. and Barros, F. C. P. D. : Optimal Damping Between Two Adjacent Elastic Structures, *Earthquake Engineering and Structural Dynamics*, Vol. 27, pp. 649 – 659, 1998.

(8) Zhang, W. S. and Xu, Y. L. : Dynamic Characteristics and Seismic Response of Adjacent Buildings Linked by Discrete Dampers, *Earthquake Engineering and Structural Dynamics*, Vol. 28, pp. 1163 – 1185, 1999.

Chapter 6

Semi-Active Pseudo-Negative Stiffness Control

6.1 General Remarks

In this chapter, the pseudo-negative stiffness (P.N.S.) control method is introduced as a simple but powerful control algorithm for the controllable damper. This technique can be regarded as one of the semi active control methods in which the control force is given by the combination of the negative stiffness element plus positive damping element. An efficacy of the proposed PNS control is examined both algebraically and numerically. As a result, it is shown that the control method is advantageous over the passive device in terms of absolute acceleration reduction. Furthermore, results of the actuator loading experiment so as for the MR damper to realize the PNS control are shown.

6.2 Concept of the Pseudo-Negative Stiffness (PNS) Control

The PNS control is originally intended to be realized by the active control method, in which the control force of the device is given by the following algorithm[1)].

$$F(t) = K_D x(t) + C_D \dot{x}(t) \tag{6.1}$$

Where,

$$K_D\,(<0)\,:\,\text{Apparent Negative Stiffness}$$
$$C_D\,(>0)\,:\,\text{Apparent Damping}$$

Since the natural period of the system can be apparently elongated by giving the negative stiffness to the structural system, this method can work effectively for reducing the acceleration. This method is also advantageous from the viewpoint of the application to the structural system because only stroke and stroke velocity at the damper locations are required for determining the control force, which is clear contrast to the traditional sophisticated but complicated active control algorithms. In addition, its clear physical meanings in elongation of the natural period and increasing system dampings make the controller design easier compared to the other sophisticated but complicated algorithms.

Despite these advantages, this strategy requires the devices to move the opposite direction from that of the velocity, and it might make the structural system unstable. Moreover, it is not economical to install large scale active device such as hydraulic actuators, followed by many sophisticated device control equipments.

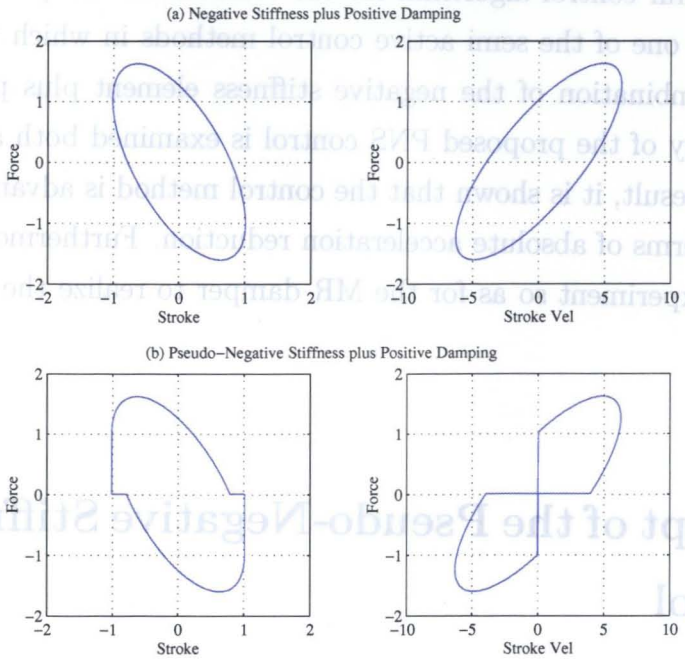

Figure 6.1: Negative and Pseudo Negative Stiffness Device Hysteresis

Alternatively, much more attentions have been paid to the semi active controlled devices, particularly an MR damper. Since semi active device can alter its dynamic characteristics in real time, most of the algorithms designed for the active devices can

be directly applied within the constraints of the device. Its constraint is, however, even advantageous when it comes to the realistic applications from the viewpoint of the system robustness. The semi active device itself has no ability to generate the energy, it does not excite the structural system.

The objective of the PNS control is to realize the combined hysteresis of the apparent negative stiffness and positive damping elements while considering the physical constraints. Figure 6.1 shows the idealized and feasible displacement versus force and velocity versus force relations. In clear contrast to the idealized hysteresis which can be realized by the active device, semi active device can not generate the force in the second and fourth quadrants of the velocity versus force relation. The term 'pseudo' is then used for the semi active devices in terms of realizing the commanded purely negative stiffness within such constraints of the device. As the target device, the MR damper is again used in this research.

6.3 Effectiveness of the Negative Stiffness for a SDOF Structure

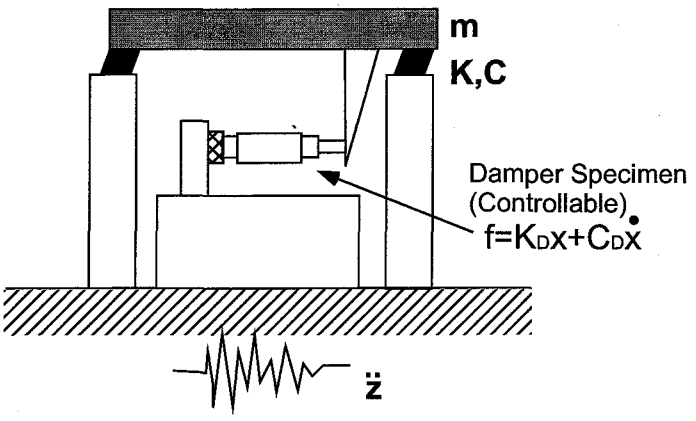

Figure 6.2: Hypothetical SDOF Structure with Controllable Damper

To begin with, the effectiveness of the negative stiffness plus damping elements is examined algebraically by introducing the hypothetical SDOF structure. Suppose the SDOF structure with additional damping C_D and stiffness K_D as depicted in Figure 6.2. These supplemental elements are assumed to be realized by the damper specimen. The equation of motion of the hypothetical SDOF structure exposed to the earthquake $\ddot{z}$ can be written as follows,

$$m\ddot{x} + (c + C_D)\dot{x} + (k + K_D)x = -m\ddot{z} \tag{6.2}$$

or equivalently,

$$\ddot{x} + 2h\omega\sqrt{1+\gamma}\,\dot{x} + (1+\gamma)\omega^2 x = -\ddot{z}. \tag{6.3}$$

Where,

$$\omega' = \sqrt{\frac{k+K_D}{m}} = \sqrt{1+\gamma}\,\omega \tag{6.4}$$

$$\frac{c+C_D}{m} = 2h\omega' = 2h\sqrt{1+\gamma}\,\omega \tag{6.5}$$

In order to generalize the discussion, ground motion is assumed to be the impulsive motion, that is

$$\ddot{z} = \delta(t) \tag{6.6}$$

Then, unit impulse response functions with regard to the displacement, velocity, and acceleration can be obtained as follows.

$$x(t) = \frac{e^{-\sqrt{1+\gamma}\,\omega ht}}{\omega\sqrt{(1+\gamma)(1-h^2)}}\sin(\omega_h t) \tag{6.7}$$

$$v(t) = \frac{e^{-\sqrt{1+\gamma}\,\omega ht}}{\sqrt{1-h^2}}\left\{h\sin(\omega_h t) - \sqrt{1-h^2}\cos(\omega_h t)\right\} \tag{6.8}$$

$$a(t) = \frac{\sqrt{1+\gamma}\,\omega e^{-\sqrt{1+\gamma}\,\omega ht}}{\sqrt{1-h^2}}\left\{-2h^2\sin(\omega_h t) + 2h\sqrt{1-h^2}\cos(\omega_h t) + \sin(\omega_h t)\right\} \tag{6.9}$$

Where,

$$\omega_h = \sqrt{(1+\gamma)(1-h^2)}\,\omega.$$

Substituting $C_D = 0$ and K_D=0 gives the ordinary unit impulse response functions. The times that give the maximum values of Eq.(6.7),(6.8),and(6.9) are given as follows.

$$t_{\text{maxd}} = \frac{1}{\omega_h}\arctan\left(\frac{\sqrt{1-h^2}}{h}\right) \tag{6.10}$$

$$t_{\text{maxv}} = \frac{1}{\omega_h}\arctan\left(\frac{2h\sqrt{1-h^2}}{2h^2-1}\right) \tag{6.11}$$

$$t_{\text{maxa}} = \frac{1}{\omega_h}\arctan\left(\frac{(4h^2-1)\sqrt{1-h^2}}{(4h^2-3)h}\right) \tag{6.12}$$

Corresponding maximum displacement, velocity, and absolute acceleration are then obtained as

$$x_{\max} = -\frac{1}{\omega\sqrt{1+\gamma}} \exp\left\{-\frac{h \arctan\left(\frac{\sqrt{1-h^2}}{h}\right)}{\sqrt{1-h^2}}\right\} \tag{6.13}$$

$$v_{\max} = \exp\left\{-\frac{h \arctan\left(\frac{2h\sqrt{1-h^2}}{2h^2-1}\right)}{\sqrt{1-h^2}}\right\} \mathrm{sign}(2h^2-1) \tag{6.14}$$

$$a_{\max} = -\sqrt{1+\gamma}\omega \exp\left\{-\frac{h \arctan\left(\frac{(4h^2-1)\sqrt{1-h^2}}{h(4h^2-3)}\right)}{\sqrt{1-h^2}}\right\} \mathrm{sign}(4h^2-3). \tag{6.15}$$

Where,

$$\mathrm{sign}(x) = \begin{cases} +1 & \text{if} \quad x > 0 \\ 0 & \text{if} \quad x = 0 \\ -1 & \text{if} \quad x < 0 \end{cases}$$

From these results, following things can be expected by introducing the negative stiffness to the device control. As seen in Eq.(6.15), device with negative stiffness and positive damping gives smaller amount of the maximum acceleration compared to that with positive stiffness and damping. It can be also proved by considering the response spectra. The response spectra with regard to both El Centro NS and Kobe NS inputs are depicted in Figure 6.3. Maximum accelerations in both earthquakes are scaled to 100 gal. It is a well known fact that the system with longer natural period shows smaller amount of the maximum acceleration, which can be clearly seen in the figure[2)]. On the other hands, it is found from the definition of the natural frequency Eq.(6.4) that taking γ negative corresponds to elongate the apparent natural period of the total structural system.

Also, given that constant damping ratio h and negative γ, required damping coefficient C_D to realize the designated damping ratio can take the smaller value compared to the the case that γ is positive. This advantage can be found from the definition Eq.(6.5). In other words, negative stiffness gives the larger damping ratio compared to the positive stiffness even if the damping coefficient C_D are the same in both devices.

To sum up, it is advantageous to introduce the negative stiffness control from the viewpoints of reducing the maximum acceleration by elongating the natural period of the system, while restraining the maximum displacement by giving the large damping ratio.

In order to illustrate these effects, numerical study is conducted for the hypothetical SDOF structure with controllable damper subjected to the earthquake. In this study, the IFDL system is assumed to be the primary structure, and algebraic damper model is utilized to take the dynamics of the damper specimen into consideration, i.e. device control force F_c is determined as follows.

$$F_c(t) = \begin{cases} K_D x + C_D \dot{x} & \text{if } F_c(t) \cdot \dot{x} > 0 \\ 0 & \text{if } F_c(t) \cdot \dot{x} < 0 \end{cases} \tag{6.16}$$

In case of the positive stiffness and damping, commanded force is fully realized.

In the realistic situation, it is impossible to generate the zero control force. In the simulation, this zero force is substituted by the minimum control force of the device obtained from the model. As ground motions, El Centro NS and Kobe NS waves are used. Maximum accelerations are assumed to be 100 gals in both inputs.

Figure 6.4 shows the maximum displacement, velocity, and absolute acceleration under El Centro NS input with various stiffness K_D and C_D, including negative and positive stiffness. Figure 6.6 depicts the same responses under Kobe NS input. As observed in these figures, negative stiffness could give the smaller amount of the absolute acceleration, which is algebraically estimated. Figures 6.5 and 6.7 shows the changes of frequency ratio γ, corresponding damping ratio h and maximum force of the device with the changes of additional stiffness and damping. It is observed that damping ratio becomes larger even under constant additional damping coefficient by introducing negative stiffness. This increase of damping ratio restrains the increase of the displacement response that occurs by the elongation of natural period.

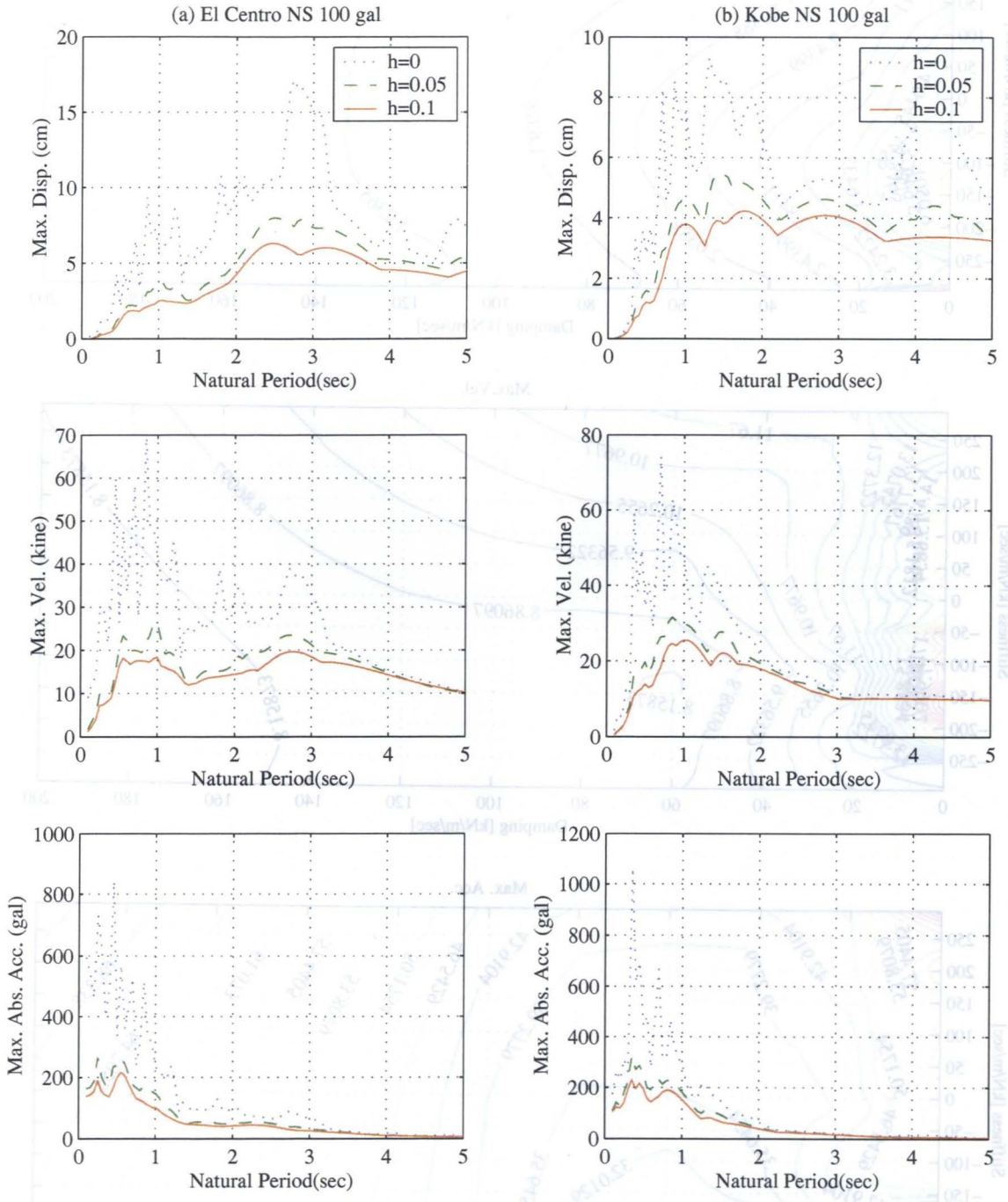

Figure 6.3: Response Spectra for ECNS and KBNS

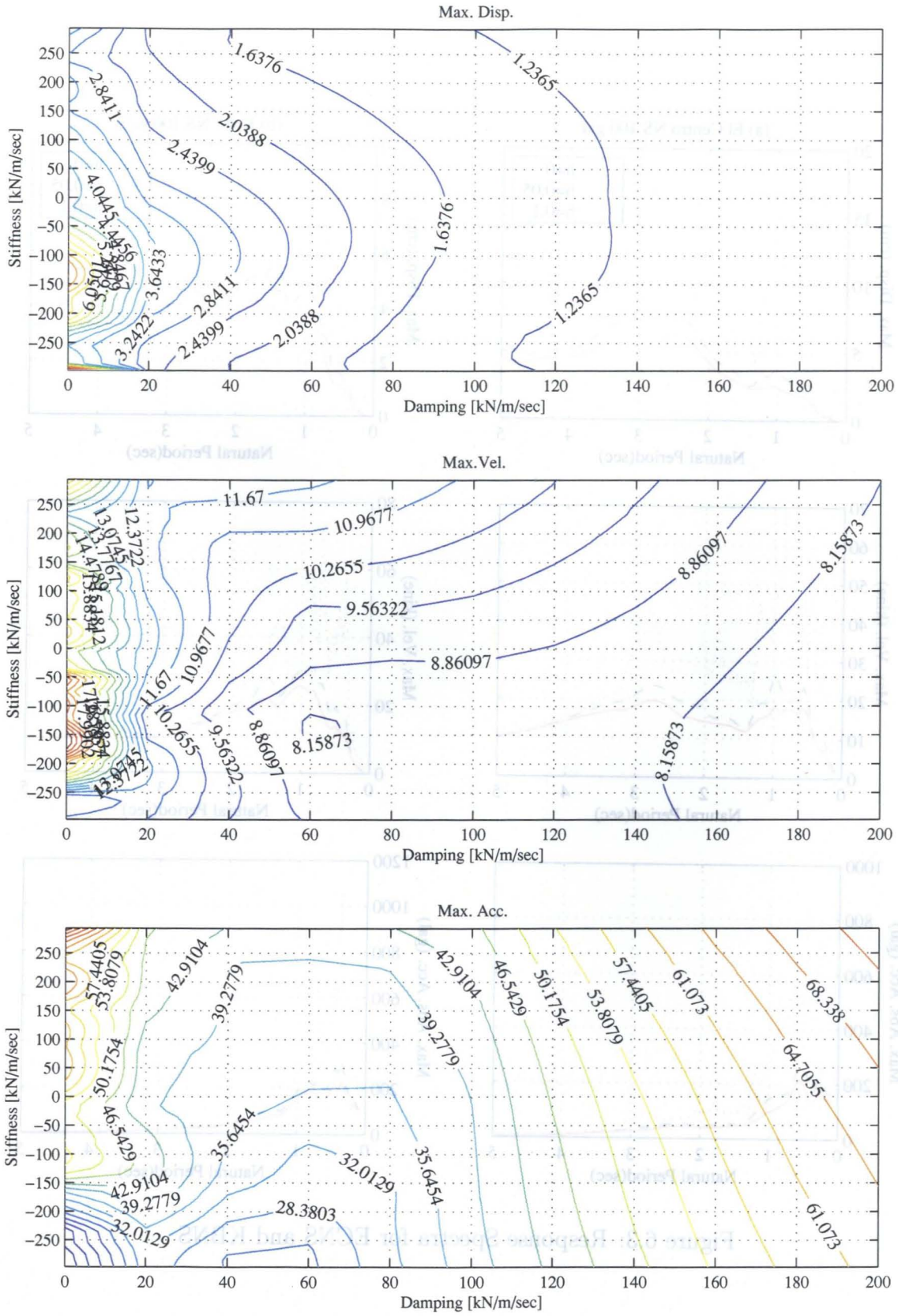

Figure 6.4: Maximum Response (ECNS 100 gal)

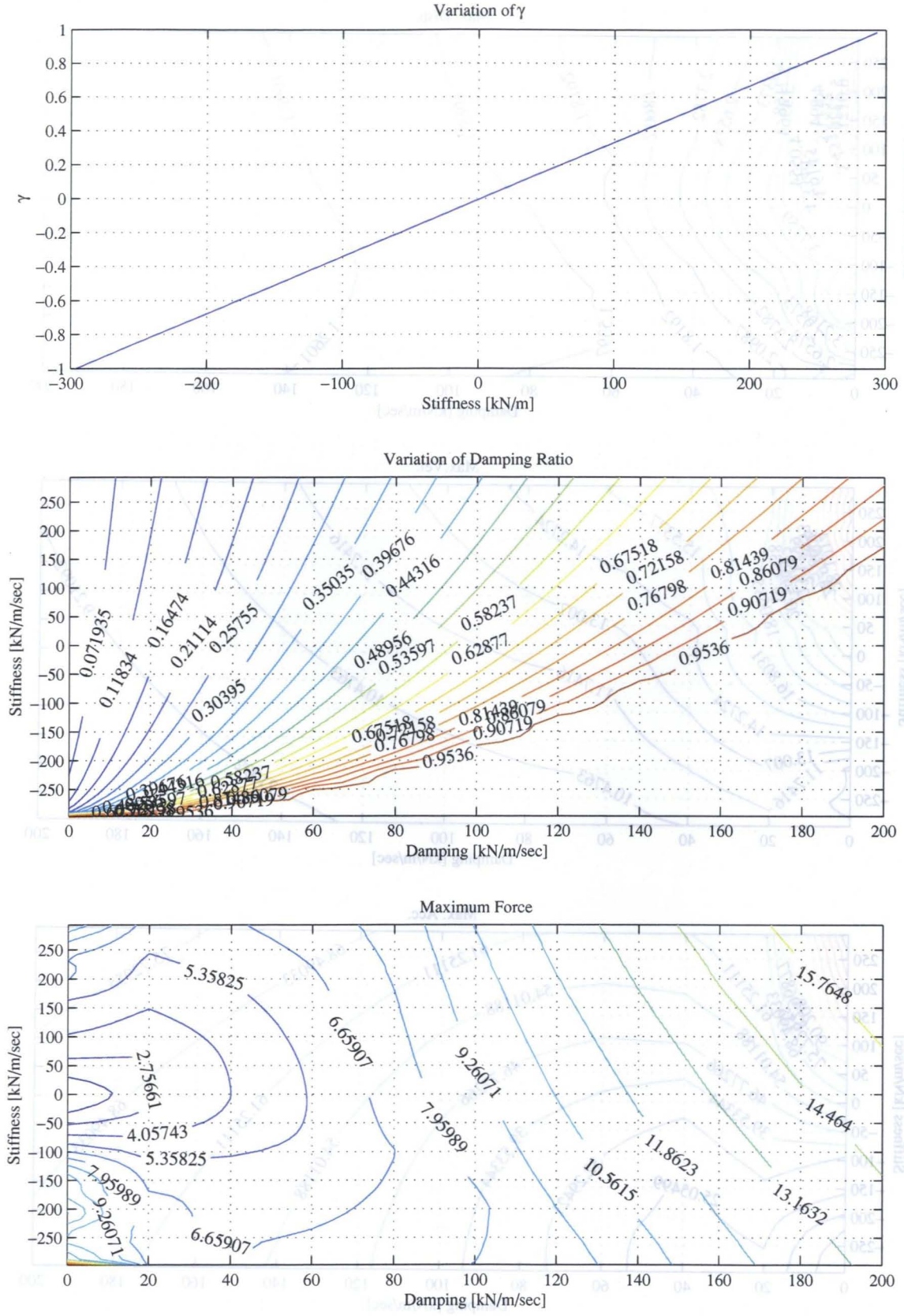

Figure 6.5: Variation of γ, h, and Damper Force (ECNS 100 gal)

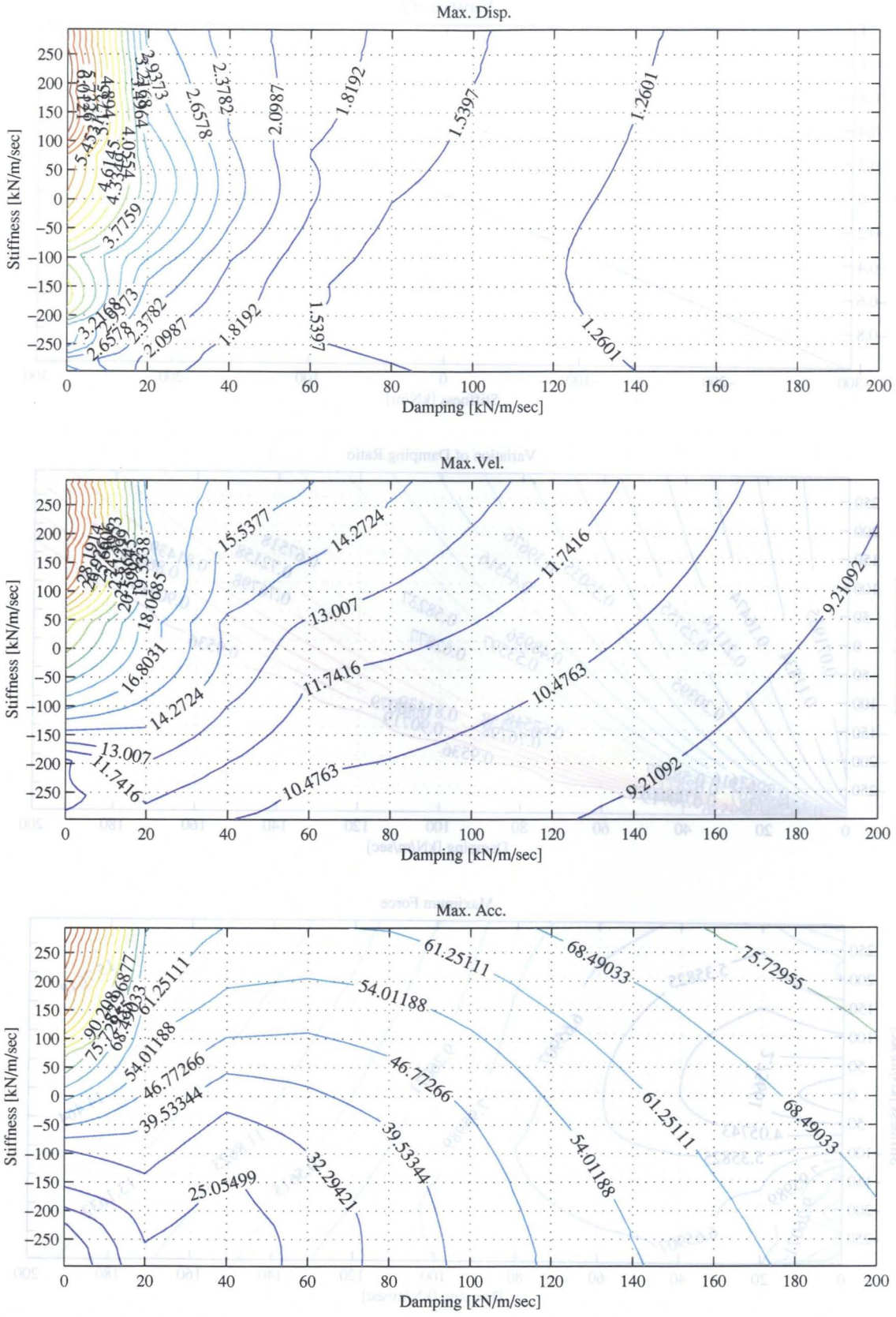

Figure 6.6: Maximum Response (KBNS 100 gal)

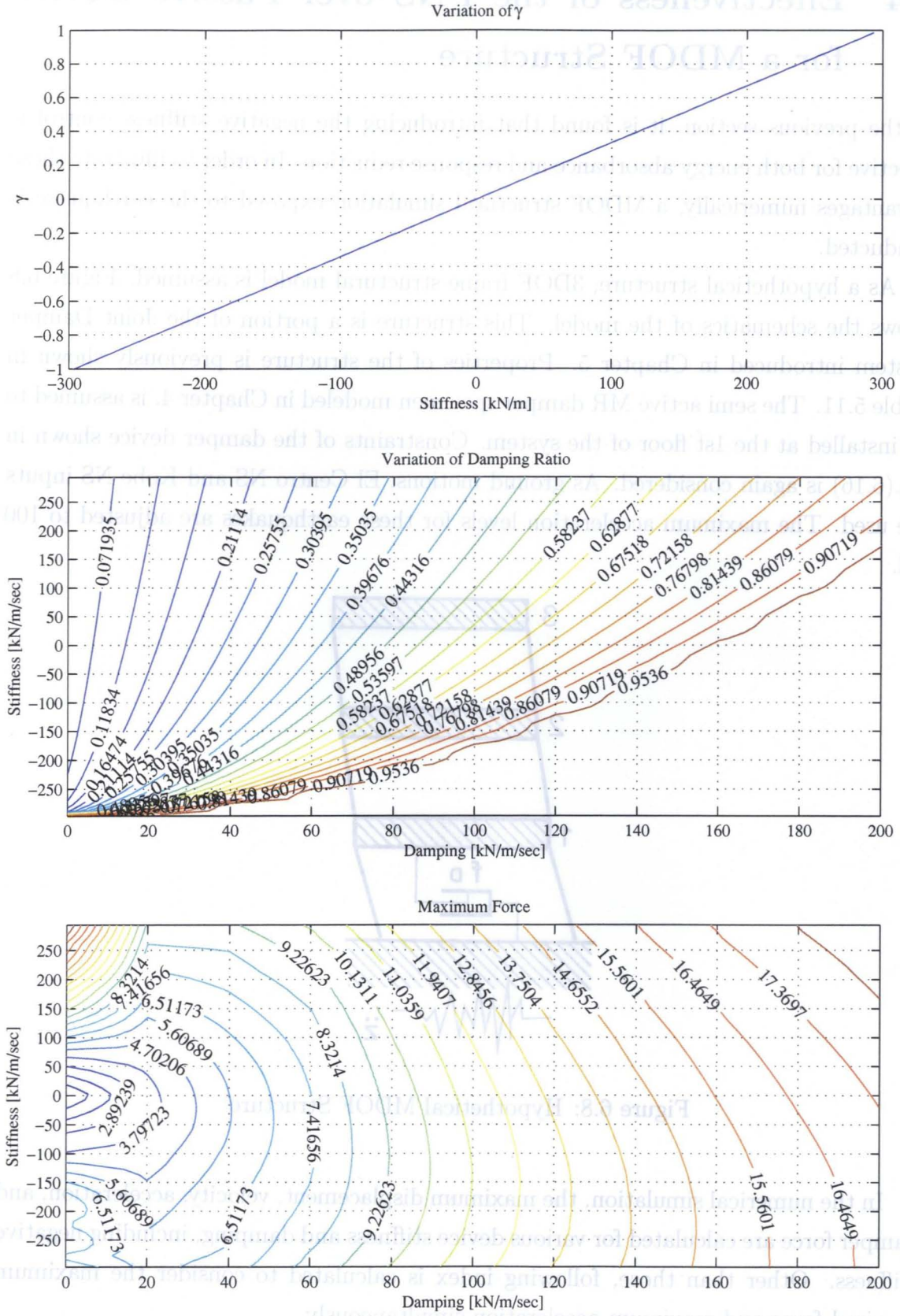

Figure 6.7: Variation of γ, h, and Damper Force (KBNS 100 gal)

6.4 Effectiveness of the PNS over Passive Device for a MDOF Structure

In the previous section, it is found that introducing the negative stiffness control is effective for both energy absorbance and response reduction. In order to illustrate these advantages numerically, a MDOF structural simulation exposed to the earthquake is conducted.

As a hypothetical structure, 3DOF frame structural model is assumed. Figure 6.8 shows the schematics of the model. This structure is a portion of the Joint Damper System introduced in Chapter 5. Properties of the structure is previously shown in Table 5.11. The semi active MR damper specimen modeled in Chapter 4, is assumed to be installed at the 1st floor of the system. Constraints of the damper device shown in Eq.(6.16) is again considered. As ground motions, El Centro NS and Kobe NS inputs are used. The maximum acceleration levels for these earthquakes are adjusted to 100 gal.

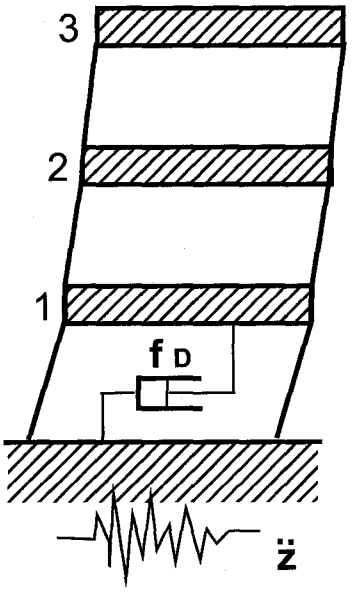

Figure 6.8: Hypothetical MDOF Structure

In the numerical simulation, the maximum displacement, velocity, acceleration, and damper force are calculated for various device stiffness and damping, including negative stiffness. Other than those, following index is calculated to consider the maximum required force and maximum acceleration simultaneously.

$$J = \max|f_D(t)| + M_{total} \cdot \max|\ddot{x}_{3F}(t)|$$

Where, $f_D(t)$ and $\ddot{x}_{3F}(t)$ are the damper reaction force and top floor absolute acceleration respectively. Also, M_{total} is the total mass of the structure, which is 61.17 ton.

For damper specimen model, same conditions with the SDOF simulation are used again in this case.

Figure 6.9 shows the changes of the maximum displacement, velocity, and absolute acceleration at 3rd floor subjected to the El Centro NS excitation with various stiffness and damping. The changes of the maximum damper force and index J are depicted in Figure 6.10. Also, Figures 6.11 and 6.12 are the same comparison under Kobe NS input. In the figure depicts the maximum force, the force norm determined by the followings is also shown.

$$N_f = \int_0^T |f(t)|dt \tag{6.17}$$

It is observed from the trends in the absolute acceleration and index J for both earthquakes, optimum response reduction can be achieved in the negative stiffness regions in both ground motions, even considering the physical constraints of the damper. Also, displacement and velocity are not so large compared to the positive stiffness, which might be the effect of the increase of the apparent damping ratio. On the contrary, magnifications in absolute acceleration are observed in case of assuming passive viscous-elastic device, despite the displacement reduction effects. This result is expected from SDOF structuresimulation, and same tendencies can be found in the MDOF simulations. From these results, it can be said that the pseudo-negative stiffness control is the simple but effective control strategy in terms of absolute acceleration reduction while restraining the displacement.

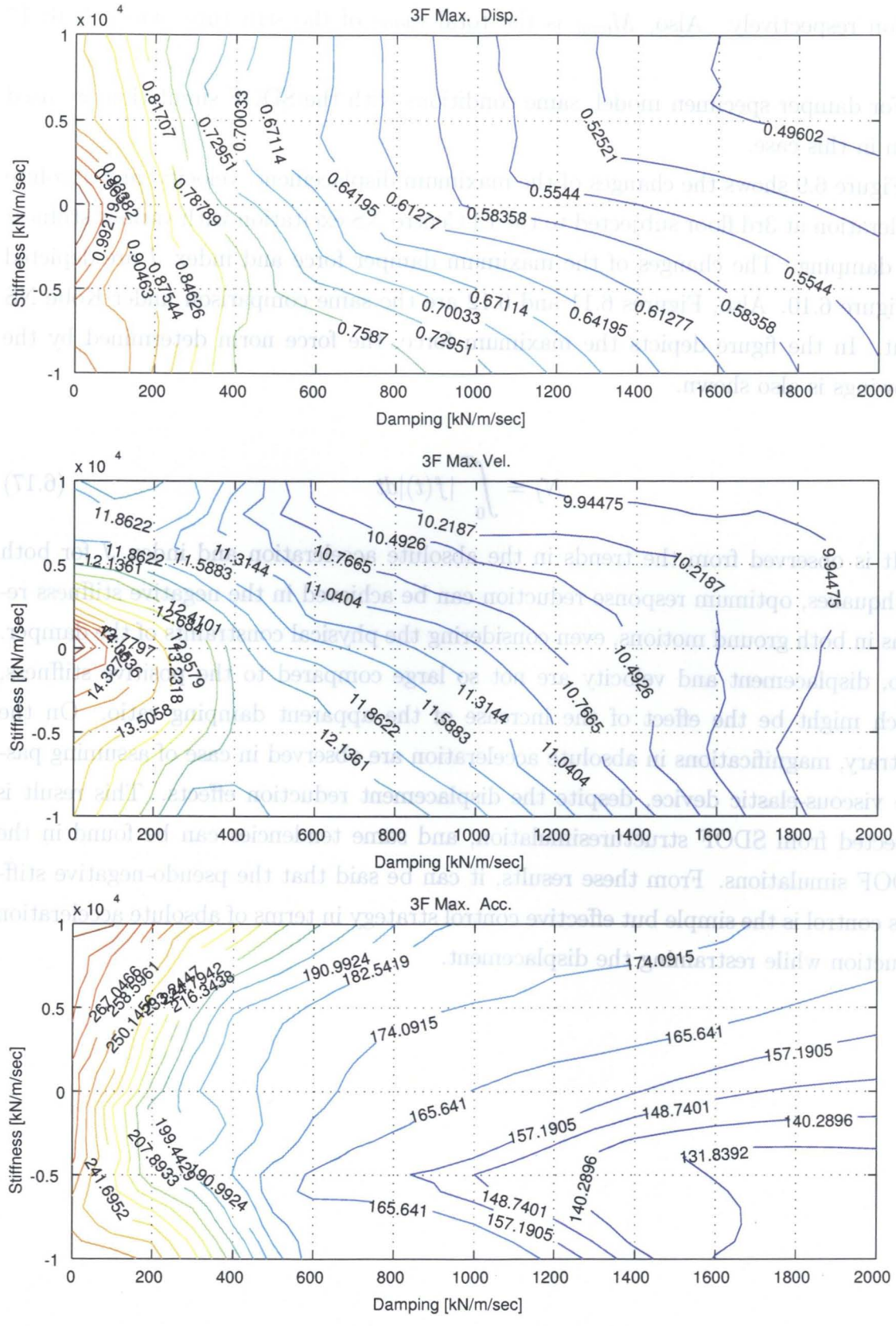

Figure 6.9: RF Maximum Responses (ECNS 100 gal)

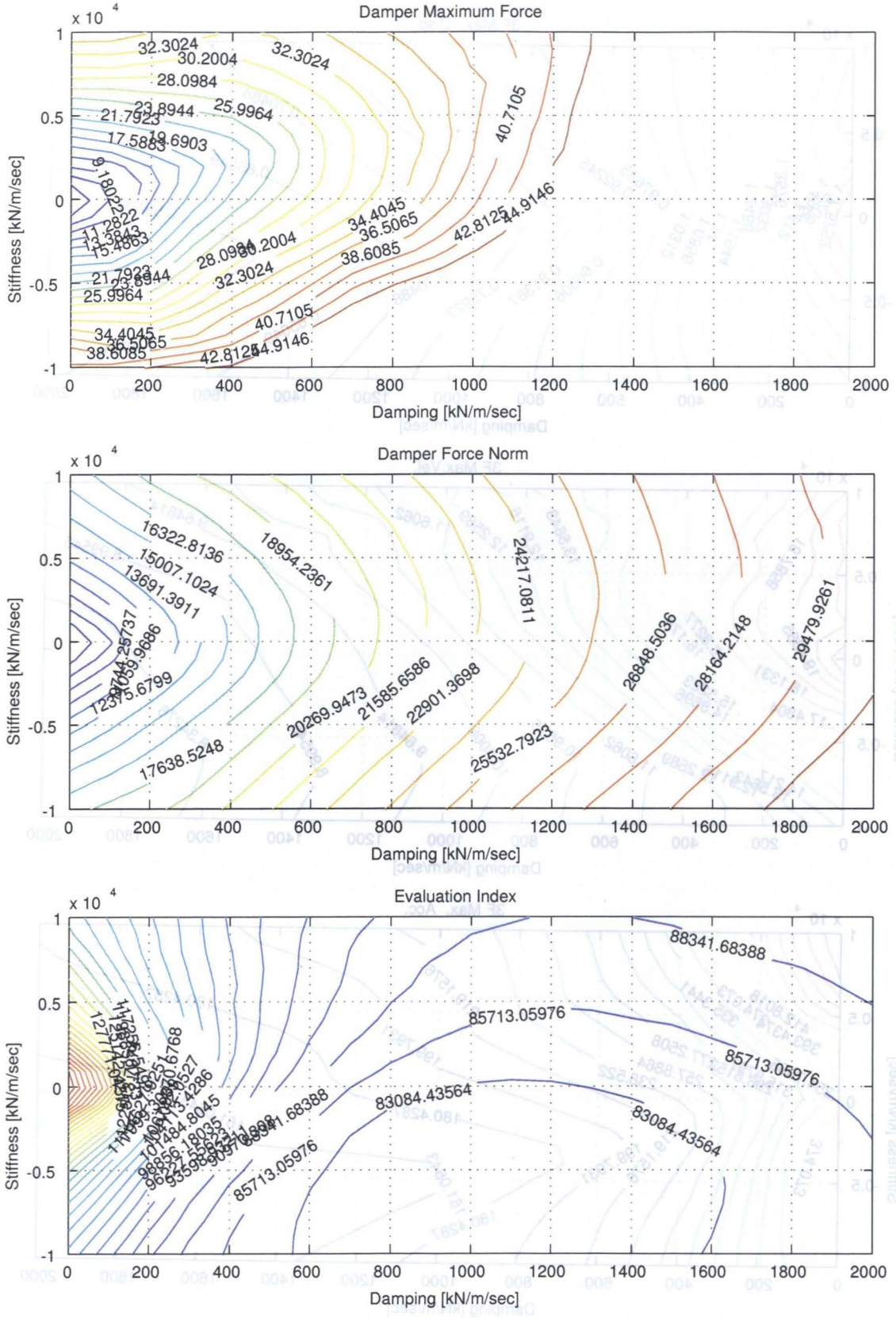

Figure 6.10: Force Response and Evaluation Index (ECNS 100 gal)

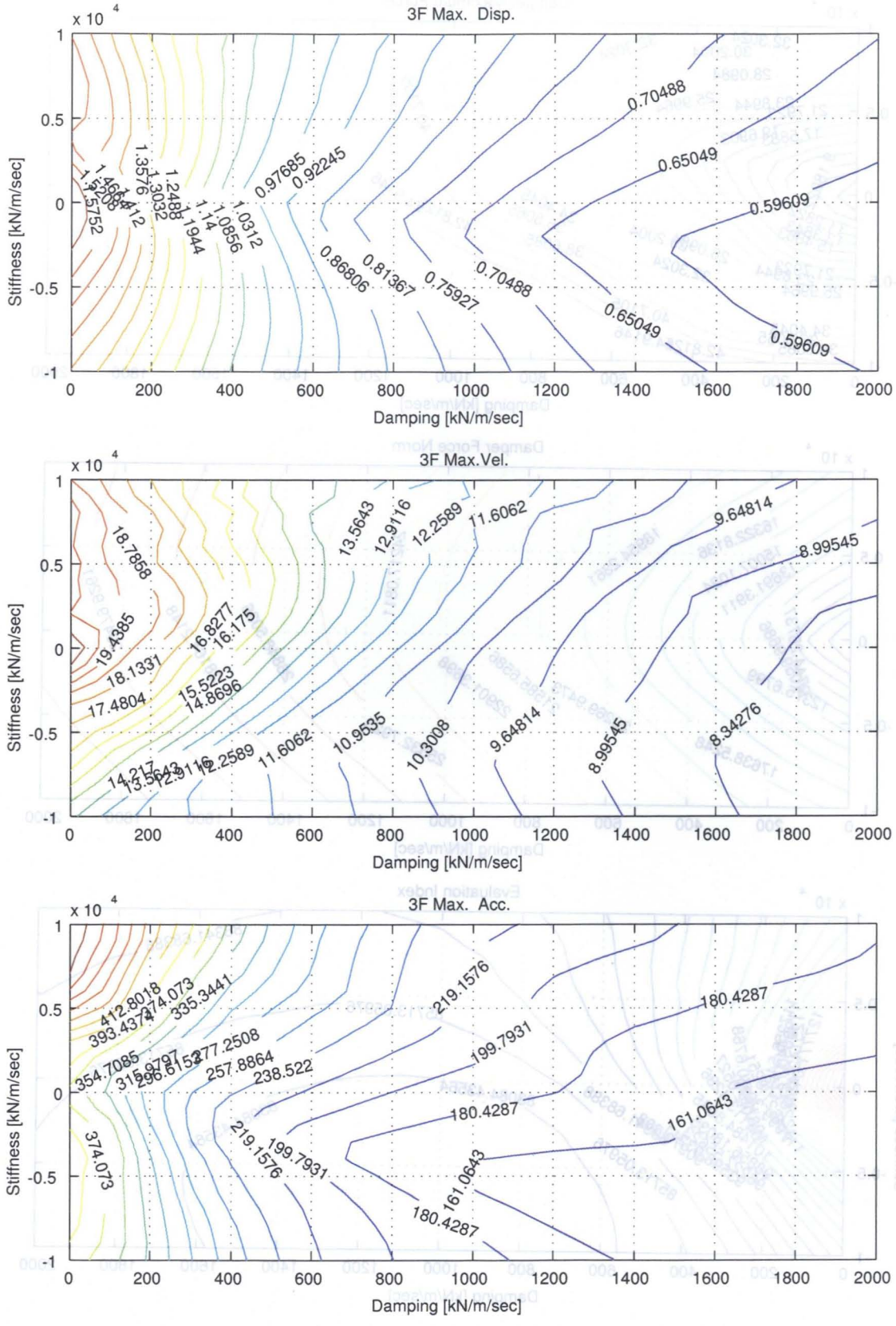

Figure 6.11: RF Maximum Responses (KBNS 100 gal)

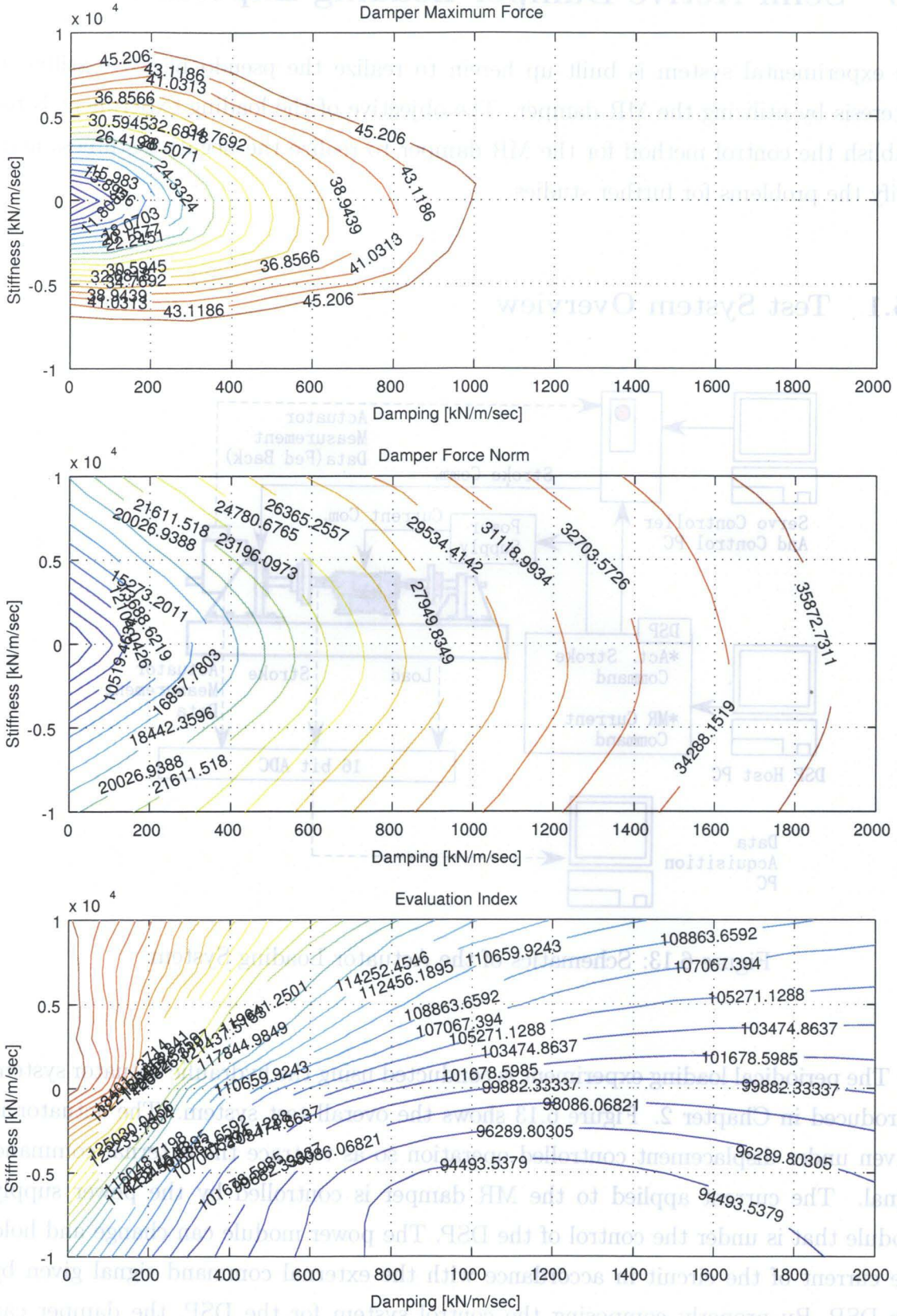

Figure 6.12: Force Response and Evaluation Index (KBNS 100 gal)

6.5 Semi Active Damper Loading Experiments

The experimental system is built up herein to realize the pseudo negative stiffness hysteresis by utilizing the MR damper. The objective of the loading experiment is to establish the control method for the MR damper to realize the negative stiffness and clarify the problems for further studies.

6.5.1 Test System Overview

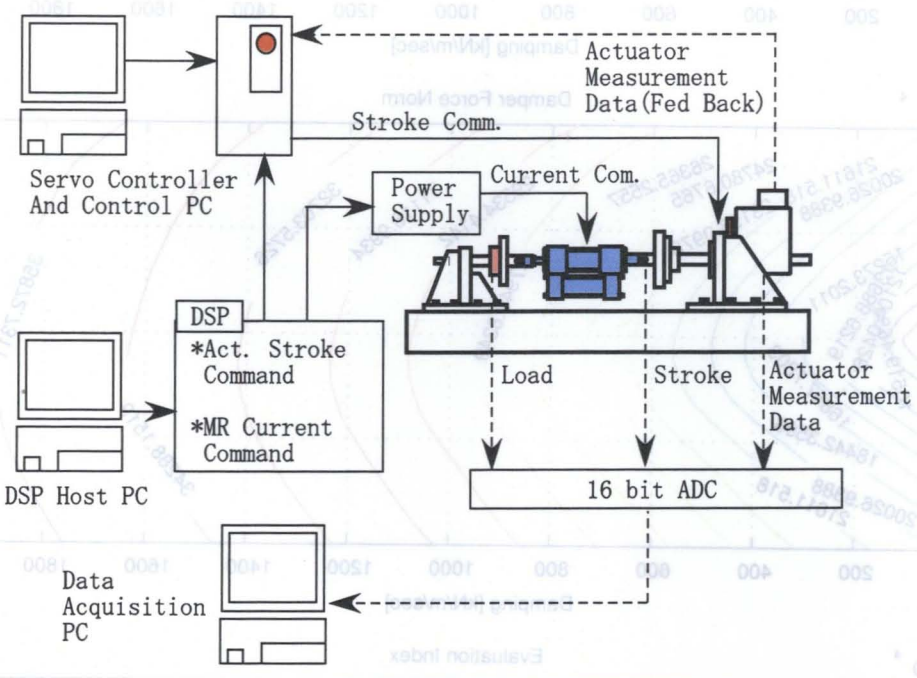

Figure 6.13: Schematics of the Actuator Loading System

The periodical loading experiment is conducted using the hydraulic actuator system introduced in Chapter 2. Figure 6.13 shows the overall test system. The actuator is driven under displacement controlled operation so as to trace the external command signal. The current applied to the MR damper is controlled by the power supply module that is under the control of the DSP. The power module can change and hold the current of the circuit in accordance with the external command signal given by the DSP. By properly composing the control system for the DSP, the damper can generate the various types of the hysteresis. Due to the rapidness of the change of the characteristics, constant current control is used for controlling the MR damper in real time[3, 4].

6.5.2 Power Supply Module Dynamics

Although the power supply module used here has a capability to keep the circuit current or voltage constant, it takes several time steps before the commanded current is being realized and settling to the target value. In order to comprehend the dynamics of the time-varying controlled MR damper, this time delay effect should be examined.

The periodic excitation test is then conducted for detecting the time delay from command to the force realization. The MR damper is excited with the 1 cm, 0.5 Hz of sinusoids, and command current is suddenly changed from 0 A to 2 A. The command current signal is given by the 1 Hz of square wave. The transfer function from command current to the force's being stable is determined so as for the calculated reaction force to trace the measured response. Consequently, a transfer function is obtained as follows,

$$H(s) = \frac{11.36}{s + 11.36} \tag{6.18}$$

Figure 6.14 shows the comparison of the measured and calculated force time histories as well as stroke versus force, stroke velocity versus force hysteresis. For reference, calculated force without considering the dynamics of the power supply module is also depicted. Also, Figure 6.15 shows the relations between stroke, stroke velocity, and command current time histories. It is found that transfer function for the power supply module can trace the moderate time response of the force with the change of the command current, which is clear contrast to the response without considering the dynamics. The overall force norm error between measured force f_{meas} and estimated force f_{est} defined by followings,

$$E = \frac{\int_0^T (|f_{meas}| - |f_{est}|)\, dt}{\int_0^T |f_{meas}| dt} \tag{6.19}$$

is reduced from 14.48 % to 3.19 % by taking the dynamics of the power supply module into account. Figure 6.16 shows the step response of the Eq.(6.18). It is found from this figure that this device takes about 0.5 second before command force is realized.

6.5.3 Periodical Loading Experiment

The periodical loading tests under stroke control mode are carried out with conditions shown in Table 6.1.

Command force is calculated by given command stiffness and damping as well as stroke and velocity measurement data. Command signal to the power module is determined by the inverted damper model, which is Eq.(4.4) and Eq.(4.5). Also, inverted

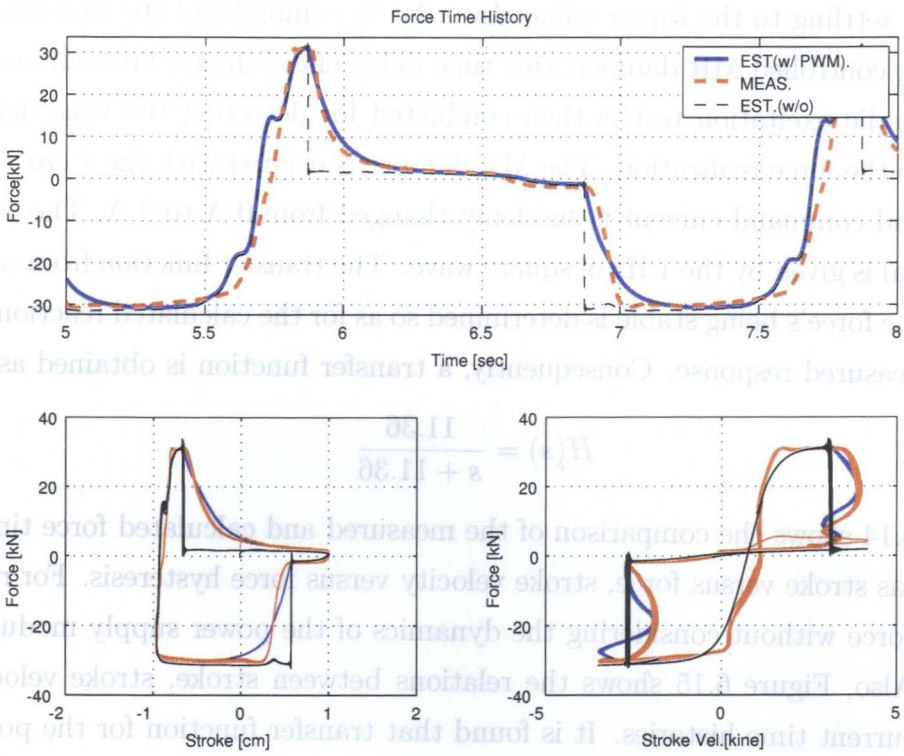

Figure 6.14: Comparison of the Measured and Calculated Forces

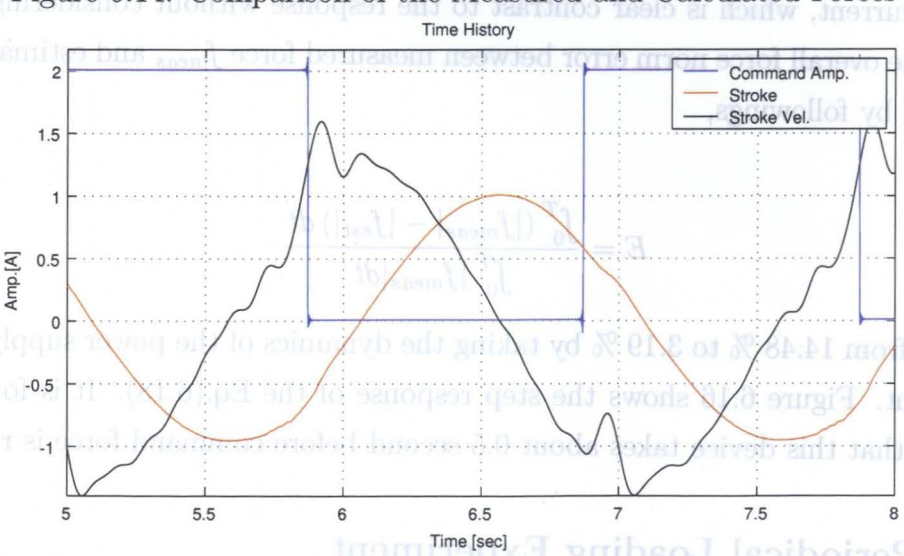

Figure 6.15: Comparison of the Response Time History (Scaled)

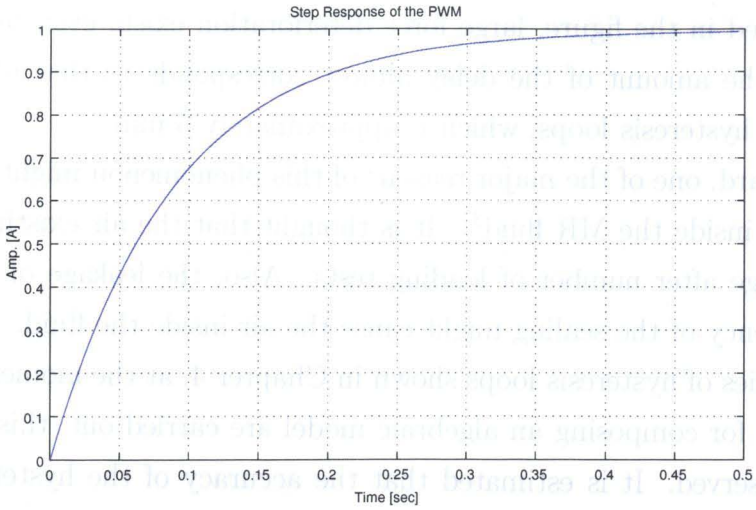

Figure 6.16: Step Response of the Identified Transfer Function

Table 6.1: Test Conditions

Stroke (cm)	Freq. (Hz)	Stiffness (kN/m)	Damping (kN/m/sec)
1.0	0.5, 0.75, 1.0	-1800	0
1.0	0.5, 0.75, 1.0	-1800	500

transfer function of Eq.(6.18) is applied between command current determination block and D/A block for compensating the dynamics. Since this inverted transfer function contains the derivative block, the control system might be vulnerable to the noise signal. For this reason, improper differentiation is utilized for implementation.

Figures 6.17~6.22 shows the comparison of the command and realized forces. Assumed stiffness is also depicted in each figure. From these results, several things are observed.

Firstly, negative slope can be observed in all of the hysteresis loops and good agreements are obtained with regard to the maximum force level. In other words, the identified inverted model has a good accuracy.

Secondly, the existence of the time delay is still observed even utilizing the inverted filter for the compensation.

Thirdly, the existence of the large delay observed at around the maximum velocity quite deteriorates the overall realized force. As for this problem, periodical loading tests under constant command currents are conducted in order to clarify whether this phenomenon arises from control system or not. Figure 6.23 shows the results of the tests under 1 cm, 0.5 Hz, and 1cm, 1.0 Hz of sinusoids with various constant currents.

As clearly observed in the figure, large force deterioration exists even under constant currents. Also, the amount of the delay almost corresponds to that of the pseudo-negative stiffness hysteresis loops, which is approximately 5 mm.

With this regard, one of the major reasons of this phenomenon might be caused by the 'trapped air' inside the MR fluid[3]. It is thought that the air existing in the MR fluid might emerge after number of loading tests. Also, the leakage of the MR fluid due to the deficiency of the sealing might cause the air inside the fluid.

As seen in series of hysteresis loops shown in Chapter 4, at the moment the periodical loading tests for composing an algebraic model are carried out, this phenomenon is not clearly observed. It is estimated that the accuracy of the hysteresis could be greatly improved by overcoming the problem existing in the device itself.

6.6 Summary

In this chapter, pseudo-negative stiffness (P.N.S.) control method, which is the simple but effective semi-active control algorithm, is introduced. In this method, the control force is given by the combination of the negative stiffness element plus positive damping element. An efficacy of the proposed PNS control is examined both algebraically and numerically. It is shown from SDOF and MDOF simulations exposed to the earthquake that the control method is advantageous over the passive device in terms of acceleration reduction. Also, periodical loading tests are conducted in order for the MR damper to realize the PNS hysteresis. Consequently, it is observed that negative stiffness could be successfully generated by making use of the inverted model for the MR damper.

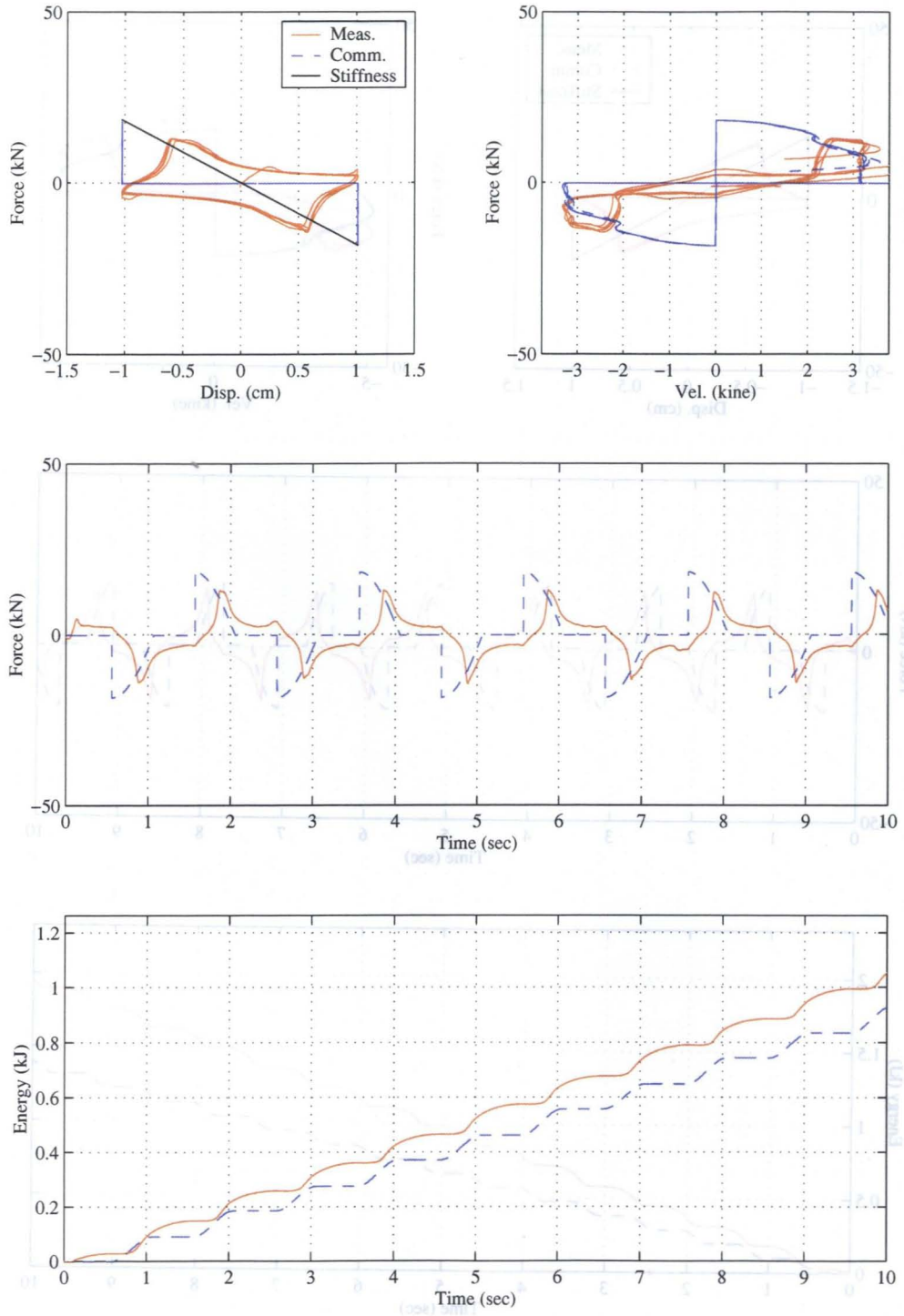

Figure 6.17: Comparison of the Hysteresis at K_D=-1800, $C_D = 0$ (1cm, 0.5 Hz)

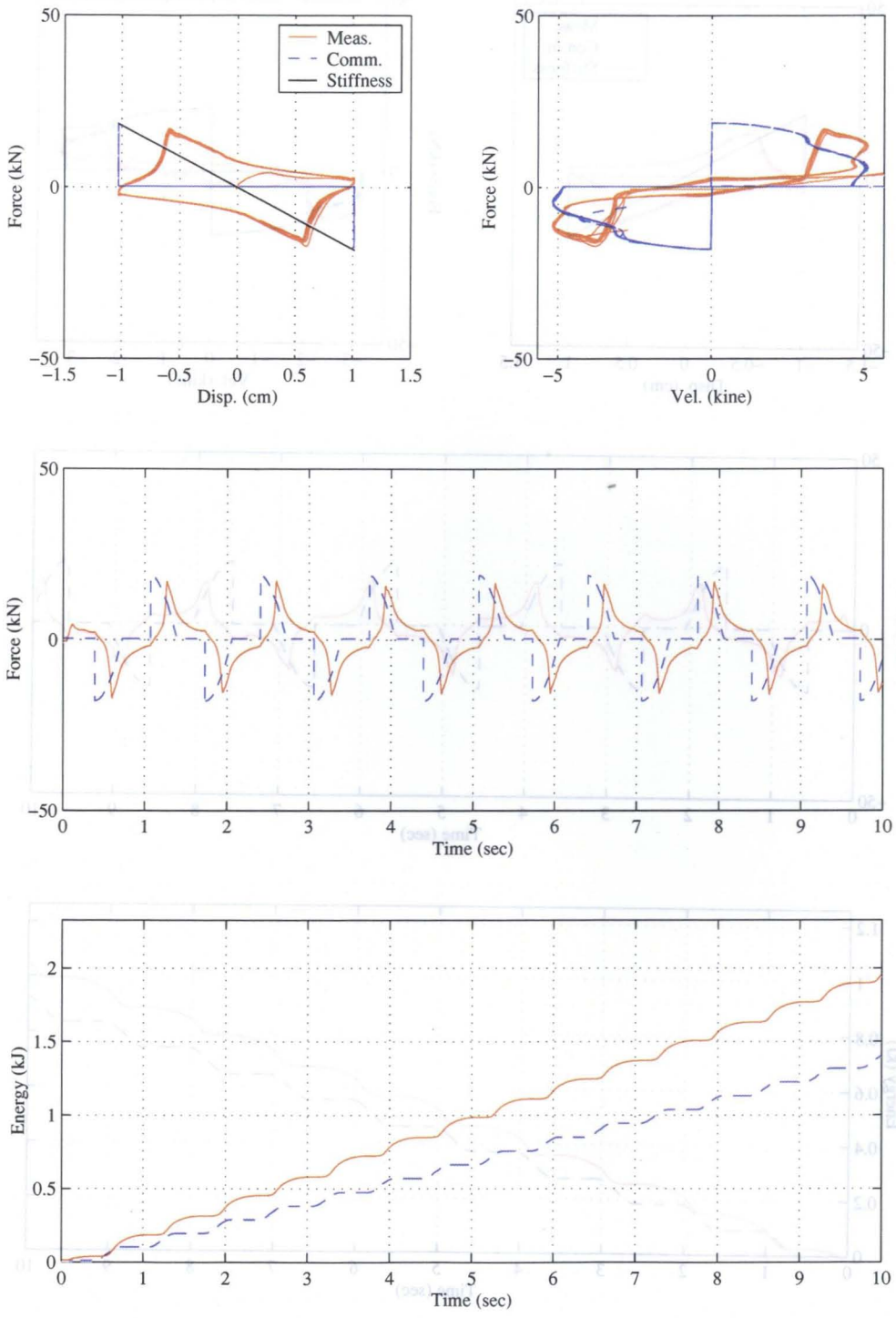

Figure 6.18: Comparison of the Hysteresis at K_D=-1800, $C_D = 0$ (1cm, 0.75 Hz)

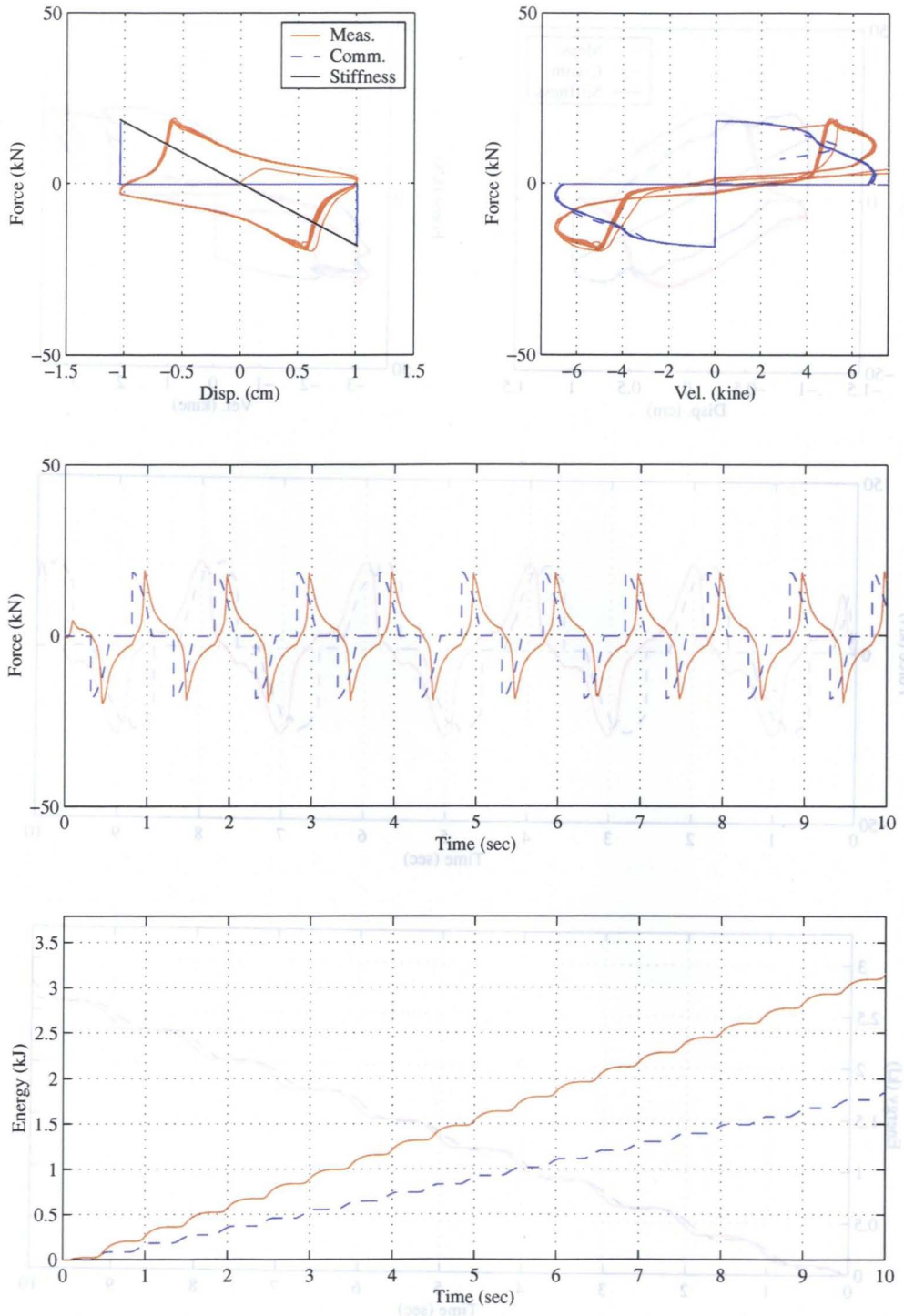

Figure 6.19: Comparison of the Hysteresis at K_D=-1800, $C_D = 0$ (1cm, 1 Hz)

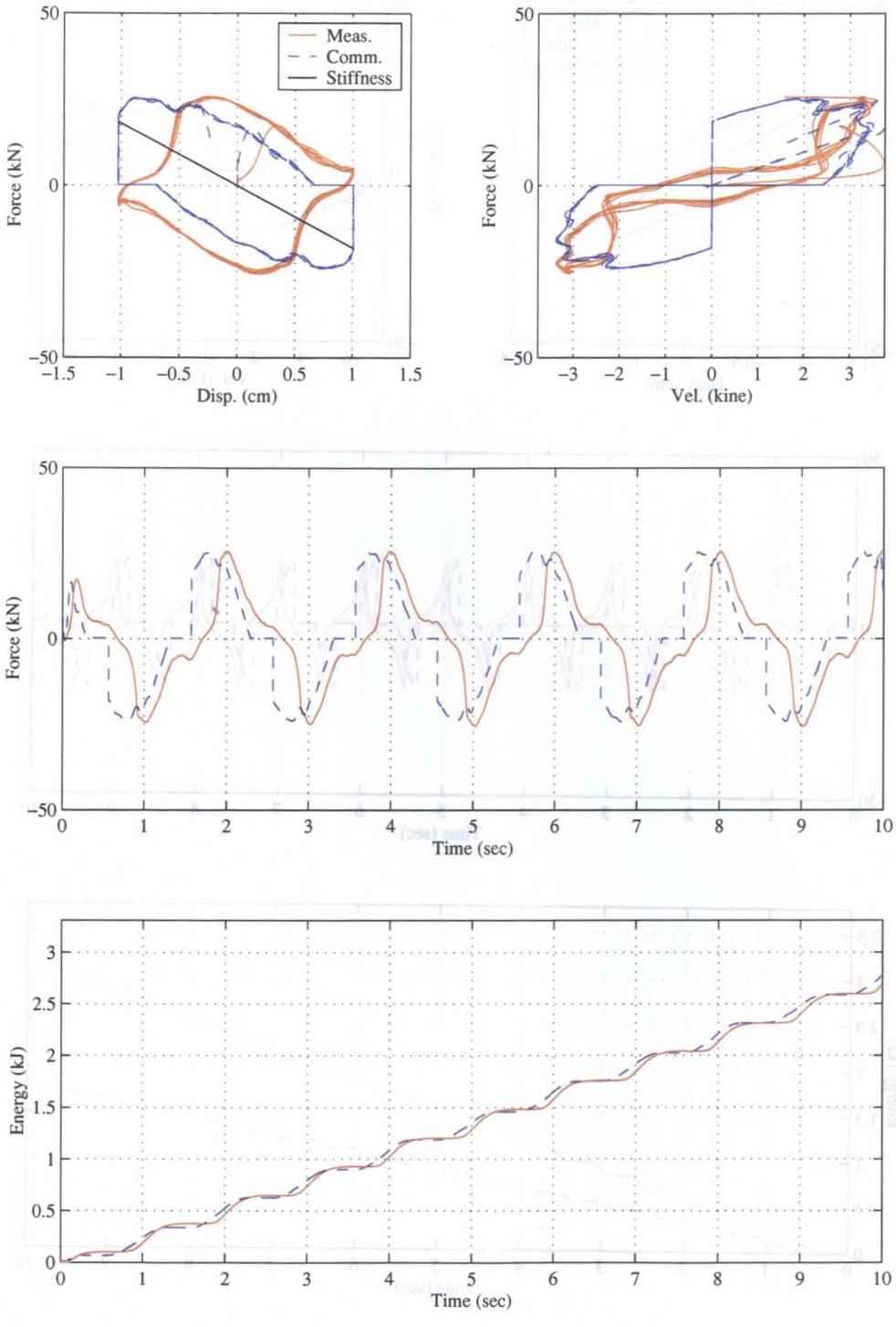

Figure 6.20: Comparison of the Hysteresis at K_D=-1800, C_D = 500 (1cm, 0.5 Hz)

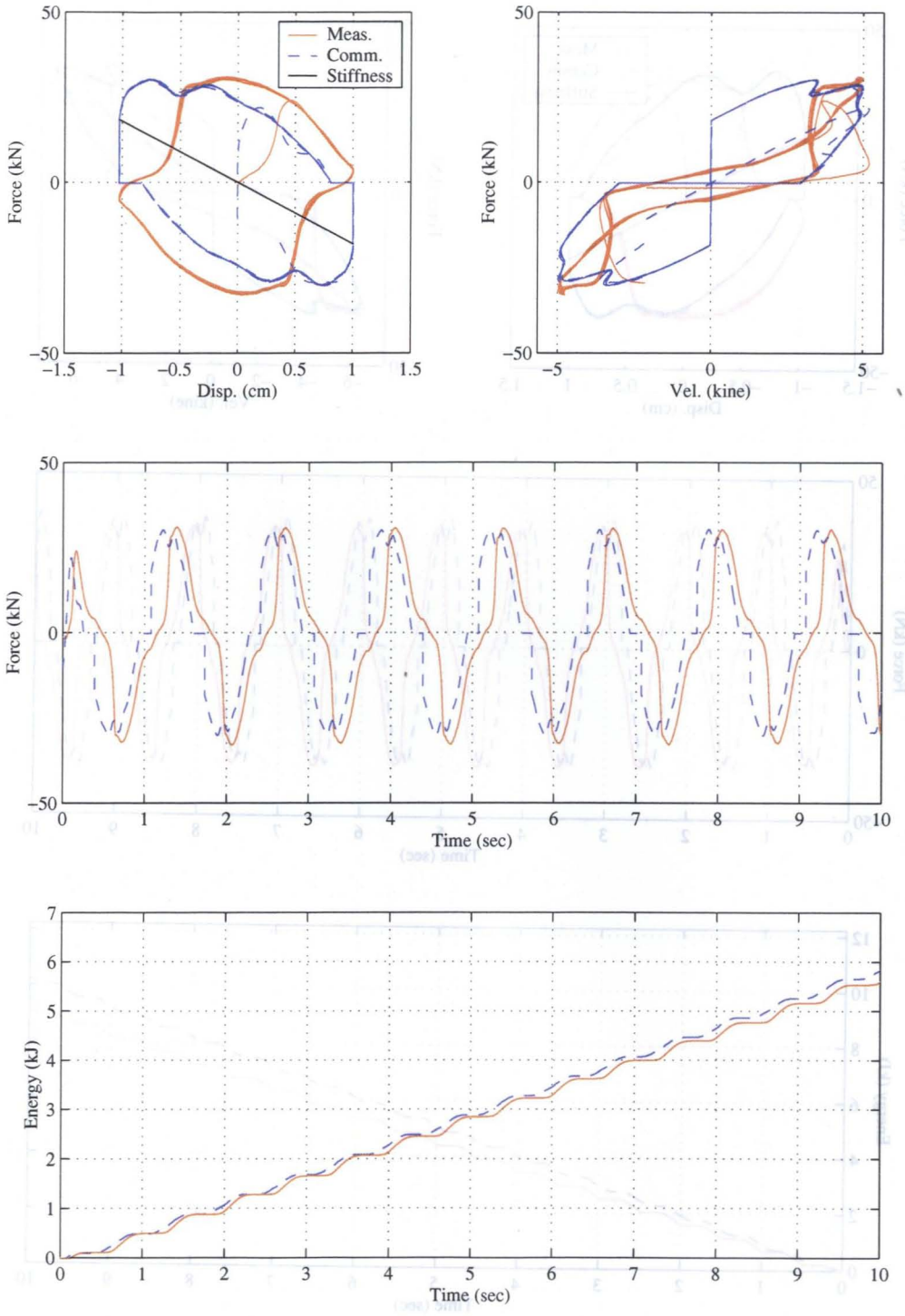

Figure 6.21: Comparison of the Hysteresis at K_D=-1800, C_D = 500 (1cm, 0.75 Hz)

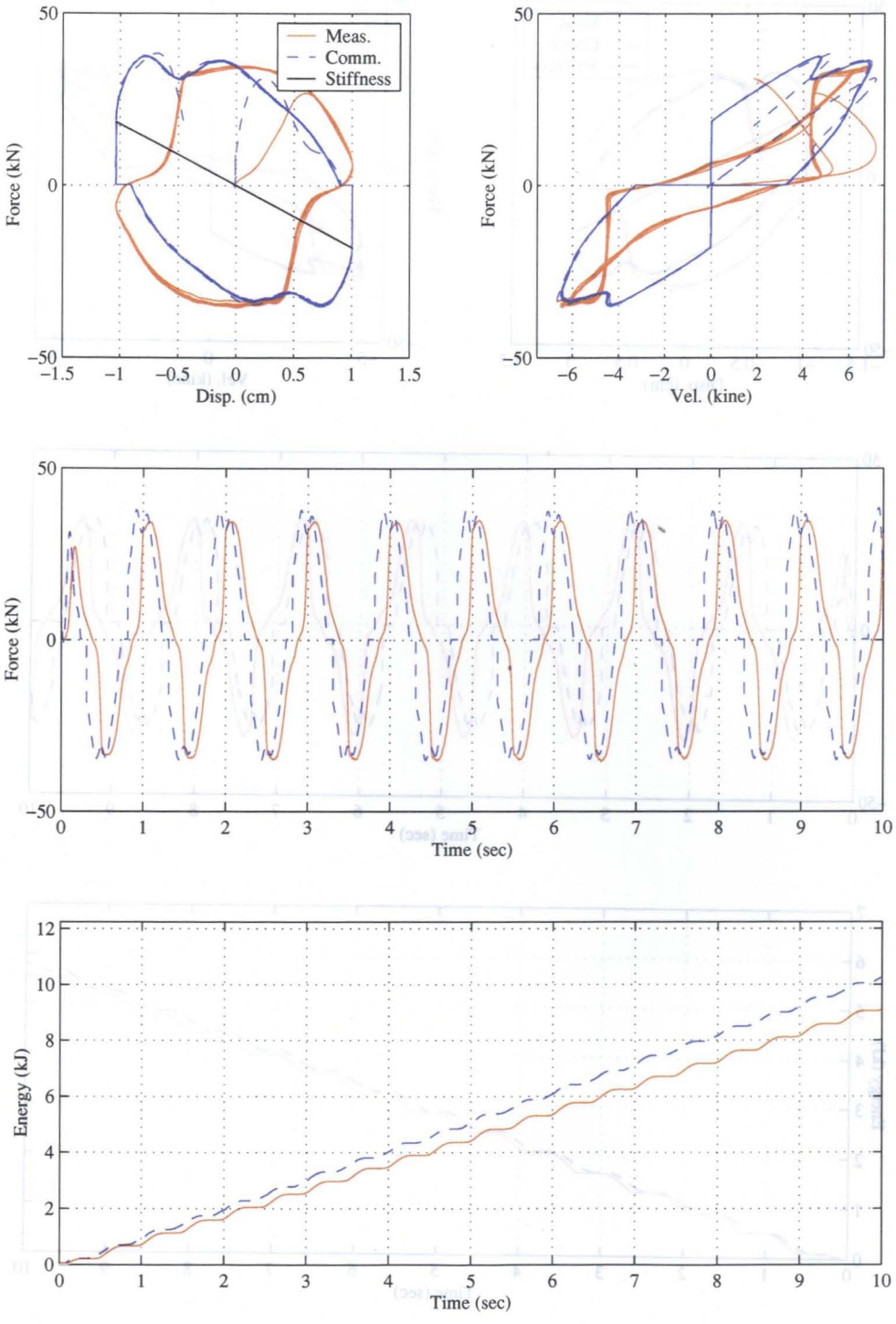

Figure 6.22: Comparison of the Hysteresis at K_D=-1800, C_D = 500 (1cm, 1 Hz)

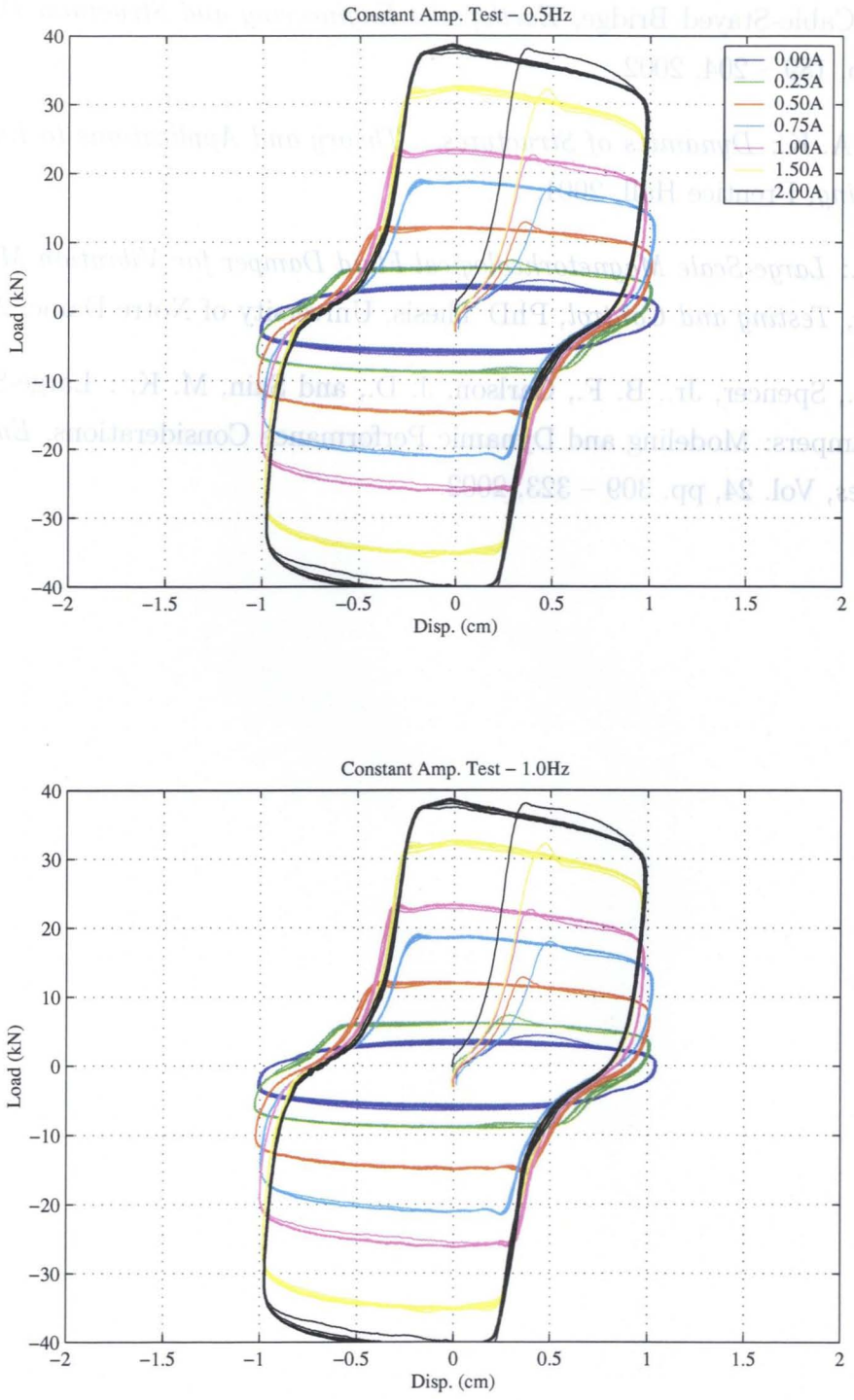

Figure 6.23: Periodical Excitation Tests under Constant Current

References

(1) Iemura, H. and Pradono, M. H. : Passive and Semi-Active Seismic Response Control of a Cable-Stayed Bridge, *Earthquake Engineering and Structural Dynamics*, Vol. 9, pp. 189 – 204, 2002.

(2) Chopra, A. K.: *Dynamics of Structures – Theory and Applications to Earthquake Engineering*, Prentice Hall, 2001.

(3) Yang, G.: *Large-Scale Magnetorheological Fluid Damper for Vibration Mitigation: Modeling, Testing and Control*, PhD Thesis, University of Notre Dame, 2001.

(4) Yang, G., Spencer, Jr., B. F., Carlson, J. D., and Sain, M. K. : Large-Scale MR Fluid Dampers: Modeling and Dynamic Performance Considerations, *Engineering Structures*, Vol. 24, pp. 309 – 323, 2002.

Chapter 7

Conclusion

In this dissertation, the Inertia-Force-Driven-Loading test system is newly developed. This test system has a capability to conduct a precise and economical loading tests while considering the structure-device interactions. In this research, a shaker control method for the IFDL test system to be utilized as the real time hybrid loading system is proposed, and its efficacy is confirmed through full-scale experiments. Also, as another objective of this research, pseudo-negative stiffness (P.N.S.) control method, which is the simple but effective semi-active control algorithm, is introduced. The effectiveness of the PNS control is examined through numerical simulations. Then, the periodical loading experiments are conducted so as for the MR damper to realize the PNS hysteresis. The achievements of the dissertation are presented as follows.

In Chapter 2, total setup of the IFDL test system including the sensors, shaker, and control devices is described. The features as well as the locations of devices are closely mentioned, which would be used for the loading experiments.

In Chapter 3, basic algorithm of the shaker control method for the IFDL system to realize the real-time hybrid loading experiment is proposed. In the proposed method, the shaker is commanded so as for the equation of motion regarding the IFDL to consistent with that of the assumed structure.

It is shown that any kinds of structural system including nonlinearity and damper specimen can be conducted by utilizing the precisely controlled shaker. The error arises from the existence of the time delay between command and realize of the shaker velocity is analyzed. It is found that existence of the time delay might cause the distortion of the response at around the natural frequency of the test system.

Also, feasible ground motion level and hypothetical structural properties are examined from the viewpoint of satisfying the physical constraints of the IFDL test system.

It is found that the shaker control force capacity should be the major concern for conducting the large-scale experiments.

In Chapter 4, preliminary identification tests with regard to the IFDL test system, damper specimen, and shaker device are carried out. It is indispensable to comprehend the dynamic characteristics for these devices from the viewpoints of conducting the precise numerical simulation and periodical loading experiment. As to damper specimen, it is shown that the dynamics of the device can be well traced by utilizing the algebraic model, which is a function of the current applying to the device. For shaker dynamics compensation, a PID controller and band-pass filter are designed.

In Chapter 5, real-time hybrid loading experiments are carried out. As hypothetical structures, single-degree-of-freedom (SDOF) as well as multi-degree-of-freedom (MDOF) systems is chosen, both are supposed to be exposed to the resonance periodical motion and historical earthquakes. As test specimen, the MR damper applying 0 A of constant current is utilized.

From SDOF experiment, the IFDL test system as well as the proposed control method are quite effective for the real-time hybrid experiment under not only periodical resonance motion but also historical earthquake inputs. In case of the MDOF simulation, results of hybrid loading experiment are compared to those of the past research that uses the assumed real-scale frame structure. It is shown that the developed experiment system could capture the structural responses under the influence of the multiple modes. It is also shown that the experimentally obtained characteristics can well trace the tendency that was observed in the past research.

In Chapter 6, a pseudo-negative stiffness (P.N.S.) control method is introduced. In this method, the control force is given by the combination of the negative stiffness element plus positive damping element. An efficacy of the proposed PNS control is examined both algebraically and numerically. It is shown from analytical approach for the SDOF system that acceleration could be reduced by elongating the natural period, while restraining displacement due to the increase of the apparent damping ratio. Also, it is shown from MDOF simulation exposed to the earthquake that the control method is advantageous over the passive device in terms of acceleration reduction. Also, periodical loading tests are conducted in order for the MR damper to realize the PNS hysteresis. Consequently, it is observed that negative stiffness could be successfully generated by making use of the inverted model for the MR damper.

For further studies, following problems should be overcome.

As to the IFDL system, the hybrid loading system using the semi-active controlled damper could not carry out due to the limitations of the shaker, and input ground motion levels are also limited to the small amounts. It is required to design the more capable test system and shaker, taking the achievements of the dissertation into account.

Also, efficacy of the obtained results from the MDOF experiments together with constant-current controlled MR damper should be confirmed by conducting the full-scale loading experiment using the real frame structures.

For the PNS control, the substructure hybrid experiments should be carried out in order to confirm the efficacy of the negative stiffness, which effectiveness was analytically shown in the dissertation.